A thesis submitted for the degree of

Doctor of Philosophy
at
Oxford Brookes University

Analysis of prior strain history effect on mechanical properties and residual stresses in beams

OXFORD
BROOKES
UNIVERSITY

Guillermo Urriolagoitia Sosa

August 2005

THE FOLLOWING HAVE NOT BEEN COPIED ON INSTRUCTION FROM THE UNIVERSITY

Figure 2.3 page 15

Figure 2.6 page 20

Figure 2.7 page 21

Figure 2.8 page 24

Figure 2.9 page 27

Table 2.1 page 29

Table 2.2 page 30

Table 2.3 page 31

Table 2.4 page 32

Figure 6.3 page 136

Figure 6.4 page 138

Figure 6.5 page 139

Figure A1 page 228

Abstract

The crack compliance method (CCM) has attracted a lot of interest as an inexpensive method for the determination of residual stresses in materials compared to the use of X-ray and neutron diffraction methods. The vast majority of the work found for the application of the CCM in the literature concentrated on the determination of residual stresses in annealed beam specimens. There is very little evidence of the verification of the method in cases where the material might have experienced prior strain loading effect such as Bauschinger effect before the residual stress is induced. This thesis has applied the CCM for the determination of residual stresses in beams that were under Bauschinger effect before the residual stress was induced. The thesis also briefly considers the application of the CCM for the study of cyclic loading effect on the relaxation of residual stresses in beams.

In order to achieve the aims highlighted above, the thesis develops a new efficient solution for the simultaneous determination of tensile and compressive stress-strain behaviour in materials under Bauschinger effect. The determination of these properties helps with the verification of the results of the CCM by using another relatively simple and inexpensive method based on the superposition of loading and unloading stresses. A new simple support method for beams subjected to electro-discharge machining (EDM) is also introduced. The new cutting arrangement allows free deformation of beams during cutting and allows the plane of cutting to be maintained without deviation. The experimental testing and verification procedure considers several factors such as different materials, heat treatment conditions, various levels of pre-straining and different fatigue load amplitudes. Several aspects of the crack compliance method are verified. The results obtained in all cases are generally very encouraging.

List of figures

List of tables

Symbols

α Direction of σ_1 or the back-stress

δU Difference in the elastic energy stored before and after the extension of the crack

ε Nominal strain

ε^{pl} Equivalent plastic strain

$\varepsilon_{\theta\theta}$ Strain measured in the tangential direction

$\varepsilon_{1,2,3}$ Values of the relaxed strains at 0, 45^0 and 90^0 respectively

ε_A Strain acting in the axial direction

$\varepsilon_{A'}$ Relaxed strain in the axial direction

$\varepsilon_{a,b,c}$ Relaxed strains measure at 0^0, 45^0 and 90^0

ε_c Nominal compressive strain

ε_{cm} Compressive strain value at increment m

$\varepsilon_{T'}$ Relaxed strain in the transverse direction

ε_t Nominal tensile strain

ε_{tm} Tensile strain value at increment m

ε_y Yield strain

ε_{zz} Strain measured in the axial direction

Φ Direction of σ_{Max} or σ_{Min} relative to ε_1

γ Rate at which kinematic modulus decreases with plastic deformation

ν Poisson's ratio

π Pi = 3.1416

σ Nominal stress

$\sigma_{\theta\theta}$ Stress in the tangential direction

$\sigma|_o$ Initial yield stress

$\sigma_{1,2}$ Magnitude of the principal stresses at a given depth

σ_c Nominal compressive stress

σ_{cm} Compressive stress value at increment m

σ_t Nominal tensile stress

σ_{tm} Tensile stress value at increment m

σ_{Max} Maximum principal stress

σ_{Min} Minimum principal stress

σ_o Current yield stress

σ_{rr} Stress in the radial direction

σ_t Nominal tensile stress

σ_y Yield stress

σ_{zz} Stress in the axial direction

a Crack or slot length

A Enclosed area

A_c Area under the compression stress-strain curve

A_i Coefficients used in the crack compliance method

A_t Area under the tensile stress-strain curve

b Rate at which the size of the yield surface changes as plastic straining develops or base of the beam

C Initial kinematic hardening modulus

$C_i(a,s)$ Response compliance function of the strain gauge at a reference location when a stress distribution is applied to the crack length

E Young's modulus

E' Generalized Young's modulus

F Force

h Total depth of the beam

h_c Distance from the compression surface to the neutral axis

h_t Distance from the tensile surface to the neutral axis

$h(x,a)$ Weight function

L Length

M Bending moment

M_c Effective bending moment carried by the part of the section of the beam under compressive stress

M_t Effective bending moment carried by the part of the section of the beam under tensile stress

P_i Power series, x^0, x^1, x^2, ... x^n etc., Legendre polynomials or other functions

Q_∞ Maximum change in the size of the yield surface

r Radius from the specimen axis

r_o Specimen outside radius

s Distance between the arbitrary point and the point of the application of the force

U Elastic store energy

W Specimen width

w Uniform distributed load

$Z(a)$ Geometry dependent function which reflects the sensitivity of the strain at reference point with respect to stresses released at the crack tip

z Current groove depth

Acknowledgment

To the beloved memory of my mother Teresita Sosa Najera, you have always been in my heart. To my father Dr. Guillermo Urriolagotia Calderón with my greatest admiration and gratitude.

The work described in this thesis was carried out in the School of Technology in the Department of Engineering at Oxford Brookes University. To Dr. J. F. Duroldola who supervised me during this project and to whom I'm grateful for the encouragement and guidance. To Dr. N. A. Fellows who was always ready to offer helpful assistance.

To Mr. Michael Hartman, my most sincere gratitude for his friendship and support in times of difficulties. Mike, thank you very much. You are a great person!

To Mr. Chris Boram who offered helpful experimental experience and technical support. My appreciation to my friends; David Harvey, Adolfo Lopez-Castro and Jean-Francois Jouin. For some years we shared the same office and try to solve many of the world problems. I will always keep you in my thoughts.

To the Consejo Nacional de Ciencia y Tecnología for the funding to carry out this research and to the Instituto Politécnico Nacional for all the unconditional support.

To my dearest wife Ms. Vivian Schaan Pessano, for her patience, care and love (you are my greatest inspiration). To my daughter and sons Teresita Isabel (TEISA), Guillermo Manuel (GUI) and Benjamín (BEN) with all my love. Also to my brothers Alejandro, Eduardo, Ricardo, José Carlos, Francisco Javier and my sister Beatríz, thanks.

1.1. Introduction.

Residual stresses are stresses existing in a material, component or structure when no external mechanical or thermal loads are applied. They can be beneficial or detrimental to the strength of a material, component or structure depending on the service load conditions.

Residual stresses are induced whenever a material is permanently deformed or distorted in a non-uniform manner during processes, such as:

1. Cold forming or working (shot peening, rolling, grinding, etc.).
2. Heating or cooling (welding operations, heat treatment, surface hardening).
3. Electro deposition.

A significance of residual stresses derives from the role they play in material failures such as fatigue, creep, wear, stress corrosion cracking, fracture, buckling, etc. They also cause dimensional instability, such as distortion after heat-treatment or after machining a part. The combined effects of external loads, environmental effects and residual stresses cause notable damage. In the presence of residual stresses, fatigue failures can occur at loads and environmental conditions that would not normally cause failure. In the past, fatigue failure was considered as being a surface initiated phenomenon. It is now obvious that high internal residual stresses in a body can lead to internal failures rather than surface initiated failures in some cases.

Residual stresses used in a controlled way can be beneficial. A typical example is that in shot peening and autofrettagging components where early yielding on the surface of the material is suppressed and thereby inhibits nucleation of cracks from the surface.

In view of the benefits and detrimental effects of residual stresses highlighted in the foregoing, they are receiving increasing attention by the engineering community. This is driven by the desire to decrease the cost of materials used in structures, reduce weight of components and improve service performances. In particular, attention to residual stress effects can lead to higher reliability and longer useful life for structural components.

Most of the existing measurement techniques for residual stresses such as Sach's electro-chemical machining, layer removal, hole drilling, crack compliance, X-ray and neutron diffraction methods are destructive or very expensive.

The ability to model and measure residual stresses accurately, quickly and easily would enable designers to account for their presence and magnitude properly. Such efforts would promote increased productivity and resource conservation and also improve quality assurance in manufactured components and assemblies.

The crack compliance method has attracted a lot of interest as a relatively cheap method of determining residual stresses in materials. Only the elastic constants of the material and data on strain relaxation, when a slot is introduced into the material are required for the application of the method. One of the strengths of the crack compliance method that is hardly emphasised is that no prior knowledge of loading history of the material is

required. Virtually all published work on the analysis of the method has made every effort to eliminate the effects of prior loading history.

This thesis presents the use of the crack compliance method for the determination of residual stresses in beams having prior strain history, i.e. under Bauschinger effect.

Chapter 2

Background

2.1. Introduction.

The aim of this chapter is to highlight some of the background details related to the origin and classification of residual stresses. This background information also covers methods for determining residual stresses in materials, parameters that are considered in the selection of measurement techniques and the determination of residual stresses.

2.2. Classification, origin and effects of residual stresses.

Several technical terms are used to refer to residual stresses, these include; internal stresses, initial stresses, inherent stresses, reaction stresses, body stresses, self stresses, forming stresses, fabrication stresses or locked-in stresses [*Masubuchi, 1980*]. Residual stresses have been defined as self-equilibrating stresses existing in a body in the absence of externally applied forces and under uniform temperature distribution. The stress state must be in static equilibrium, i.e. the total force acting on any cross-section must be zero and secondly the total moment of the forces on any section must also be zero. These conditions are usually expressed as [*Treuting, 1952*];

$$\int \sigma \, dA = 0 \qquad 2.1$$

and

$$\int dM = \int \sigma \, r \, dA = 0 \qquad 2.2$$

r being the distance of the elemental area dA on which the stress σ acts from an appropriate axis through the section.

Residual stresses have in a general way, in the literature, been divided in two categories, macroscopic or microscopic depending on the size of the zone over which they act [*Masubuchi, 1980 and Parlane, 1979*].

Macroscopic Residual Stresses are residual stresses distributed over appreciable areas, from entire surfaces to a group of grains in a material. They are also known as body stresses of the 1st kind [*Masubuchi, 1980*]. Examples of these stresses are those produced by grinding a metal component, welding pieces of metals together, heating a structure causing thermal distortions and plastically bending a bar.

Microscopic Residual Stresses are residual stresses that vary from grain to grain or within a grain (also know as residual stresses of the 2nd kind). The exact influence of these stresses is still not very well understood, but they are identified as having some relationship with processes such as age hardening, precipitation and diffusion in alloys that result in changes in physical properties. Examples are stresses produced in areas of martensitic transformation in steels, or stresses that exist on the atomic scale in areas near dislocations.

There is another widely standardized classification proposed by *Macherauch and Kloos* [*1986*] categorising the residual stresses into three different types:

1st Kind.- This type of residual stresses are macro-stresses that are nearly "homogenous" (the term "homogenous" is used to mean constant in magnitude and direction) across large areas of several material grains and are in equilibrium over the bulk of the component. Any type of interference with a part of a component containing this kind of stresses will result in a change of the shape of the component. This research is focused on residual stresses of the 1st kind.

2nd Kind.- This type of residual stresses are micro-stresses that are nearly "homogenous" across microscopic areas about the sizes of a grain in a material, and are in equilibrium across a number of grains.

3rd Kind.- These residual stresses are also micro-stresses and are "inhomogeneous" across sub-microscopic areas of material (some atomic distance within the grain). No macroscopic changes in the dimensions of the material will occur if the equilibrium of the stresses are disturbed.

Several processes required for the fabrication of components can cause residual stresses. Some of main processes are described below.

a) *Machining Processes.*- These processes are described as those mechanical operations that remove or cut material to manufacture a new piece. Examples of these operations are drilling, planning, reaming, honing, broaching, band sawing, turning, milling and grinding. These standard machining processes usually create compressive stresses in the cut zones of the metal [*Bainbridge, 1969*]. The magnitude of the residual stresses can be high or low depending on the mechanical properties of the material, the cutting force, the velocity used to cut, the tool sharpness, the depth of the cut, the feed rate, the nature of the cooling fluid and the geometry of the tool.

b) *Forming Process.*- These are processes in which loads are applied to permanently deform a component without removing material. Some examples of forming processes are rolling, drawing, bending, flanging, twisting, dimpling,

forging, rectification, tension, compression, pressing, spinning, blasting and shot peening. They can generate tensile and/or compressive residual stresses in the component surfaces depending on the process. The bending forming operation was used in this project to induce residual stresses in beams. When a metal bar is bent beyond the yield point, plastic deformation takes place on both tensile and compression sides. The stresses due to loading plastically are generally not linearly distributed through the depth of the bar, but the unloading stress is elastic and linearly distributed [*Timoshenko and Gere, 1991*]. The residual stress state that acts on the bar upon unloading can be obtained by superposition, (Figure 2.1) by using Equation 2.3.

$$\sigma_{Re\,sidual}(x) = \sigma_{Loading}(x) - \sigma_{Unloading}(x) \qquad 2.3$$

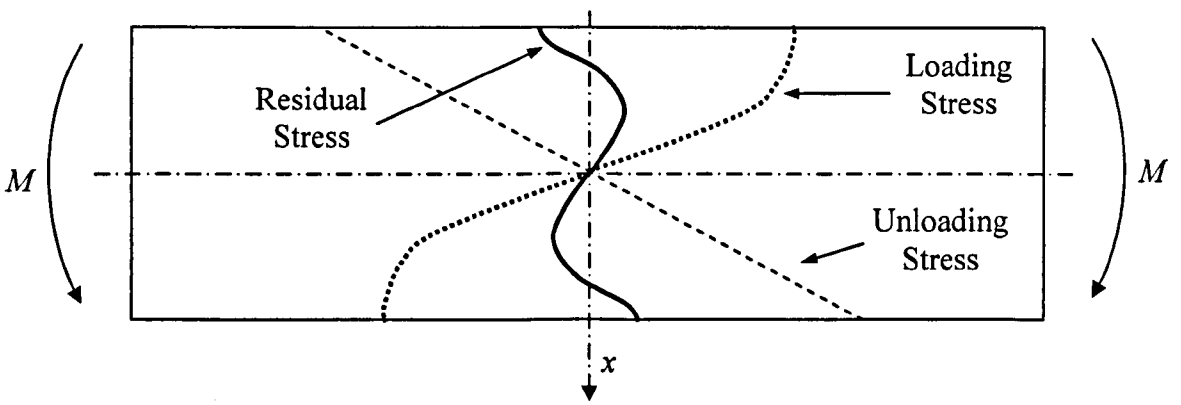

Figure 2.1.- Residual stresses superposition

where x describes the depth location in the bar. Residual stresses of opposite sign will occur in the outer regions of the bar that were originally under tension or compression.

c) *Heat Treatment Processes.*- These processes could produce residual stresses even if the treated material does not experience crystalline structure changes. For example, when aluminium is rapidly cooled after heat treatment, the resulting temperature gradient causes dissimilar rates of contraction at the surface and interior [*Bonner, 1996*].

d) *Joining Processes.*- The processes denoted here involve operations that join two or more pieces together permanently [*Bonner, 1996*]. Some examples of this kind of processes are welding, soldering, brazing and adhering. The mechanisms involved in the production of residual stresses in the joining processes (principally welding and soldering) are many and varied and their interactions can be complex. The primary source of induced residual stress is localised shrinkage during cooling or drying of the union. However other sources can be identified depending on the joining process [*Huang, et. al. 1988 and Dye, et. al. 2000*].

e) *Coating Processes.*- These processes refer to techniques for application of a thin layer of one material to another. They are widely used to enhance and alter the physical properties and appearance of a component. Coating and lamination are applied to various materials including metals, plastics, composites, ceramics and fabrics. Some examples of this kind of operations are; depositing, cladding, spraying, electroplating, plating and galvanising.

The induction of residual stresses by one or more of the operations highlighted above can result in a multiplicity of effects, like; changes in metal properties, alteration of the

electrical conductivity, magnetic permeability and magnetostriction, chemical potential and reactivity, phase transformation, precipitation, plastic deformation, work hardening, fatigue, creep, elastic and plastic after effects, recovery and re-crystallization, internal friction, elastic properties, mechanical strength, fabrication qualities, and dimensional stability. The knowledge of inhomogeneous dimensional changes resulting in residual stresses can be used to explain several observable effects such as indicated in the following:

1. *Mechanical Properties.*- The response of a component to static loading (tensile and/or compression) can be altered by the induction of residual stresses. The external loading produces stresses that add to the pre-existing stresses. When the sum of these stresses exceeds the yield strength of the material, plastic flow will occur earlier than expected and failure will consequently take place earlier than expected.

2. *Fatigue.*- The introduction of residual stresses can result either in a reduction or an increase in the resistance to crack initiation and propagation. They significantly affect the crack initiation and alter the crack growth rate, either by keeping the crack closed by compressive residual stresses, or by opening the crack when the stresses are tensile.

3. *Stress Relief Annealing.*- The main objective of stress relief annealing is to elevate the temperature of the component in order to eliminate inherent residual stresses whilst not producing high levels of softening in the material. But some times the stress relief process does not accomplish this purpose. If a component

having high tensile residual stresses is put in a furnace and heated too quickly, the thermal stresses from the inhomogeneous expansion may be tensile and compound to cause the cracking of the component [*Treuting, 1952*].

4. *Dimensional Stability.*- Relief of residual stresses by thermal operations causes a redistribution that tends to disturb the static equilibrium, which then must be continuously re-established. Inequality of stress relaxation results in distortion, because the required maintenance of equilibrium is accomplished by dimensional changes to neutralize the forces, and bending to neutralize the moments. The simplest example of dimensional instability is the elastic after effect in which the relief of longitudinal stresses is accompanied by longitudinal contraction. Stress distribution can also be altered when a part of a material and its share of the stresses are removed along with it. This upsets the static equilibrium, through the generation of internal forces and moments to be balanced out by gross dimensional changes and by bending. One of the methods for determining residual stresses based on this observable effect is the crack compliance method, which is used in this work and is explained in Chapter 6.

2.3. Methods for the measurement of residual stress.

The knowledge of the magnitude and direction of residual stresses acting in a material is of great importance, but unfortunately residual stresses cannot be determined directly in the manner that stresses due to applied loads are calculated [*Ruud, 1982*]. Residual stresses are determined by measuring the corresponding strains that exist within the material. These strains are elastic in nature and are usually obtained by mechanical, X-ray

or Neutron Diffraction methods and the corresponding stresses are usually calculated from elastic theory formulations.

The determination of residual stresses is generally carried out using a number of methods. The classification of these methods can be separated into three groups; destructive, semi-destructive and non-destructive methods [*Wadsley, 1994*].

2.3.1. Destructive methods.

Usually these methods involve cutting or slicing parts of a component and measuring the resulting strain caused as the component changes shape. As a consequence, the specimen will be permanently damaged. These procedures only measure the average strain across the specimen and can be very reliable; examples are:

- *Crack compliance Method (CCM).*- The principle of the method is to introduce a thin slot of increasing depth into the piece and measure the deformation produced nearby by using strain gauges [*Cheng, Finnie and Vardar, 1991, Schindler, 2000 and Prime, Rangaswamy and Bourke, 2000*]. A more detailed explanation of this method is given in Chapter 6 of this thesis.

- *Sachs' method.* This method is used in cases where the residual stresses have rotational symmetry and are uniform in the axial direction (Figure 2.2). The routine involves the determination of the progressive variation on the surface strain as several circumferential layers are removed thus causing partial relaxation [*Sachs and Espey, 1941*].

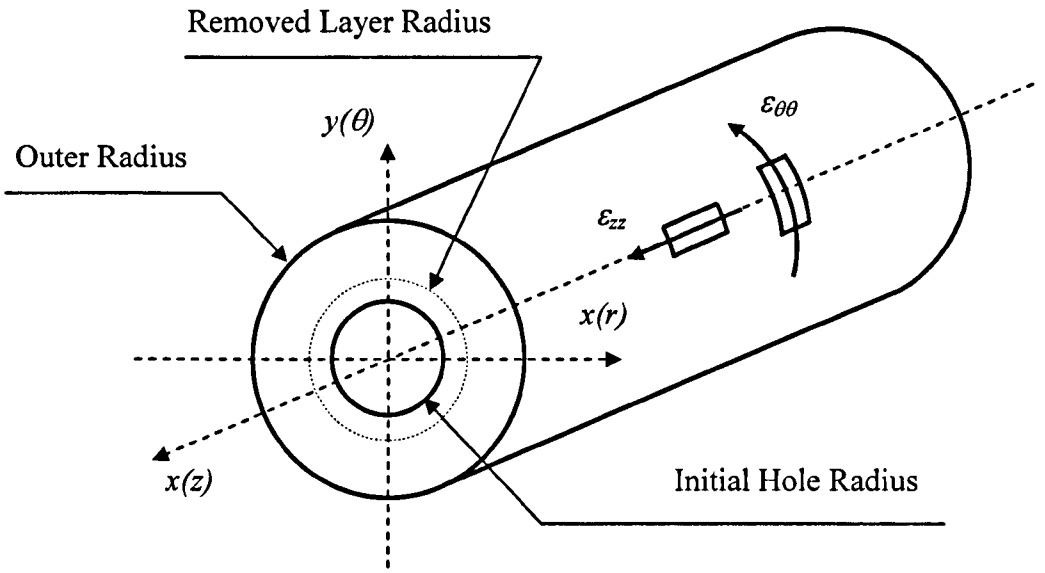

Figure 2.2.- Sach's boring method layout

The technique is applied to tubes and solid cylinders. When layers are removed successively from the inner part, axial and tangential strains are measured at the outside surface. If layers are removed from the exterior part, strains are measured on the inside. The relevant formulas for determining residual stresses are given in Equation 2.4.

$$\sigma_{rr}(r) = \frac{E}{1-v^2}\frac{(A(r_0)-A(r))}{2A(r)}\theta$$

$$\sigma_{\theta\theta}(r) = \frac{E}{1-v^2}\left[(A(r_0)-A(r))\frac{d\theta}{dA(r)} - \frac{(A(r_0)-A(r))}{2A(r)}\theta\right] \qquad 2.4$$

$$\sigma_{zz}(r) = \frac{E}{1-v^2}\left[(A(r_0)-A(r))\frac{d\Lambda}{dA(r)} - \Lambda\right]$$

where $\theta = \varepsilon_{\theta\theta} + v\varepsilon_{zz}$ *and* $\Lambda = \varepsilon_{zz} + v\varepsilon_{\theta\theta}$. With $\sigma_{rr,\theta\theta,zz}$ equal to the residual stresses in the radial, tangential and axial directions respectively; r is the radius from the specimen axis; r_o is the outside radius of the specimen; E is Young's modulus; v is Poisson's ratio; A is the enclosed area up to a given radial

distance; and $\varepsilon_{\theta\theta,zz}$ are the strains measured in the tangential and axial directions respectively. The equations are also applicable if layers are removed from the exterior part, however $A(r_o)$ is replaced by $A(r_i)$ where r_i is the inside radius of the specimen. The specimen must have an axial length of at least 4 to 6 r_o and since the above relations assume elastic behaviour, errors will arise if any plasticity occurs. The values of θ and Λ must be plotted against $A(r)$ and smooth curves fitted carefully through the data points, in order to reduce any local anomalies and obtain the required first derivative with enough accuracy. Three devices are required to be able to perform this type of measurements; strain gauges attached to the surface of the specimen to detect the deformation during the removal of the layers, a micrometer to measure the specimen diameters and a device to perform the removal of the layer. The removal of layers can be done by using different methods. One method is mechanical machining, but this tends to introduce more residual stresses and is considered to be unsuitable. Chemical etching is better because it does not cause additional stresses. However, it is a time consuming operation and can result in an uneven thickness. Electrical machining is considered to be the best option because it is stress free, suitable for high strength materials and produces a smooth finish. The method often offers a high degree of accuracy, but can only be applied in the laboratory (Figure 2.2) [*Sachs and Espey, 1941*].

2.3.2. Semi-destructive methods.

Semi-destructive methods are based on the fact that material removal results in a partial or full relaxation of the residual stress state and hence of the strain state, and are not restricted to crystalline solids. The elimination of material is performed without

significantly affecting the structural integrity of the piece. The elimination of material is usually performed by introducing a small perforation not too deep into the specimen. The disadvantages of semi-destructive methods are: lack of accuracy, low depth penetration and they can be expensive. However, they can in principle be applied to every piece in a production lot, not only during production but in service as well [*Beaney and Procter, 1974*]. Examples of these techniques are:

- *Centre hole drilling method.* The method relies on partial stress relief that is induced at the surface region of the specimen by drilling a small circular hole. In particular, the initial radial residual stress is reduced to zero at the edge of the hole and varies into the material of the specimen (Figure 2.3).

Figure 2.3.- Elastic radial stress relaxation due to drilled hole [*Beaney and Procter, 1974*]

The relief strain corresponding to the stress changes is as illustrated by the shaded region in Figure 2.3 and is detected by resistance strain gauges that are aligned radially. A biaxial stress field with unknown principal stress direction is generally assumed to be present. This state of stress can be determined by the measurement of the strain in three different directions, hence a three-element strain rosette is normally used, Figure 2.4.

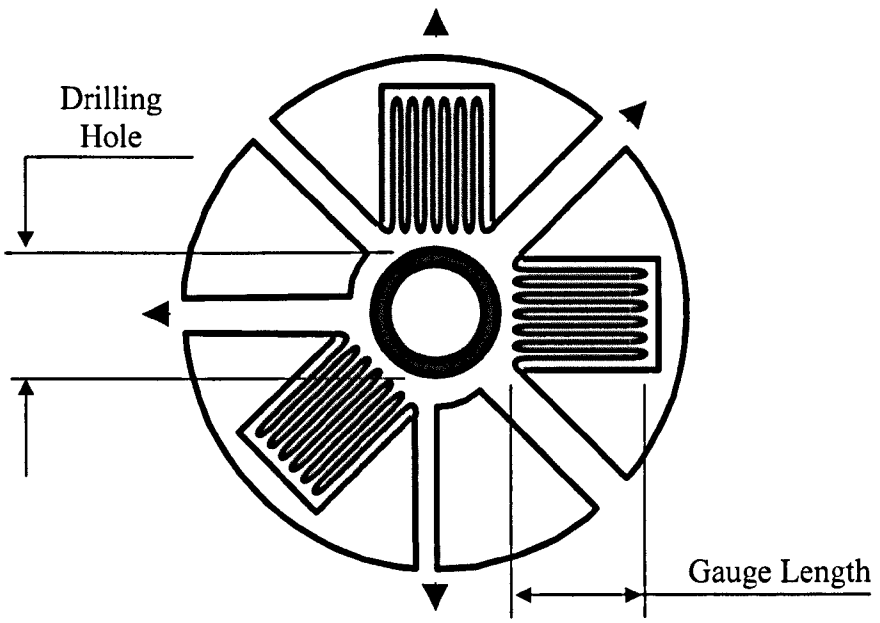

Figure 2.4.- 45^0 rectangular rosette diagram for residual stress measurement

Beaney et. al. [*1974*] presented a solution for the relationship between the measured relaxed strains, the residual stresses and the direction of the stresses as given in Equations 2.5 and 2.6:

$$\sigma_{Max,Min} = \frac{E}{2K_1}\left\{\frac{\varepsilon_1+\varepsilon_3}{1-\frac{\upsilon K_2}{K_1}} \pm \frac{1}{1+\frac{\upsilon K_2}{K_1}}\sqrt{(\varepsilon_1-\varepsilon_3)^2+[\varepsilon_1+\varepsilon_3-2\varepsilon_2]^2}\right\} \quad 2.5$$

$$\Phi = \frac{1}{2}tan^{-1}\left(\frac{\varepsilon_1+\varepsilon_3-2\varepsilon_2}{\varepsilon_3-\varepsilon_1}\right) \quad 2.6$$

σ_{Max}, σ_{Min} are the maximum and minimum principal stresses respectively; $\varepsilon_{1,2,3}$ are the values of the relaxed strains at 0, 45^0 and 90^0 respectively; Φ is the direction of σ_{Max} or σ_{Min} relative to ε_1. The constants K_1 and K_2 are given by Equations 2.7 and 2.8:

$$\frac{1}{K_1} = \frac{\varepsilon_A}{\varepsilon_{A'}} \quad 2.7$$

$$\frac{\upsilon K_2}{K_1} = \frac{\varepsilon_{T'}}{\varepsilon_{A'}} \quad 2.8$$

where ε_A is the strain acting in the axial direction; $\varepsilon_{A'}$ is the relaxed strain in the axial direction; and $\varepsilon_{T'}$ is the relaxed strain in the transverse direction. Advantages of the method are that: the equipment for the measurement of the strains is highly mobile, the method is not expensive and the entire process only takes a few hours. Disadvantages consist of the induction of additional residual stresses into the material if wrongly applied. The hole can act as a crack initiator in brittle material or with cyclic loading, and the measure of the strains can only be done to shallow depths [*Beaney, 1976 and Cardenas-Garcia, 2000*]. Figure 2.5 is an illustration of the equipment used to cut holes and to measure the hole dimensions.

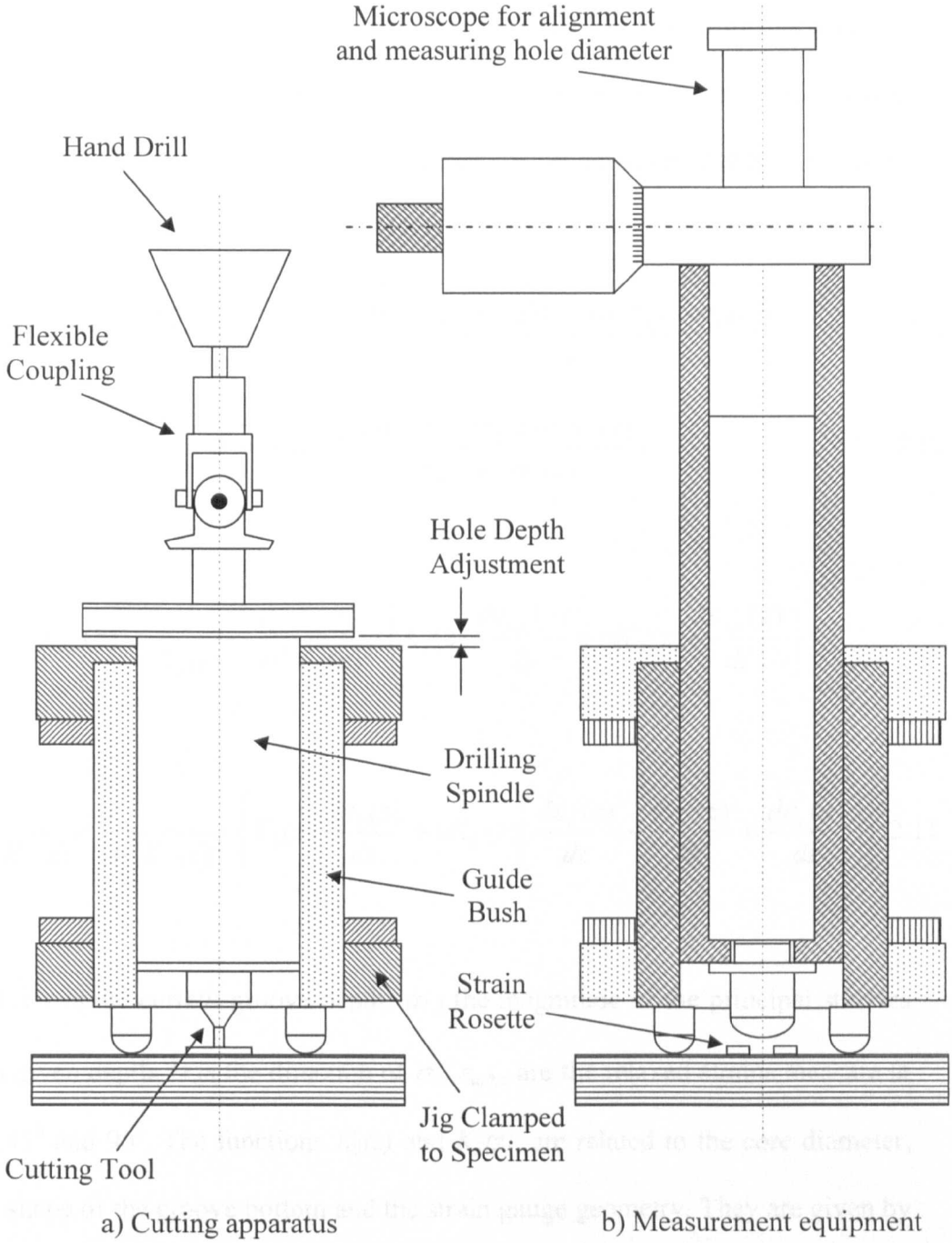

Figure 2.5.- Hole cutting apparatus and measurement equipment

- *Ring-Coring method.* This method is similar to the centre hole drilling, except that an annular groove is produced instead of a circular hole. A ring core rosette is fixed centrally over a measurement point and the relief strains determined with increasing depth of the annular groove. The trepanning groove releases the

stresses in the core and the strain variation recorded in three directions on the surface [*Wern, 1997*]. The original principal residual stresses can be obtained as a function of depth by the strain variations, using equations 2.9 to 2.11 [*Keil, 1992*]:

$$\sigma_{1,2}(z) = \frac{\sigma_a(z)+\sigma_c(z)}{2} \pm \sqrt{\frac{(\sigma_b(z)-\sigma_a(z))^2 - (\sigma_b(z)-\sigma_c(z))^2}{2}} \qquad 2.9$$

$$\alpha = \frac{1}{2}\tan^{-1}\left(\frac{2\sigma_b(z)-\sigma_a(z)-\sigma_c(z)}{\sigma_a(z)-\sigma_c(z)}\right) \qquad 2.10$$

where

$$\sigma_{a,c}(z) = \frac{E}{K_1(z)^2 - \upsilon^2 K_2(z)^2}\left\{K_1(z)\frac{d\varepsilon_{a,c}(z)}{dz} + \upsilon K_2(z)\frac{d\varepsilon_{c,a}(z)}{dz}\right\}$$

and

$$\sigma_b(z) = \frac{E}{K_1(z)^2 - \upsilon^2 K_2(z)^2}\left\{K_1(z)\frac{d\varepsilon_b(z)}{dz} + \upsilon K_2(z)\left[\frac{d\varepsilon_a(z)}{dz} - \frac{d\varepsilon_b(z)}{dz} + \frac{d\varepsilon_c(z)}{dz}\right]\right\} \qquad 2.11$$

where z is the current groove depth; $\sigma_{1,2}$ the magnitude of the principal stresses at a given depth; α is the direction of σ_1; $\varepsilon_{a,b,c}$ are the relaxed strains measure at 0^0, 45^0 and 90^0. The functions $K_1(z)$ and $K_2(z)$, are related to the core diameter, the shape of the groove bottom and the strain gauge geometry. They are given by equations 2.12:

$$K_1(z) = \frac{E}{\sigma_1}\frac{d\varepsilon_1(z)}{dz} \qquad \text{and} \qquad K_2(z) = \frac{E}{\upsilon\sigma_1}\frac{d\varepsilon_2(z)}{dz} \qquad 2.12$$

Some of the disadvantages of the technique are that it can turn into a destructive method and it can be extremely time consuming because the leads of the gauge have to be changed before completing each milling step and replaced afterwards. Electric discharge machining can be used to overcome these two problems, but

the method can only be carried out in the laboratory. In addition, the greater accuracy of the latter makes it the preferred option in the majority of cases, because it can be used to determine residual stresses to far greater depth than the hole drilling methods (Figure 2.6).

Figure 2.6.- Ring coring measurement [*Keil, 1992*]

- *Deep hole method.* This technique is also based on partial stress relaxation induced by drilling process. It is assumed that the complete stress field can be determined by assuming uniformity and linear stress-strain behaviour on stress relieving [*Leeman and Hayes, 1966*]. The method measures the distortion of a reference hole drilled through the component. A schematic diagram of the operations is shown in Figure 2.7. Prior to drilling the reference hole, small steel blocks are glued to the surface of the component. A reference hole is drilled through the component. Accurate measurement of the diameter of the hole is

made at a number of distances through the wall. Then a column of material containing the reference hole as its axis is trepanned free of the component. Any changes in the axial dimension of the column during trepanning are measured, provided that there is access for displacement transducers placed on the opposite side of the component wall. After trepanning, the reference hole is re-measured, and the changes in diameter and column height are used to determine the residual stresses. The main disadvantage of the deep hole method, over the last two methods described is its increased destructiveness, with each hole created by the trepanning process having a diameter up to 25 mm or more. The advantage of the method is that it gives reasonably accurate determination of residual stresses to depths of 100 mm and above (Figure 2.7) [*Smith, Bouchard and George, 2000*].

Figure 2.7.- Basic process of deep hole residual stress measurement

2.3.3. Non-destructive methods.

The non-destructive methods allow the determination of residual stresses acting in a component without removing material and without causing any form of damage to the specimen. Non-destructive techniques are based on the measurement of the variation of the material properties due to residual stresses and are usually applicable to crystalline materials. Electro-magnetic methods are based on magnetic field strength changes in a ferromagnetic material. The principal difficulty with the non-destructive methods is that they are all indirect and the quantities determined are influenced not only by the stresses but also by material parameters such as metallurgical structure. The most difficult problem with these methods is thus the interpretation of the results and the certainty of the values obtained. The most common, reliable and truly non-destructive methods are X-ray diffraction and Neutron diffraction methods [*Bonner, 1996*] and these are described in more details in what follows.

- *X-ray diffraction.* When a material is stressed, the resultant elastic strains cause the atomic planes in the metallic crystal structure to change their spacing. This follows because metals are composed of atoms arranged in a regular three-dimensional array to form a crystal. Most metallic components of practical use consist of many tiny grains randomly oriented with respect to their crystalline arrangement and are fused together to make a bulk solid [*Middleton, 1987*]. When such a polycrystalline material is subjected to stress, elastic strains are produced in the crystal lattice of the individual crystallite. The X–ray method has the capability to measure the inter-atomic spacing (d-spacing), which is indicative of the elastic strain in the specimen. Changes in the inter-atomic spacing can, therefore, be related to the elastic strain in the material and hence,

to the stress. The X-ray beam is directed onto the sample surface at the location of interest. A position-sensitive proportional counter detects the diffracted beam. The angular position (2ϕ) of the diffracted beam is used to calculate the d-spacing between parallel planes of atoms using Bragg's law. A series of measurements made at different X-ray beam approach angles (ψ) are used to fully characterise the d-spacing [*Cohen, 1992* and *Prevéy, 1986*]. Calculation of stresses by this method is very localised and can be point values associated with the sample surface region only. X-Rays may have a penetration of about 0.1 mm in steel. This is inconvenient when a thick component with residual stresses needs to be analysed. The method, is in general capable of good precision and resolution, and is ideally suited to regions of high stress gradient [*Prevéy, 1986*]. The disadvantages are that the method is expensive, time consuming and surface finish has to be very good. Mechanical surface cleaning methods induce compressive surface stresses therefore electro-etching is one of the methods recommended to clean the surface [*Prevéy, 1986*].

- *Neutron diffraction.* This method, like the X-ray method, determines the component of strains directly from the measurements of changes in lattice spacing of crystals. Contrary to the X-ray method, the readings are not limited to near surface measurements. The penetration of neutrons can be several centimetres into most metals, since the neutrons are energetic and uncharged, allowing stress determination inside the material. Neutron diffraction method is also based on Bragg's law, as the X-ray method. The method uses two different approaches. The first involves the use of a monochromatic neutron beam, with the analysis similar to the X-ray method. The second uses a polychromatic beam

and requires fixed angle measurements of the differences in neutron beam flight time when testing stressed and unstressed samples [*Lambrineas, et. al. 1987*]. The main advantages of this technique are that its measurements are based on neutron counts (that is volume sample and counting time). There is an inherent statistical error, which can be reduced by increasing the counting time and/or increasing the volume sampled. The disadvantages are that the method is very time consuming and also very expensive. Sensitivity and resolution are dependent on angular dispersion, and crystalline anisotropy affects the measurements (less than in the case of X-ray diffraction method) Figure 2.8 [*Lambrineas, et. al. 1987*].

Figure 2.8.- Schematic of twin axis neutron diffractometer employing steady state source

- *Acoustic methods.* The method is based on the measurement of the speed of propagating ultrasonic waves. The speed variation is caused by the anisotropy condition arising from the inducted residual stress state in the material. Some

examples of these techniques are; *ultrasonic birefringe, ultrasonic attenuation, ultrasonic surface waves, ultrasonic goniometry and ultrasonic beam interaction* [*Stänhlkopf and Egan, 1979*]. The principal advantages of these methods are that they are extremely fast to apply, inexpensive and very accurate for the determination of bulk stresses at up to 10 mm depth and for stresses at the surface. One disadvantage is that small surfaces cannot be analysed (less that 30 mm^2) because they can lead to inaccuracies in regions of high stress gradients. Also stresses tend to change the velocity of ultrasounds by an amount (between 0.1 to 1.0 %) that is similar to the changes that can be produced by metallurgical inhomogeneities. Information about the stress free state is required for the calculation of the residual stress state, which in some cases is very difficult to obtain [*Stänhlkopf and Egan, 1979*].

- *Magnetic and/or Electrical methods.* Contrary to the X-ray and ultrasonic methods the magnetic technique is restricted to ferromagnetic materials. A comparative calibrated material state is needed. The calibrated piece is used to derive the relationship between the magnetic and magneto-elastic measured quantities. The basic principle of the method relies on the fact that all ferromagnetic materials exhibit a domain type structure, where regions with differing magnetisation directions are separated by interfaces (Bloch walls). On magnetisation, the material changes its shape in order to minimise the increase in internal energy density. The magneto-elastic reaction occurs at a microscopic level as magnetostrictive quarter turns on the interfaces (Bloch walls). Some examples of using the measurement of magnetic field strength to determine the stress state are: *(1) Magnetic Barkhausen Noise;* This method reads the electrical

impulse induced in a magnetic-inductive sensor located close to the specimen. The penetration is less than 1mm and the minimal sampling area is around 0.1 mm^2 [*Gauthier, Krause and Atherton, 1998 and Pacyna and Kokosza, 1999*]. *(2) Acoustic Barkhausen Noise;* Unlike the last method, this method attenuates approximately as an inverse square of distance, so that the depth is limited by the magnetisation field frequency only. Alternating and changing magnetic fields are superimposed and the intensity/sign of the exited signals are examined. The penetration is in the range of 5 to 10 mm and the area cannot be smaller than 100 mm^2 [*Vanderveld, Carpenter and Dahmen, 2000*]. *(3) Incremental Permeability;* Is a magnetisation process and is used in the same manner as the acoustic Barkhausen noise method. The penetration is about 5 mm and the smallest area that can be tested is 1 mm^2 [*Grimberg, et. al. 1996*]. *(4) Dynamic Magnetostriction;* This method is based on the magnetic anisotropy of a ferromagnetic material induced by the stress state. Penetration is very poor at about 0.1 mm and the smallest area for determination is about 100 mm^2 [*Sarnatski, et. al. 2001*]. Electro-magnetic methods are used to determine several different physical properties that are related to the residual stress field acting in the material. There are problems with these methods due to the fact that structural states of materials affect physical properties. The effect arising from the variations in the structural and the stress states must therefore be separated. In addition the specimens must be ferromagnetic and magnetostrictive materials, so that stress calculations can be quantitatively carried out. Calibration must be carried out for each material. The method is expensive because of the cost all of the equipment involved. Advantages include the short time required in the

process of determining the residual stress state and the reliability of the technique (Figure 2.9) [*Kashiwaya, Sakamoto and Inoue, 1989*].

Figure 2.9.- Schematic representation for electro-magnetism measurements

- *Coating methods.* These techniques are confined to surface measurement and are unsuitable to environments under high temperatures. The two principal methods based on this principle are photo-elastic coating and brittle lacquers. Hole drilling and trepanning are conducted at the same time to relax the strain previously induced into the material. This enables the determination of the elastic residual stress in the regions of interest.

A review of some of the most important methods to determine residual stresses has been presented. It would be almost impossible to cite all the methods available to determine residual stresses because of the enormous number of techniques in use and the continuous development of new ones.

2.4. Selection of appropriate techniques for the evaluation of residual stresses.

Kandil, et. al. [*2001*] produced a number of tables that can be used to aid selection of appropriate methods for the determination of residual stresses in different materials. Tables 2.1 to 2.4 are included in the thesis for completeness.

Table 2.1. Practical issues.- Deals with matters such as cost, availability of equipment, portability, measurement speed, existence of standard procedures and level of expertise required.

Table 2.2. Material issues.- Covers factors such as the class of materials that can be examined using different techniques, property information required, surface preparation, etc.

Table 2.3. Measurement.- Include information on the physical characteristics of each technique including the resolution, penetration, stress-averaging area or volume, stress state, stress gradient and uncertainty.

Table 2.4. Summary.- Gives the advantages and disadvantages of various techniques.

Table 2.1.- Practical issues [*Kandil, et. al. 2001*]

1 Depending on the type of the instrument used, size and geometry of sample.
2 Thick coating only.
3 can be destructive if used for depth profiling.

Table 2.2.- Material issues [*Kandil, et. al. 2001*]

Table 2.3.- Physical characteristics [*Kandil, et. al. 2001*]

Table 2.4.- Summary [*Kandil, et. al. 2001*]

2.5. Summary.

In this chapter it has been shown that residual stresses are generated in a component as a result of mismatch changes in the microstructure and dimensions. The material suffering from the mismatch adjusts in order to maintain equilibrium in the specimen. The adjustment produces strain and instigates residual stresses. Also reviewed in this chapter are the classification and effects of residual stresses.

Typical methods used for the determination of residual stresses in materials have been summarised. To determine residual stresses the associated elastic strain has to be detected and measured. Some methods therefore embody a reversal of the process by which the strains were produced. In order to obtain the residual stress field of the whole body, material from the body is removed and the resulting dimensional changes are determined and analysed.

Due to the enormous number of techniques implemented for determining residual stresses and the continuos development of new ones, only the main current techniques have been highlighted. Additionally, a series of tables have been included in this chapter to facilitate the selection and use of a method to determine residual stresses. The tables presented in this thesis deal with matters such as; Practical issues; Material issues; Physical characteristics of each technique and the advantages and disadvantages.

Chapter 3

Review of Literature

3.1. Introduction.

The review of literature presented in this chapter covers the two main areas that form the basis of the work in this thesis. The two areas are the Bauschinger effect and the crack compliance method for the determination of residual stresses.

3.2. Bauschinger effect.

In order to carry out a proper mechanical analysis of a material it is necessary to account for the strain history in the material [*Dowling, 1993*]. It is known that the pre-straining of metals induces them to behave anisotropically. This means that many of the properties become a function of the direction of further plastic deformation. If the direction of straining of a material is reversed after yielding has occurred, the stress-strain curve that is followed differs from the initial monotonic behaviour, as illustrated in Figure 3.1.

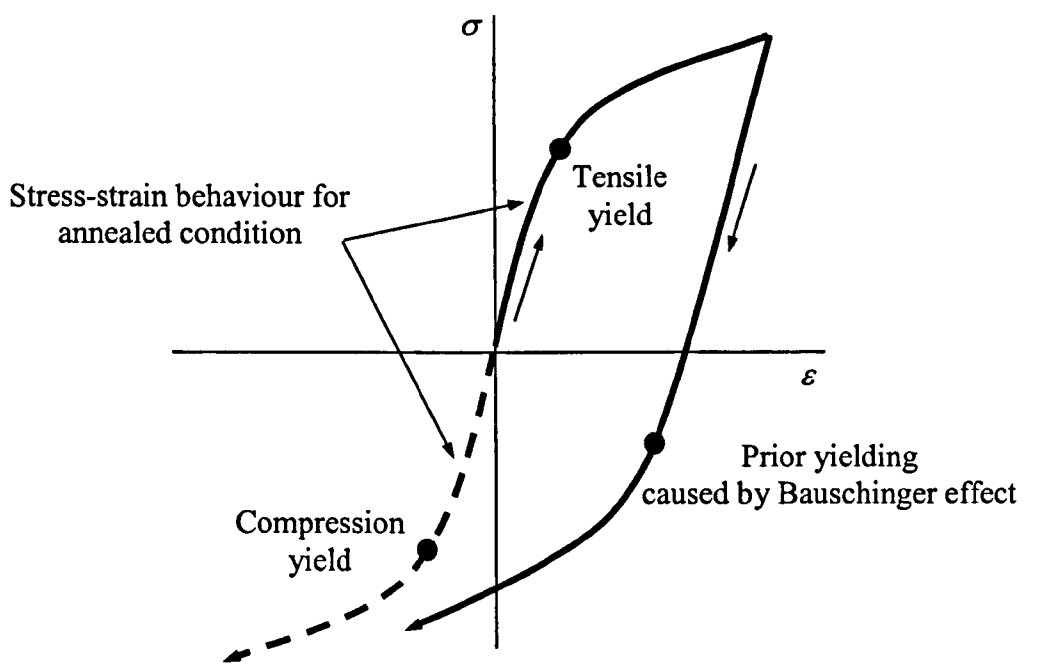

Figure 3.1.- Monotonic stress-strain curve showing hardening and Bauschinger effect

This early yielding behaviour is called Bauschinger effect, after *Jonathan Bauschinger* who first studied the phenomenon. *Bauschinger* work's on mild steel [*1881 and 1886*], found that by loading a bar in tension past its plastic range and unloading and reloading the bar in the same direction increased the elastic limit. But if the reloading of the bar occurred in the opposite direction to that of the first applied load, there will be a reduction in the elastic limit and in some cases the elastic behaviour can vanish.

3.2.1. Previous works on Bauschinger effect.

Bauschinger [*1881*] started to study the directional strengthening of metals in *1881*. He presented the work and experimental conclusions in *1886* in Germany. Because of the importance of the work, it was translated and published in English several years later [*Bauschinger, 1881 and 1886*]. The experimental work was carried out on wrought iron and Bessemer steel, and the results can be summarized briefly as follows:

- Plastic pre-strain increases the elastic limit of deformation in the same direction as the pre-strain. This rise in the elastic limit is kept in the material as a new mechanical property when the load is removed.

- Plastic pre-strain decreases the elastic limit of deformation in the reverse direction to the pre-strain. If the magnitude of the pre-strain is increased, the elastic limit in the reverse direction can be reduced to zero.

- Strain hardening is possible when loading along the direction suffering from Bauschinger effect. The yield strength produced by repeatedly strain hardening

along this direction will however never be as high as that of the annealed material.

- The phenomenon is not time dependent.

The main limitations of *Bauschinger's* results at the time were the lack of sensitivity in equipment used to measure the strains accurately. It took several years before work related to Bauschinger effect was again carried out. *Bairstow* [*1911*] conducted a series of fatigue tests to establish two theorems relating to Bauschinger effect. He firstly postulated that the elastic limit in the starting loading direction can only be raised by a corresponding drop in the elastic limit in the inverse loading direction. And secondly, that there is an existing limit that the yield stress can be raised.

3.2.1.1. Observation of Bauschinger effect.

By *1920, Moore and Beckinsale* [*1920*] found that it was possible to eliminate Bauschinger effect from brass components by a suitable annealing heat treatment process. *Bader and Lode* [*1930*] studied the problem of the curved transitions from the elastic to the plastic part of stress-strain curves. *Nadai* [*1931*] studied Bauschinger effect in mild steel by the application of load induced by twisting a component into the plastic region and re-twisting in the opposite direction. Similar results were obtained to the ones produced in uniaxial loading.

Similar to Nadai's work, *Canal* [*1956*] started experimenting on hollow tubes specimens in torsion improving the sensitivity of the resulting stress and strain measurements in *1956*. The materials tested were copper, aluminium, brass, nickel, and magnesium. He

concluded firstly that during reversal of deformation, not only is the initial yield stress lower than the original deformation, but the entire stress-strain curve shifts in the negative stress or positive strain direction and that the stress-strain relation changes its characteristic parabolic form. Secondly, that by heating the specimens above re-crystallization temperature, all traces of Bauschinger effect disappear.

Work continued on the observation of the Bauschinger effect for the next two decades, showing that the reduction in the yield stress on reversal of loading of pre-strained material was only one of the manifestations of the Bauschinger effect. Other manifestations include; the well-rounded appearance of the initial plastic portion of the reverse stress-strain curve, the increase in the reverse work hardening rate and permanent softening. Similar results were obtained by *Wilson* [*1965*], *Ashby* [*1966*], *Gould, Hirsch and Humphreys* [*1974*], *Atkinson, Brown and Stobbs* [*1974*] *and Lloyd* [*1977*].

By *1989, Takeda and Nasu* [*1989*] performed several bending tests to determine the tensile and compressive strength of anisotropic steel plates. Bauschinger effect and the planar anisotropy of the material were examined using bending specimens cut at various angles to the pre-straining direction. This lead to the proposal of an anisotropic yield function.

Fairly recently *Thakur, Nemat-Nasser and Vecchio* [*1996*] published their observations on dynamic Bauschinger effect. Their experimental procedure was carried out on a tension split Hopkinson bar under dynamic loading. They tested two types of materials HAYNES 230 alloy and AL-2024 alloy. Tensile specimens were subjected to a single tension pulse of known magnitude and then unloaded. The uniformly deformed gauge

sections of the tension samples were then sectioned and reloaded in compression using the same strain rate as in the initial tensile loading. The Al-2024 alloy did not exhibit Bauschinger effect at any strain rates. The Hayes 230 alloy exhibited Bauschinger effect only under high strain rate conditions [*Thakur, Nemat-Nasser and Vecchio, 1996*].

At the end of century, *Zhang et. al.* [*2000*] published their results on the effect of pre-tensile straining on the compressive yield strength in Ti-6Al-2Cr-2Mo-2Sn-Zr (Ti-6-22-22). Tensile and compression tests were performed to measure the retention of compressive yield stress after stress relieving. The retention of the compressive yield strength indicates an effective stress relieving process. Reduction of the compressive yield stress is dependent on the magnitude of pre-tensile strain. X-ray analysis showed that all pre-strained samples exhibited very low compressive residual stresses.

3.2.1.2. Explanation of Bauschinger effect.

Heyn [*1918*] presented the first accepted explanation of the Bauschinger effect in *1918.* He assumed firstly that the material consists of small volume elements, which have ideal stress-strain curves and that the elastic limits of various volume elements are not equal to each other. This assumption can explain the initial curvature of the stress-strain curve at the elastic-plastic transition. Secondly, during deformation, strain is homogeneously uniform across the material and it is assumed that the absolute value of the elastic limit of any volume element is independent of the direction of deformation, i.e. it is the same in tension and compression. Therefore during plastic deformation the stress distribution is not uniform in such a material after unloading. Residual stresses arise due to the non-uniform yielding of the volume elements and are responsible for Bauschinger effect.

The following simplified plot can be used to visualize the physical behaviour of this model (Figure 3.2). Consider a specimen made of volume elements *A* and *B* that have the same elastic constants. Assume that volume element *B* has a higher elastic limit than volume element *A*. Assume further that both elements deform plastically without hardening, i.e. elastic-perfectly plastic.

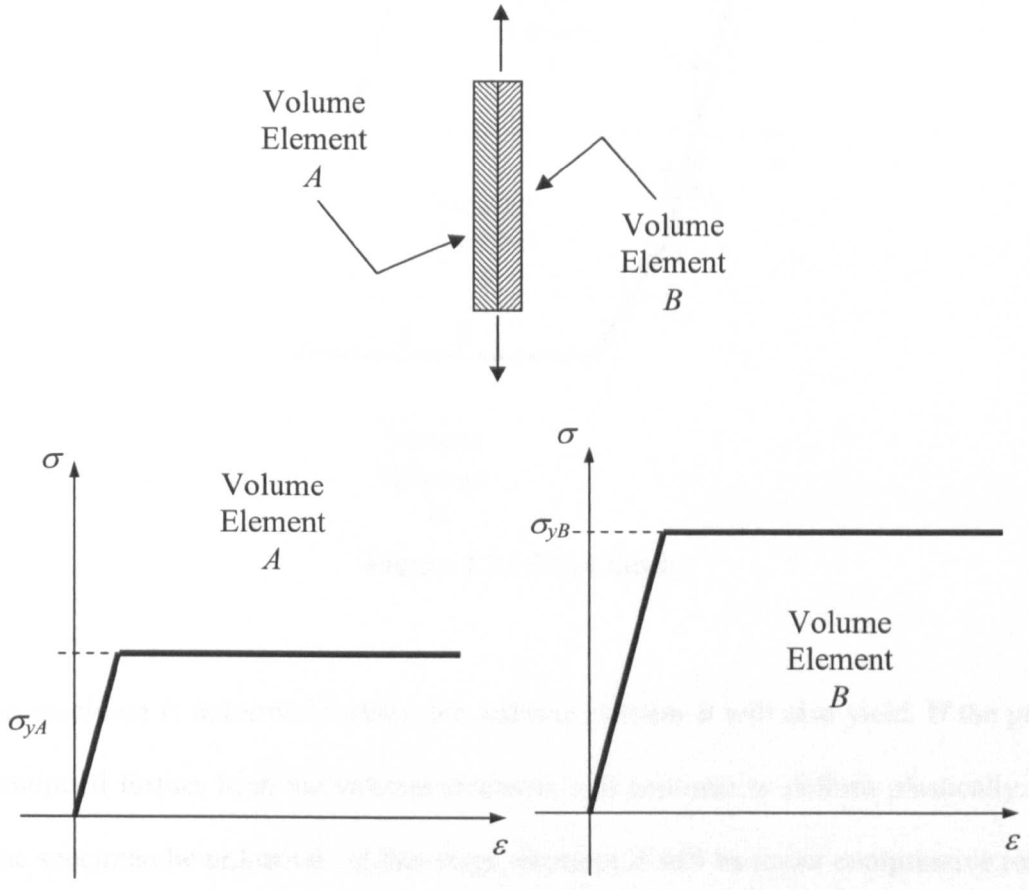

Figure 3.2.- *Heyn* schematic simplification theory

If the specimen is tested in tension and compression in a rigid testing machine the stress-strain curve is an average of both volume elements as shown in Figure 3.3. If the specimen is uniaxially loaded in tension, both of the volume elements will initially deform elastically. Immediately after the volume element *A* yields a change in the gradient of the combined curve appears. From this instant the deformation in the

specimen will be non-homogeneous and residual stresses will be created if the load is removed.

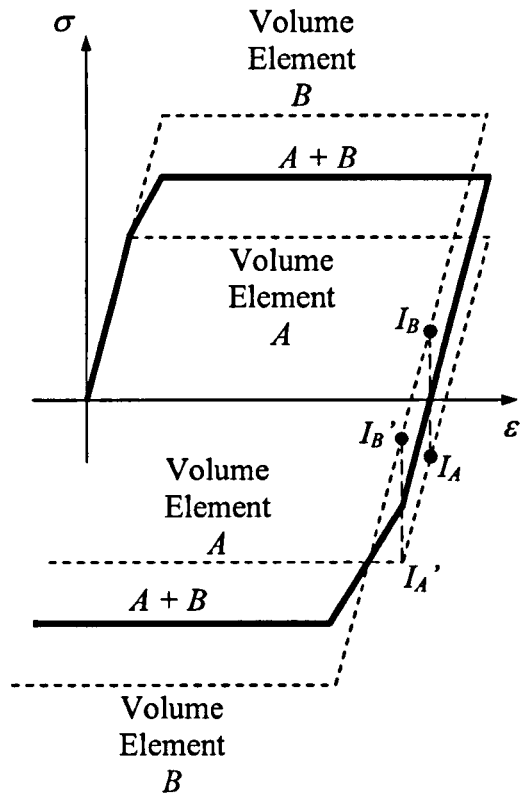

Figure 3.3.- *Heyn* theory

If the specimen is deformed further, the volume element *B* will also yield. If the process is continued further both the volume elements will continue to deform plastically. Then let the specimen be unloaded. At this stage, element *A* will be under compressive residual stress as highlighted by location I_A and element *B* will be in tensile residual stress as shown by position I_B (Figure 3.3). Then let the specimen be loaded in compression to the same magnitude as it was originally loaded in tension. Element *A* will experience early yielding at I_A' and consequently promoting early yielding of the combined volume. This simple model demonstrates that the average yield stress for reverse deformation is lower than it is for the original deformation. The residual stresses at I_A and I_B (Figure 3.3) are commonly known as *Heyn* stresses.

Masing [*1925*] supported this theory by conducting a series of experiments on brass (tension and compression tests) and on iron, copper and aluminium (torsion tests). These experiments did show a fair agreement with the calculated reverse stress-strain curve. *Masing's* experiments were done at very small pre-strain values. Deformation was reversed after 0.5% to 1% strain and under such circumstances the theory does give a rough quantitative agreement. Nevertheless, at higher pre-strain values the experimentally observed Bauschinger effect is quite different from the effect predicted by *Heyn's* theory.

Sachs and Shoji [*1927*] investigated the Bauschinger effect in brass single crystals by using tensile and compressive tests. The observations from the work disproved the belief that Bauschinger effect was induced by strain discontinuities at grain boundaries, which were due to the varying orientations of neighbouring grains, as suggested by *Heyn* [*1918*].

Woolley [*1953*] completed a study of Bauschinger effect using many kinds of F.C.C. and B.C.C. metals. He observed that the strain associated with the Bauschinger effect is approximately proportional to the stress applied to produce work hardening divided by the Young's modulus, and is almost independent of the grain size. He presented an explanation of the Bauschinger effect in terms of the rearrangement of dislocations present in the work hardened lattice. Latter in *1958* he disproved *Masing's* theory [*Wooley, 1958*] and also his own previous theory for explaining Bauschinger effect [*Wooley, 1953*].

Historically the theoretical models used to describe Bauschinger effect have been of two main types *Macroscopic or Microscopic.* The macroscopic approach was based on continuum theories of plasticity, the most commonly used models of work hardening are the isotropic and kinematic models. Isotropic work hardening theories are based on the uniform expansion of an initial yield surface and as such are unsuitable for solely describing the Bauschinger effect. The kinematic hardening laws, on the other hand, are founded on the translation of the original yield surface in stress space and accordingly are more suited to an explanation of the directional dependence of the stress strain relationship. *Mroz [1967]* proposed a combined kinematic and isotropic macroscopic model, which is generally believed to give a full description of Bauschinger effect. The nearest to giving a full microscopic theory of Bauschinger effect is proposed by *Orowan [1959]*. He suggested that the initial rounded portion of the reverse flow curve was permeable obstacles to dislocation movement and that the downward displacement of the same curve was due to back stress which would relax after reverse straining.

3.2.1.3. Bauschinger effect on residual stresses.

It was clear from this literature review that there was limited work on determining the influence of Bauschinger effect on the formation of residual stress fields. One of the aims of this research is to investigate how this effect relates to the distribution of residual stress fields. This information can be useful in selecting materials and processing autofretagging. Although this work does not seek to explain the causes of Bauschinger effect, it will investigate the change it causes to mechanical properties of different materials and simplify the process of obtaining these properties (Chapter 4 and 5).

Sidebottom and Chang [1963] highlighted the influence of Bauschinger effect in reducing the magnitude of residual stresses in an in-elastically deformed beam as well as lowering the load-carrying capacity of such beams when the direction of the load is reversed. The results showed that both the residual stresses and the load carrying capacity of the beam were appreciably lower than the theoretical values, which were derived on the assumption of no Bauschinger effect.

Al-Hassani [1981] studied the Bauschinger effect on residual stress fields induced by shot peening. As expected the results showed a significant difference between the stresses calculated by theoretical formulation and those obtained by experimental procedure.

Chen [1986] similarly carried out an investigation of Bauschinger and hardening effects on residual stresses in autofrettaged thick-walled cylinders. The research was carried out on commercial steel EN 1a and EN 24. Once again the induced residual stress state expected by theoretical formulation was different from the states found by experimental tests. However a model based on kinematic hardening showed some numerical accuracy compared with tests results.

It is clear that more work is necessary to comprehend the effects and consequences of Bauschinger effect. The use of kinematic hardening rules to assist in the process of determining residual stresses [*Chen, 1988*] is approximate due to the inadequacies of the rules. The use of methods such as the compliance method, which does not require hardening rules, provides a good means to study the interaction of Bauschinger effect on residual stress fields. This work aims to use the crack compliance method (CCM) to

study consequences of Bauschinger effect on residual stress fields. The review of CCM is carried out in the next section.

3.3. Crack compliance method.

The crack compliance method (CCM) is based on the cutting of a thin slot of increasing depth into a specimen and measuring the distortion produced nearby using strain gauges (Figure 3.4).

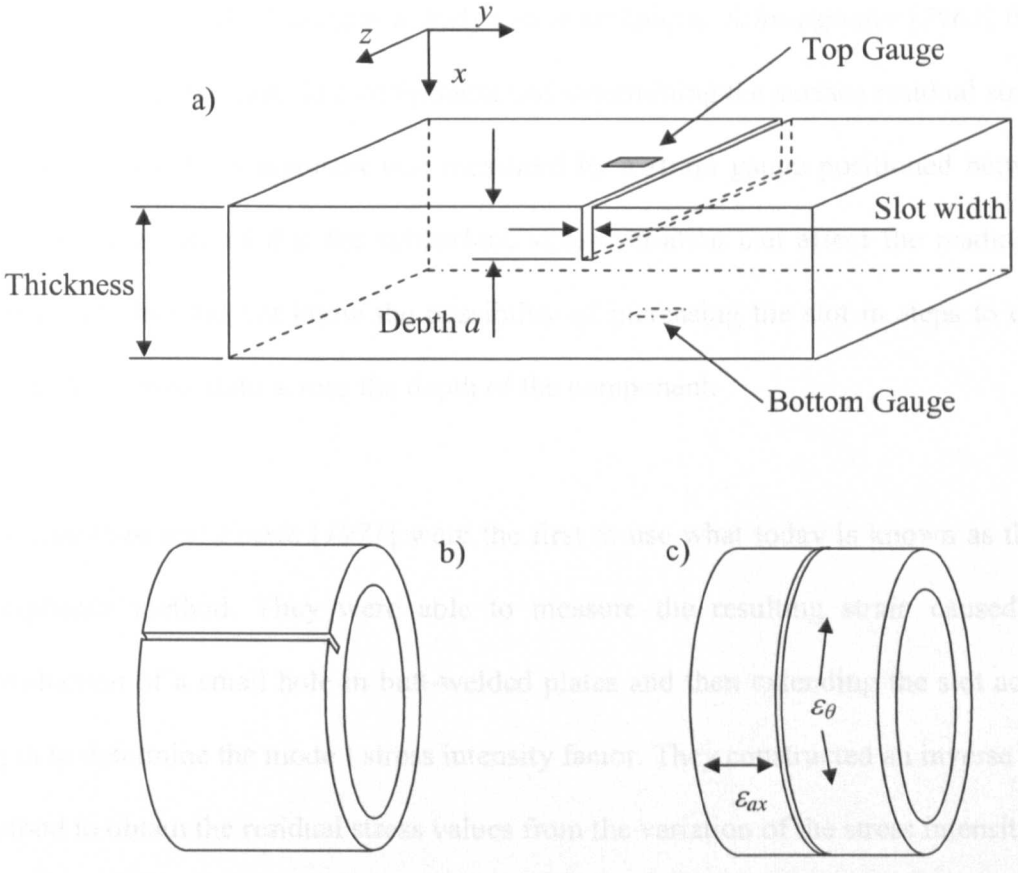

Figure 3.4.- Schematic representation of the CCM in different geometries
a) cut in plates and beams b) axial cut in tubes c) circumferential cut in tube

It is assumed that the stresses do not vary along the length of the slot and that linear-elastic stress relaxation occurs during the cutting process. In this way, usually the direct

residual stresses normal to the slot and in some cases the shear residual stresses parallel to the specimen surface can be determined throughout the depth.

3.3.1. Review of previous work using the crack compliance method.

The work reviewed in this section is related to the calculation of residual stress by introducing an incremental slot or cut into a component containing residual stresses. In reality this technique does not measure stress but strain or deformation, and the corresponding residual stresses are then subsequently calculated. The introduction of a slot to measure residual stress is a fairly recent technique. *Schwaighofer* [*1964*] first used it by machining two slots in a component and determining the surface residual stress. The deformation of the component was measured by a strain gauge positioned between the two slots. He noticed that the subsurface stress variation can affect the reading of the deformation but did not know the possibility of increasing the slot in steps to calculate the residual stress state across the depth of the component.

Vaidyanathan and Finnie [*1971*] were the first to use what today is known as the crack compliance method. They were able to measure the resulting strain caused by the introduction of a small hole in butt-welded plates and then extending the slot across the depth to determine the mode I stress intensity factor. They constructed an inverse solution method to obtain the residual stress values from the variation of the stress intensity factor. The method was successful, but there was little with which to compare the results.

There are two components to the analytical calculation in the CCM, the forward and inverse solutions. The forward solution determines what strains to measure for a given stress distribution. The inverse solution uses results from the forward solution to

determine a stress distribution that "best" matches the experimentally measured strains. These two steps are necessary because a direct calculation of residual stresses from measured deformation is not possible. The literature review presented in this section considers the forward solution and inverse solution aspects as well as other general solution methods.

3.3.1.1. Forward solution.

The main aim of the forward solution is to obtain the compliance function. The compliance function, C, is the relaxed strain obtained as a function of crack depth in a residual stress field.

Cheng and Finnie [*1985*] obtained compliance functions by using the stress intensity factor K_I solution for an arbitrary loading case of a crack on a surface. In *1987*, they revisited this solution and gave compliances in tabular form [*Cheng and Finnie, 1987*]. *Cheng and Finnie* [*1986*] also calculated compliances in a thin-walled cylinder for the case of axisymmetric hoop residual stresses. They considered an axial crack, starting at the outer surface. Hoop strain on the outer surface was calculated with a stress intensity factor K_I solution for arbitrary loading on the crack faces. The solution was valid for strain gauges located at least a wall thickness away from the cut. *Cheng and Finnie* [*1990*] added corrections to the previous solution for the case of thick-walled cylinders.

Ritchie and Leggatt used the finite element method to calculate compliances for a slot sawed through the thickness of a strip in *1987*. The geometry modelled was a 2-D slot including the actual slot width and considering all to be plane stress. *Wu and Carlsson* [*1991*] published a compendium of fracture mechanics weight function solutions for the

most common geometries used in the engineering field. This has greatly facilitated the calculation of the needed compliance function.

Schindler [*1994, 1995 and 1997*] calculated compliance functions for a solid disk with an axial crack. He calculated surface hoop strains with a weight function solution and gave procedures that ensured accuracy for near-surface or very deep cracks where weight functions may not be correct. *Fett and Thun* [*1996*] also calculated compliances for a solid disk with an axial crack using weight function and additionally included a solution for a central internal crack. These researchers gave the basis for the determination of the relevant functions for a beam or strip used in this thesis. The solutions found were as accurate as the fracture mechanics solutions available.

A totally different approach based on the dislocation density method was used by *Nowell, Tochilin and Hills* [*2000*] to obtain the compliance functions for a through-thickness crack.

Fracture mechanics with numerical methods are now commonly used to determine the compliance function. In recent years, the use of the finite element method for the calculation of the compliance function and other related functions has saved much effort in the application of the CCM.

The main contribution in this thesis towards the forward solution approach is the development of an evaluation method for weight functions used in the method. This removes the need to rely on tabulated values for the evaluation of the crack compliance functions.

3.3.1.2. Inverse solution.

The forward solution gives the deformation that would be measured for a given arbitrary stress distribution. The inverse solution is used to obtain the stress distribution that best matches the actual strain measurements when slots of increasing depths are introduced into a component of interest that has an inherent residual stress field.

A step by step inversion method has been used by many researchers to determine residual stress distribution in components. The equivalent stress is determined for each step or increment based on the strain reading at that stage and the stresses from previous increments [*Ritchie and Leggatt, 1987*]. This can carry forward errors arising from previous increments. *Ritchie and Leggatt* [*1987*] used a least squares fit to minimize errors in the incremental approach. Strains were measured at a distinct location for each increment of the slot depth. The objective is to combine all increments into a single fit to reduce the propagation error produced by the incrementing slot. The method requires multiple deformation measurements at each depth.

Beghini and Bertini [*1990*] measured residual stress fields in steel plates with various weld geometries. They developed an approach with one more unknown than the number of depth increments. They considered a residual stress distribution that varied linearly within each of the m increments. Considering continuity, this was characterised by a single stress value at $m + 1$ nodes. Readings from strain gauges at multiple locations allowed a least square fit to find the $m + 1$ nodal stresses that best reproduced the measurements.

In *1992, Gremaud et. al.*, determined stresses near the surface through the thickness of a layer and into its substrate by using the crack compliance method. The inverse solution method used was a series expansion of the stress using separate series in the layer and substrate. The result gave strong evidence of the crack compliance method's ability to resolve stress variation with depth.

Gremaud et al. [*1994*] proposed a spline-based Overlapping Piecewise Functions method for stress fields that cannot be accurately fitted with continuous polynomials. They divided the region of stress variation into a set of overlapping intervals and the stresses in the intervals were expressed as a linearly or quadratically varying series expansion by using a least squares fit. The fit of the intervals was done sub-sequentially, with the effect of each previous interval considered. It was also demonstrated that the series expansion inverse is quite tolerant of zero-shift and random errors in the strain measurements.

There are two major limitations on inverse solutions that apply to all inverse methods: Firstly, the spatial resolution is inherently limited by the distance between the location for the strain measurement and the location of the desired interior stresses. A solution to this problem can be attempted by using small increment (much less than 1 mm). This will not however be totally sufficient because the strain changes resulting from each cut must be measurable and significant. Secondly, the stability and uniqueness of the inverse must be considered. When relaxed strains are measured at the top surface of a part, the inverse solution will become unstable at some depth. This is a consequence of lack of sensitivity on the surface gauge as the slot grows. The depth at which the inversion is unstable is not well defined for crack compliance measurements. No direct contribution was made in this thesis towards further development of the inverse solution method.

3.3.1.3. Other solutions.

Two new methods used to determine residual stresses are highlighted in this section. Both methods work by employing the same experimental procedure to produce the incremental slot as in the crack compliance method. But in these two procedures there is no need to measure the resulting strains caused by the cutting of the material or calculate any weight or influence functions. The methods are referred to as the contour method and the radius of curvature method.

Prime [*2001*] pioneered a contour method for residual stress determination using one of the resulting surfaces obtained from cutting a part in two. The contour of the resulting new surface is measured thus determining the displacements caused by releasing the residual stresses acting in the part. Analytically, for example using finite element method, the opposite of the measured contour is applied to the surface as a displacement boundary condition to obtain the stresses. The method is based on a variation of *Bueckner's* superposition principle. Figure 3.5 presents an illustration in 2-D for simplicity, although the principle applies equally in 3-D.

The undisturbed residual stresses are represented in Figure 3.5a. The cut deforms the part, because of the release of the residual stresses caused by the separation procedure (Figure 3.5b. In Figure 3.5c, the free surface created by the cut is forced back to its original shape. So, it can be concluded that superimposing the state in b) with the change in stress from c) gives the original residual stresses throughout the part. This superposition principle assumes that the material behaves elastically during the relaxation of residual stress and the process of cutting does not introduce stresses of sufficient magnitude to affect the measured displacement. The superposition principle described uniquely

determines the original σ_x and τ_{xy} (and τ_{xz} in the 3-D case) residual stress distribution on the plane cut.

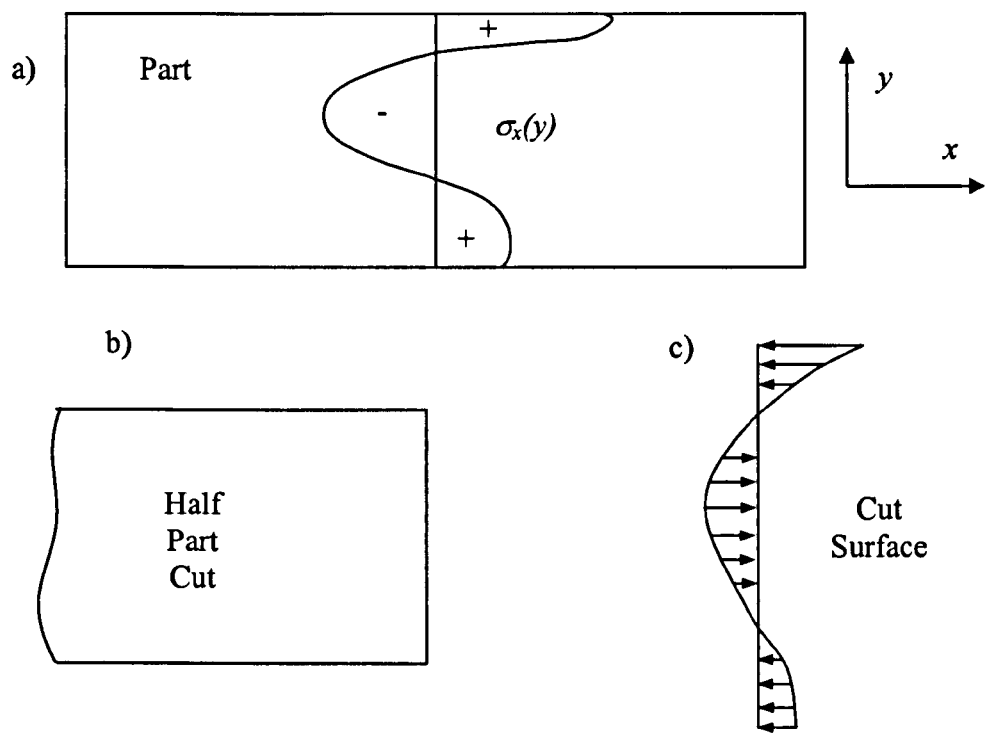

Figure 3.5.- Superposition principle a) original residual stress distribution
b) part cut in half, stresses relieved on face of cut
c) cut surface forced back to original state. All stress back to original values

For the contour method, accurate cutting and measurement of the deformed surface are critical to the accuracy of the technique. The ideal cutting process for separating the part should:

- Make a precisely straight cut.
- Not remove any additional material as surfaces are cut.
- Not introduce any plastic deformation.

Wire electric discharge machining (EDM) is generally used. There is no physical contact between the wire and the part being machined and so there is no cutting force present. This non-contact approach does not induce localised plastic deformation compared with the large contact forces that can be generated with conventional machining. The wire-control mechanisms can achieve positional precision of a fraction of a micrometer, especially for a straight cut.

The second method is the radius of curvature, which derives from *Timoshenko's* layer removal method [*1956*]. The principle of the method is to remove a complete layer of material from a beam or strip that has been plastically bent. The removal of a layer will disturb the residual stress field which was in an equilibrated state, thus resulting in a change in shape (curvature). This change in shape is measured as a change of curvature so the original state of residual stresses can be determined. The method assumes that the material is bent beyond the yield point and that unloading follows *Hooke's* law. The layer removal method can be applied not only to cases of bending but also to other cases including prismatic bars subjected to longitudinal plastic deformation. The method has been successfully applied to measure residual stresses in cold drawn brass tubes.

Güngör in *2001* presented results of residual stresses determined by applying the radius of curvature method to two Ti/SiC unidirectional composite panels with thick cladding. The variation of in-plane residual stresses in the cladding of the materials was measured, and the average fibre stresses were determined from the results. The calculations of residual stresses were made on the simple bending theory analysis of the curvature induced by the introduction of a successively growing slot. The results were validated by finite element analysis. The longitudinal fibre strains were measured from the relaxation

of fibres upon dissolving the matrix in a part of the composite by using a matrix etching technique. The stresses in the fibre and the matrix were determined using a concentric cylinder model.

3.4. Relaxation or maintainability of residual stresses.

Relaxation of residual stresses in materials can be associated with two cases; thermal or mechanical. Since residual stresses induced during manufacturing can be detrimental to the integrity and the service behaviour of a component, stress relief operations are an integral step in many sequences. Nevertheless, beneficial residual stress distributions can relax during service, leading to loss of their worth. The classification best known techniques that bring about residual stress relaxation are [*Vöhringer, 1987*] annealing (heat treatment), uniaxial deformation (drawing, stretching), cyclic deformation, temperature cyclic loading, quenching, neutron bombardment. The focus of this review is on the loss of beneficial residual stresses by fatigue-induced relaxation.

3.4.1. Review of relevant work.

Buehler and Buchlotz [*1933*] initiated the study of stress relaxation under cyclic loading. They presented a paper showing the effect of residual stresses upon bending fatigue strength and how the relaxation of these stresses was present as the cycles advance and failure occurred. *Rosenthal, Sines and Zizicas* [1949] induced residual compressive stresses in notched 61S aluminium specimens. They found a redistribution of residual stresses when the specimens were under cyclic loading. In fact, the stress at the notch was found to vanish completely. *Wallace and Frankel* [*1949*] checked the behaviour of induced residual tensile stresses on a notch after a single fatigue cycle load in an aluminium specimen. They heated one side of the hole while the other half of the hole

was immersed in water thus inducing residual stresses in the notch. The magnitude of the stresses was measured by the X-Ray method. The specimen was then subjected to one complete cycle of stress, the very close to the yield strength of the alloy. The results showed that the residual stresses at the base of the notch were relieved during the first cycle. This was expected because the magnitude of the applied cyclic stress caused the sum of itself and the residual stresses to exceed the yield point.

Badr [*2000*] presented his study on residual stress maintainability in materials subjected to fatigue. He manufactured a special keyhole specimen (modified compact-tension specimen, ASTM standard E 647-91). Before applying the overloaded (to create the residual stress state) and the constant cyclic load (fatigue load), a strain gauge was installed along the circumferential direction with the centre of the gauge at the point were the maximum normal stress occurs. The residual stress created by the overloading was simulated by finite element analysis. Trapezoidal cyclic loading was then applied using the maximum and minimum load and held constant during the whole test. Two specimens were overloaded to different loads to produce dissimilar residual stress fields in the parts and one specimen was not loaded. All three specimens were then subjected to the same amplitude of cyclic loading. The results from the paper showed that all three specimens had an incremental resulting strain as the number of the cycles increased, inducting stress relaxation. The maximum strain relaxation (570 microstrain) was present on the specimen with the highest overload and the minimum was found for the specimen subjected to no-overload (250 microstrain), the second overloaded specimen having similar values (270 microstrain).

Lindgren and Lepistö [*2002*] presented a study on the effect of mean stress on residual stress relaxation in steel specimens. The material studied was a mild steel type S235JRG2 in three different conditions; as received, annealed and strained 3% in tension. They treated the residual stress as a mean stress and studied its relaxation during fatigue. The strain amplitudes for systematic study were 0.05% and 0.06% but some experiments were also carried out with the strain amplitude set at 0.08%. Initial mean stresses ranged from 100 to around 200 MPa and the experiments were halted if 10^6 cycles were completed. To confirm the relaxation or maintainability of residual stresses, the stresses in the specimen surfaces were characterised before and after testing by means of X-ray diffraction. The conclusions were summarised in four points:

- Strain amplitudes of 0.05 and 0.06% result in mean stress relaxation to a stable value in mild steel. This value is dependent on the material condition.

- Crack growth and temperature variations significantly affect the results of mean stress relaxation experiments. Their effect must be taken into account when evaluating the reliability of experimental data.

- The stress relaxation exponent can be divided into two parts, where the first part includes the mean stress decrease due to yielding, and the second part includes the mean stress decrease as a result of cyclic mean stress relaxation. The first part is dependent on the mean stress i.e. the occurrence of plastic deformation, and the second part does not depend on the mean stress.

- Residual stresses at the specimen surface change during a mean stress relaxation experiment, even though the mean stress does not relax.

A lot of work has been carried out on the relaxation of residual stresses. Residual stress relaxation has been measured using a strain gauge approach or by the use of X-ray or neutron diffraction methods. The results produced by the strain gauge method are qualitative. While the results of X-ray and neutron diffraction methods are quantitative, the examinations have been surface based. The aim of the work carried out in this thesis is to use both the strain gauge approach and the crack compliance method to assess relaxation of residual stresses and to reveal the through thickness residual stress re-distribution profile due to stress relaxation in beams.

3.5 Summary.

From the literature reviewed in this chapter, it is clear that more work is necessary to comprehend the effects and consequences of the Bauschinger effect. Examples of areas of research interest are types of processes that promote Bauschinger effect and how the Bauschinger effect influences residual stress distribution. Additionally, the use of isotropic and/or kinematic hardening rules to assist in the process of determining residual stresses is approximate due to the inadequacies of the rules. The use of methods such as the compliance method, which does not require hardening rules, provides a good means to study the effect of Bauschinger effect on residual stress fields. This work therefore aims to use the CCM to study the interaction of Bauschinger effect on residual stress fields.

Chapter 4

Beam method for the simultaneous determination of tensile and compressive stress-strain behaviour of materials with prior strain history

4.1. Introduction.

It is usually assumed that most metals in the annealed condition have the same stress-strain behaviour in compression as in tension. If however they are strain hardened by loading beyond yield, either in tension or compression, and the direction of loading is reversed, the yield stress in the reverse direction is in most cases found to be lower than that in the original direction of loading [*Bauschinger, 1881 and 1886*]. Thus if a beam is made out of a material that has been uniaxially loaded beyond yield and then loaded in bending into the plastic range, the stress-strain behaviour on the tension and compression sides will not be the same.

The effect of prior plastic strain history manifests itself in many metals as the Bauschinger effect. Typically, whereas strain hardening during loading in one direction leads to increasing yield strength, reversing the direction of the loading subsequently leads to lower yield strength. Several attempts have been made to describe this anisotropic hardening behaviour using empirical rules [*Edelman and Drucker 1951, Prager, 1956, Hodge, 1957, Ziegler, 1959, Baltov and Sawczuk, 1965, Rees, 1981 and Stouffer 1996*]. Kinematic hardening assumes that the initial yield surface translates rigidly in the stress space but does not change shape [*Stouffer, 1996*]. This means that the elastic range is preserved. On the other hand isotropic hardening assumes that the initial yield surface grows in the stress space. The elastic range is however not preserved. These rules are known to underestimate the Bauschinger effect considerably [*Rees, 1981*].

It has been observed that the Bauschinger effect includes translations, expansion or contraction of the yield surface. Therefore combined isotropic / kinematic hardening rules that account for all these effects, apart from the yield surface contraction case, are better

able to account for the Bauschinger effect than kinematic hardening rules only [*Stouffer, 1996*]. Contraction of the yield surface due to softening is generally excluded from the theory of yield surface plasticity [*Stouffer, 1996*]. Anisotropic hardening rules including Bauschinger effect are usually based on the use of plastic pre-strain coefficients that are derived from tests involving loading in different directions [*Rees, 1981*]. In axial test cases, tensile and compression stress-strain behaviours are required to be studied.

One of the customary explanations for the occurrence of Bauschinger effect is that a back-stress is produced due to dislocation pile up when a material is strain hardened by loading in one direction. The back-stress compounds with reverse applied stress when the material is loaded in the opposite direction to cause early onset of yielding [*Dieter, 1981*].

This chapter presents a method for the simultaneous determination of tensile and compression stress-strain behaviours for materials under Bauschinger effect from bend tests only. The method is based on the application of simple tensile and bending moment equilibrium conditions to derive the two stress-strain behaviours (tension and compression). This concept was first used by *Herbert* [*1910*] and later by *Bach and Bauman* [*1924*]. Procedures based on the concept have subsequently been described by a few authors [*Nadai, 1950, Laws, 1981 and Marin, 1962*]. The procedures are however implicit in nature rather than explicit so that the required stresses are either obtained iteratively or by using graphical methods [*Nadai, 1950*]. *Mayville and Finnie* [*1982*] have used a similar derivation approach but obtained more readily applicable solutions. The approach derived in this work is similarly readily implemented using bending moment and surface strain data to obtain tensile and compression stress-strain curves.

Whereas previous derivations required differentiation of integral expressions [*Herbert, 1910, Bach and Bauman, 1924, Nadai, 1950, Laws, 1981, Marin, 1962 and Mayville and Finnie, 1982*], the approach developed in this work solves the integrations by using a simple Simpon's rule integration method [*Press, et al 1987*]. The final form of the solutions obtained independently in this work is slightly different from those of *Mayville and Finnie* [*1982*] but the results from both methods agree closely and are effectively indistinguishable.

4.2 The beam method.

Imagine that the tensile and compressive stress-strain of a material previously loaded in tension beyond yield is as composed in Figure 4.1.

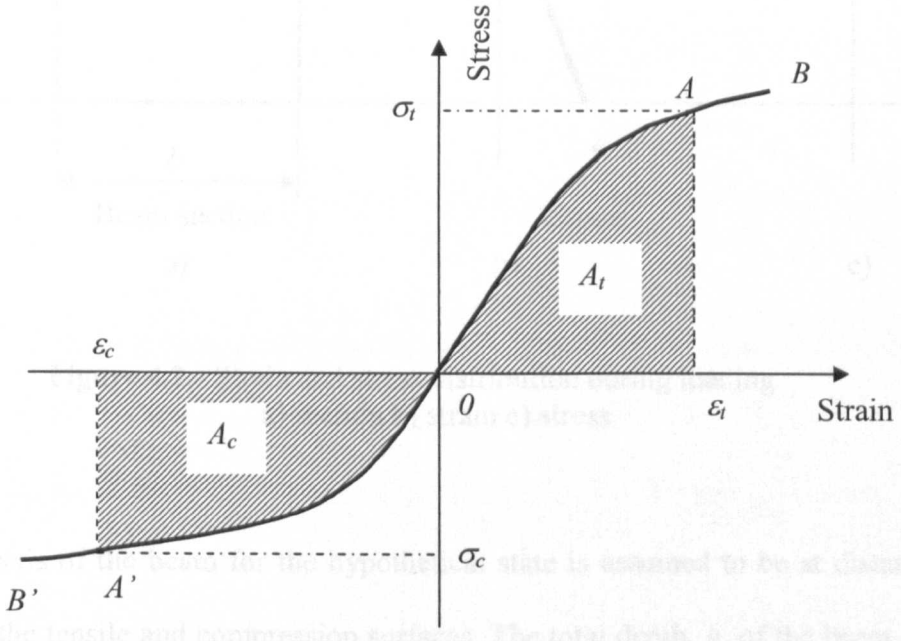

Figure 4.1.- Graphical illustration of the stress-strain curve
(strain hardening in tension and Bauschinger effect in compression)

Assume further that the beam from the material has a cross section as shown in Figure 4.2a and that a bending moment M has been applied to it such that the top and bottom surfaces of the beam are at strain and stress, (ε_t, σ_t) and (ε_c, σ_c) respectively, as shown in Figure 4.2b and 4.2c.

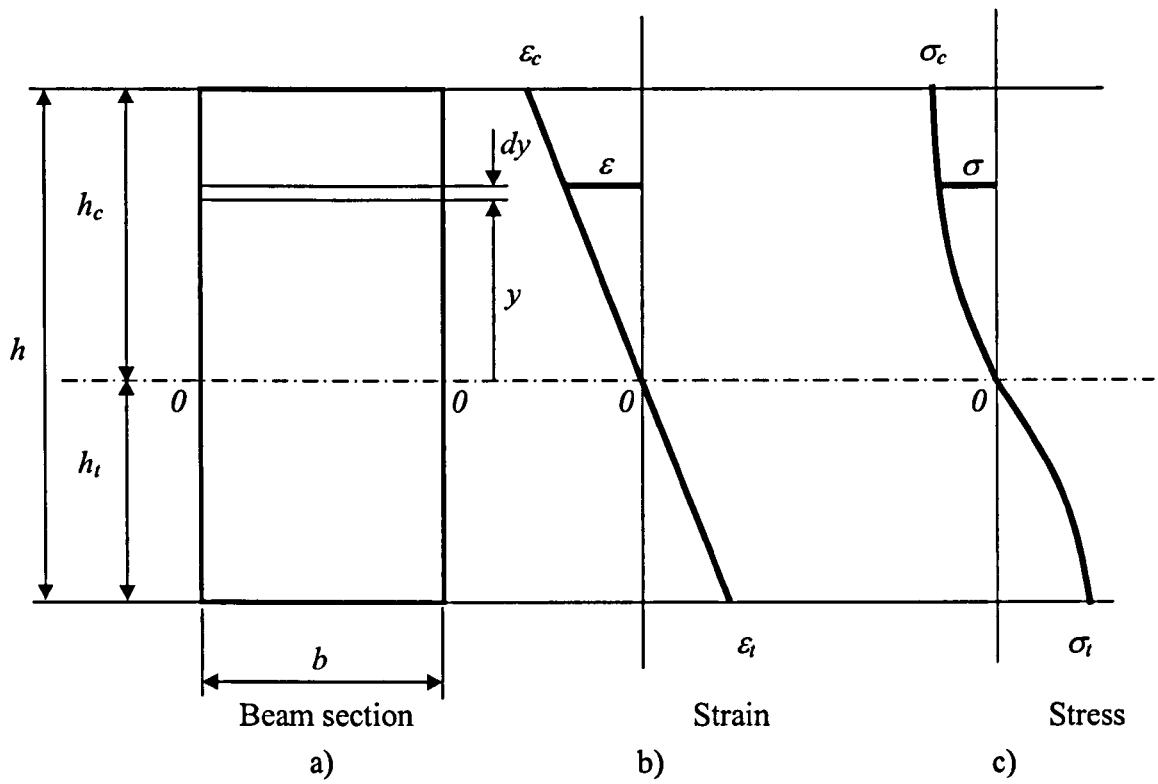

Figure 4.2.- Strain and stress distribution during loading
a) section b) strain c) stress

The neutral axis of the beam for the hypothetical state is assumed to be at distances h_t and h_c from the tensile and compression surfaces. The total depth, h, of the beam equals the sum of h_t and h_c, i.e.

$$h = h_t + h_c \qquad 4.1$$

The corresponding strain and stress distributions through the depth are as illustrated in Figures 4.2b and 4.2c. The strain distribution is assumed linear following Timoshenko's

assumption of plane sections remaining plane before and after bending [*Gere and Timoshenko, 1997 and Dowling, 1993*]. Let the loading stress at a position y, Figure 4.2c be given by;

$$\sigma_l(y) = f_l(y) \tag{4.2}$$

where $f_l(y)$ is the function which describes how the loading stress varies through the depth of the beam. The above procedure is based on the assumption that the stress-strain curves *OAB* and *O'A'B'*, Figure 4.1, are available from experimental tests or partly predicted using kinematic hardening rules. However, the behaviour of some materials such as annealed steels that yield abruptly on monotonic loading is poorly predicted by kinematic hardening rules [*Dowling, 1993, Rees, 1981, Korsunky and Whithers, 1997 and Timoshenko, 1981*].

The aim of this chapter is to show that both curves *OAB* and *O'A'B'* can be simultaneously determined from the knowledge of the bending moment and corresponding strain data at the top and bottom surfaces of beams during bend testing.

Under a pure bending condition, the neutral axis is located by imposing the equilibrium condition that the total axial force vanishes. This condition together with the Timoshenko's linear strain distribution through the depth of the beam leads to the equality condition given in Equation 4.3 [*Gere and Timoshenko, 1997*];

$$A_t = A_c \tag{4.3}$$

where A_t and A_c are the areas under the tensile and the compression stress-strain curves as illustrated in Figure 4.1. This condition is more explicitly written as;

$$\int_0^{\varepsilon_c} \sigma_c d\varepsilon_c = \int_0^{\varepsilon_t} \sigma_t d\varepsilon_t \tag{4.4}$$

Furthermore the condition of equilibrium of internal and external moments requires that;

$$M = M_t + M_c \tag{4.5}$$

where M_t and M_c are effective moments carried by the part of the section of the beam under tensile and under compressive stresses respectively. These component parts are given by;

$$M_t = \frac{bh_t^2}{\varepsilon_t^2}\int_0^{\varepsilon_c} \sigma_t \varepsilon_t d\varepsilon_t \tag{4.6}$$

$$M_c = \frac{bh_c^2}{\varepsilon_c^2}\int_0^{\varepsilon_c} \sigma_c \varepsilon_c d\varepsilon_c \tag{4.7}$$

respectively [*Timoshenko and Gere, 1991*].

The strain range ε_t in the bend test can be divided into a series of m strain increments $\Delta\varepsilon_{tj}$, $j=1, m$ and the corresponding matching compression strain increments, $\Delta\varepsilon_{cj}$, can be found for ε_c from logged strain results. Following this approach, we can re-write the integral Equation given in 4.3 and 4.4 as;

$$\sum_{j=1}^{m} \sigma_{tj} \Delta\varepsilon_{tj} = \sum_{j=1}^{m} \sigma_{cj} \Delta\varepsilon_{cj} \tag{4.8}$$

where σ_{tj} and σ_{cj} are the average stress values over the corresponding strain increments. The following equality condition, Equation 4.9, holds for corresponding strain increments;

$$\sigma_{tj} \Delta\varepsilon_{tj} = \sigma_{cj} \Delta\varepsilon_{cj} \tag{4.9}$$

for all $j = 1, m$. It has previously been shown [*Urriolagoitia-Sosa, Durodola and Fellows, 2003*], that if either the tensile and compressive stress-strain data is known, Equation 4.9 can be used to determine the unknown tensile or compressive stress-strain data. Following a similar integration procedure as highlighted for Equation 4.8, the total external moment M applied at increment m is as given in Equation 4.10 below;

$$M_m = \frac{bh_{tm}^2}{\varepsilon_{tm}^2}\sum_{j=1}^{m}\sigma_{tj}\varepsilon_{tj}\Delta\varepsilon_{tj} + \frac{bh_{cm}^2}{\varepsilon_{cm}^2}\sum_{j=1}^{m}\sigma_{cj}\varepsilon_{cj}\Delta\varepsilon_{cj} \qquad 4.10$$

Subscript m is used to denote total number of increments over the strain ranges. By simple proportions, we have, similar to $\frac{y}{\varepsilon} = \frac{h_t}{\varepsilon_t} = \frac{h_c}{\varepsilon_c}$, that $\left(bh_t^2/\varepsilon_t^2\right) = \left(bh_c^2/\varepsilon_c^2\right) = [bh^2/(\varepsilon_t + \varepsilon_c)^2]$. Equation 4.10 can therefore be rewritten as;

$$M_m = \frac{bh^2}{(\varepsilon_{tm} + \varepsilon_{cm})^2}\sum_{j=1}^{m}\left[\sigma_{cj}\varepsilon_{cj}\Delta\varepsilon_{cj} + \sigma_{tj}\varepsilon_{tj}\Delta\varepsilon_{cj}\right] \qquad 4.11$$

By using the equality condition in Equation 4.9 for every increment j, Equation 4.11 can be written as;

$$M_m = \frac{bh^2}{(\varepsilon_{tm} + \varepsilon_{cm})^2}\sum_{j=1}^{m}\left[\sigma_{tj}\Delta\varepsilon_{tj}(\varepsilon_{cj} + \varepsilon_{tj})\right] \qquad 4.12$$

Assuming that the stresses and strain at increments *1* to *k-1* have been determined, the tensile stress at any increment k can be obtained from Equation 4.12 as;

$$\sigma_{kt} = \left[\overline{M}_k - \sum_{j=1}^{k-1}\bar{\varepsilon}_j\sigma_{tj}\Delta\varepsilon_{tj}\right] / \left[\bar{\varepsilon}_k\Delta\varepsilon_{kt}\right] \qquad 4.13$$

where;

$$\overline{M}_k = M_k \Big/ \left[\frac{bh^2}{(\varepsilon_{tm} + \varepsilon_{cm})^2}\right] \qquad 4.14$$

and $\bar{\varepsilon}_k = (\varepsilon_{ck} + \varepsilon_{tk})$. Alternatively we can write Equation 4.12 as;

$$\overline{M}_m = \sum_{j=1}^{m}\left[\sigma_{tj}\Delta\varepsilon_{tj}(\varepsilon_{cj} + \varepsilon_{tj})\right] \qquad 4.15$$

and by considering any two consecutive increments *k-1* and k, and generalising for tensile and compression stresses, we can write, following from Equation 4.15, that;

$$\sigma_{\alpha k} = \frac{\overline{M}_k - \overline{M}_{k-1}}{\bar{\varepsilon}_k \Delta\varepsilon_{\alpha k}} \qquad 4.16$$

where $\alpha = t$ for tension stresses and $\alpha = c$ for compression stresses. Equation 4.16 gives the average stresses at any increment $k = 1..m$. Although equations types 4.13 and 4.16 can be used to obtain the stresses, Equation 4.16 will be more readily implemented as only information over a specific increment is required to obtain the corresponding stresses for the increment. Thus the tensile and compressive stresses were obtained in this work using Equation 4.16.

In summary, if the moment, strain and strain increments are known at any stage of loading from the bending test, Equation 4.16 can be used to obtain both the tensile and compressive stresses. At the first increment, $k = 1$, the term, $\overline{M}_{k-1}$ term in Equation 4.16 is zero, and hence $\sigma_{t1} = \overline{M}_1 \,/\, \bar{\varepsilon}_1 \Delta\varepsilon_{t1}$ and similarly $\sigma_{c1} = \overline{M}_1 \,/\, \bar{\varepsilon}_1 \Delta\varepsilon_{c1}$. Equation 4.16 can then used progressively for $k = 2 \ldots m$ to obtain the stresses at subsequent increments up to the last increment m.

4.3. FEA of the beam method.

The aim of this section of the thesis was to verify the performance of the beam method presented in section 4.2 on simulated data prior to experimental testing. FEA was used to generate the simulated data.

4.3.1. Modelling of the beam.

The procedure for the derivation of the tensile and compressive stresses is based on the strain response of a bent beam. The beams are modelled in 2-Dimensions in order to allow variations of stresses and strains through the depth to be determined. Quadratic

order elements where used instead of linear elements, in order to obtain smooth variations of stress and strain through the depth of the beams.

In the ANSYS FE package [*2004*], the element is defined by eight nodes having three degrees of freedom at each node; translation in the nodal *x* and *y* direction and rotation in the *z* axis (UX, UY and ROTZ). Only translation degrees of freedom exist at the nodes for the same type of elements in the ABAQUS FE package [*2002*]. The elements have plasticity, creep, swelling, stress stiffening, large deflection and large strain capabilities.

The beam was loaded in a four-point bend configuration with the force located on two separate nodes as illustrated in Figure 4.3.1a. The maximum value of the moment applied in each case was 11.5 Nm. This produced plastic deformation in the beam for all material elastic-plastic behaviour cases considered.

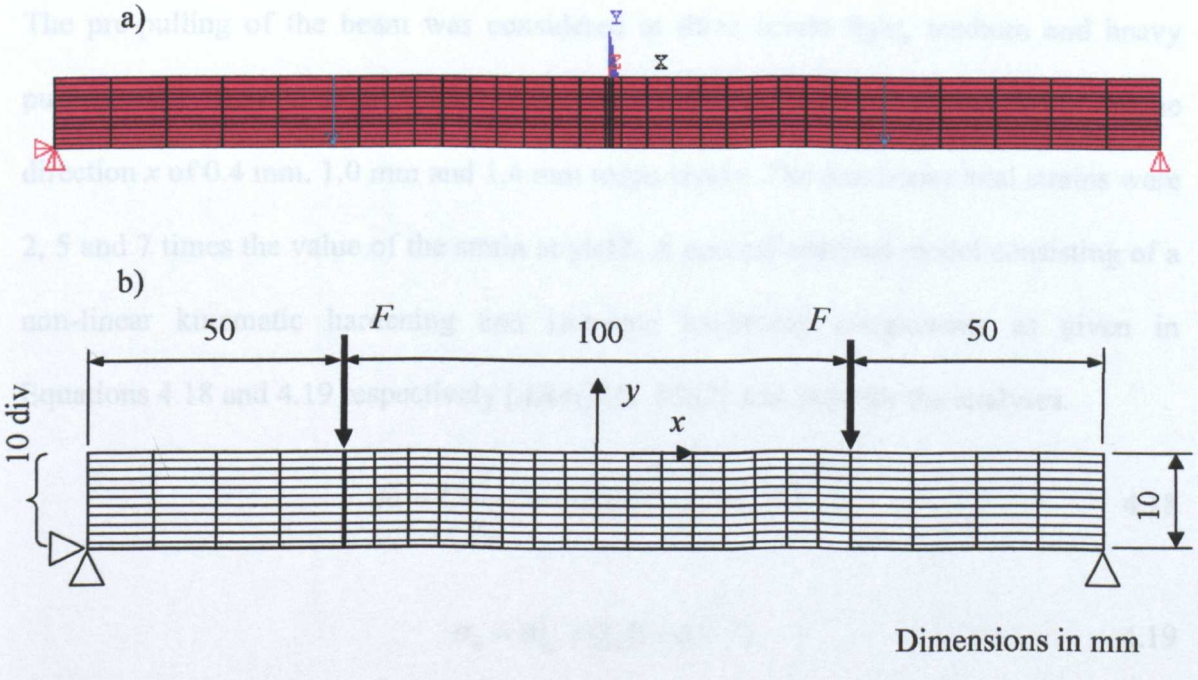

Figure 4.3.1.- Four-point bending beam model
a) FEA model b) schematic representation of the FEA model

Boundary conditions were applied at the extreme end nodes at the bottom (Figure 4.3.1b). One node was restricted in both the x and y directions and the other was only restricted in the y direction. All the nodes were let free to rotate about z as shown in Figure 4.3.1b. Care was taken to produce small elements in the middle part of the beam, where the strain data was obtained for the evaluation of the simultaneous method. Ten elements were used across the depth of the beam and twenty across the length.

Plane stress analysis was carried out and the loading was applied in a total of 100 sequentially increasing increments. The resulting strain in the x direction, produced by the action of the bending loading was recorded for each loading increment. The convergence of the model was checked by refining the mesh and verifying that there were no significant differences between results from the meshes. Theoretical calculations were also carried out to validate simulation results wherever possible.

The pre-pulling of the beam was considered at three levels light, medium and heavy pulling with respect to the yield strain. These correspond to a displacement in the direction x of 0.4 mm, 1.0 mm and 1.4 mm respectively. The maximum total strains were 2, 5 and 7 times the value of the strain at yield. A general material model consisting of a non-linear kinematic hardening and isotropic hardening components as given in Equations 4.18 and 4.19 respectively [*ABAQUS, 2002*] was used for the analyses.

$$d\alpha = C\frac{1}{\sigma_o}(\sigma - \alpha)d\bar{\varepsilon}^{pl} - \gamma\ \alpha\ d\bar{\varepsilon}^{pl} \qquad 4.18$$

$$\sigma_o = \sigma|_o + Q_\infty(1 - e^{-\bar{\varepsilon}^{pl} b}) \qquad 4.19$$

$\bar{\varepsilon}^{pl}$ is the equivalent plastic strain, α is the back-stress, C is the initial kinematic hardening modulus, γ determines the rate at which kinematic modulus decreases with

plastic deformation, σ_o is the current yield stress, $\sigma|_o$ is the initial yield stress, Q_∞ is the maximum change in the size of the yield surface and b defines the rate at which the size of the yield surface changes as plastic straining develops.

Equation 4.18 describes the translation of the yield surface in the stress space due to the back-stress, α, while Equation 4.19 describes the change of the equivalent stress defining the size of the yield surface, σ_o, as a function of plastic deformation. The different hardening models used for these examples are explained as follows:

Isotropic hardening.- Through hardening, the elasticity domain in stress space expands or shrinks in an isotropic way around the centre (Figure 4.3.2a) $\sigma = 0$. $\sigma|_o$ is the virgin yield stress at the first time of loading. In the case of isotropic hardening, the yield surface transforms into $|\sigma_o| = z\,|\sigma|_o|$, where z is > 1.

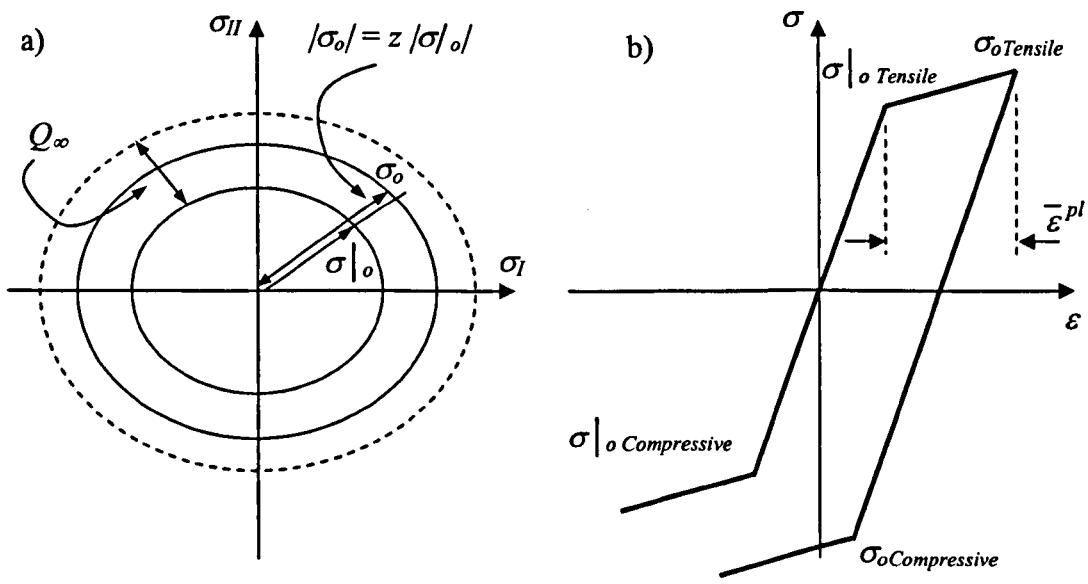

Figure 4.3.2.- Common isotropic hardening model
a) Yield surface diagram b) Stress-strain curve

However, there is also a maximum limiting size that the yield surface can reach. This is given by $\sigma|_o + Q_\infty$. In Figure 4.3.2a, the loading and reverse loading for an isotropic hardening model is represented, where an increase in the reversed yield stress is apparent. The equivalent plastic strain in multi-axial case is given by $\bar{\varepsilon}^{pl} = \sqrt{\frac{2}{3}\varepsilon_{ij}^{pl}\varepsilon_{ij}^{pl}}$.

Kinematic hardening.- Through hardening, the elasticity domain undergoes a translation in stress space, while maintaining its volume (Figure 4.3.3a). This translation in the stress space is described by a translation of the centre, $\sigma = 0$. Let $\sigma|_o$ be again the initial yield stress of a virgin material at the first time of loading. The translation of the stress space can be described by $/\sigma - \alpha/ = /\sigma^0/$.

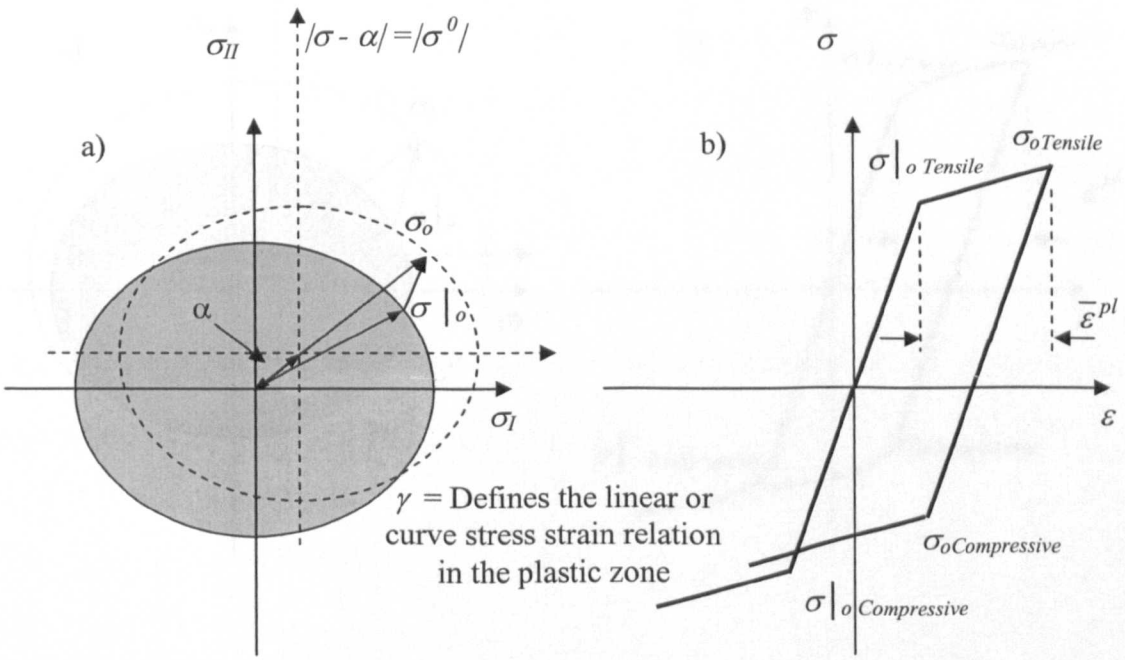

Figure 4.3.3.- Common kinematic hardening model
a) Yield surface diagram b) Stress-strain curve

During plastic loading, the elastic domain preserves its value in the translation, where α corresponds to the measurable translation of the centre in stress space (Figure 4.3.3a). In Figure 4.5b, the loading and reverse loading for a kinematic hardening model is represented, where a decrease in the reversed yield stress is apparent.

Combined hardening.- The two previous hardening models can be joined to give the combined isotropic and kinematic hardening model. For this model the elasticity domain undergoes a translation and expansion in stress space. The volume is not maintained (Figure 4.3.4a). In Figure 4.3.4b, the loading and reverse loading for a combined hardening model is represented.

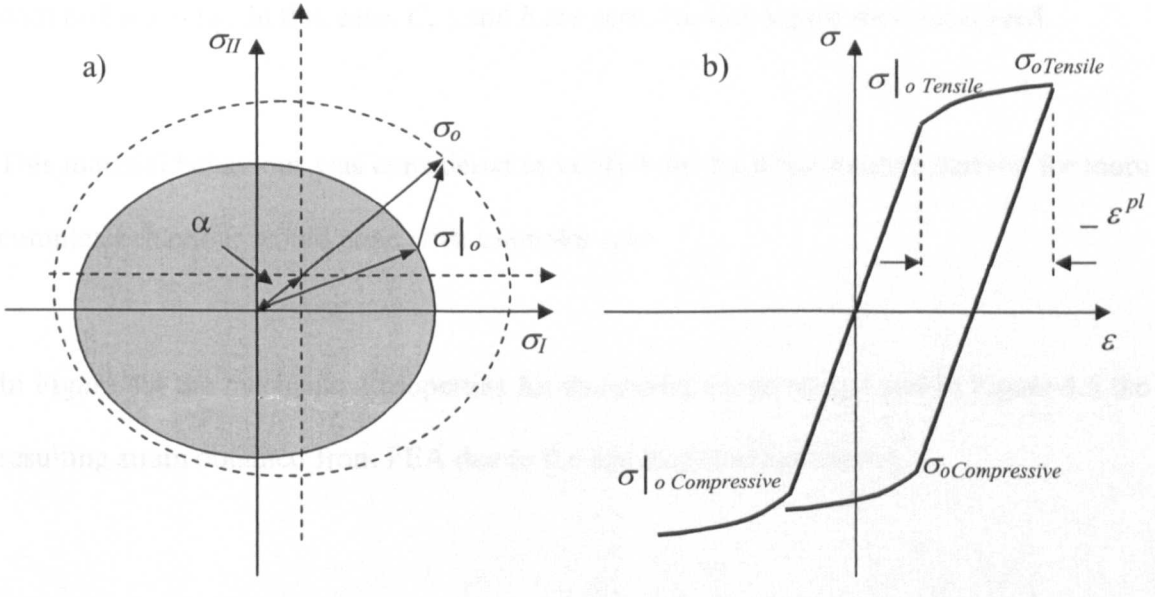

Figure 4.3.4.- Common combined hardening model
a) Yield surface diagram b) Stress-strain curve

A sample model material used for the verification of the combined isotropic / kinematic hardening procedure in Equation 4.18 and 4.19 were in the ABAQUS packages. The material properties used were E = 200 x 10^3 N/mm^2, $\sigma|_o$ = 200 N/mm^2, ν = 0.3, Q_∞ = 333 N/mm^2, b = 666, C = 22220 N/mm^2 and γ = 34.65.

These properties were used for the analysis of the various hardening cases, to test the beam approach proposed for the simultaneous determination of the tensile and compressive properties from bend tests.

4.3.2. Elastic-perfectly plastic behaviour.

This first analysis considered a situation where the mechanical properties of the material are supposed to be identical in tension and compression (annealed state of the material) with no hardening. In this case, C, γ and b are zero. No initial pull was considered.

This material behaviour was considered to verify how the beam method derived for more complex behaviour would cope with a simpler case.

In Figure 4.4 the mechanical properties for the model are presented and in Figure 4.5 the resulting strain obtained from FEA due to the bending load are shown.

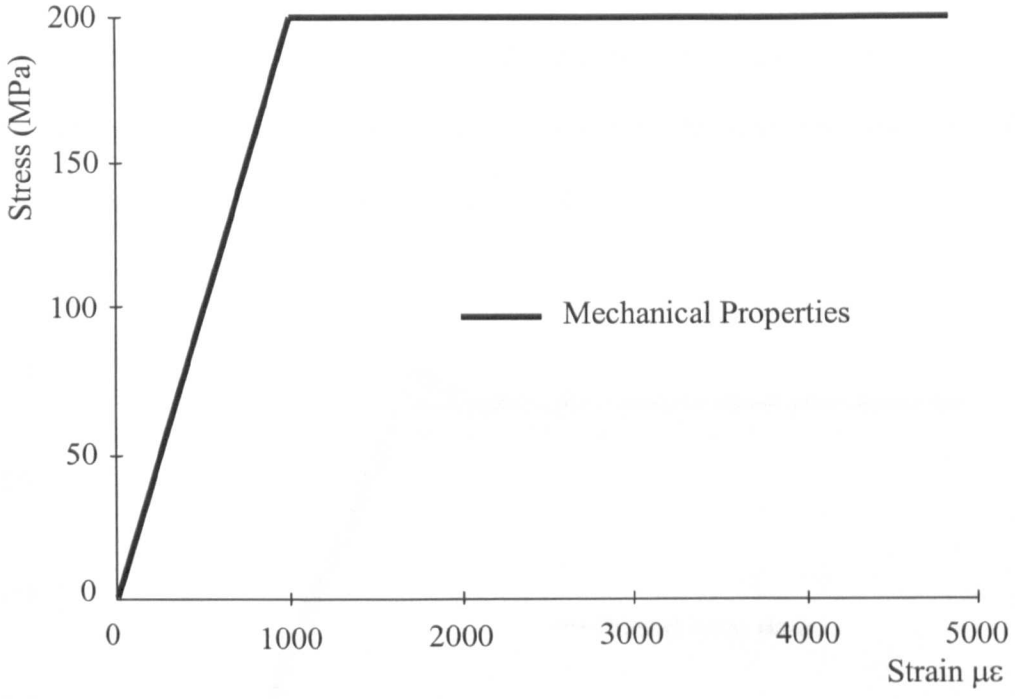

Figure 4.4.- Elastic-perfectly plastic stress-strain behaviour

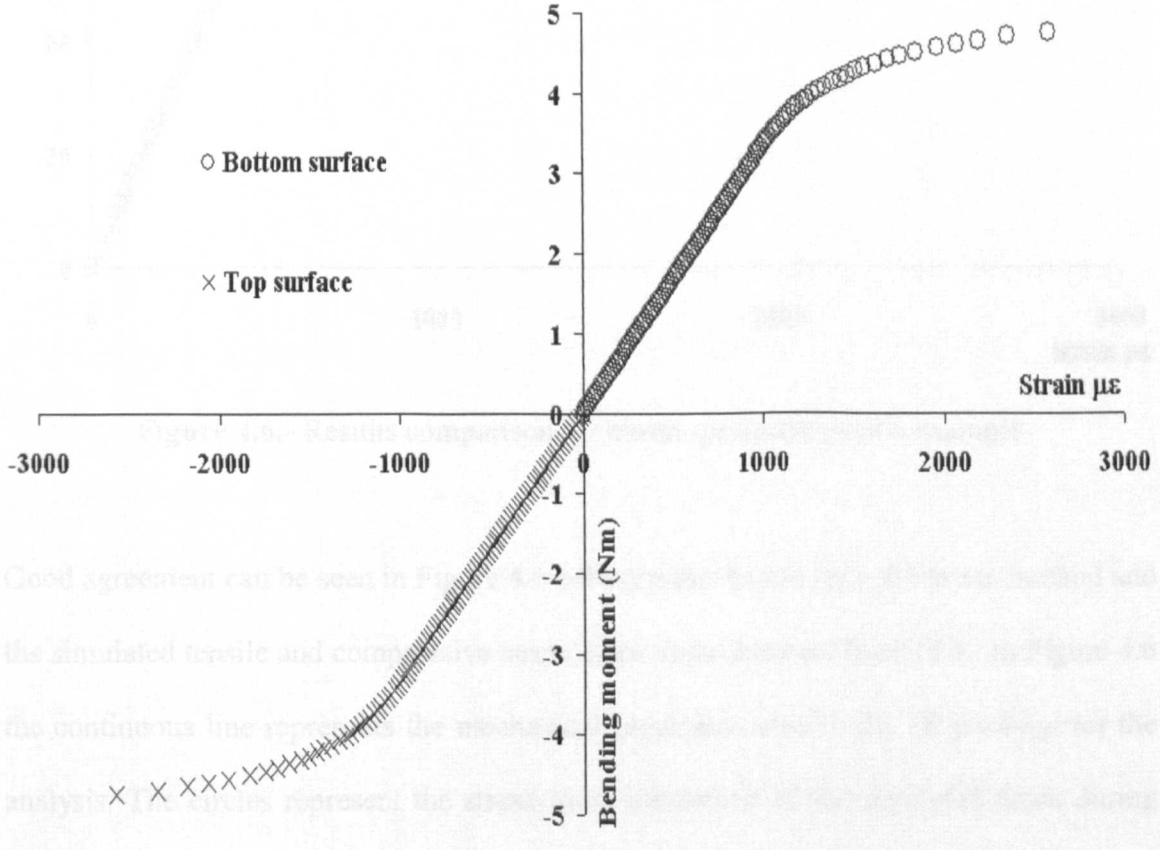

Figure 4.5.- Actual tensile and compressive strain results produced by bending

The results obtained using the beam method described in section 4.2 (using Equation 4.16) are shown in Figure 4.6. The results are compared against the stress-strain data from finite element analysis. The stress-strain results obtained at the surface of the beam as loading increased are also indicated in the plot.

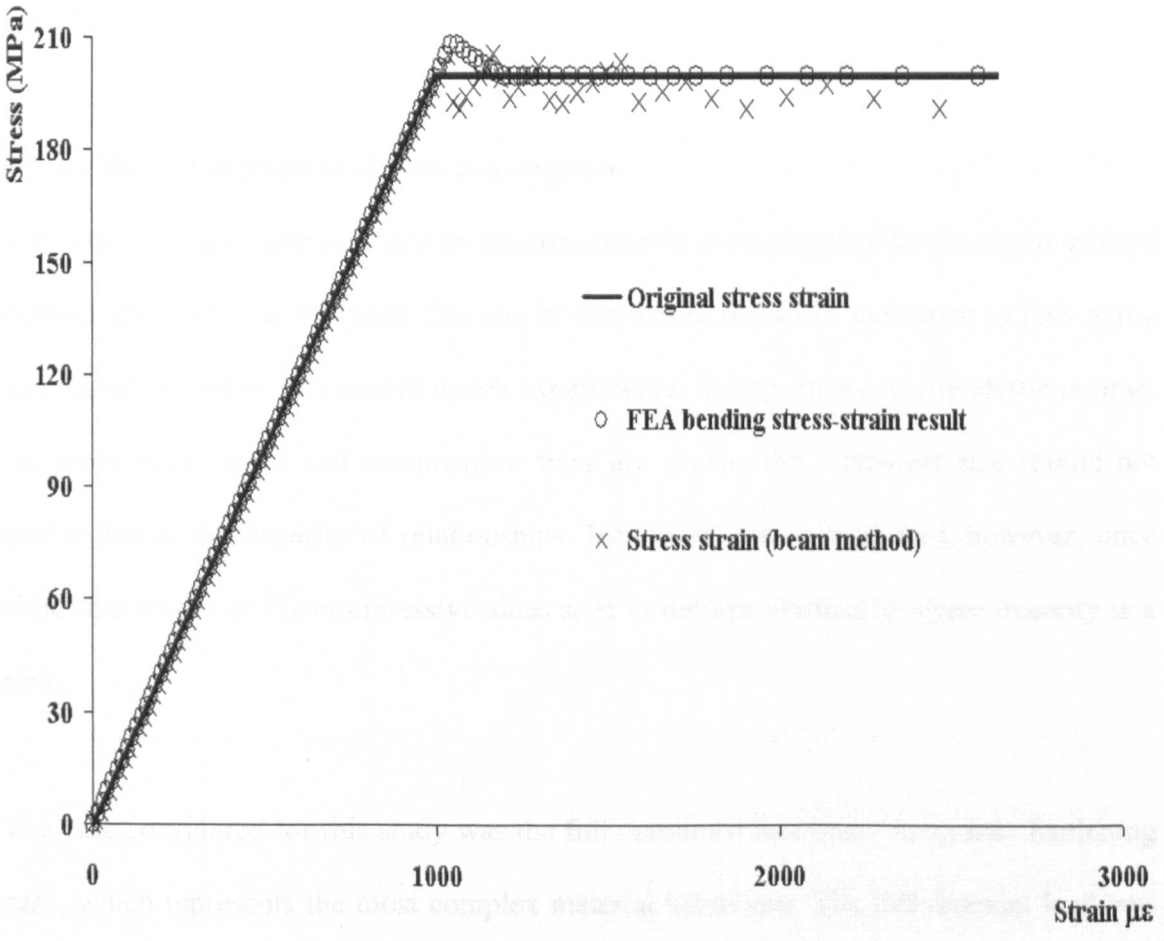

Figure 4.6.- Results comparison for elastic-perfectly plastic example

Good agreement can be seen in Figure 4.6 between the results from the beam method and the simulated tensile and compressive stress-strain data obtained from FEA. In Figure 4.6 the continuous line represents the mechanical properties used in the FE package for the analysis. The circles represent the stress-strain behaviour of the simulated beam during loading. It can be seen that there is a difference between the behaviour of the original

stress-strain line and the loading stress-strain line. A small peak on the loading stress-strain behaviour is apparent after yielding has occurred. This can be made smother by increasing the increments of the loading analysis. Nevertheless, this peak cannot be eradicated completely due to the inability to match the abrupt change that occurs at yield. It can also be seen that the calculation stabilizes quickly and follows the expected shape at higher strains.

4.3.3. Effect of increment size on convergence.

The effect of load increment size on the convergence characteristics for the beam method derived approach was analysed. The aim of this was to obtain an indication of how many increments would be essential to match experimental testing. In the totally elastic regime, i.e. when both tensile and compressive sides are elastic, the increment size should not matter due to the linearity of relationships. Increment size is important, however, once either the tensile or the compressive sides start to deform plastically where linearity is a rarity.

The case considered for this study was the full combined isotropic / kinematic hardening case, which represents the most complex material behaviour. The full moment load was applied in 10, 50, 100, 200 and 500 increment cases. The plots of the results obtained for the tensile and the compression stresses are as indicated in Figure 4.7. It can be seen that no significant improvements in convergence is obtained with number of increments higher than 100. It should be indicated that the increment sizes used are uniform from the beginning to the end of the loading process. This approach was followed, as it is practically difficult to know in advance when the plastic deformation stage will set in.

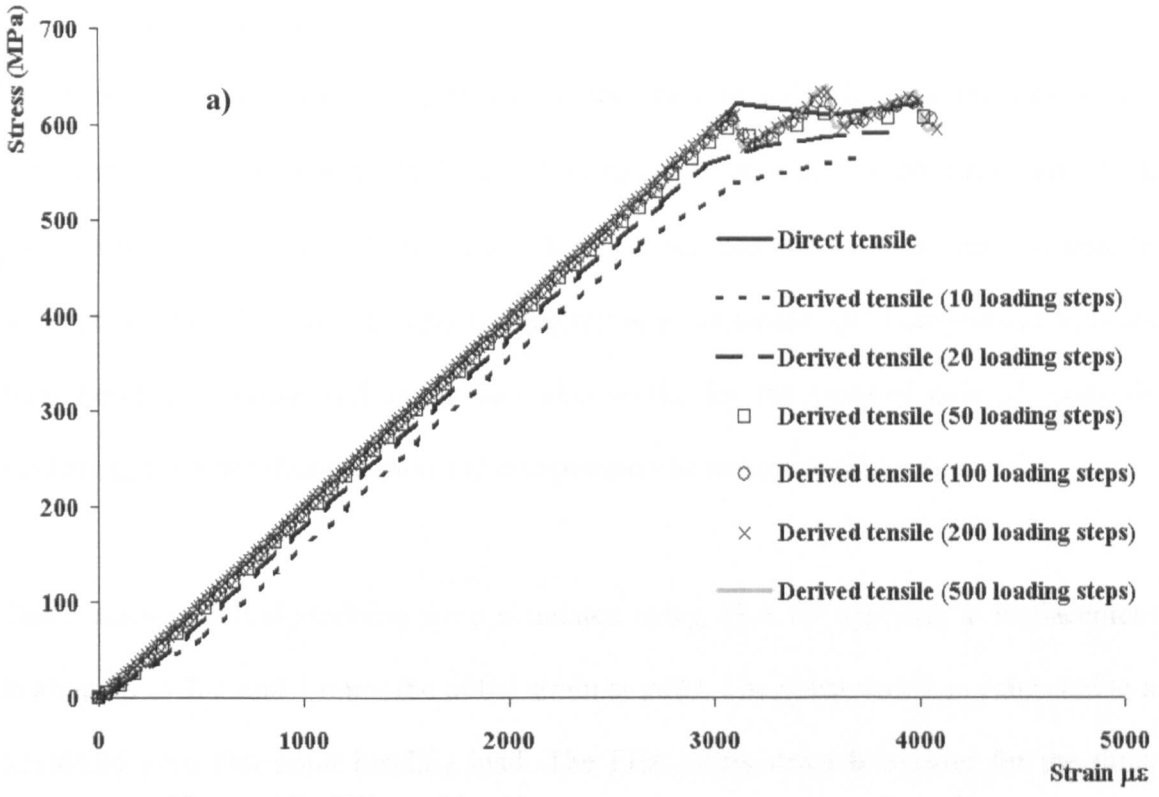

Figure 4.7.- Effect of load increment on convergence of results.
a) tensile properties

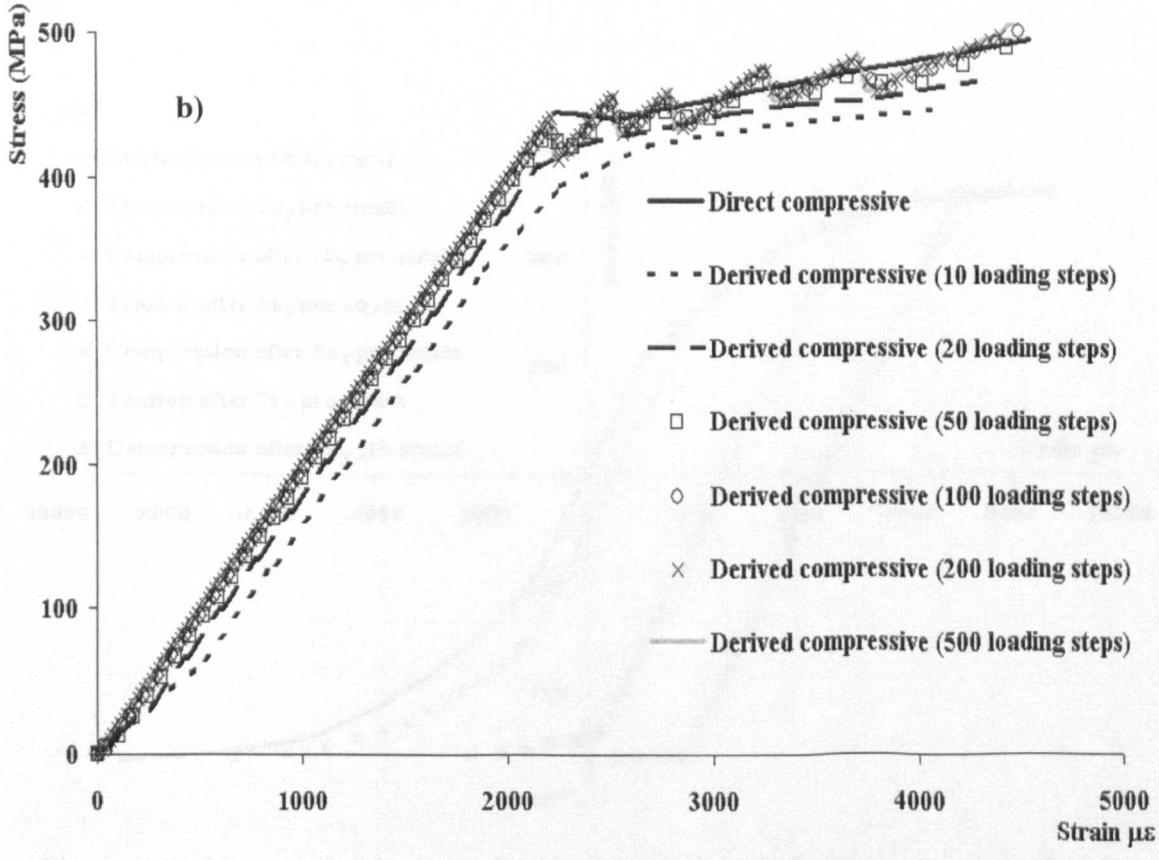

Figure 4.7.- Effect of load increment on convergence of results.
b) compressive properties

4.3.4. Isotropic hardening.

The general combined isotropic / kinematic hardening model reduces to the simple case of isotropic hardening when C and γ are equal to zero so that there is no translation of the yield surface (Equation 4.18 and 4.19). This case was considered in the first instance to demonstrate that the beam method for determining the tensile and compressive stresses from bending moment and strain data also works for the reduced case of isotropic hardening, for which both tension and compression behaviour are the same.

Three cases of initial straining were simulated using FEA by applying a displacement loading up to 2, 5 and 7 times the initial strain at yield. The beam was then subjected to a simulated pure four-point bending load. The FEA stress-strain behaviour for the three initial (light, medium and hard) pre-straining cases are plotted superimposed in Figure 4.8a.

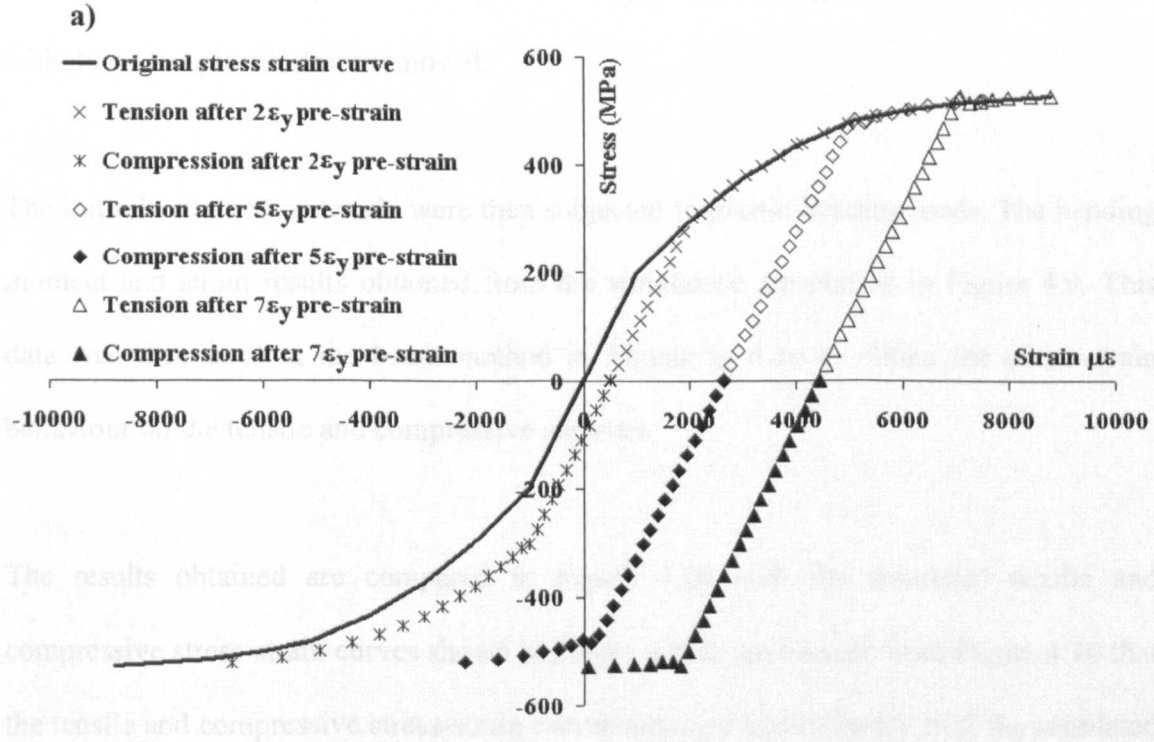

Figure 4.8.- Isotropic hardening behaviour a) effect of different levels of tensile pre-strain on tension and compression behaviour

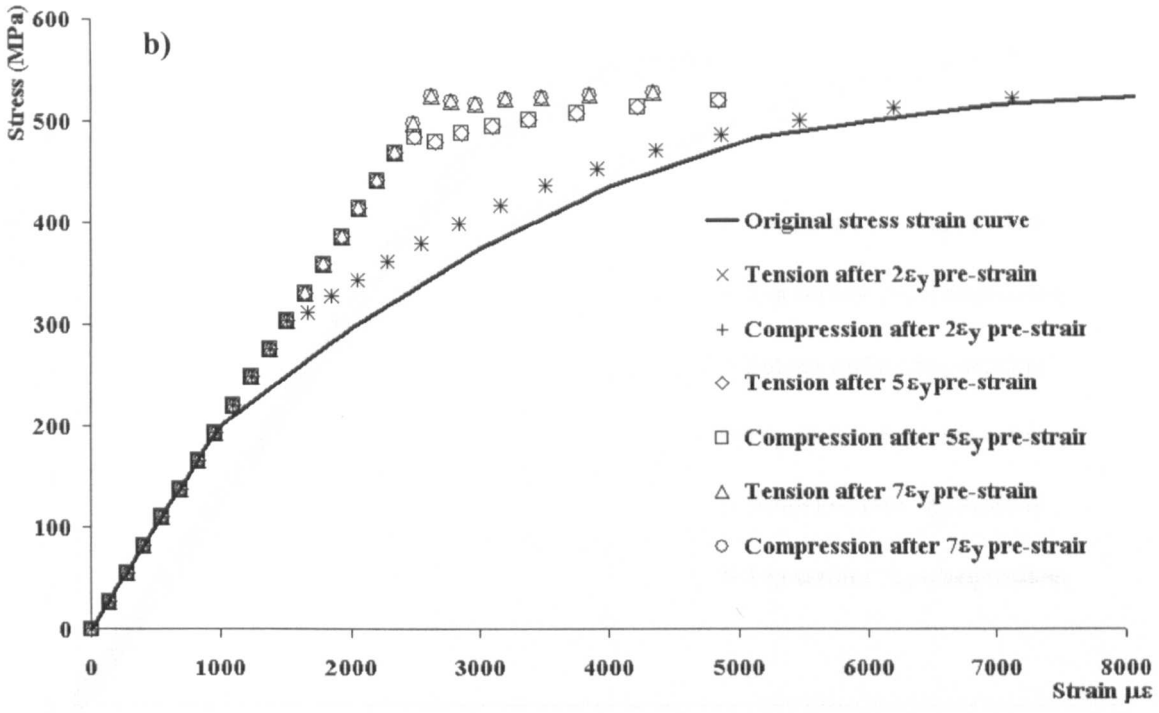

Figure 4.8.- Isotropic hardening behaviour b) comparison of stress-strain plots

It can be seen that the yield stresses in tension and compression are the same on reverse loading for these isotropic hardening cases. Figure 4.8b compares the same curves but with the initial plastic strain removed.

The initially strained materials were then subjected to plastic bending loads. The bending moment and strain results obtained from the simulation are plotted in Figure 4.9. This data was then used in the beam method in Equations 4.16 to obtain the stress-strain behaviour on the tensile and compressive surfaces.

The results obtained are compared in Figure 4.10 with the simulated tensile and compressive stress-strain curves shown in Figure 4.8. It can be seen from Figure 4.10 that the tensile and compressive stress-strain curves obtained agree closely with the simulated data.

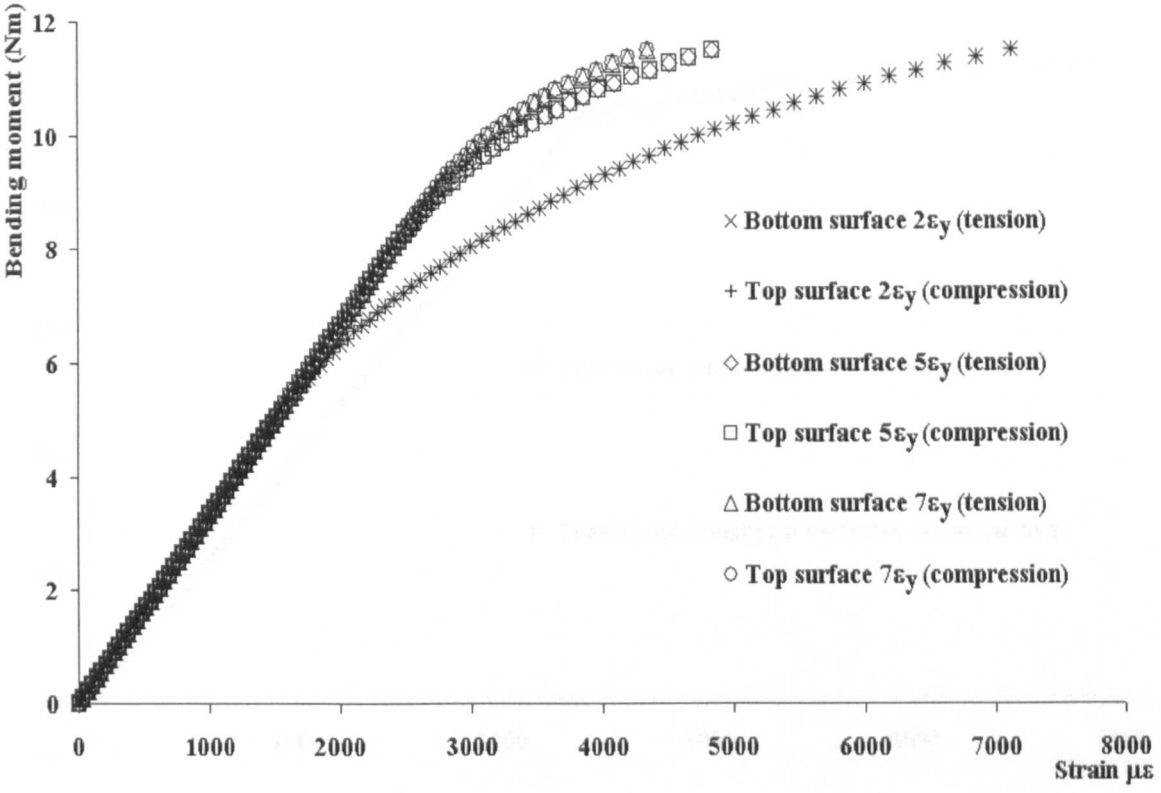

Figure 4.9.- Superposition of FEA simulated bending moment-strain data for different levels of tensile pre-strain

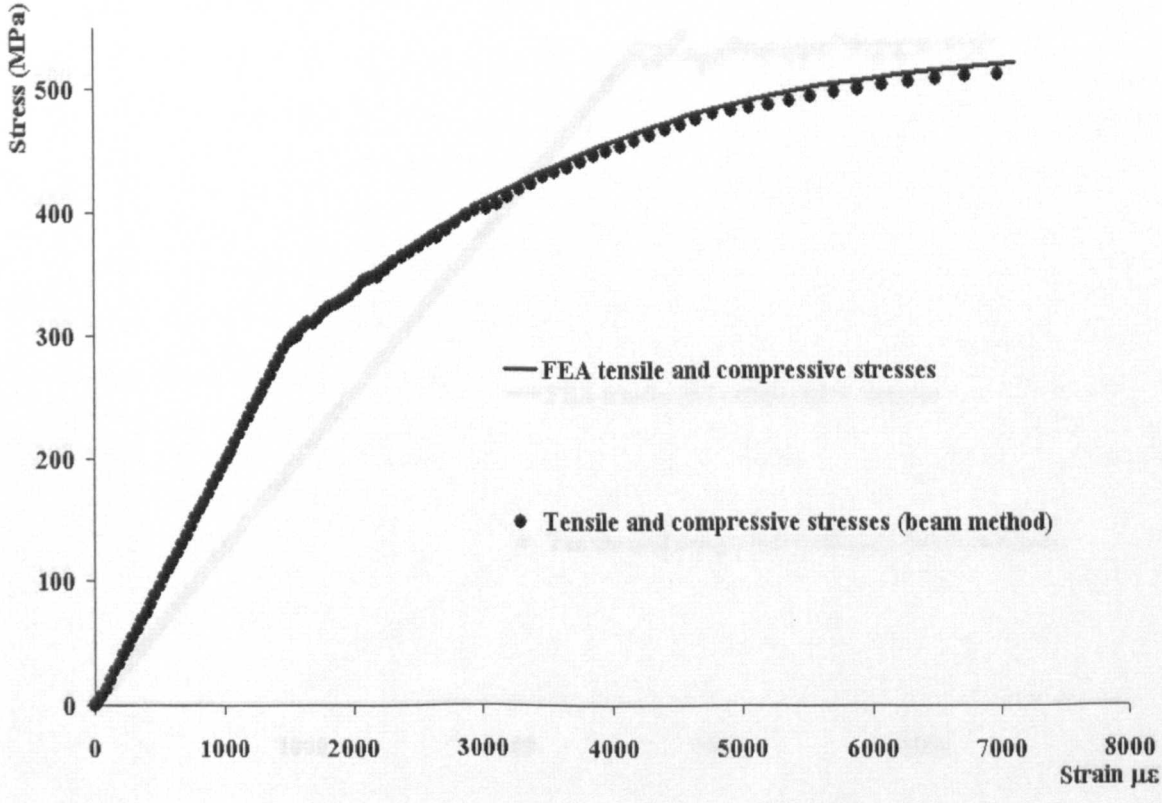

Figure 4.10a.- Comparison of stress-strain for mutual plots subjected to $2\varepsilon_y$ pre-pull for the isotropic hardening behaviour

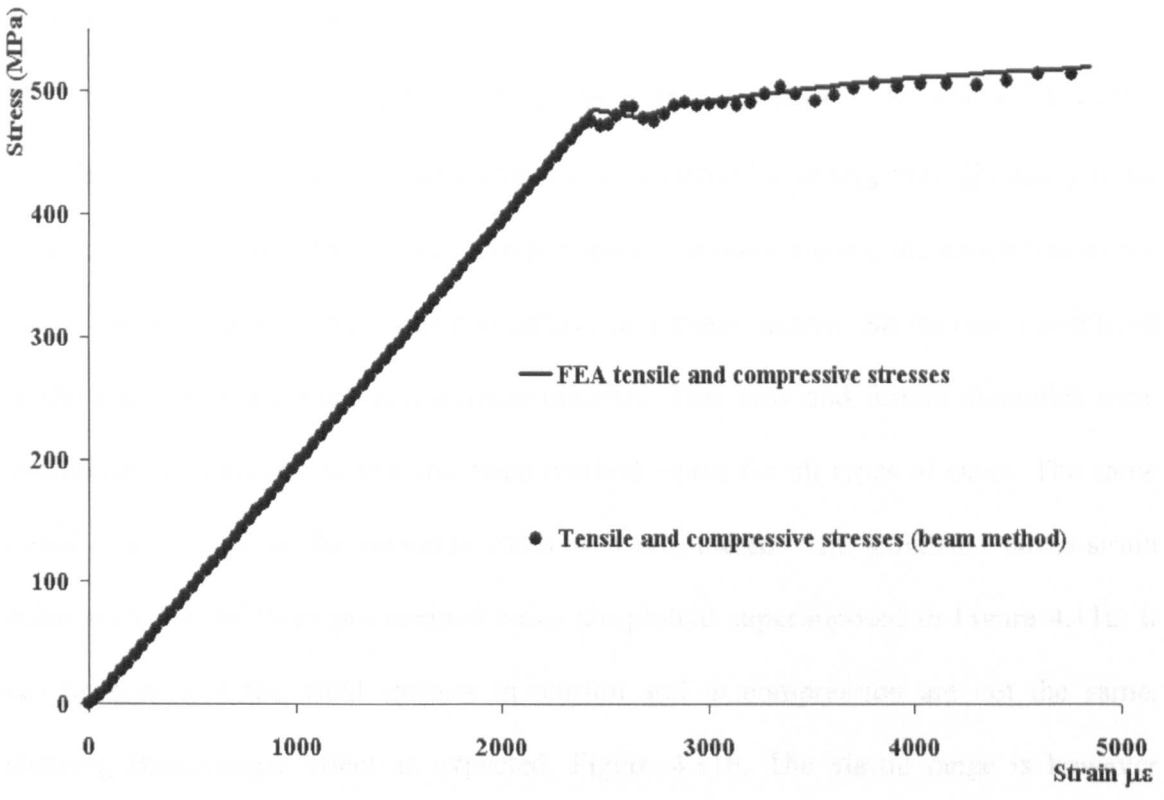

Figure 4.10b.- Comparison of stress-strain for mutual plots subjected to $5\varepsilon_y$ pre-pull for the isotropic hardening behaviour

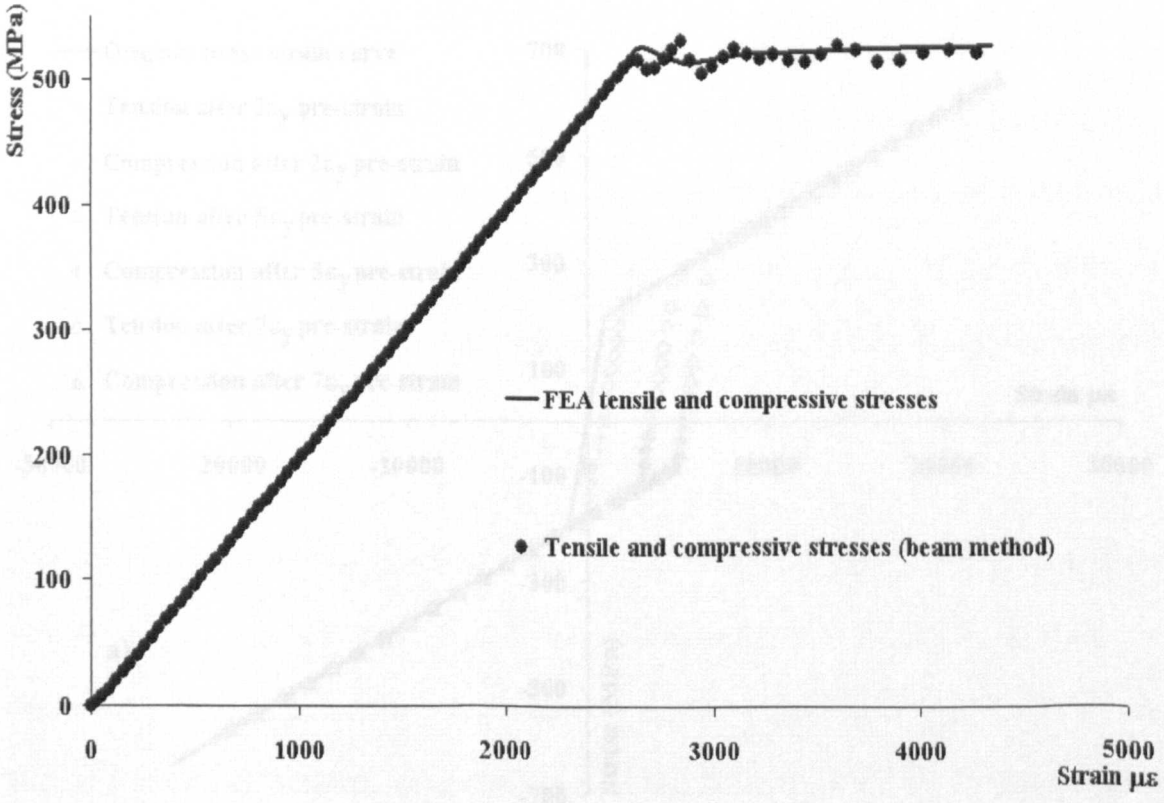

Figure 4.10c.- Comparison of stress-strain for mutual plots subjected to $7\varepsilon_y$ pre-pull for the isotropic hardening behaviour

4.3.5. Linear Ziegler hardening.

The analysis carried out in this case is similar to that described in Section 4.3.4. In this case, however, linear Ziegler hardening was considered by setting both Q_α and γ to be equal to zero. By considering these two parameters as non-existing, the simulation of the plastic region in this example tends to behave in a linear manner. So the case considered in this section of the work is a bilinear material. This case and further examples were considered to demonstrate that the beam method works for all types of cases. The same initial straining as in the previous cases was considered. The simulated stress-strain behaviours for the three pre-strained cases are plotted superimposed in Figure 4.11a. It can be seen that the yield stresses in tension and in compression are not the same, showing Bauschinger effect as expected, Figure 4.11b. The elastic range is however preserved as can be seen in Figure 4.11a.

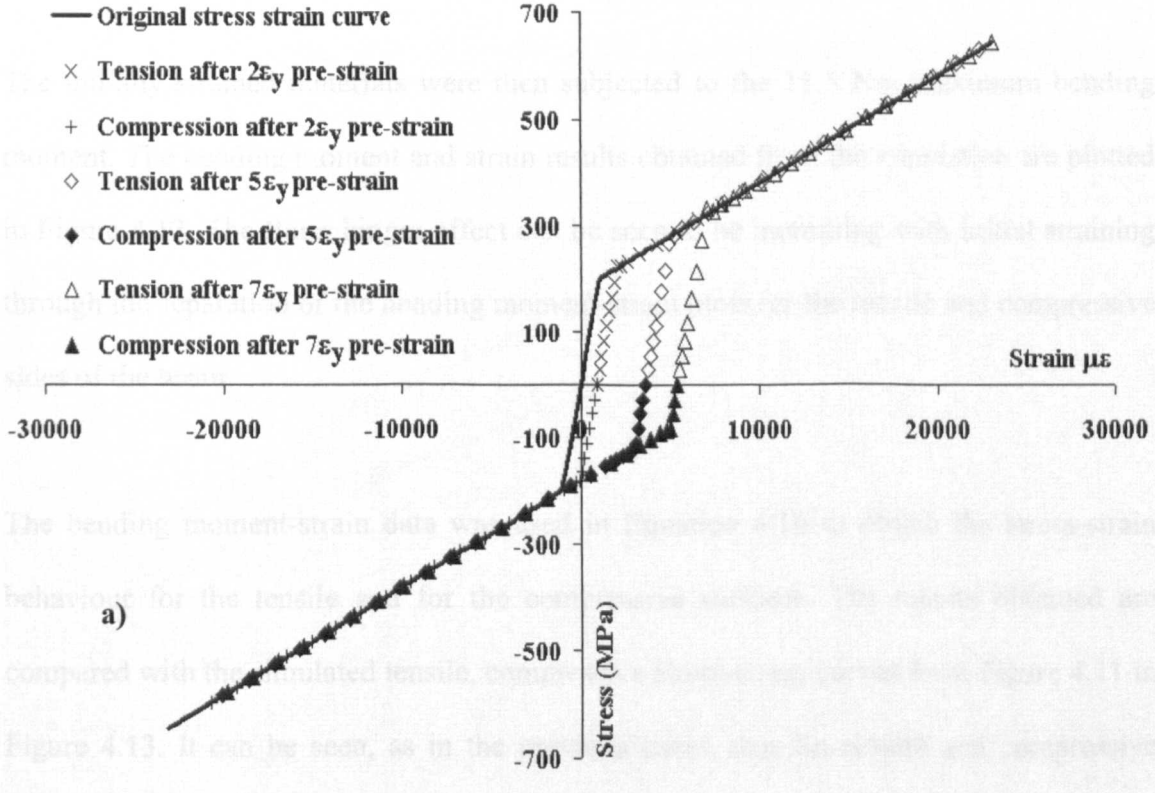

Figure 4.11.- Linear Ziegler hardening behaviour a) effect of different levels of tensile pre-strain on tension and compression behaviour

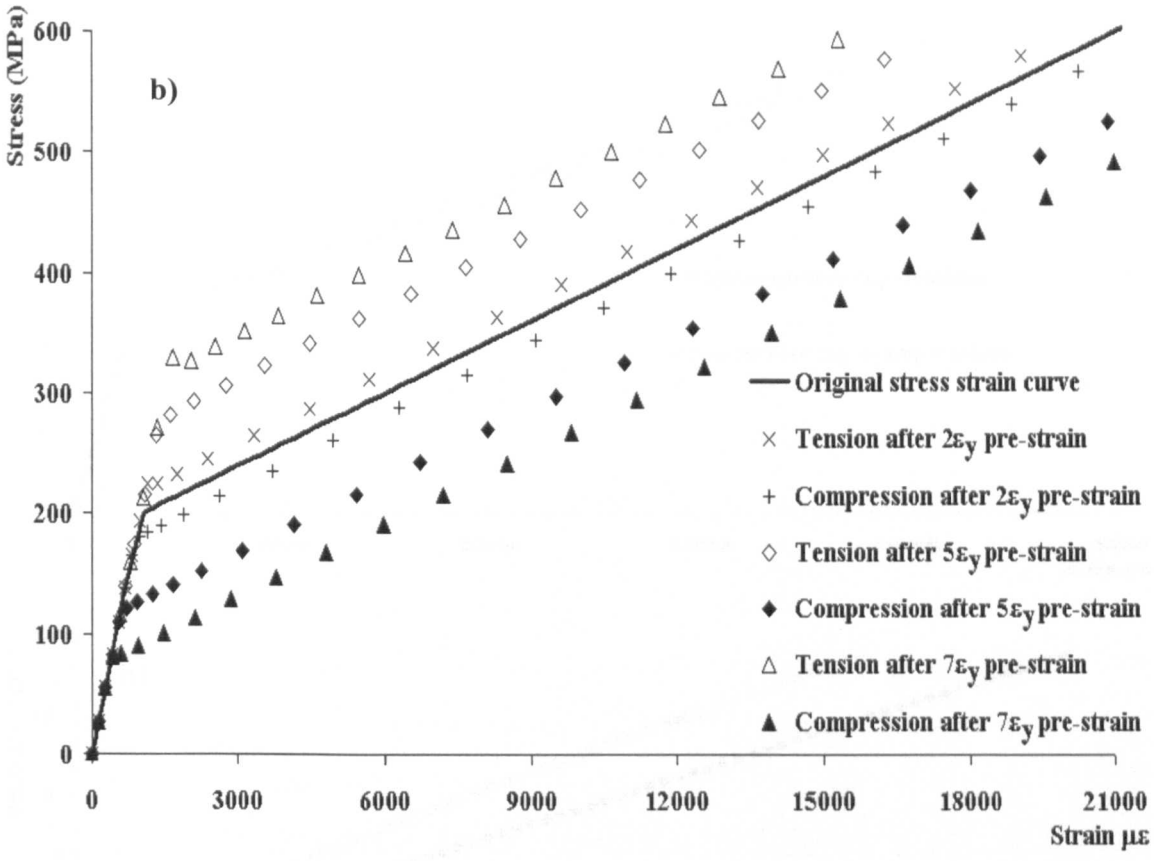

Figure 4.11.- Linear Ziegler hardening behaviour
b) comparison of stress-strain plots

The initially strained materials were then subjected to the 11.5 Nm maximum bending moment. The bending moment and strain results obtained from the simulation are plotted in Figure 4.12. The Bauschinger effect can be seen to be increasing with initial straining through the separation of the bending moment-strain plots for the tensile and compressive sides of the beam.

The bending moment-strain data was used in Equation 4.16 to obtain the stress-strain behaviour for the tensile and for the compressive surfaces. The results obtained are compared with the simulated tensile, compressive stress-strain curves from Figure 4.11 in Figure 4.13. It can be seen, as in the previous cases, that the tensile and compressive stress-strain curves and the derived curves agree closely.

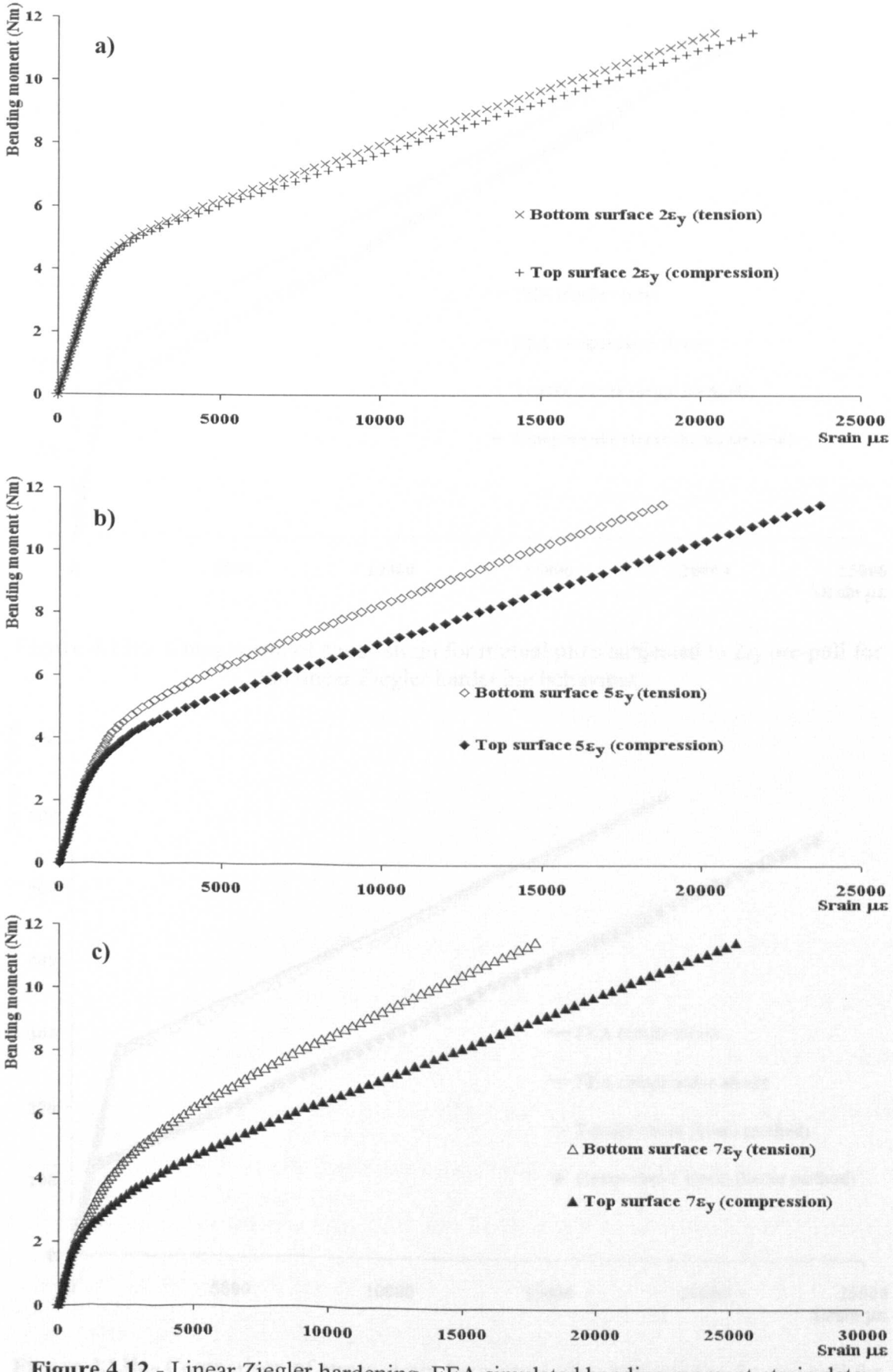

Figure 4.12.- Linear Ziegler hardening, FEA simulated bending moment-strain data a) $2\varepsilon_y$ tensile pre-strain case b) $5\varepsilon_y$ tensile pre-strain case c) $7\varepsilon_y$ tensile pre-strain case

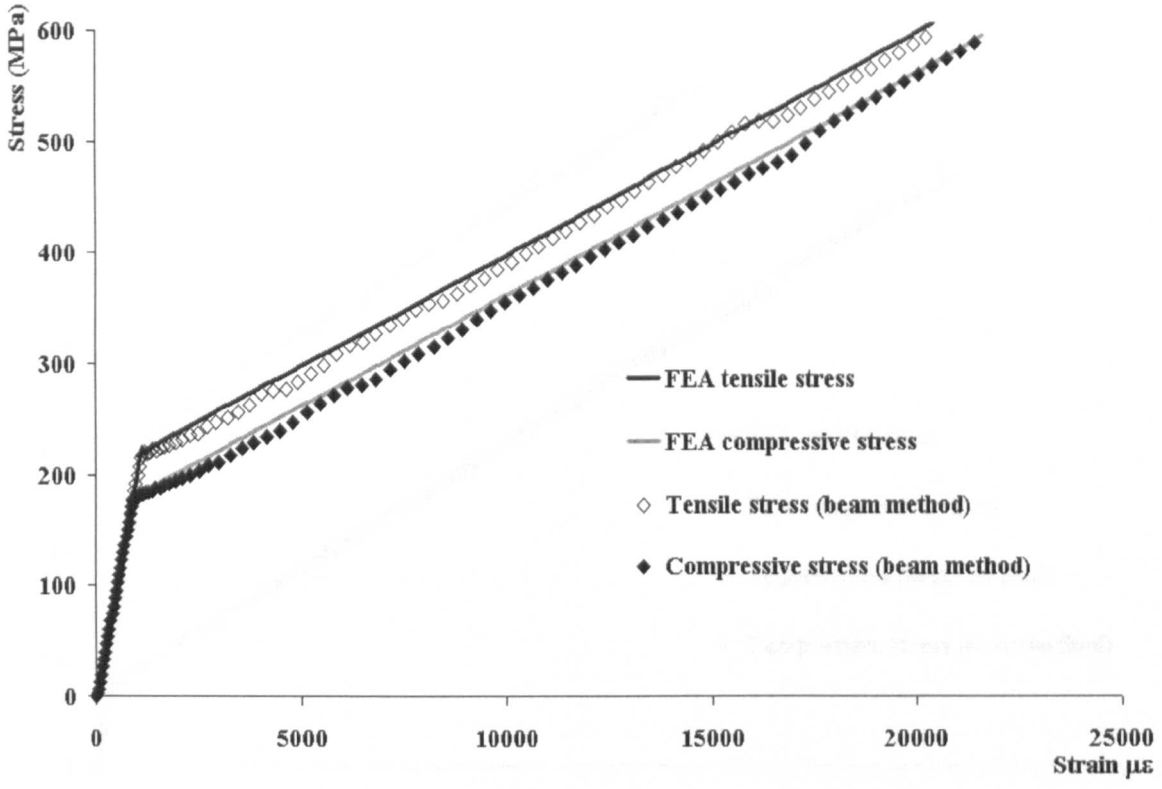

Figure 4.13a.- Comparison of stress-strain for mutual plots subjected to $2\varepsilon_y$ pre-pull for the linear Ziegler hardening behaviour

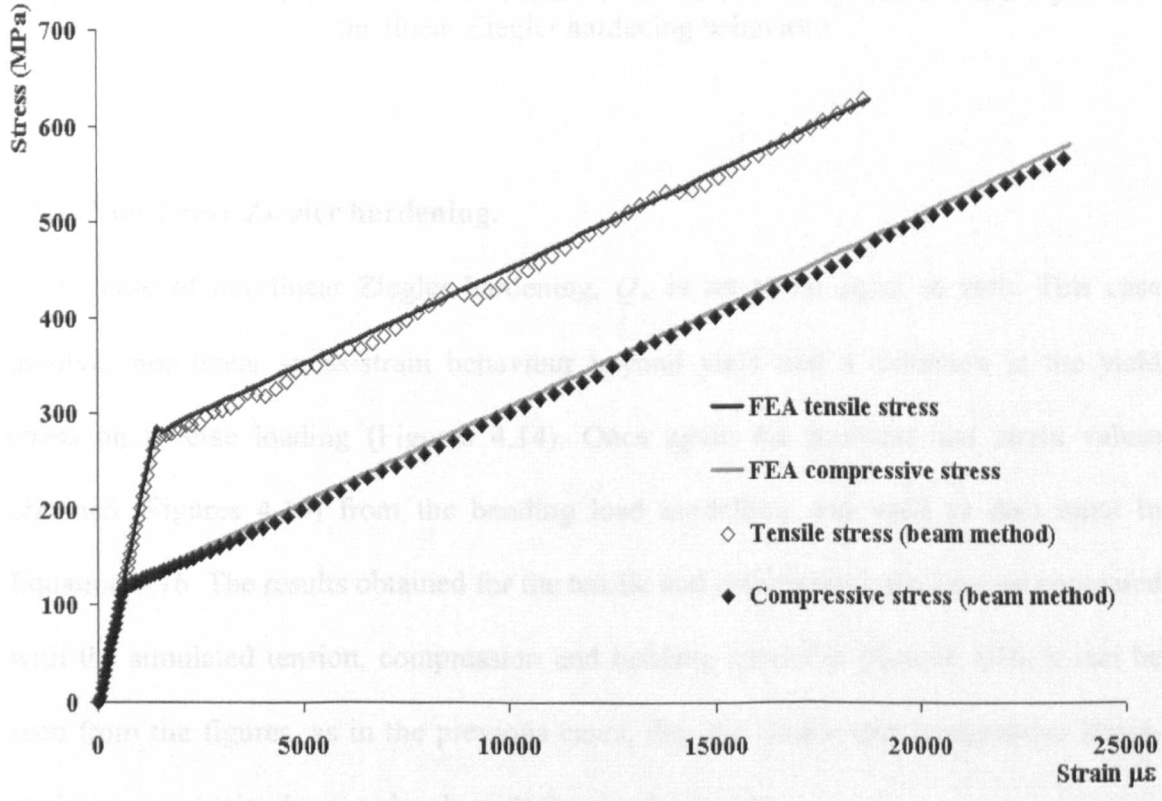

Figure 4.13b.- Comparison of stress-strain for mutual plots subjected to $5\varepsilon_y$ pre-pull for the linear Ziegler hardening behaviour

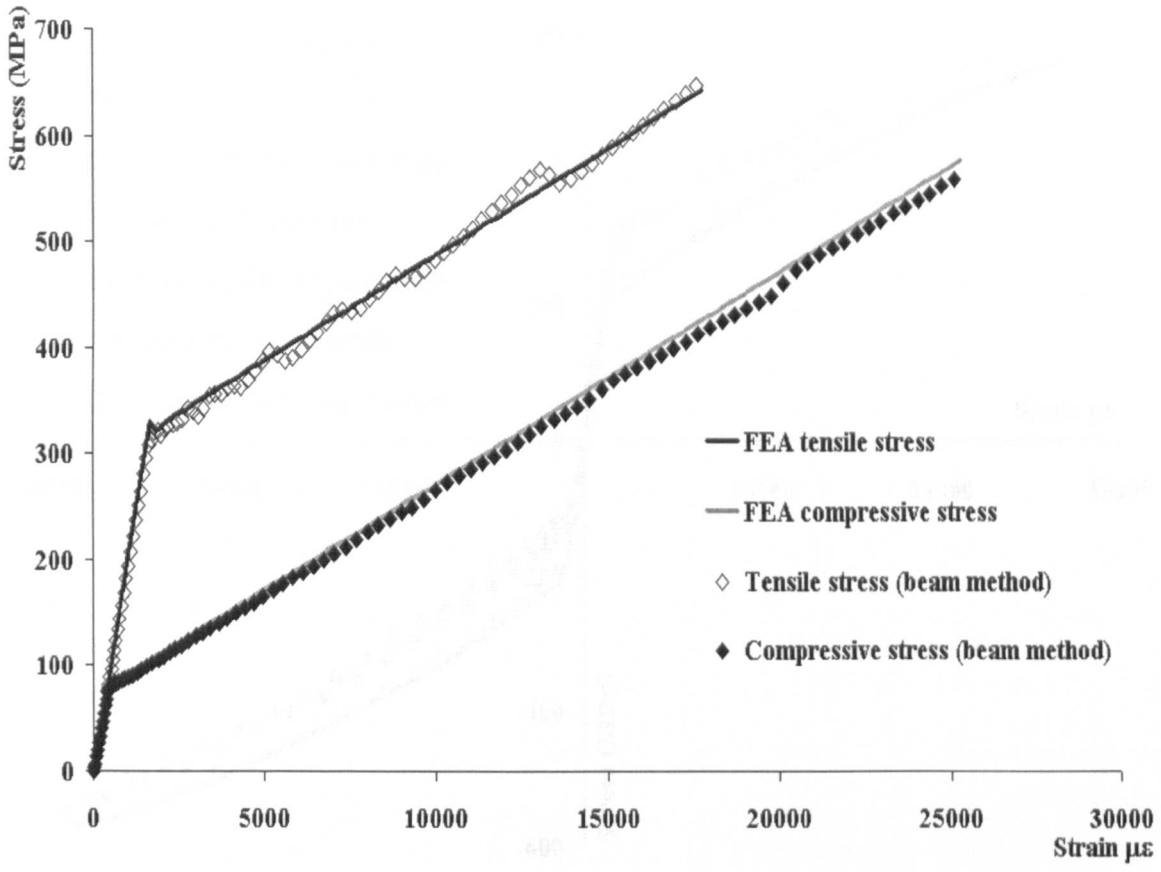

Figure 4.13c.- Comparison of stress-strain for mutual plots subjected to $2\varepsilon_y$ pre-pull for the linear Ziegler hardening behaviour

4.3.6. Non-linear Ziegler hardening.

In the case of non-linear Ziegler hardening, Q_α is set to be equal to zero. This case involves non-linear stress-strain behaviour beyond yield and a reduction in the yield stress on reverse loading (Figures 4.14). Once again the moment and strain values obtained (Figures 4.15) from the bending load modelling was used as data input in Equation 4.16. The results obtained for the tensile and compressive stresses are compared with the simulated tension, compression and bending results in Figures 4.16. It can be seen from the figures, as in the previous cases, that the tensile and compressive stress-strain curves obtained agree closely with the simulated data.

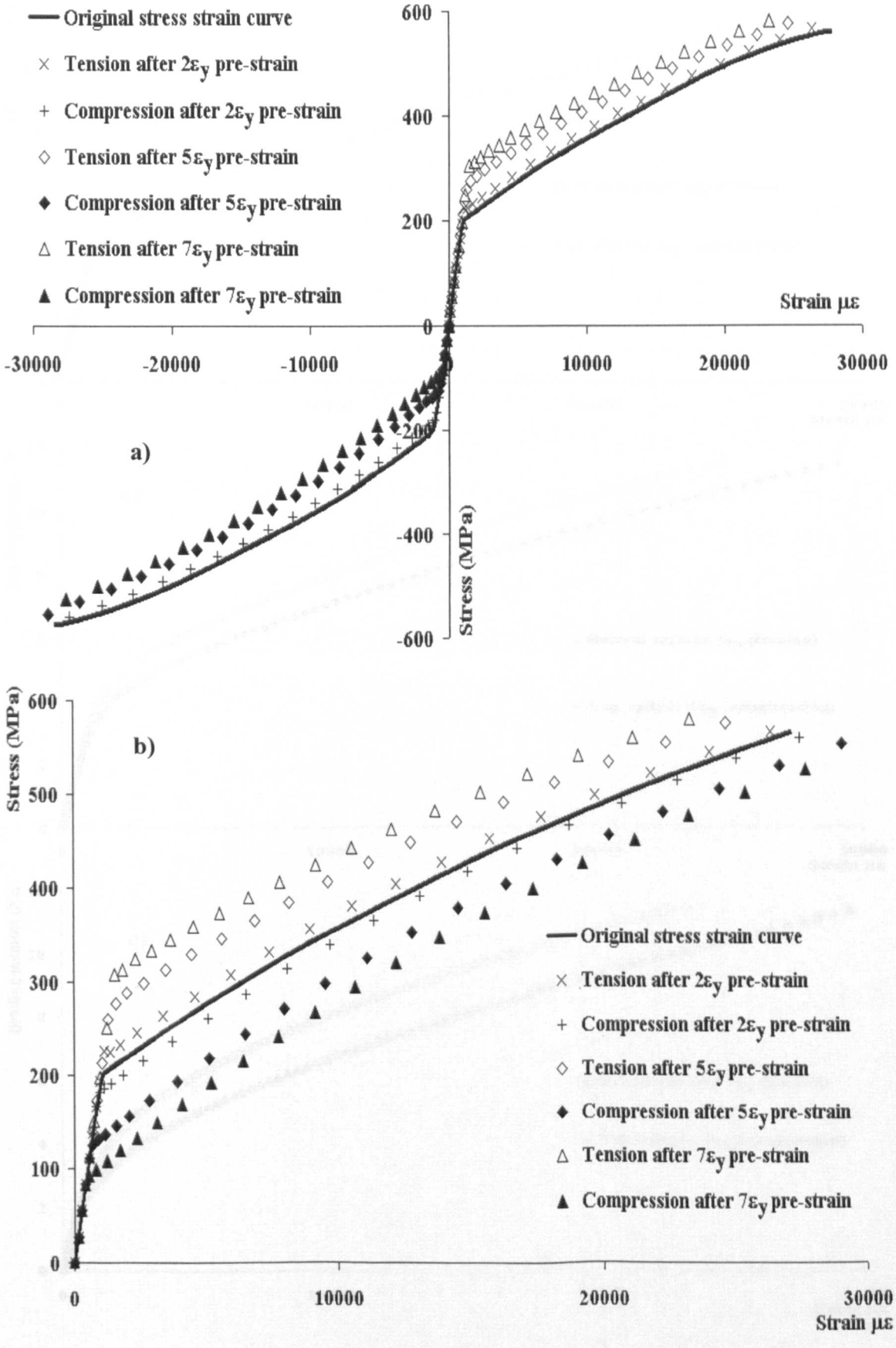

Figure 4.14.- Non-linear Ziegler hardening behaviour a) effect of different levels of tensile pre-strain on tension and compression behaviour b) comparison of stress-strain plots.

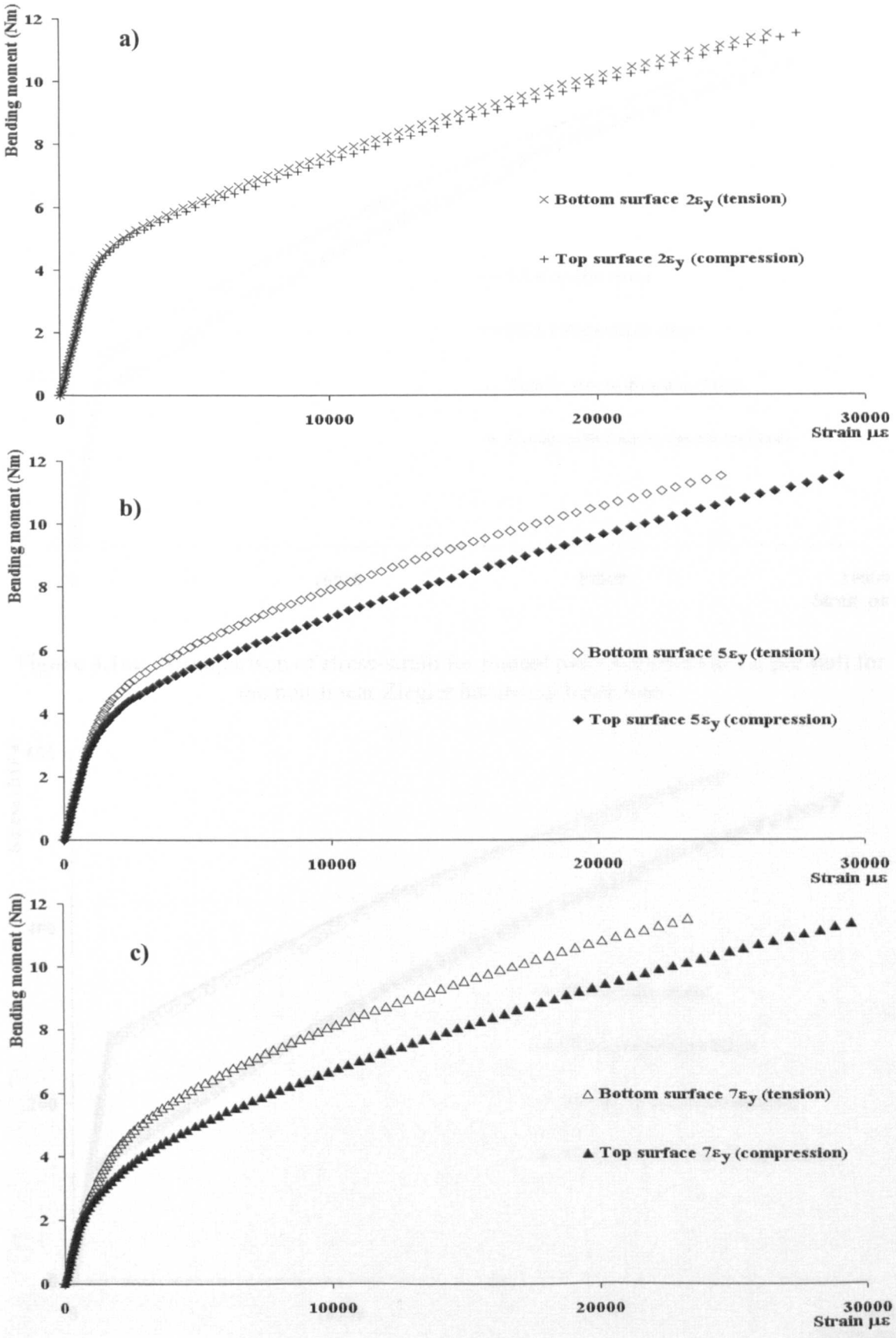

Figure 4.15.- Non-linear Ziegler hardening, FEA simulated bending moment-strain data a) $2\varepsilon_y$ tensile pre-strain case b) $5\varepsilon_y$ tensile pre-strain case c) $7\varepsilon_y$ tensile pre-strain case

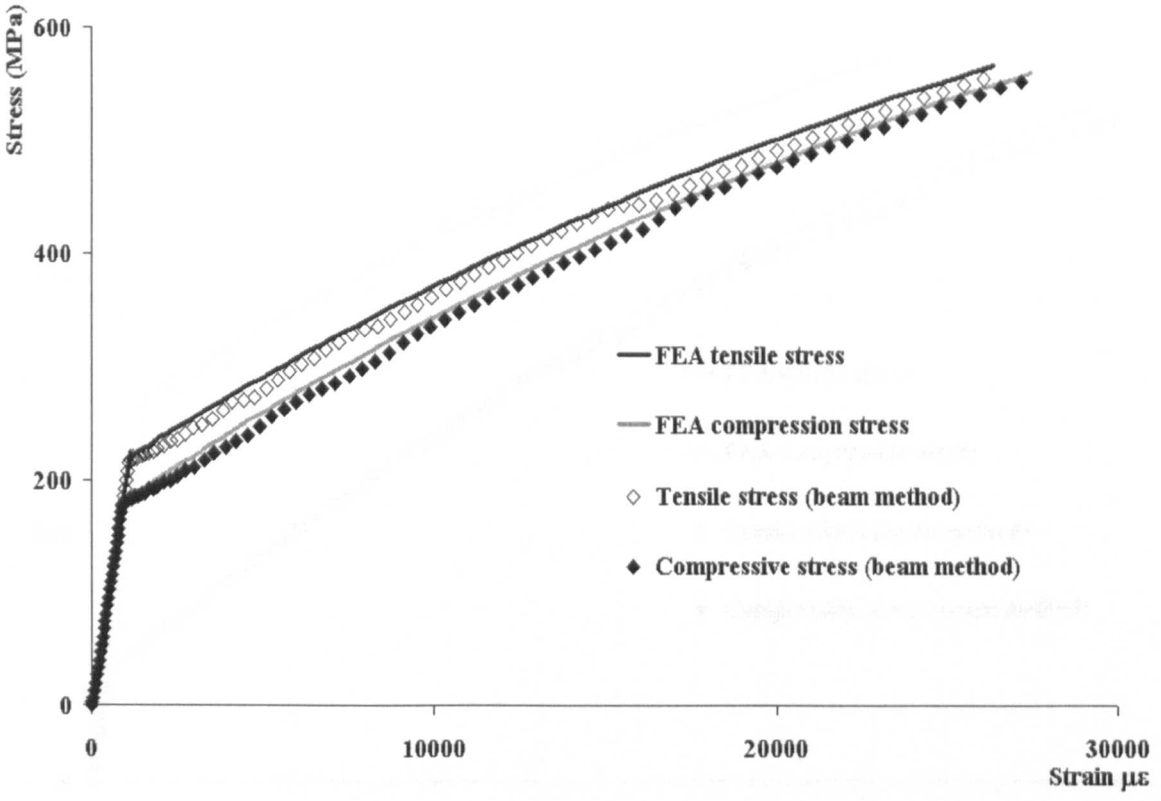

Figure 4.16a.- Comparison of stress-strain for mutual plots subjected to $2\varepsilon_y$ pre-pull for the non-linear Ziegler hardening behaviour

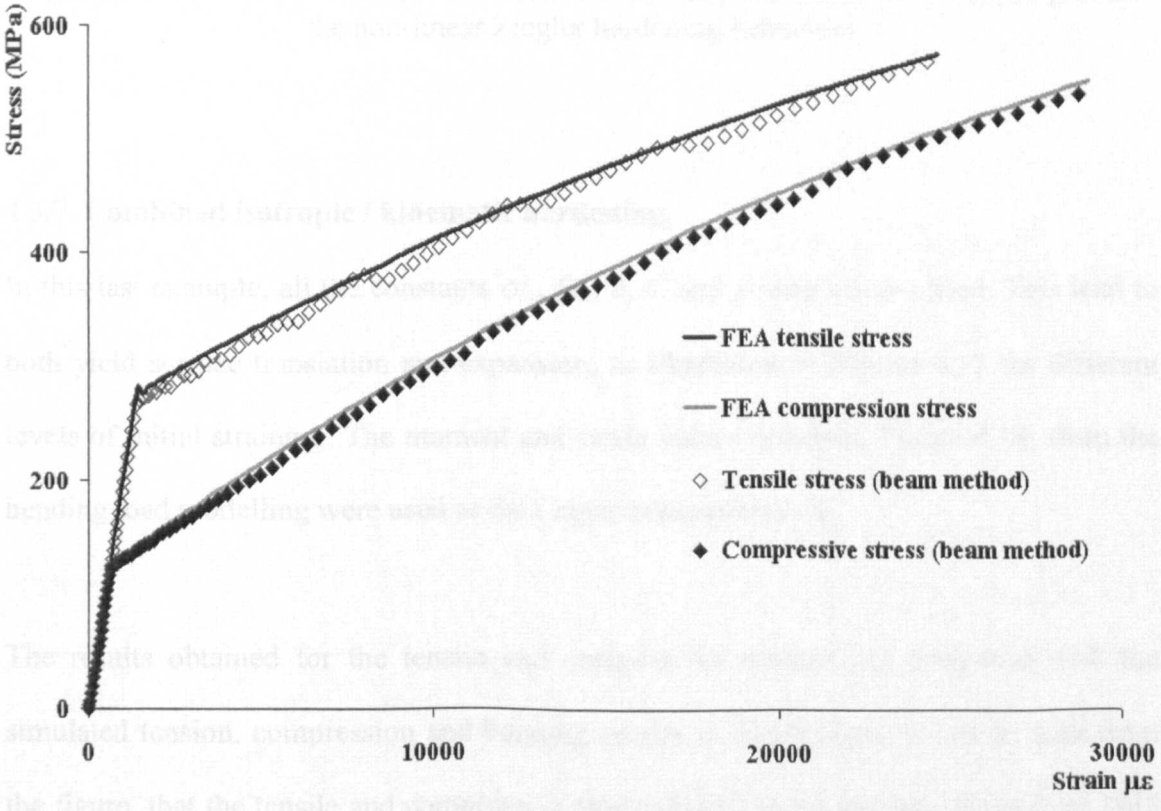

Figure 4.16b.- Comparison of stress-strain for mutual plots subjected to $5\varepsilon_y$ pre-pull for the non-linear Ziegler hardening behaviour

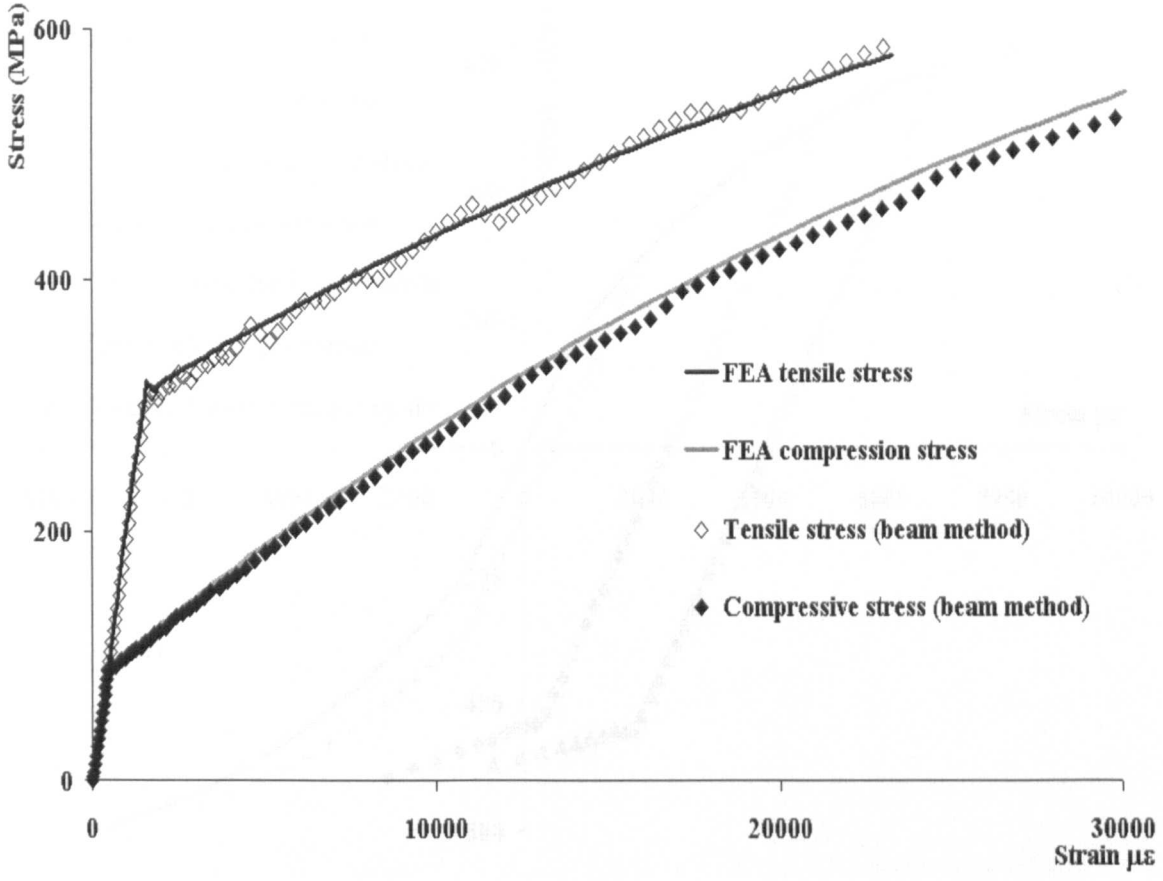

Figure 4.16c.- Comparison of stress-strain for mutual plots subjected to $7\varepsilon_y$ pre-pull for the non-linear Ziegler hardening behaviour

4.3.7. Combined isotropic / kinematic hardening.

In this last example, all the constants σ_o, Q_∞, b, C and γ were all specified. This lead to both yield surface translation and expansion, as illustrated in Figures 4.17 for different levels of initial straining. The moment and strain values obtained, Figure 4.18, from the bending load modelling were used as data input in equation 4.16.

The results obtained for the tensile and compressive stresses are compared with the simulated tension, compression and bending results in Figure 4.19. It can be seen from the figure, that the tensile and compressive stress-strain curves and the curves from both approaches agree closely.

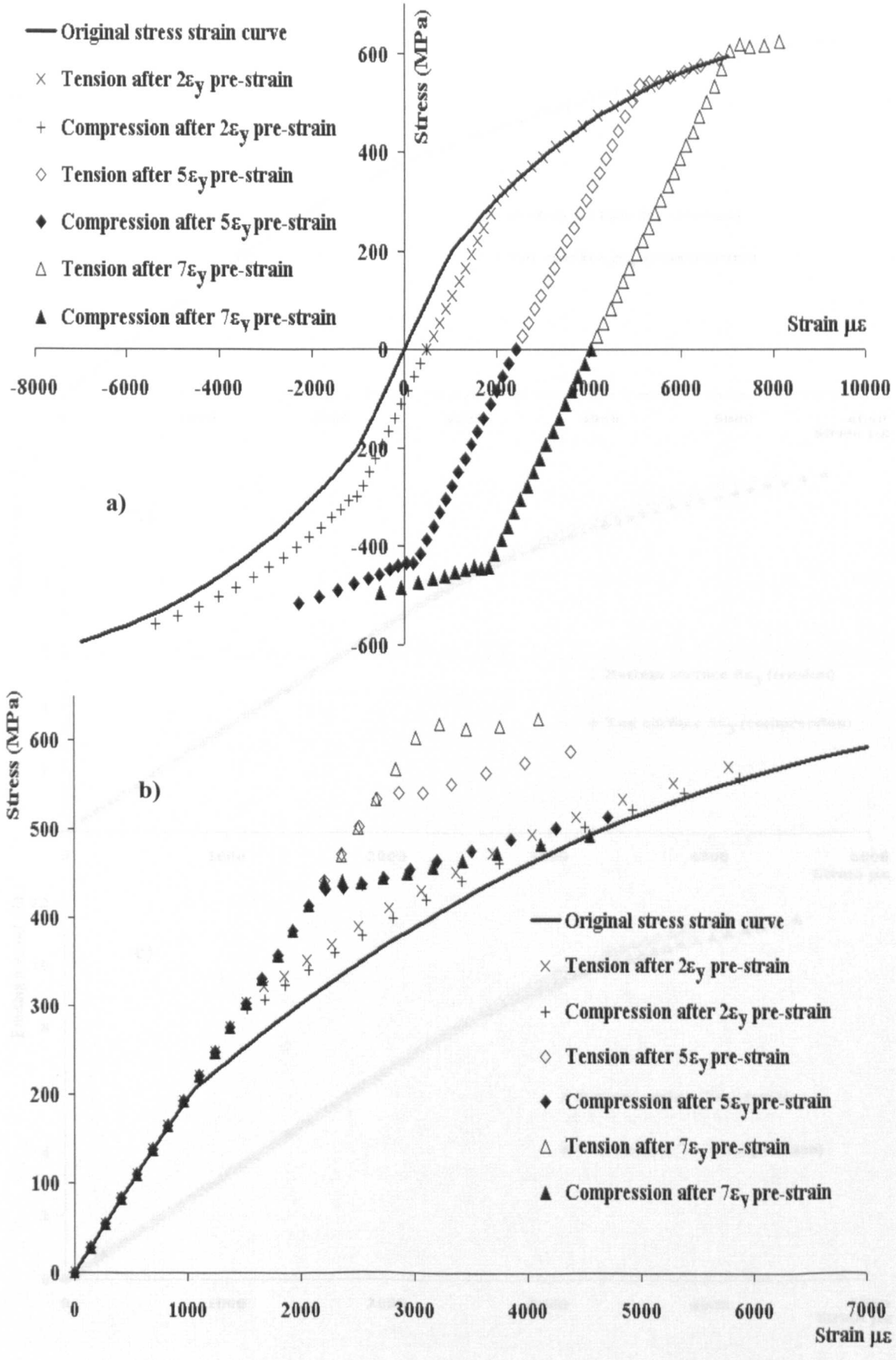

Figure 4.17.- Combined hardening behaviour a) effect of different levels of tensile pre-strain on tension and compression behaviour b) comparison of stress-strain plots.

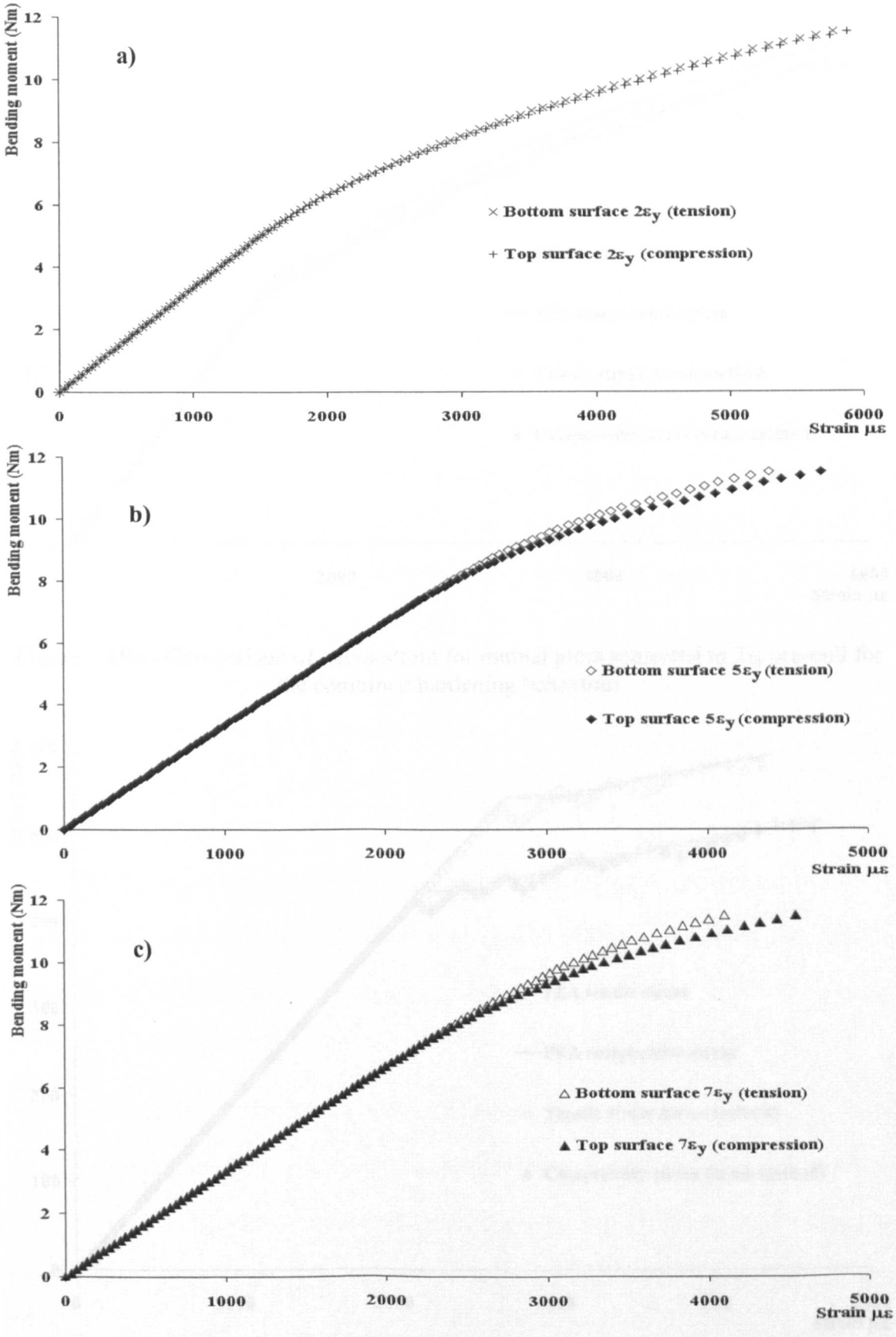

Figure 4.18.- Combined hardening, FEA simulated bending moment-strain data a) $2\varepsilon_y$ tensile pre-strain case b) $5\varepsilon_y$ tensile pre-strain case c) $7\varepsilon_y$ tensile pre-strain case

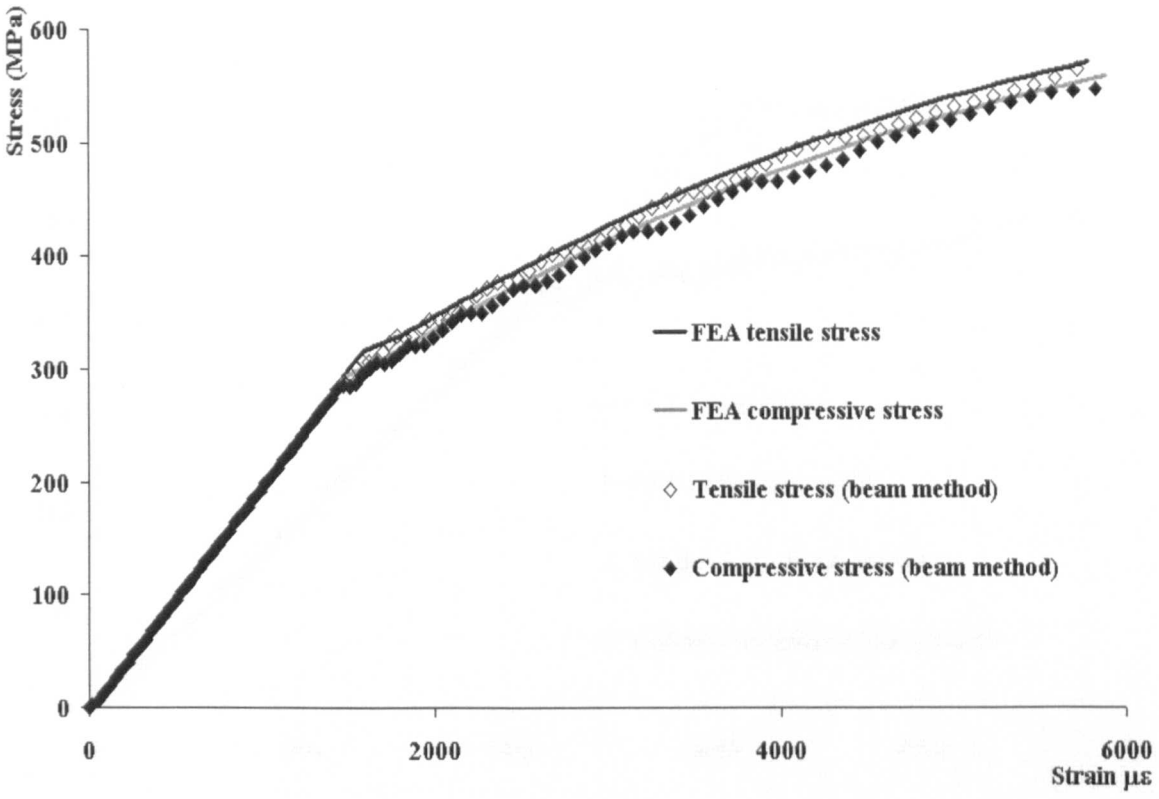

Figure 4.19a.- Comparison of stress-strain for mutual plots subjected to $2\varepsilon_y$ pre-pull for the combined hardening behaviour

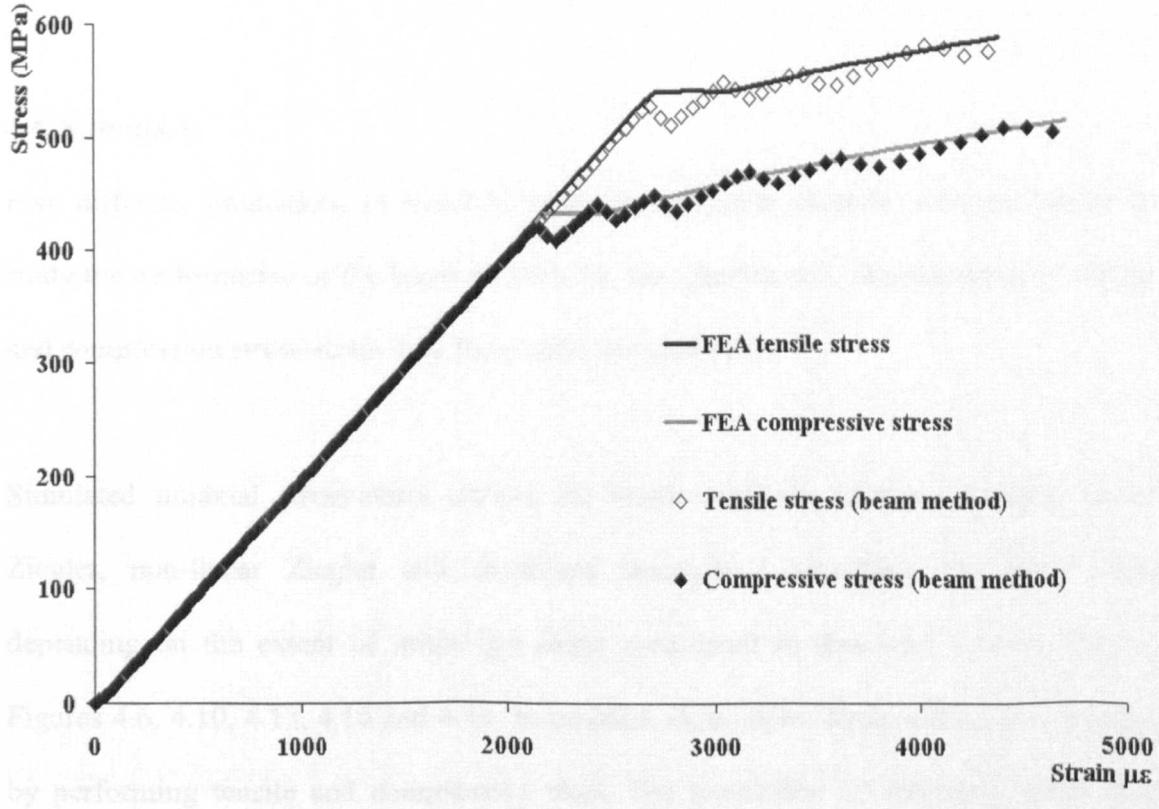

Figure 4.19b.- Comparison of stress-strain for mutual plots subjected to $5\varepsilon_y$ pre-pull for the combined hardening behaviour

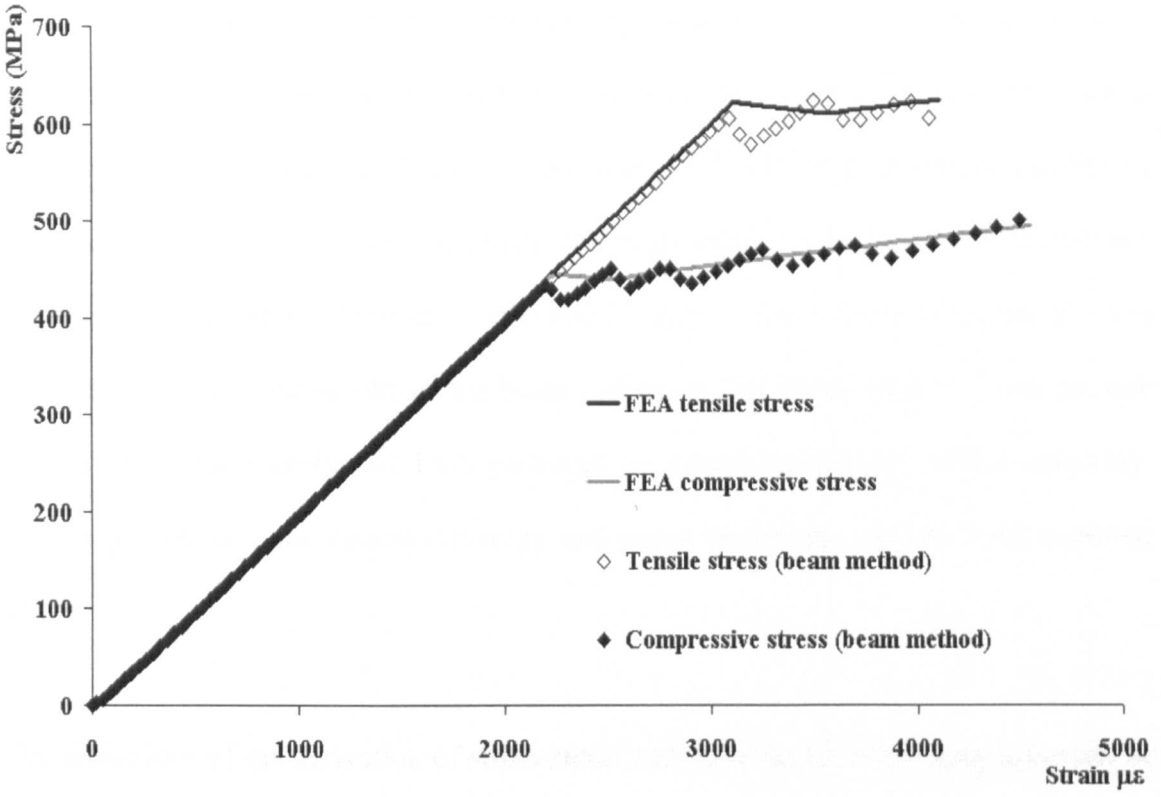

Figure 4.19c.- Comparison of stress-strain for mutual plots subjected to $7\varepsilon_y$ pre-pull for the combined hardening behaviour

4.4. Summary.

Five different simulations of material behaviour by finite element were performed to study the performance of the beam method for the simultaneous determination of tensile and compression stress-strain data from bend test data only.

Simulated uniaxial stress-strain curves for elastic-perfectly plastic, isotropic, linear Ziegler, non-linear Ziegler and combined isotropic / kinematic hardening cases depending on the extent of initial pre-strain considered in this work can be seen in Figures 4.6, 4.10, 4.13, 4.16 and 4.19. In practice, these stress-strain curves are obtained by performing tensile and compressive tests. The possibility of obtaining tensile and compressive stress-strain curves from bend tests alone will reduce the number of tests

that need to be carried out. The beam method proposed in this work provides a process of achieving this objective. The method was explored in this chapter analytically by using simulated data obtained from finite element analysis. Three initial pre-strain conditions were selected to represent low, medium and high initial strain hardening conditions. Excellent agreement is obtained in the elastic region. Some level of oscillation can however be seen in the results of the beam method in the plastic region. These are due effectively to the inability of FEA packages to model Bauschinger effect smoothly. Generally however, the results converge and agree reasonably closely with expected results.

The limitations of the derivation of stress-strain curves using beam bending approach lie primarily in the assumptions of the underlining theory. The theory assumes that the strain at any point in the beam is proportional to the distance from the neutral axis. This assumption is said to hold provided the cross sectional dimensions of the beam is much smaller than the radius of curvature, typically less than one-tenth [*Hearn, 1997*]. A further observation worthy of note with this approach compared to uniaxially testing is the absence of the possibility of necking. In this regard, the approach is not less disadvantaged compared to compression tests because barrelling occurs. None of the bending analysis considered here exceeded the 5% strain limit at which Poisson's lateral deformation effects can be considerable. Exceeding 5% strain will have necessitated the consideration of true stress-strain behaviour. This effect was considered in the calculation but did not change results significantly. *Hearn,* [*1997*] *and Mayville and Finnie* [*1982*] discuss the limitations of the use of the simple bending theory in detail. The results obtained showed that the discretisation of the load in to about 100 increments should give very good results up to the limiting bending strain of 5% considered in this work.

Although the method has been presented as a method for deriving tensile and compression stress-strain curves from bend tests for materials under Bauschinger effect, it is applicable to any situation where the stress-strain behaviour in the tensile part is unique and that in compression part is also unique. This will not be the case in situations where a material has non-uniform macro residual stress inherent. In such situations each material point will have a stress-strain behaviour that is generally different from those from other parts of the same material.

Chapter 5

Experimental testing of the beam method for the determination of stress-strain behaviour

5.1. Introduction.

In this chapter, the beam method for the simultaneous determination of tensile and compressive stress-strain data from bend tests only, developed in Chapter 4, is evaluated experimentally. The aim of the work was to validate the method for determining stress-strain curves from bend tests, especially under asymmetric behaviour such as that caused by the Bauschinger effect.

5.2. Materials.

The materials used in this investigation were steel and aluminium alloys. Two steels EN 1A (230M07) and EN 8 (080M40) [*Mac Readys, 1991*] and one aluminium alloy AA 6082 T6 [*Smithells, 1992*] were considered (steel EN 8 was only used in this section to test the rig but is used extensively in the chapter where the crack compliancy is evaluated experimentally).

These three materials are used extensively in the automotive, mechanical and general engineering industries. Applications include gears, shafts, spanners, rollers, bolts, studs, etc and the chemical compositions of alloying elements in percentage are given in Tables 5.1a and 5.1b.

Table 5.1a.- Aluminium alloy

Aluminium Alloy	Mg	Si	Mn
6082 T6	1.0	1.0	0.7

Table 5.1b.- Steels

Steel	C	Mn	S	Si	P	Pb	Te
EN 1A	0.15 max.	0.9 – 1.3	0.25 – 0.35	-	0.07 max.	0.12 -0.35	0.03 -0.05
EN 8	0.36 – 0.44	0.6 – 1.0	0.05 max	0.1 – 0.4	0.05 max	-	-

Batches of 10 mm by 10 mm by 6 m bars were obtained for the EN 1A (230M07) and 12.7 mm by 38.1 mm by 6 m for the EN 8 (080M40) materials. The material obtained for the aluminium alloy AA 6082 T6 tests had dimensions of 9.8 mm by 12.7 mm and 6 m long. Batches of specimens were prepared as described in section 5.2.3.

5.2.1. Cold drawn material.

The idea to research the Bauschinger effect arose as a result of bending tests carried out on steel EN 8 (080M40) specimens that were in the as received condition, even though annealed specimens had been ordered. For the specimens, in the as received condition, it was noticed that the action of a plastic bending moment produced a different numerical strain response at opposite surfaces of the beam. The numerical strain value obtained at the surface suffering from the compressive action of the bending moment was, in all cases, higher than the numerical strain value obtained at the surface under the tensile action (Figure 5.1). It was also noticed that early yielding occurred at the surfaces under compressive loading, Figure 5.1.

The initial thought of this strain inequality was that the bending rig was causing an additional pulling effect. In order to eliminate the supposed pulling effect, the pins on the rig were left loose and layers of PTFE were positioned between contact surfaces in order

to reduce grip due to friction. However this did not solve the apparent problem, moreover the combination of tensile and bending loading should show reduced straining on the compression side and higher strain on the tensile side as illustrated in Figure 5.2.

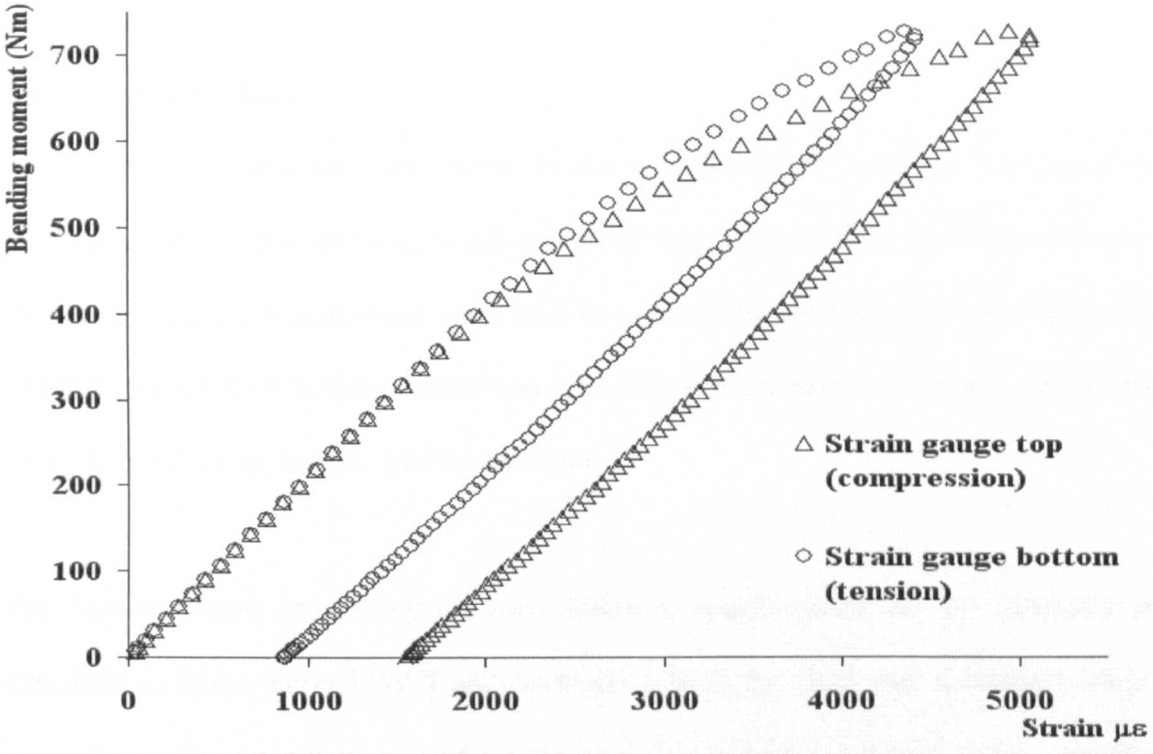

Figure 5.1.- Bending test showing Bauschinger effect

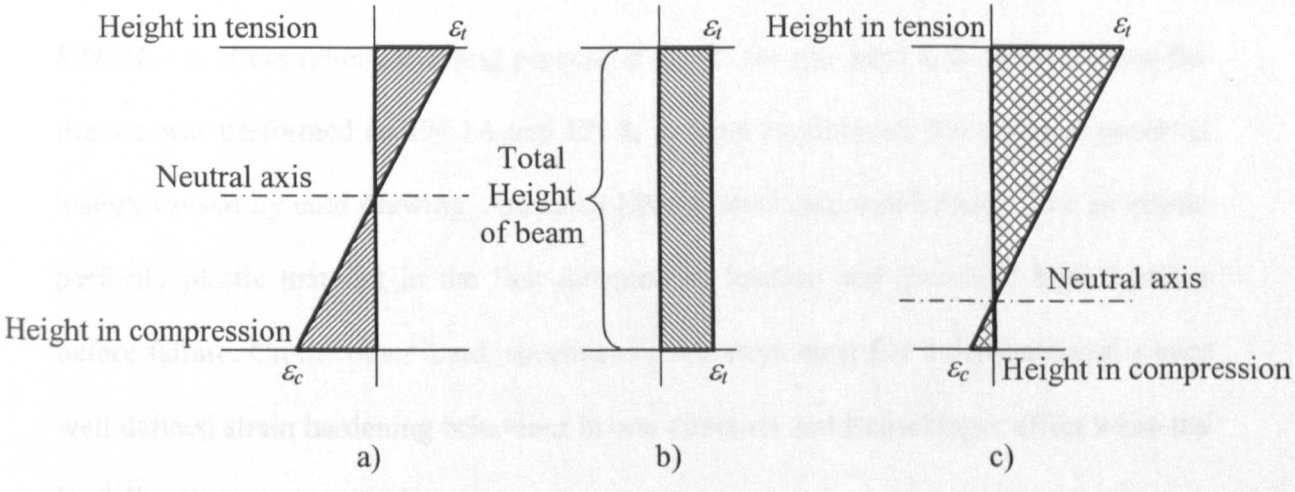

Figure 5.2.- Strain representation of bending and pulling effect in a rectangular beam
a) strain due to bending b) strain due to pull c) overall strain

It was therefore concluded that the material was exhibiting the Bauschinger effect. This was confirmed by annealing the material and repeating the bend tests; the results of which showed strain symmetry at the top and bottom surfaces. The anomaly prompted a study of the effect of prior straining on mechanical properties.

5.2.2. Heat treatment.

A number of heat treatment conditions for the materials were considered. An annealing heat treatment was chosen because this process eliminates the effects of previous history. Different annealing temperatures were used for each of the selected materials. One batch of EN 8 (080M40) (cold drawn) steel was left in the as received condition as a further test of the limit of the applicability of the methods.

The heat treatment process cycles used followed specifications for the materials as described in *Nabertherm* [*1997*] and *Smithells* [*1992*] for steel and aluminium alloys respectively. The temperatures used for the annealing and further details on the materials are as described below.

STEEL.- A stress relief annealing process at 660°C for one hour and cooling inside the furnace was performed on EN 1A and EN 8, in order to eliminate the effect of previous history caused by cold drawing. Annealed EN 1A steel responded almost like an elastic perfectly plastic material in the first direction of loading and presented high ductility before failure. On the other hand, specimens made from steel EN 8 demonstrated a very well defined strain hardening behaviour in one direction and Bauschinger effect when the load direction was reversed.

To avoid oxidation during the heat treatment process, semi-vacuum metallic bags made from thin sheets of medium carbon steel were used. The bags were pressed tightly round the specimens in order to squeeze out as much air as possible. The small quantity of oxygen left inside when sealed reacts spontaneously with the inner layer of the bag during heating in the furnace. By following this procedure, the specimens were annealed with virtually no oxidation visible.

Figure 5.3 shows a picture of the 2kW electric furnace (Wild Barfield, Model GMl) used for all annealing processing carried out. Figure 5.4 shows a picture of a metallic semi-vacuum bag used to avoid oxidation.

Figure 5.3.- Annealing furnace

Figure 5.4.- Semi-vacuum metallic bag

Aluminium.- The specimens made from the aluminium alloy (AA 6082 T6) were annealed, using two different procedures: A batch of specimens were stress relief annealed for 25 minutes at 250°C and a second batch was fully annealed for 1.25 hours at 385°C. Stress relief annealing process does not change the microstructure of the alloy, the strength and ductility of the material are slightly reduced and slightly increased respectively. On the other hand, full annealing processes change the microstructure of the alloy and produced a material with high levels of ductility. During both processes the specimens were left in the furnace to cool down slowly.

The reason for doing two annealing procedures for the aluminium alloy was to produce two different levels of ductility. When separated uniaxial tests in tension and compression were performed on these specimens it was perceived that; the stress relief annealed specimens showed low strain hardening under cyclic loading condition and when the load was uniaxially reversed in direction, a very well defined Bauschinger effect was noticed.

On the other hand, the fully annealed specimens presented a higher rise in the yield stress every time they were uniaxially strain hardened and a Bauschinger effect was unmistakable when the uniaxial loading was reversed. In all cases the fully annealed specimens showed higher ductility than the stress relief annealed specimens.

5.2.3. Specimen manufacture.

It was necessary to carry out different types of tests to meet the needs of the research. Tensile tests were carried out to characterise the stress-strain curve of the selected materials in each condition and also to induce strain hardening in some beam specimens. Dog bone uniaxial tensile specimens were manufactured following specifications from *BSI 10003* [*1990*]. Compression tests were carried out to characterise the stress-strain curves of all selected materials and to evaluate any Bauschinger effect induced in specimens by previous uniaxially loading. Compression tests for each particular condition were carried out on cylindrical specimens of 10 mm diameter and 15 mm height [*Dowling, 1993*]. All bend testing were performed on a four-point bending rig and the total length of the rectangular beams used was 250 mm.

5.3. Four-point testing rig.

Due to its conceptual elegance and simplicity, four-point bending tests have been used in structural experiments for many years [*Dowling, 1993*]. The main advantage of this type of test is that beams that are symmetrically loaded are subjected to a constant bending moment over the central portion of the beam.

A four-point bending rig was designed and manufactured for the stress-strain determination. The rig manufactured for the work is illustrated in Figure 5.5. Two square

blocks of hard steel (EN 24) were used to construct the frame. Four supports, of cylindrical shape, were positioned into semi-cylindrical slots contained in the blocks. The slots are able to support cylindrical pins allowing free rotation in order to avoid unwanted pulling of the beams. To avoid or reduce friction between the parts, PTFE silicon layers of 2 mm thick were placed between the contact surfaces of the supports and the semi-cylindrical surfaces in the blocks, Figure 5.5.

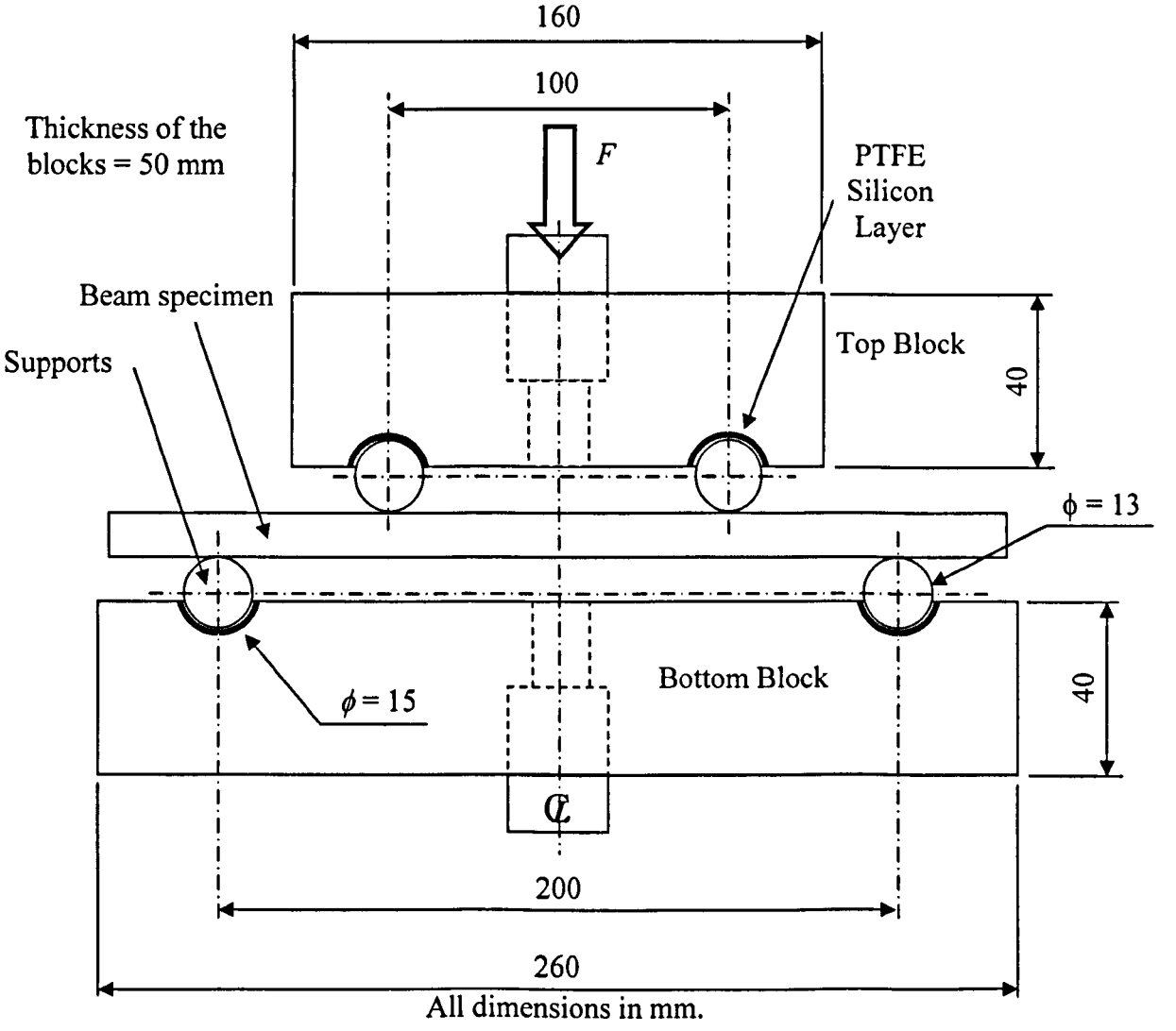

Figure 5.5.- Four-point bending rig

5.4. Strain measurement.

Strain gauges EA-06-060LZ-120 [*Measurement Group, 1992*] were attached to the tensile, compressive surfaces of the beams for the purpose of collecting strain information. The gauges were attached to the beams as illustrated in Figure 5.6.

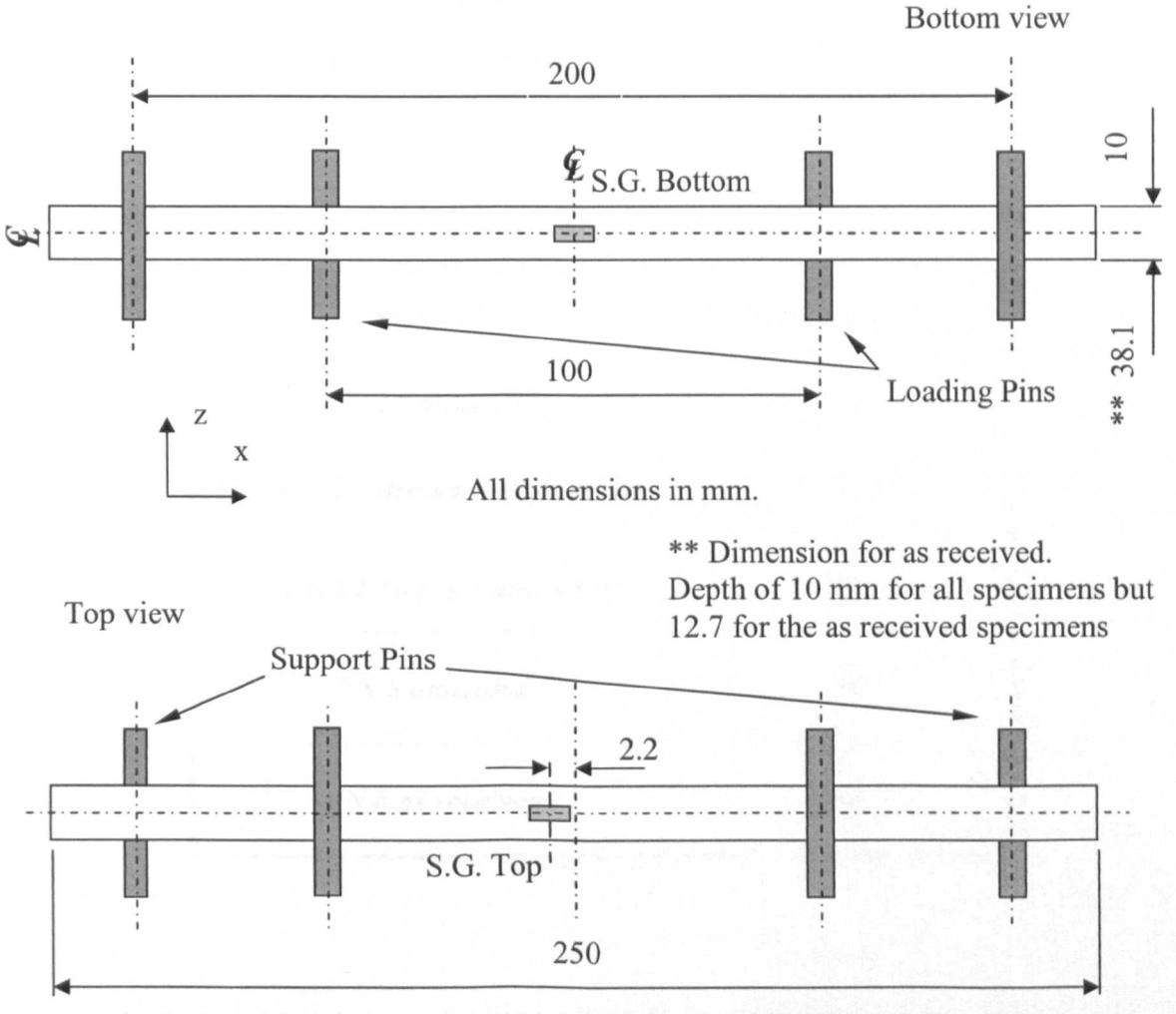

Figure 5.6.- Position of strain gauges on EN 1A, EN 8 and aluminium alloy annealed and pull beam specimens

5.5. Results.

The results of tensile, compression, pre-pulling and bending tests and calculations for the derived properties are detailed in this section. Derived results are compared against actual

tensile and compressive tests. The low and high levels of initial pre-strain hardening considered for EN 1A steel were 10,000 and 25,000 microstrain. The corresponding values for all the aluminium alloy specimens were 15,000 and 30,000 microstrain.

Different bending loads were applied to the annealed and strain hardened materials in order to achieve plastic bending, Table 5.2.

Table 5.2.- Applied bending moment

Material	Bending moment (Nm)
EN 1A annealed	75
AA 6082 T6 stress relief Annealed	55
AA 6082 T6 fully Annealed	26
EN 8 annealed	110
EN 8 as received	730

Limited amount of EN 8 steel specimens were available and only annealed and as received conditions were tested for this material.

5.5.1. Uniaxial test results.

Tensile tests were carried out on the steel and aluminium alloy material. The average tensile stress-strain curves from three tests for the annealed materials are given in Figure 5.7. This figure illustrates the variety of behaviour of the materials.

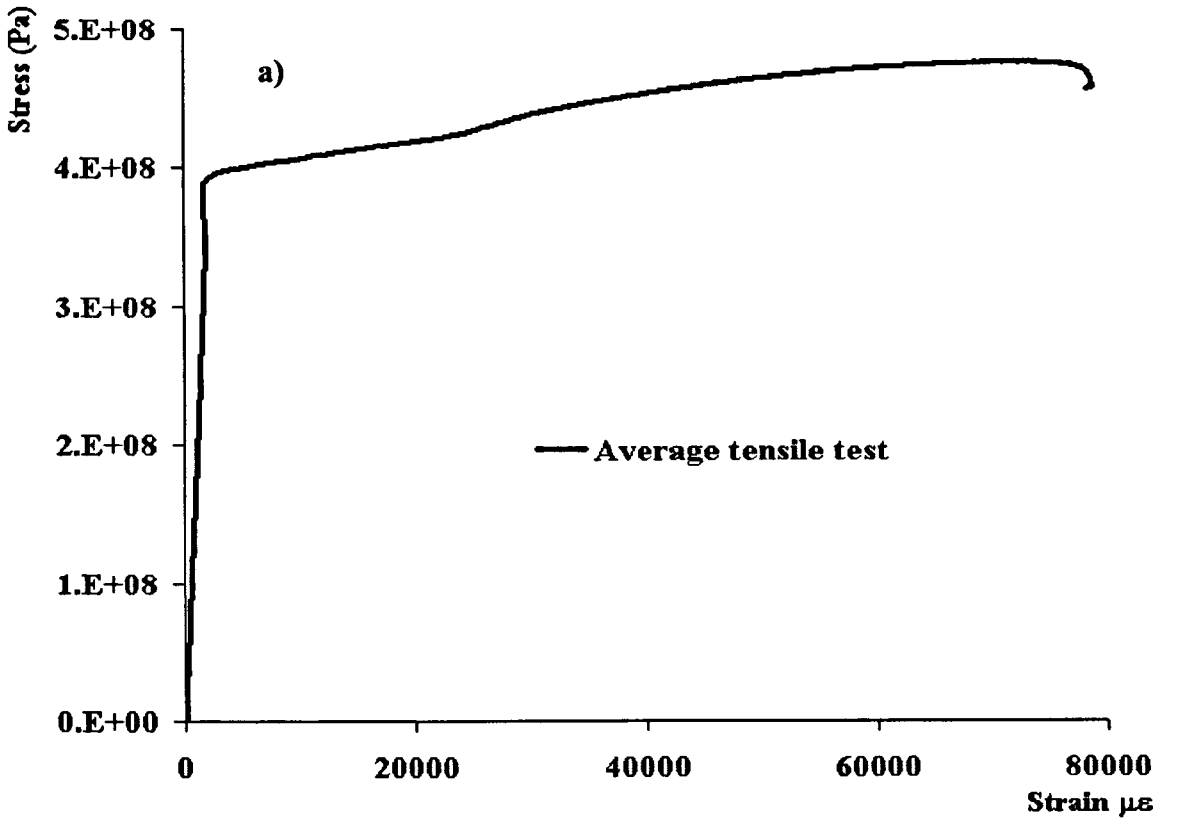

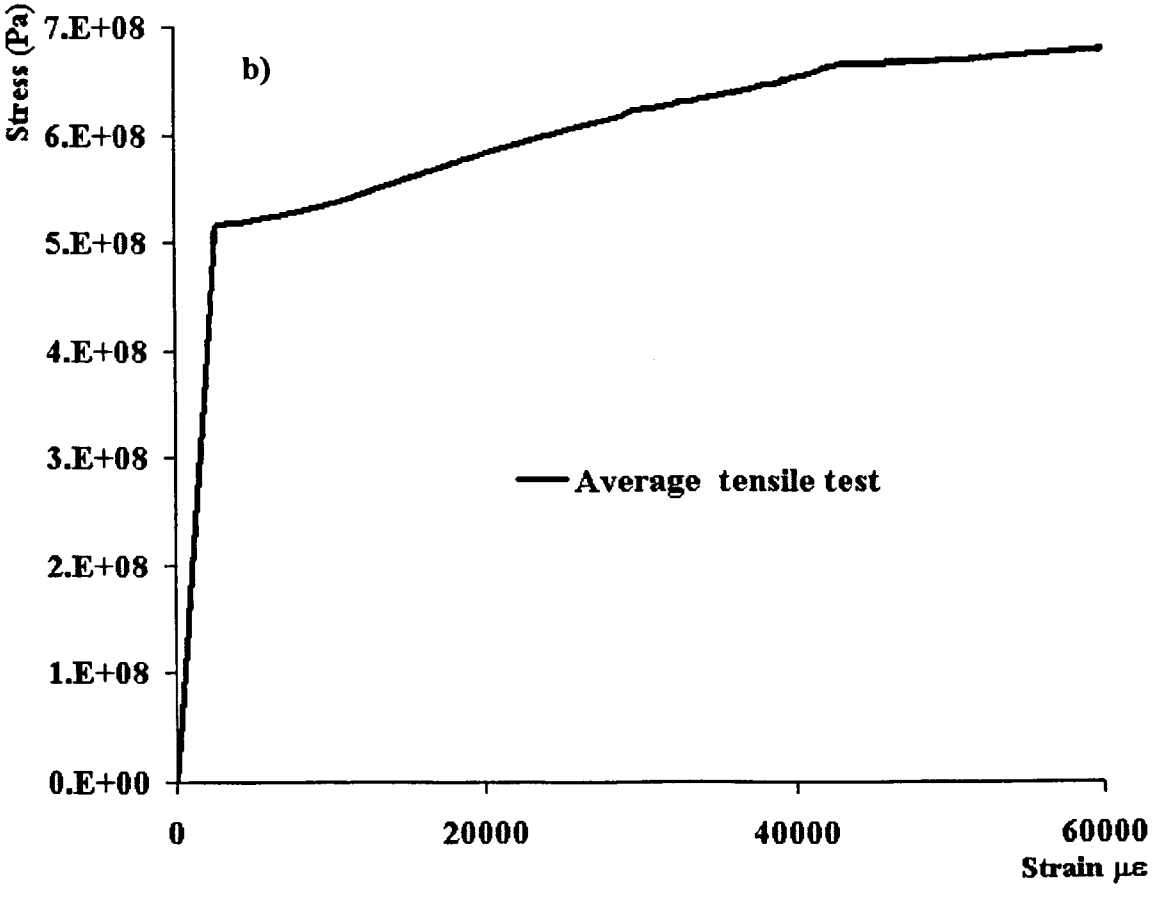

Figure 5.7.- Tensile tests results on annealed condition
a) EN 1A steel b) EN 8 steel

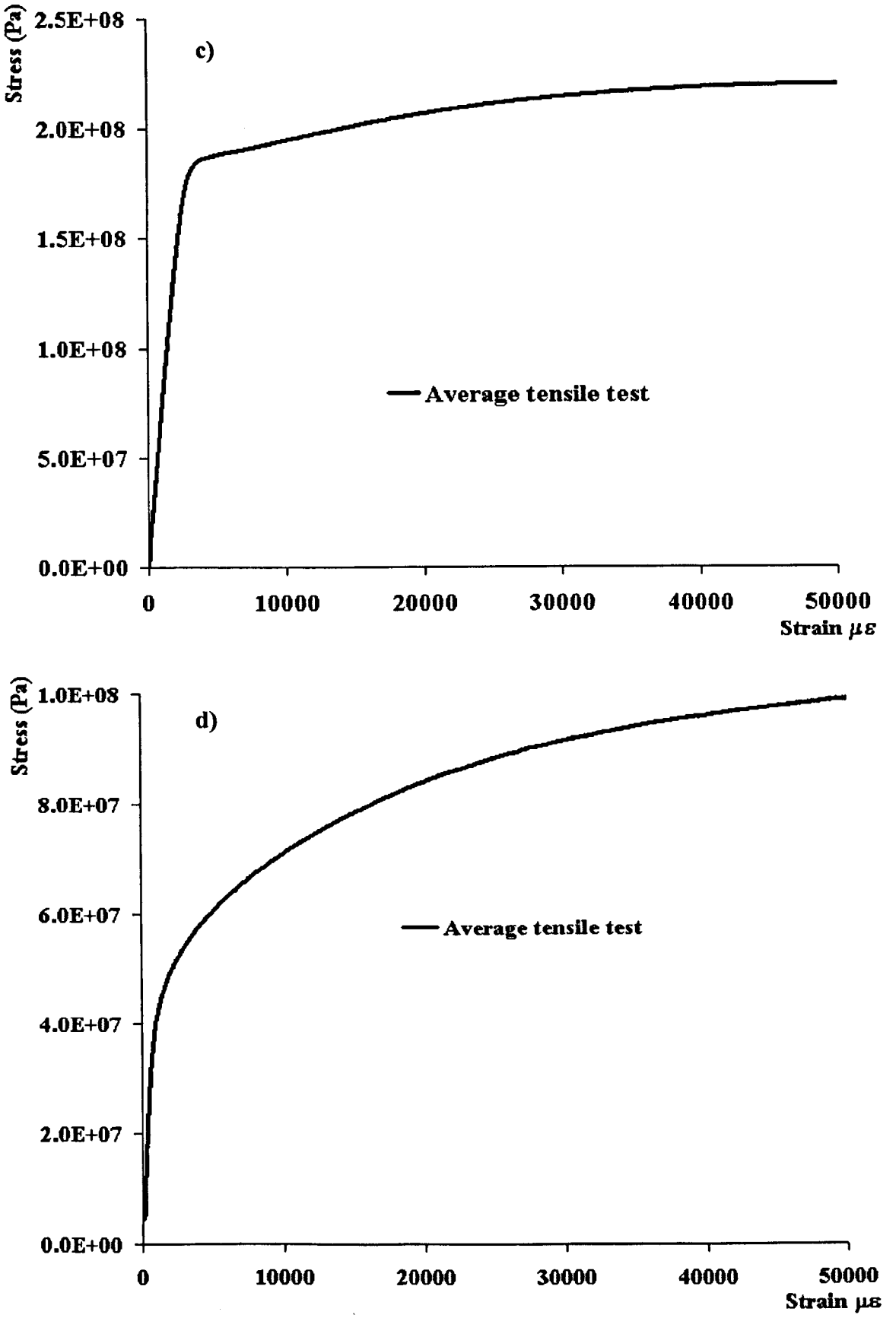

Figure 5.7.- Tensile tests results on annealed condition
c) aluminium alloy stress relief d) aluminium alloy fully annealed

5.5.2. Bending of annealed steel and aluminium beam specimens.

Bending tests were performed on annealed metals in order to provide a base reference for later comparison with the strain hardened beams having Bauschinger effect. The bending moment-strain results obtained from these tests are summarised in Figure 5.8. It can be seen from Figure 5.8 that in each case, the strain readings from the top and bottom surfaces were approximately the same. This observation means that the beam specimens displayed no effect of previous history. It is also important to express that the plots presented in each case is the average of at least three bend tests. The symmetry of the strain response seen in Figure 5.8 indicates that the bend tests had been carried out properly. It can also be seen from these figures that there is no evidence of reversed plastic deformation during the unloading process.

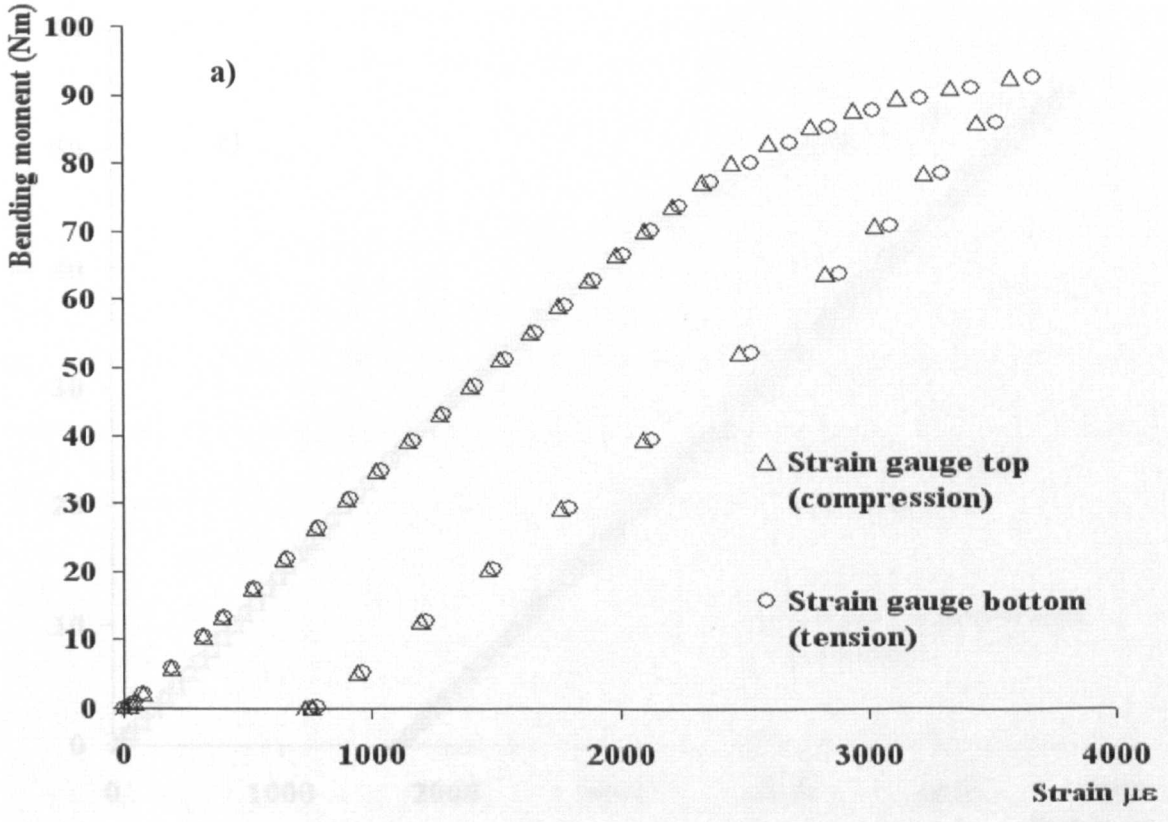

Figure 5.8.- Four-point bending tests on annealed material
a) stress relief annealed EN 1A steel

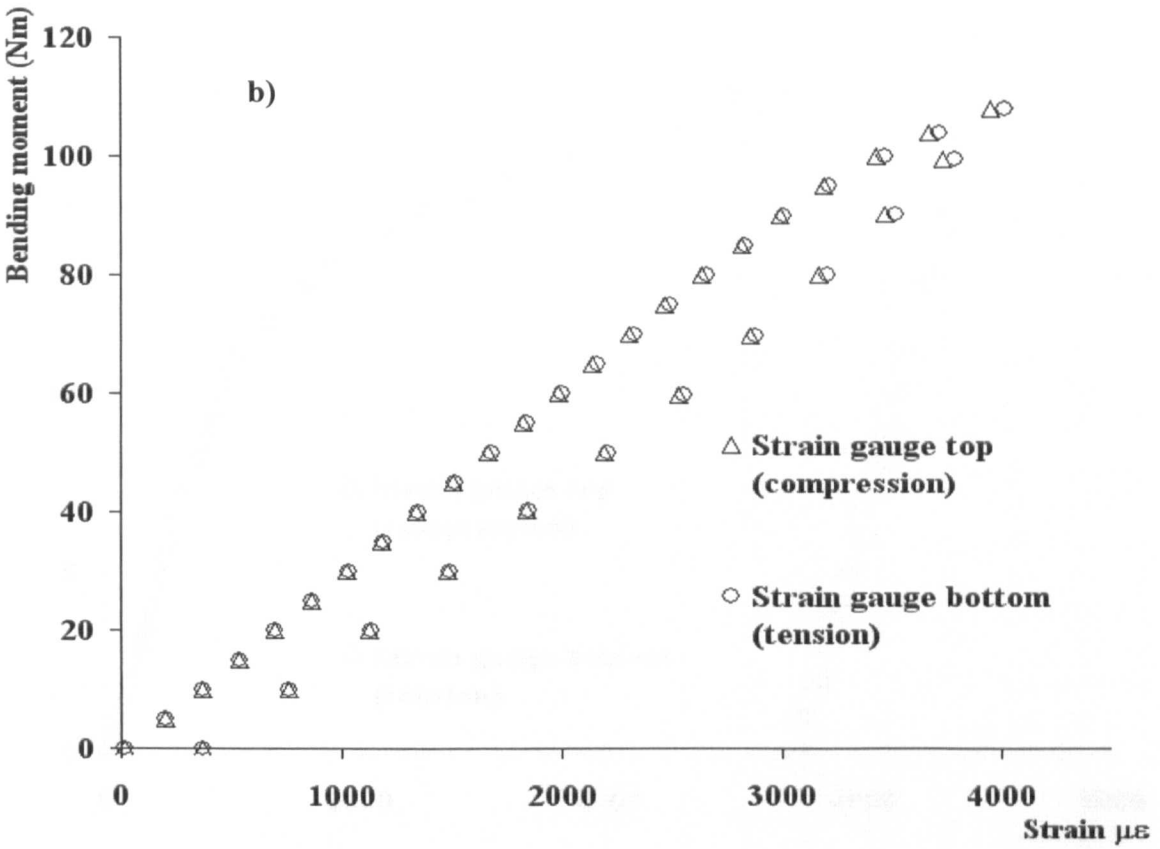

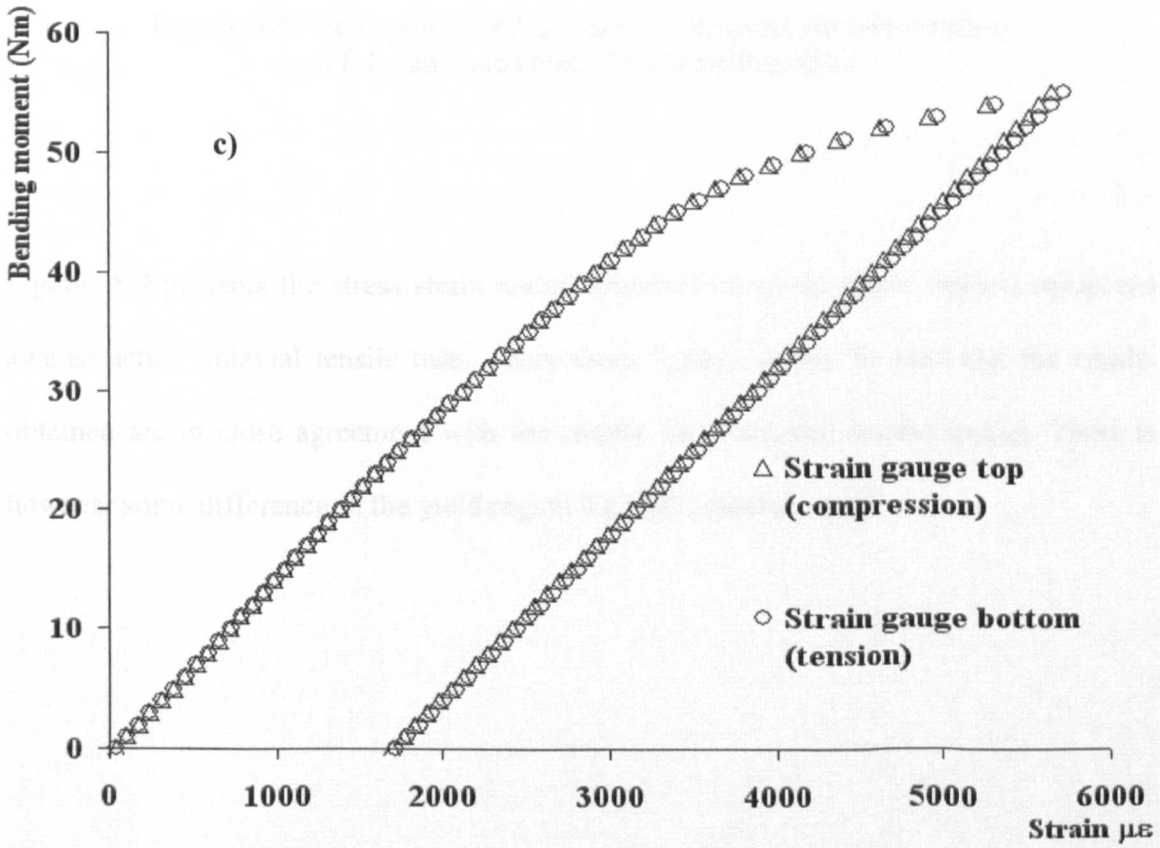

Figure 5.8.- Four-point bending tests on annealed material b) stress relief annealed EN 8 steel c) stress relief annealed 6082 T6 aluminium alloy

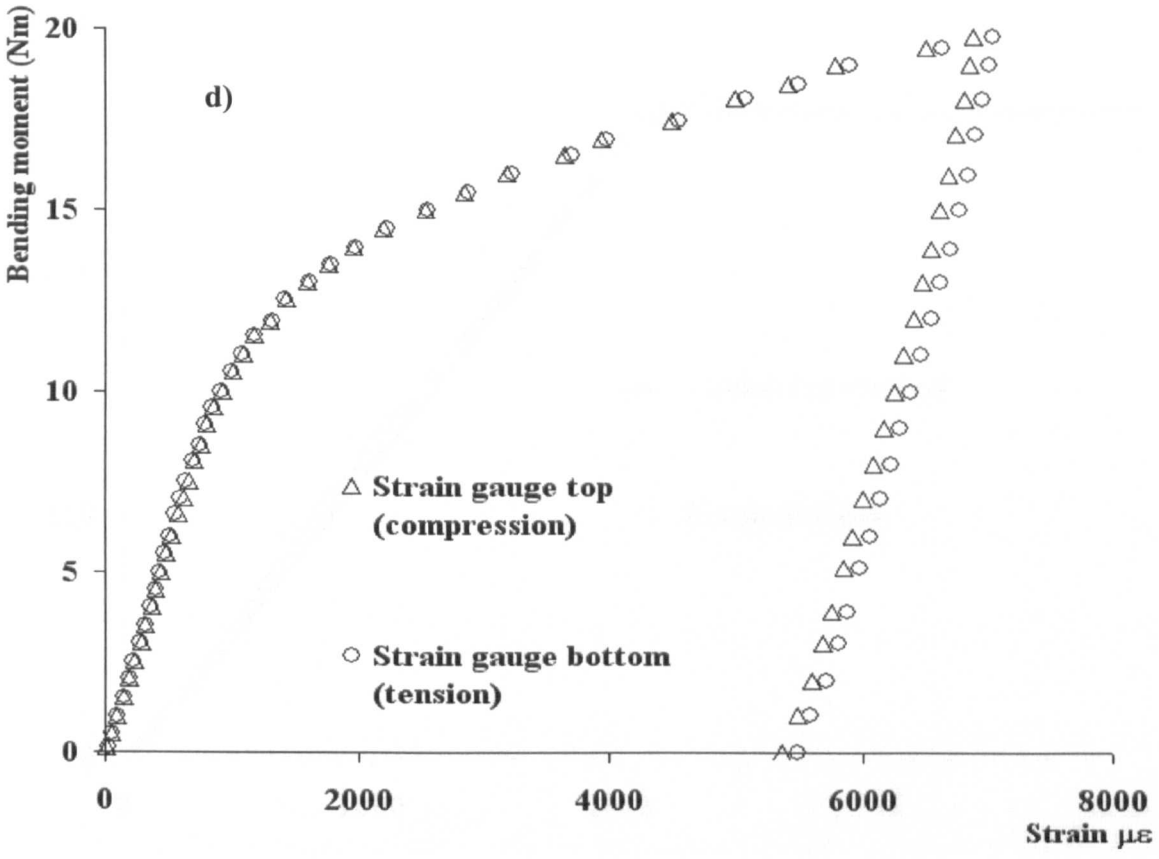

Figure 5.8.- Four-point bending tests on annealed aluminium alloy
d) fully annealed 6082 T6 aluminium alloy

Figures 5.9 presents the stress-strain results obtained using the beam method compared against actual uniaxial tensile tests. From these figures, it can be seen that the results obtained are in close agreement with the results from uniaxial tensile testing. There is however some difference in the yield region for both material types.

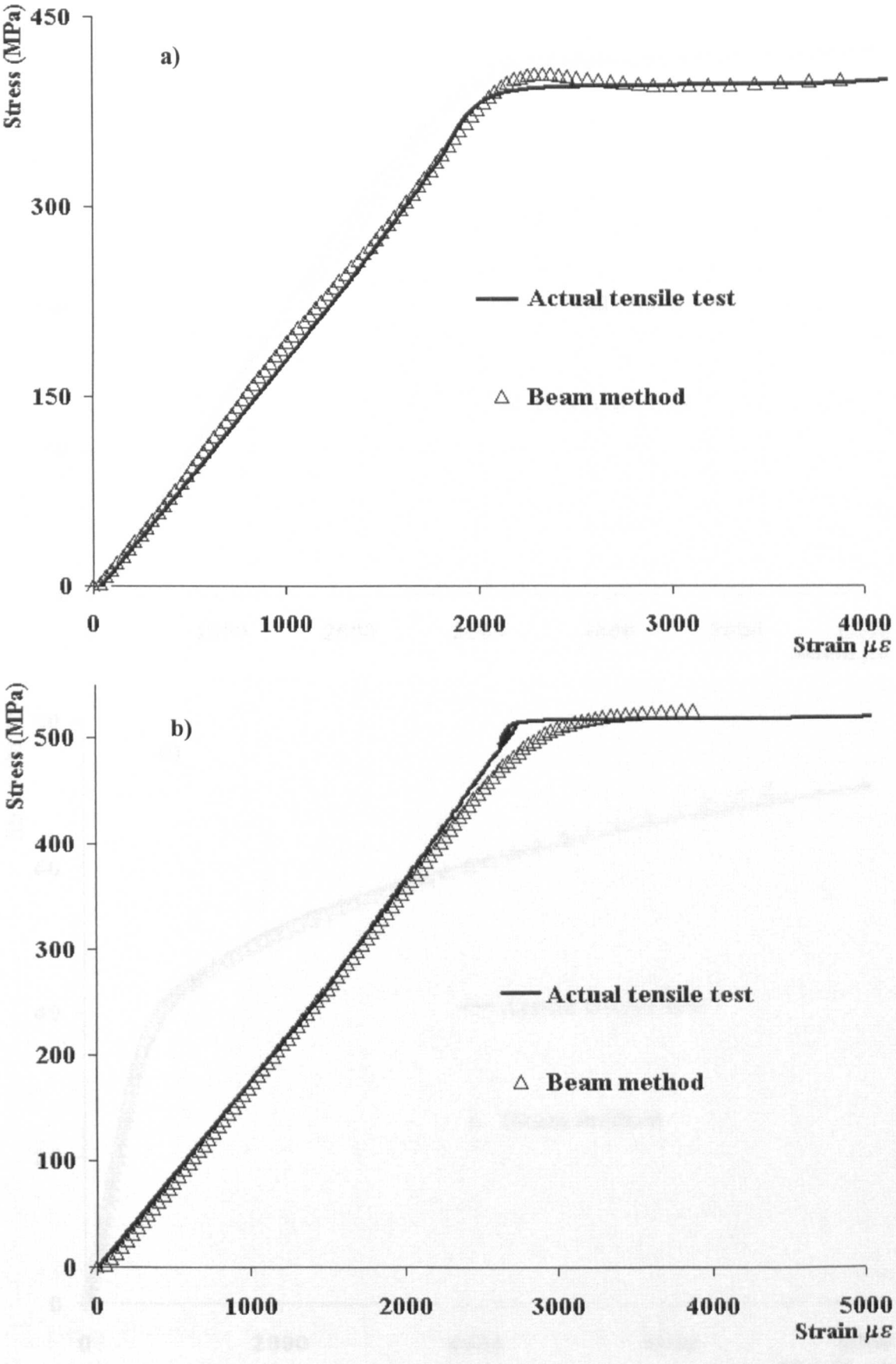

Figure 5.9.- Stress-strain results for steels in stress relief annealed condition a) EN 1A steel b) EN 8 steel

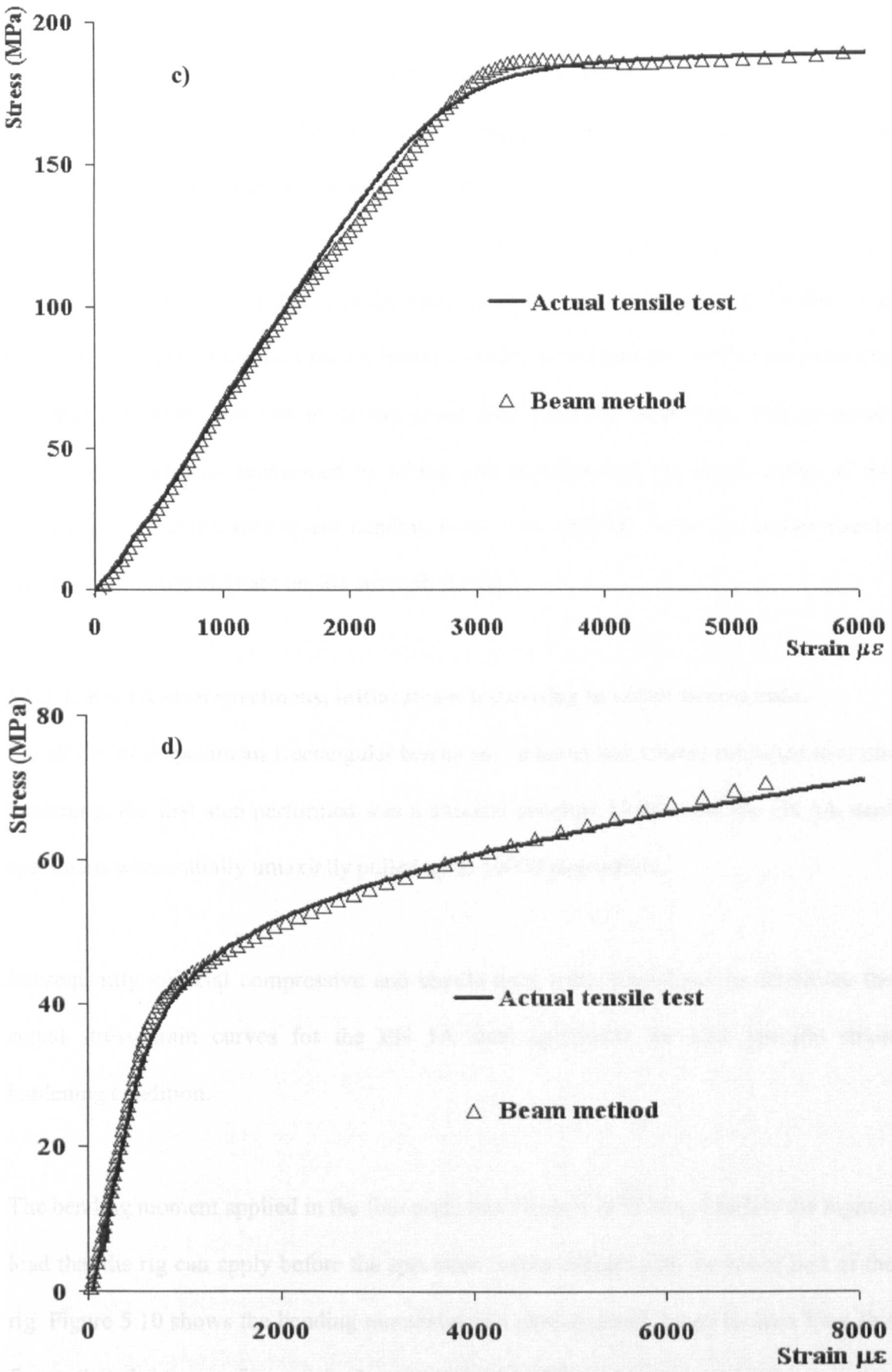

Figure 5.9.- Stress-strain results for AA 6082 T6 aluminium alloy in annealed condition c) stress relief annealed d) fully annealed

5.5.3. Bending of beams with Bauschinger effect.

The initial length of each of the rectangular beam specimens used for these tests was 400 mm. The gripped ends of the bars during pre-pulling to induce initial strain were later cut off in order to obtain a final beam length of 250 mm.

Strain gauges were attached at opposite surfaces of the beam specimens, as illustrated in Figure 5.6. Gauges were used on the beams in order to monitor the level of pre-straining for each particular case and to collect strain data from the bend tests. The pre-strain hardening extent was determined by taking into consideration the plastic range of the material and also the subsequent bending load to be applied, Table 5.2, before tensile failure occur at the ultimate tensile strength (UTS).

5.5.3.1. EN 1A steel specimens, initial strain hardening to 10000 microstrain.

For all the steel specimens (rectangular beams and uniaxial specimens) subjected to strain hardening, the first step performed was a uniaxial pre-pull. In this case the EN 1A steel specimens were initially uniaxially pulled up to 10000 microstrain.

Subsequently uniaxial compressive and tensile tests were carried out to determine the actual stress-strain curves for the EN 1A steel specimens for each specific strain hardening condition.

The bending moment applied in the four point bend tests was 75 Nm, which is the highest load that the rig can apply before the specimen makes contact with the lower part of the rig. Figure 5.10 shows the bending moment-strain plot obtained. It can be seen from this figure that the top surface of the beam (surface under compressive action) has higher

strain values than the bottom surface of the specimen (surface under tensile stress). Additionally, the surface under compression shows an early strain yielding than the surface under tension bending.

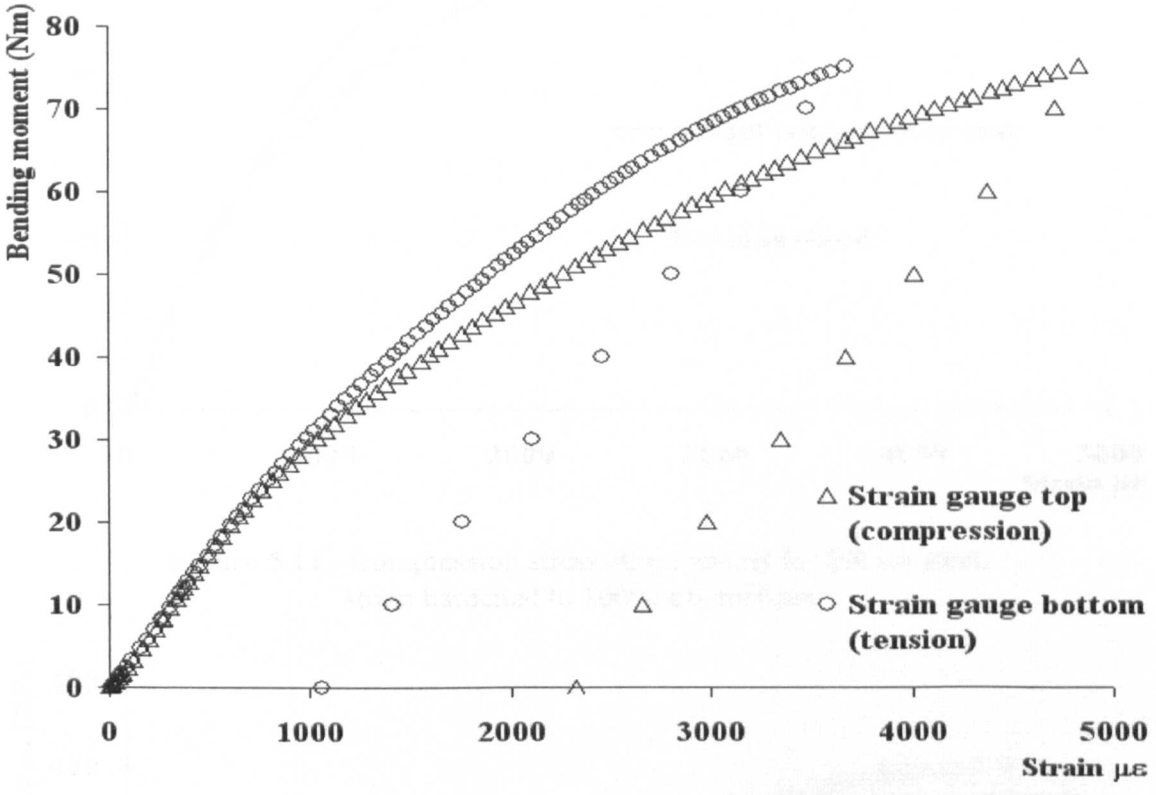

Figure 5.10.- Bending moment-strain graph for EN 1A steel specimen, strain hardened to 10000 microstrain

The tensile and compressive stress-strain data determined by the beam method is compared against uniaxial compressive stress-strain data obtained from experimental tests in Figures 5.11 and 5.12. The curves obtained in Figures 5.11 and 5.12 from the beam method followed the general trend in comparison with stress-strain uniaxial tensile and compression tests. Fairly good agreement was obtained in early parts of the elastic region. There is some variation in the yield and plastic regions. The difference in these regions is however less than 9% relative to the results of direct uniaxial tests. The difference in results can be related to difficulties with alignment on the axial testing.

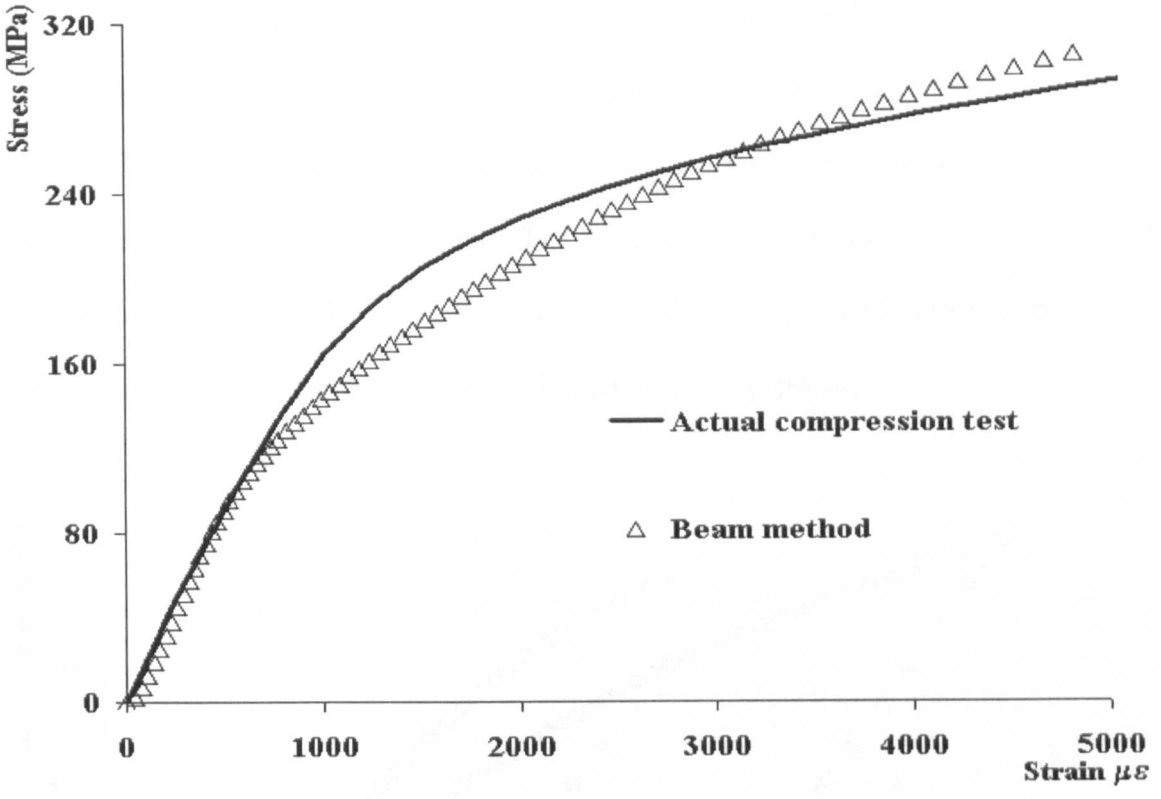

Figure 5.11.- Compression stress-strain results for EN 1A steel, strain hardened to 10000 microstrain

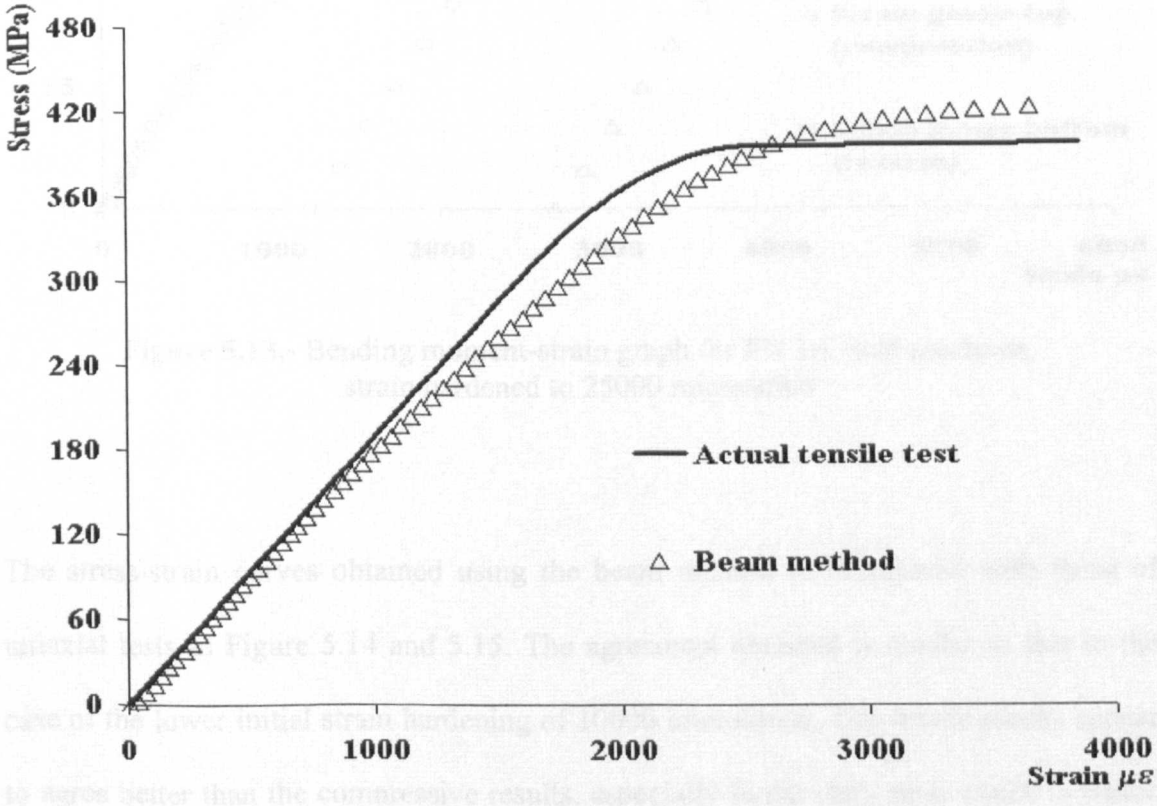

Figure 5.12.- Tensile stress-strain results for EN 1A steel, strain hardened to 10000 microstrain

5.5.3.2. EN 1A steel specimens, initial strain hardening to 25000 microstrain.

The analyses carried out in this section are similar to those ones described in section 5.3.3.1 of this chapter. In this section, the initial strain hardening considered for EN 1A steel specimens was 25000 microstrain. The bending moment against strain data obtained is presented in Figure 5.13. As in the case in section 5.3.3.1, the response of the tensile and compressive side demonstrates Bauschinger effect as expected.

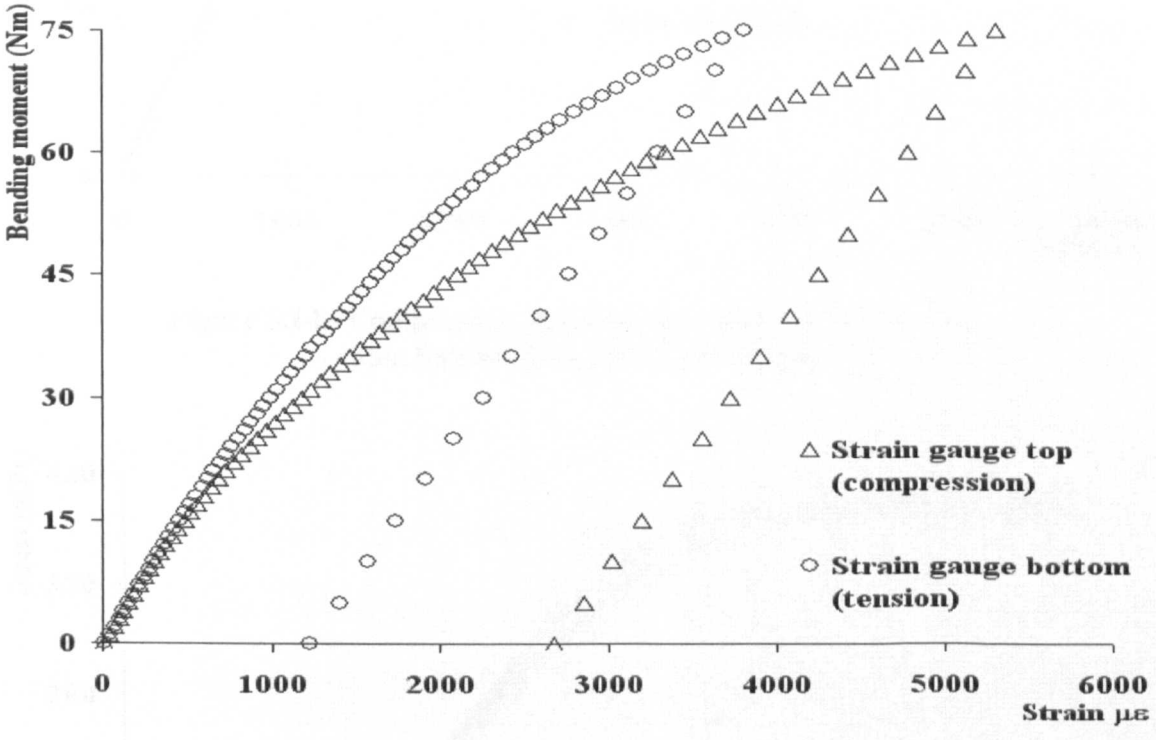

Figure 5.13.- Bending moment-strain graph for EN 1A steel specimen, strain hardened to 25000 microstrain

The stress-strain curves obtained using the beam method are compared with those of uniaxial tests in Figure 5.14 and 5.15. The agreement obtained is similar to that in the case of the lower initial strain hardening of 10000 microstrain. The tensile results appear to agree better than the compressive results, especially in the early parts which is elastic in the former but inelastic in the latter.

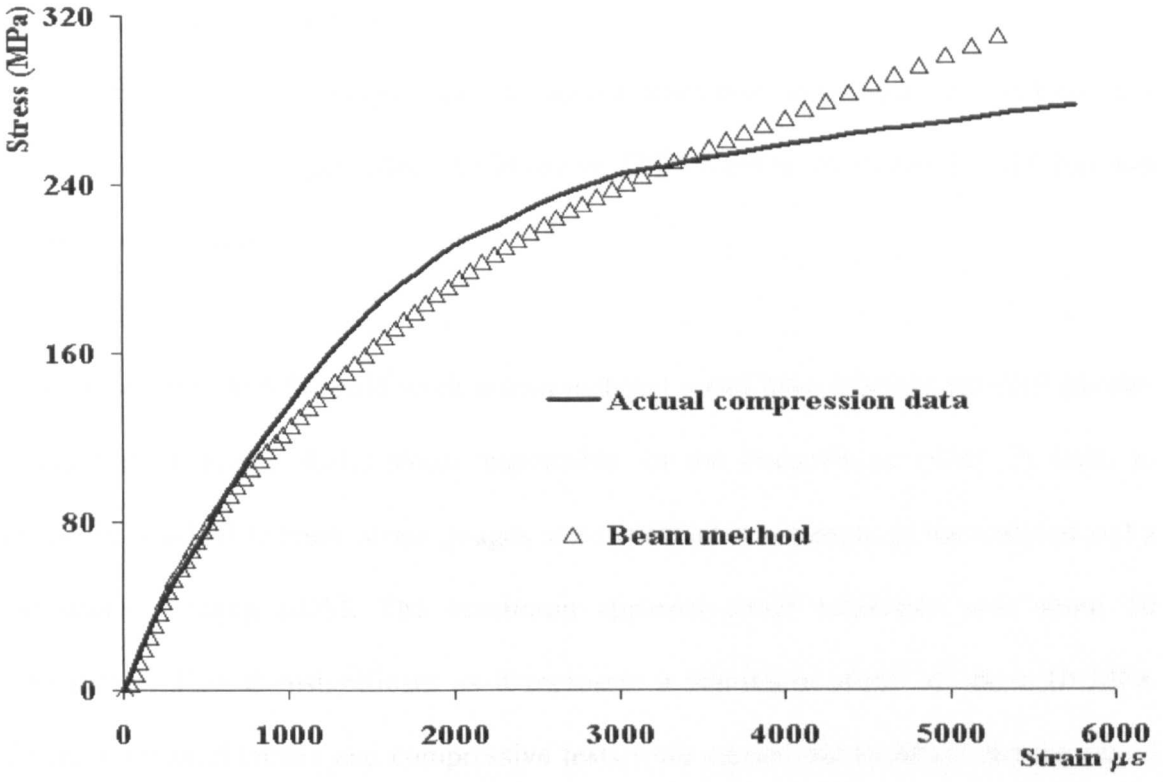

Figure 5.14.- Compression stress-strain results for EN 1A steel, strain hardening to 25000 microstrain

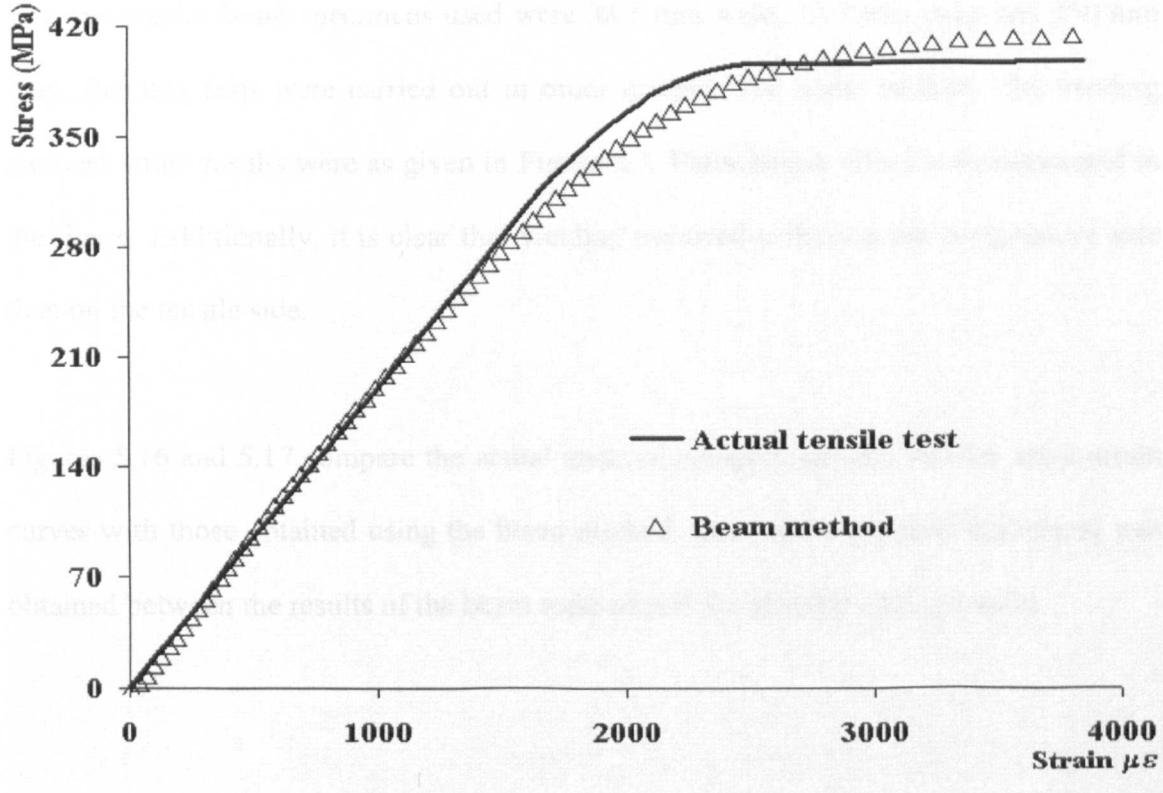

Figure 5.15.- Tensile stress-strain results for EN 1A steel, strain hardening to 25000 microstrain

5.5.3.3. As received EN 8 steel.

This example provided an opportunity to test the beam method on an as received material with inherent Bauschinger effect. Cold drawn EN 8 steel in as received condition was chosen for the study.

It is conceivable that the cold work drawn material could have inherent residual stresses in addition to initial plastic strain responsible for the Bauschinger effect. In order to check for residual stresses, strain gauges were attached to a sample of the material and a slit was cut using EDM. The maximum apparent strain relaxation was about 50 microstrain. This is insignificant as it represent a maximum stress of about 10 MPa. Separate uniaxial tensile and compressive tests were carried out to determine the actual stress-strain curves of the material.

The rectangular beam specimens used were 38.1 mm wide, 12.7 mm deep and 250 mm long. Bending tests were carried out in order to apply the beam method. The bending moment-strain results were as given in Figure 5.3. Bauschinger effect is demonstrated in the figure. Additionally, it is clear that yielding occurred earlier on the compressive side than on the tensile side.

Figures 5.16 and 5.17 compare the actual uniaxial compression and tension stress-strain curves with those obtained using the beam method. Generally very good agreement was obtained between the results of the beam method and the uniaxial testing results.

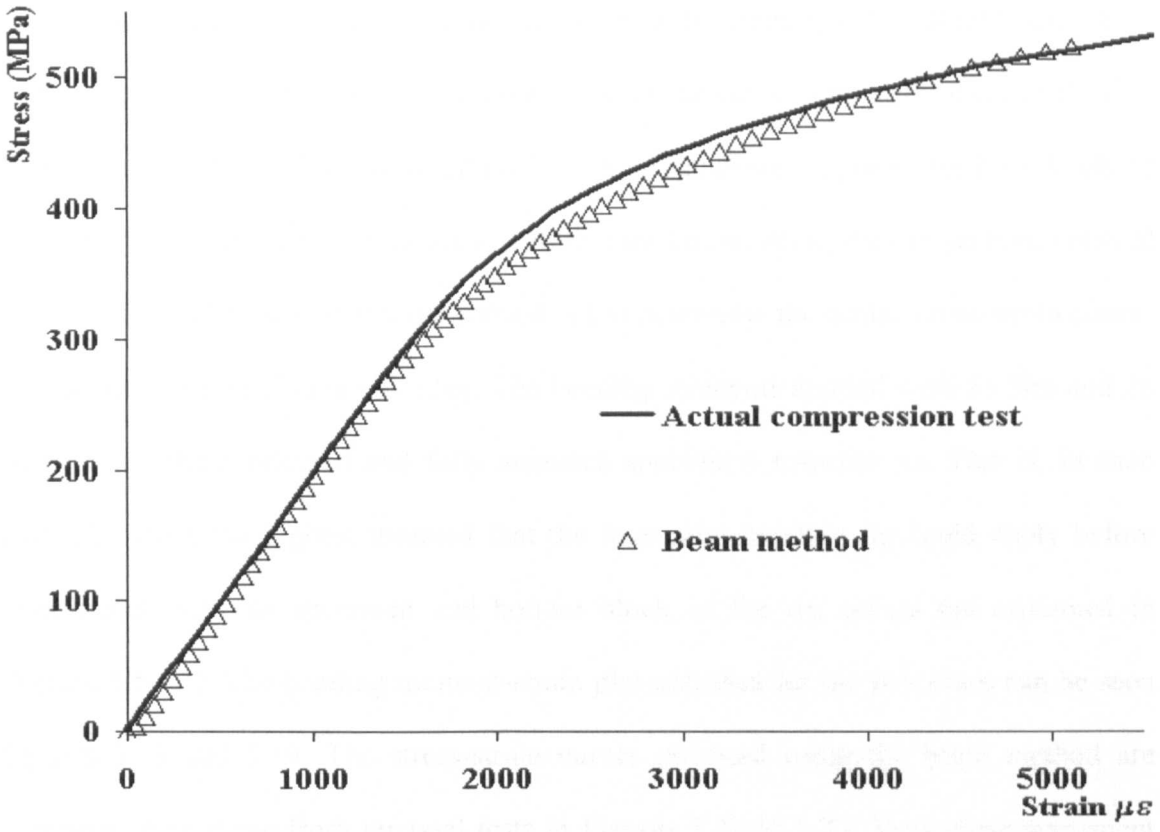

Figure 5.16.- Compressive stress-strain results for EN 8 steel cold drawn

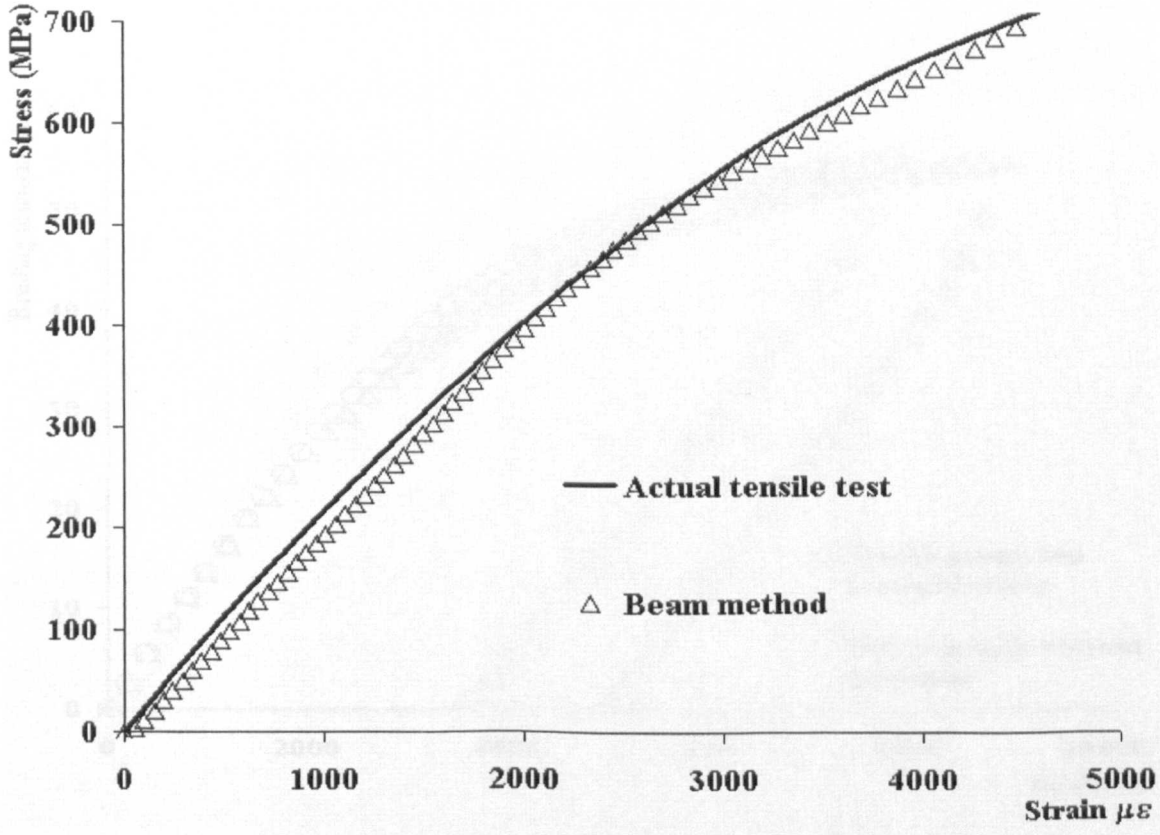

Figure 5.17.- Tensile stress-strain results for EN 8 steel cold drawn

5.5.3.4. AA 6082 T6 alloy specimens, initial strain hardening to 15000 microstrain.

In this section, two different aluminium annealed conditions were used for the evaluation of the beam method. The initial strain hardening condition imposed for both kinds of aluminium alloy specimens was set to 15000 microstrain. As in the last section, uniaxial compressive and tensile tests were carried out to determine the actual stress-strain curves for the pre-strained aluminium alloy. The bending moments applied were 55 Nm and 26 Nm for the stress relieved and fully annealed specimens respectively. This is, in each particular case, the highest moment that the four-point bending rig could apply before interference between specimen and bottom block of the rig occurs (as explained in Section 5.5.3.1). The bending moment-strain plot obtained for the two cases can be seen Figures 5.18 and 5.19. The stress-strain curves obtained using the beam method are compared with those from uniaxial tests in Figures 5.20 to 5.23. Very close agreement can be seen in all regions in these results compared to those of the steel material.

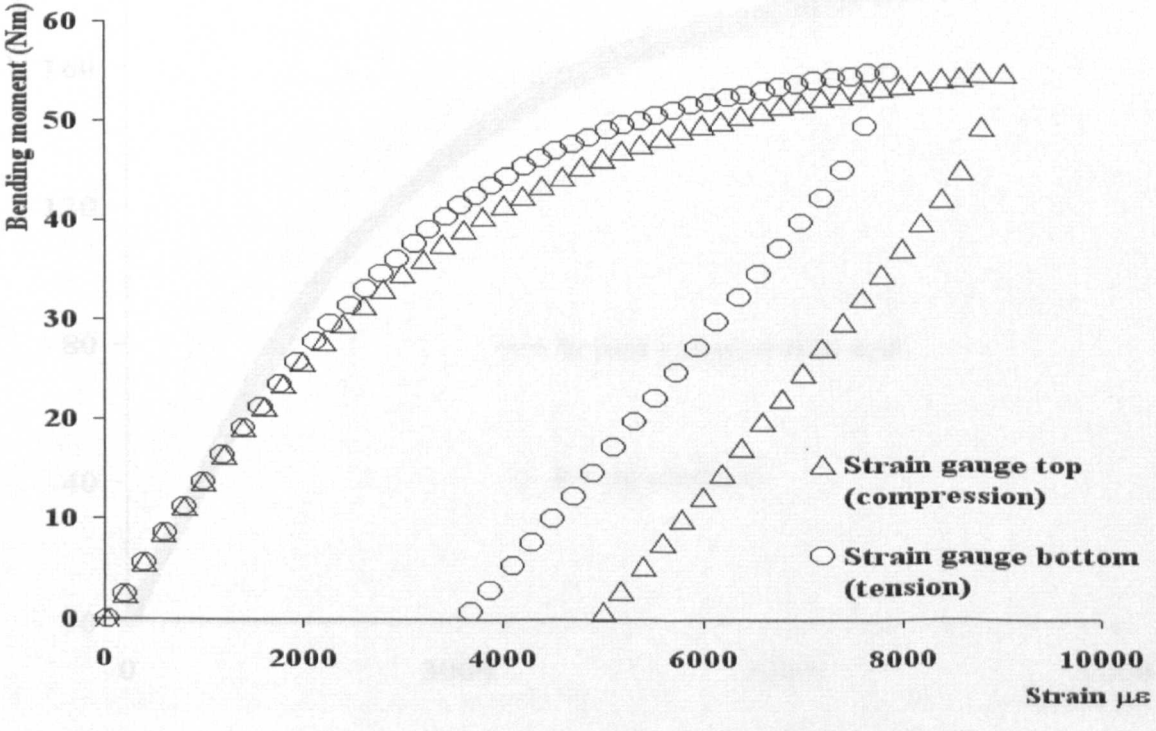

Figure 5.18.- Bending moment-strain graph for AA 6082 T6 alloy stress relief annealed specimen, strain hardened to 15000 microstrain

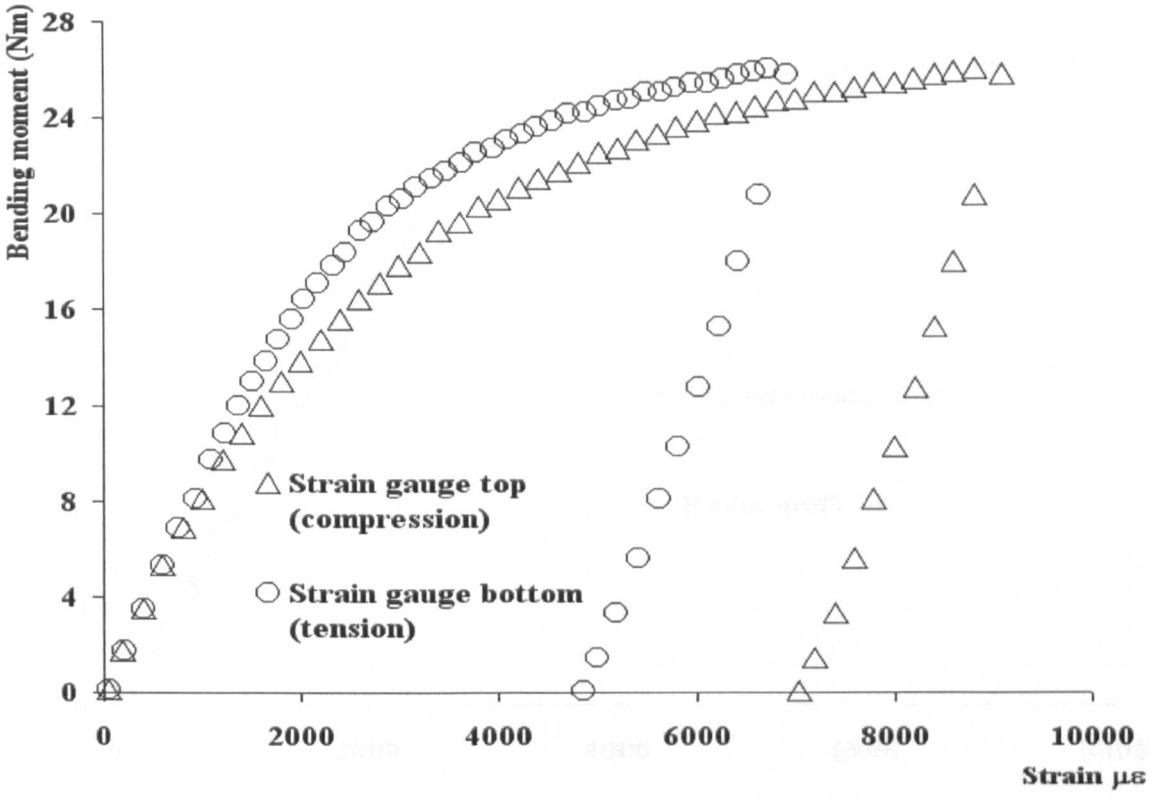

Figure 5.19.- Bending moment-strain graph for AA 6082 T6 alloy fully annealed specimen, strain hardened to 15000 microstrain

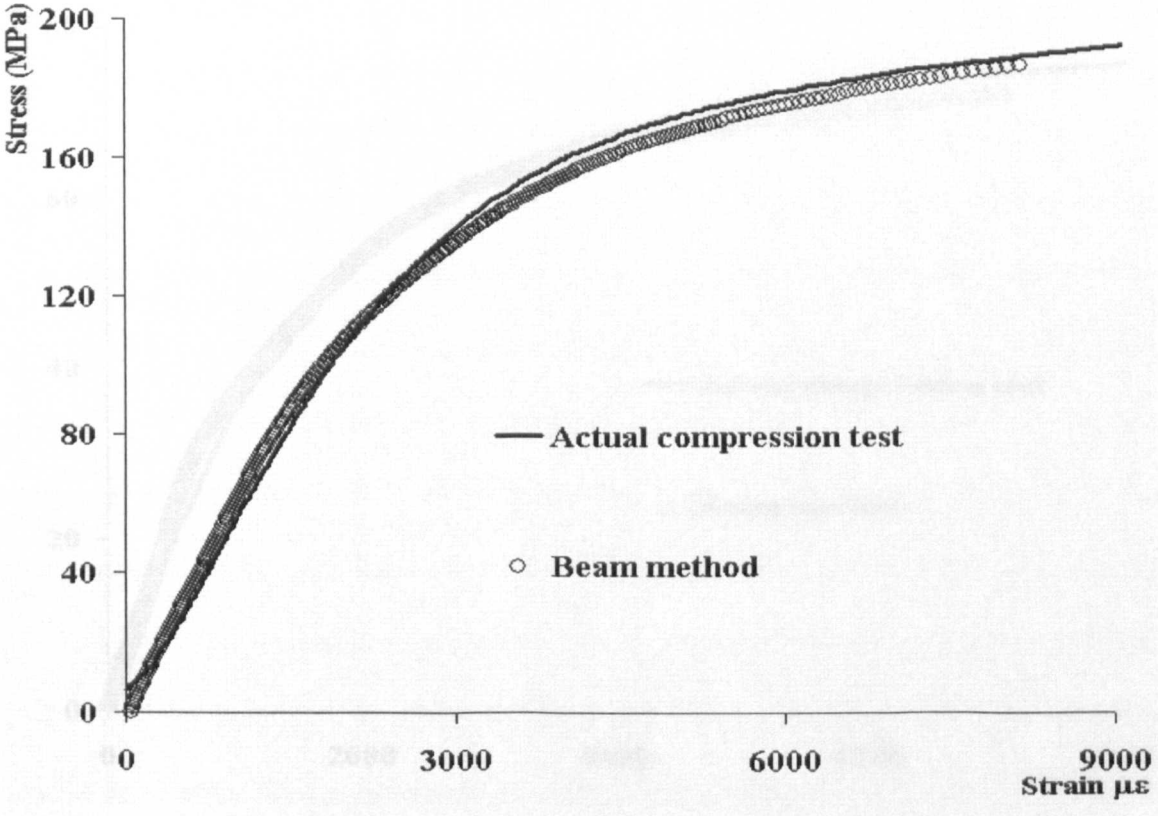

Figure 5.20.- Compressive stress-strain results for AA 6082 T6 alloy stress relief annealed, strain hardened to 15000 microstrain

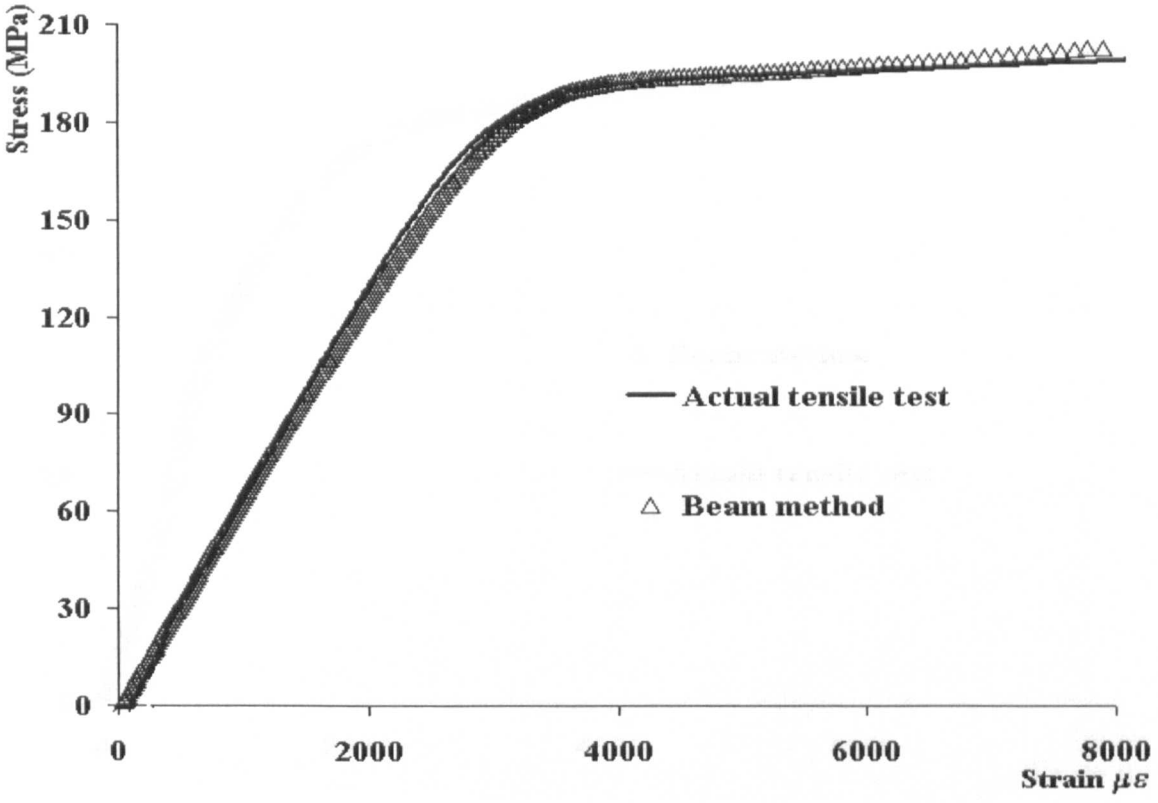

Figure 5.21.- Tensile stress-strain results for AA 6082 T6 alloy stress relief annealed, strain hardened to 15000 microstrain

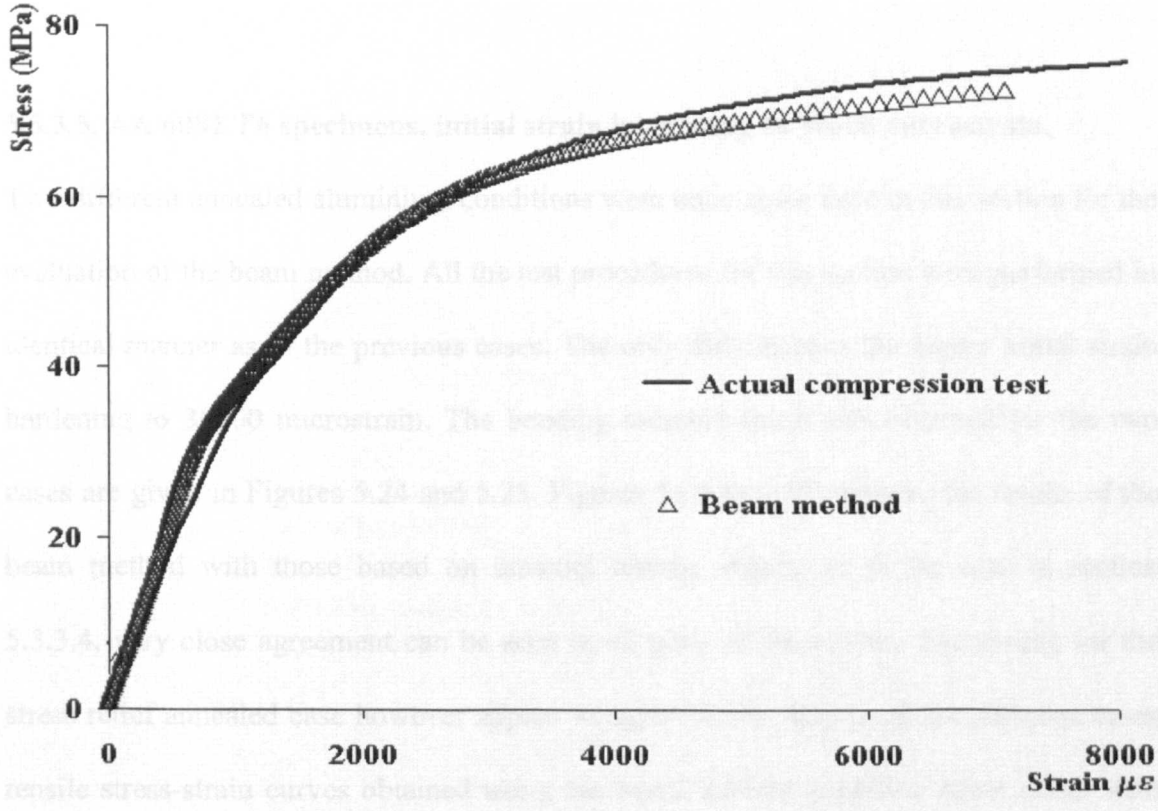

Figure 5.22.- Compressive stress-strain results for AA 6082 T6 alloy fully annealed, strain hardened to 15000 microstrain

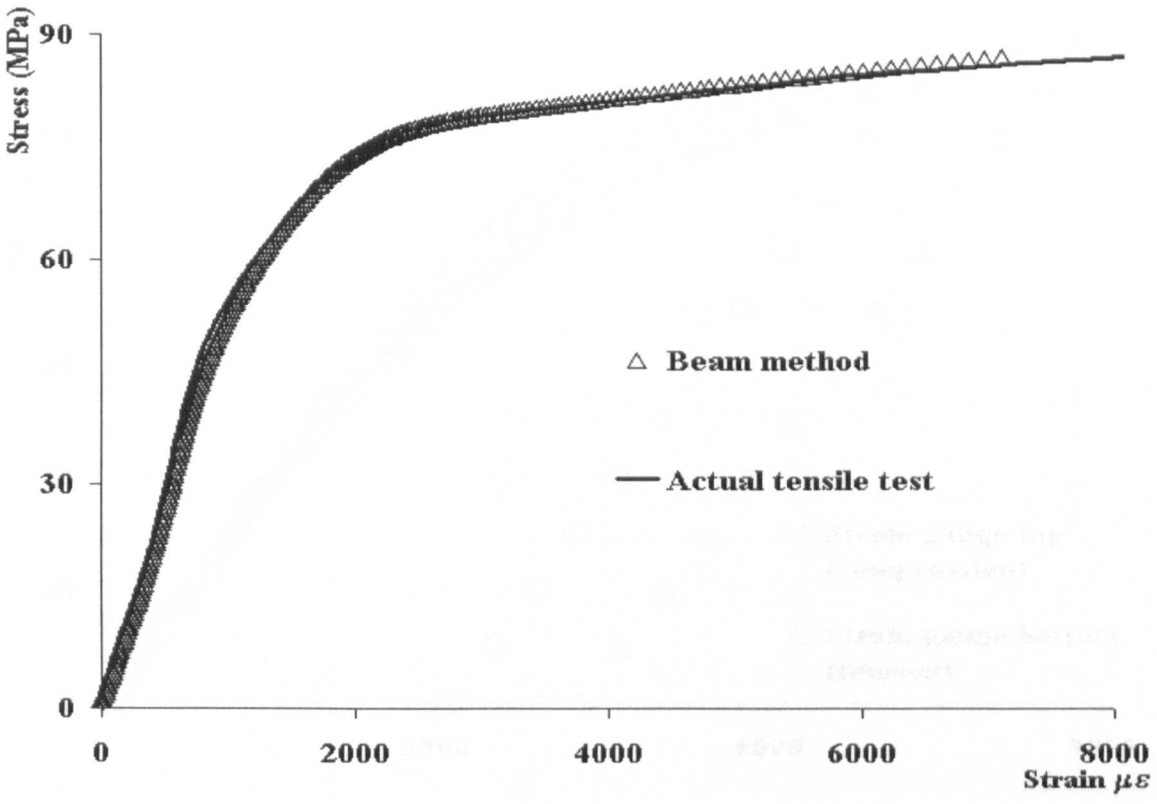

Figure 5.23.- Tensile stress-strain results for AA 6082 T6 alloy fully annealed, strain hardened to 15000 microstrain

5.5.3.5. AA 6082 T6 specimens, initial strain hardening to 30000 microstrain.

Two different annealed aluminium conditions were once again used in this section for the evaluation of the beam method. All the test procedures for this section were performed in identical manner as in the previous cases. The only difference is the higher initial strain hardening to 30000 microstrain. The bending moment-strain plot obtained for the two cases are given in Figures 5.24 and 5.25. Figures 5.26 to 5.29 compare the results of the beam method with those based on uniaxial testing. Again, as in the case in section 5.3.3.4, very close agreement can be seen in all parts of the curves. The results for the stress relief annealed case however appear to agree better. Also as in the previous cases tensile stress-strain curves obtained using the beam method appear to agree better with those from uniaxial test compared to results for compressive stress-strain curves.

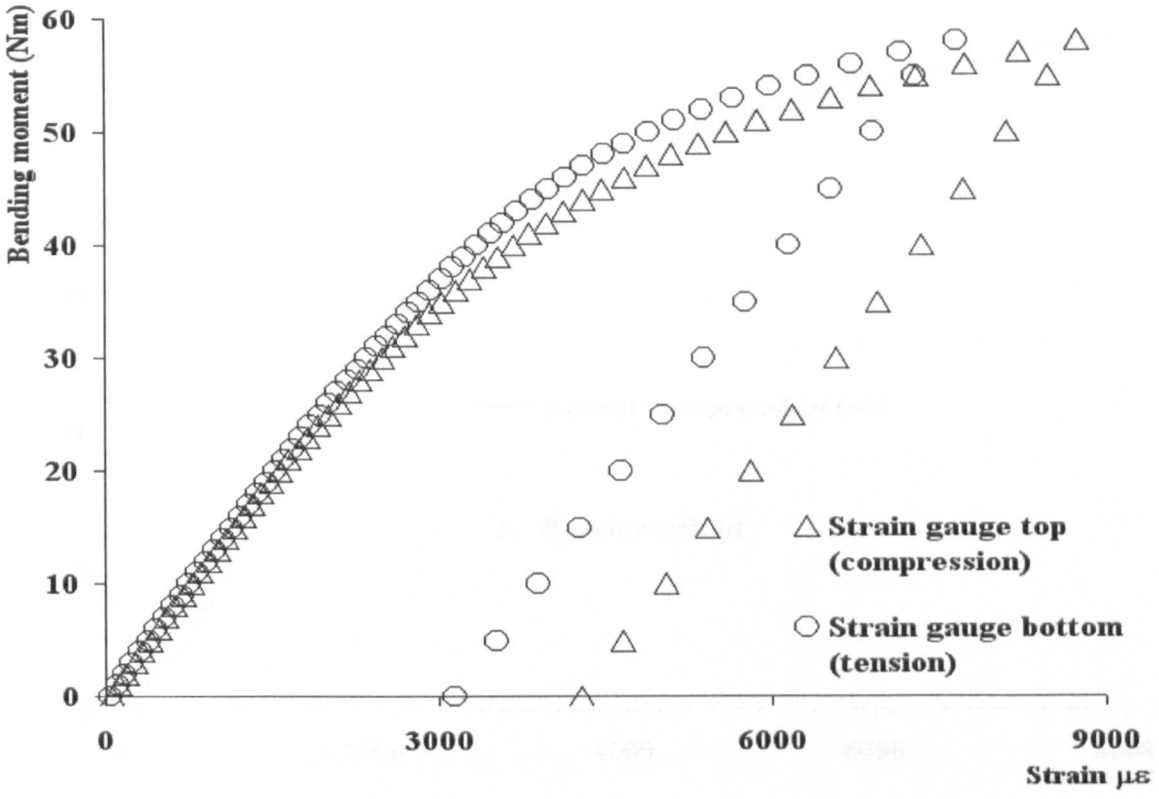

Figure 5.24.- Bending moment-strain graph for AA 6082 T6 alloy stress relief annealed specimen, strain hardened to 30000 microstrain

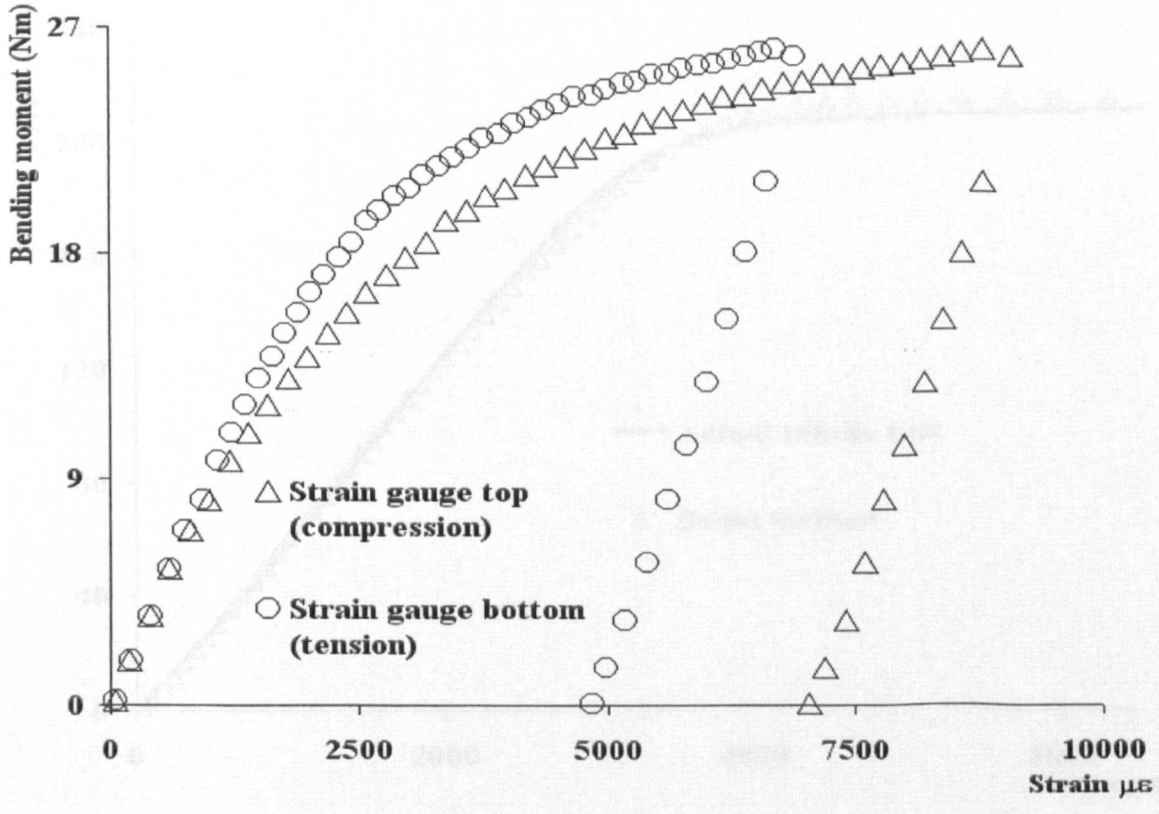

Figure 5.25.- Bending moment-strain graph for AA 6082 T6 alloy fully annealed specimen, strain hardened to 30000 microstrain

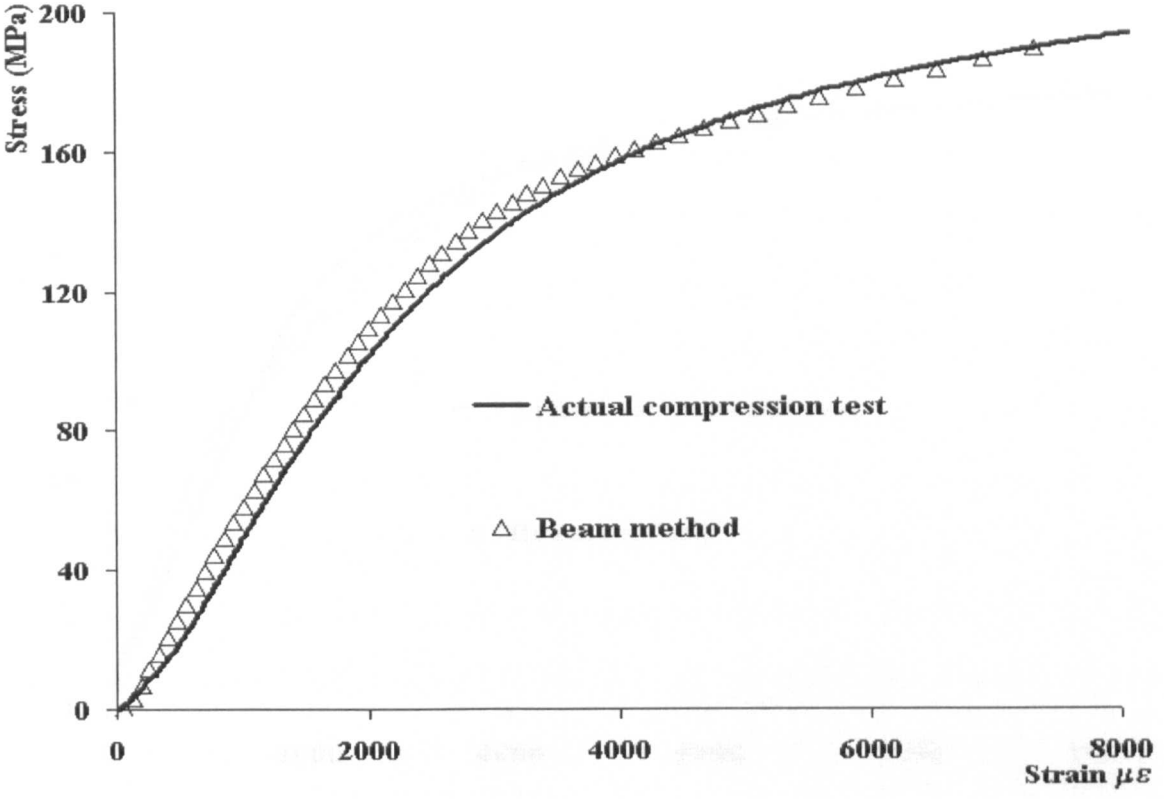

Figure 5.26.- Compressive stress-strain results for AA 6082 T6 alloy stress relief annealed, strain hardened to 30000 microstrain

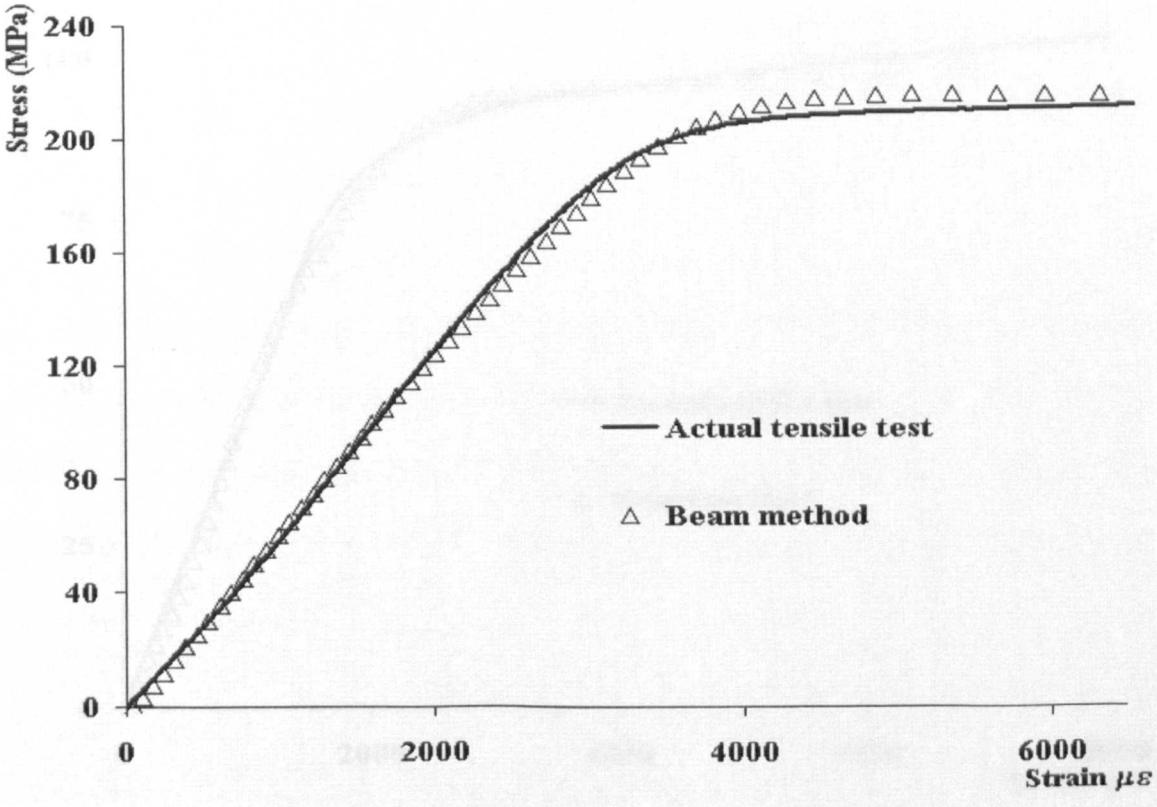

Figure 5.27.- Tensile stress-strain results for AA 6082 T6 alloy stress relief annealed, strain hardened to 30000 microstrain

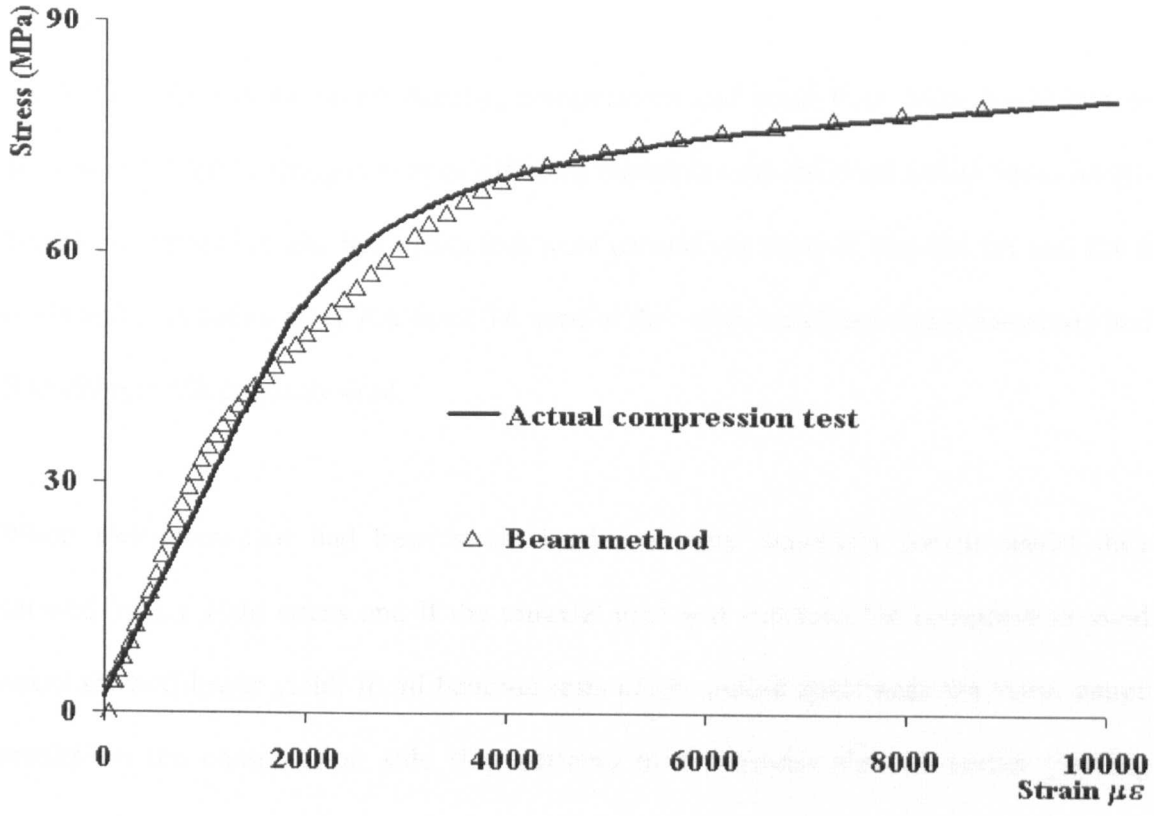

Figure 5.28- Compressive stress-strain results for AA 6082 T6 alloy fully annealed, strain hardened to 30000 microstrain

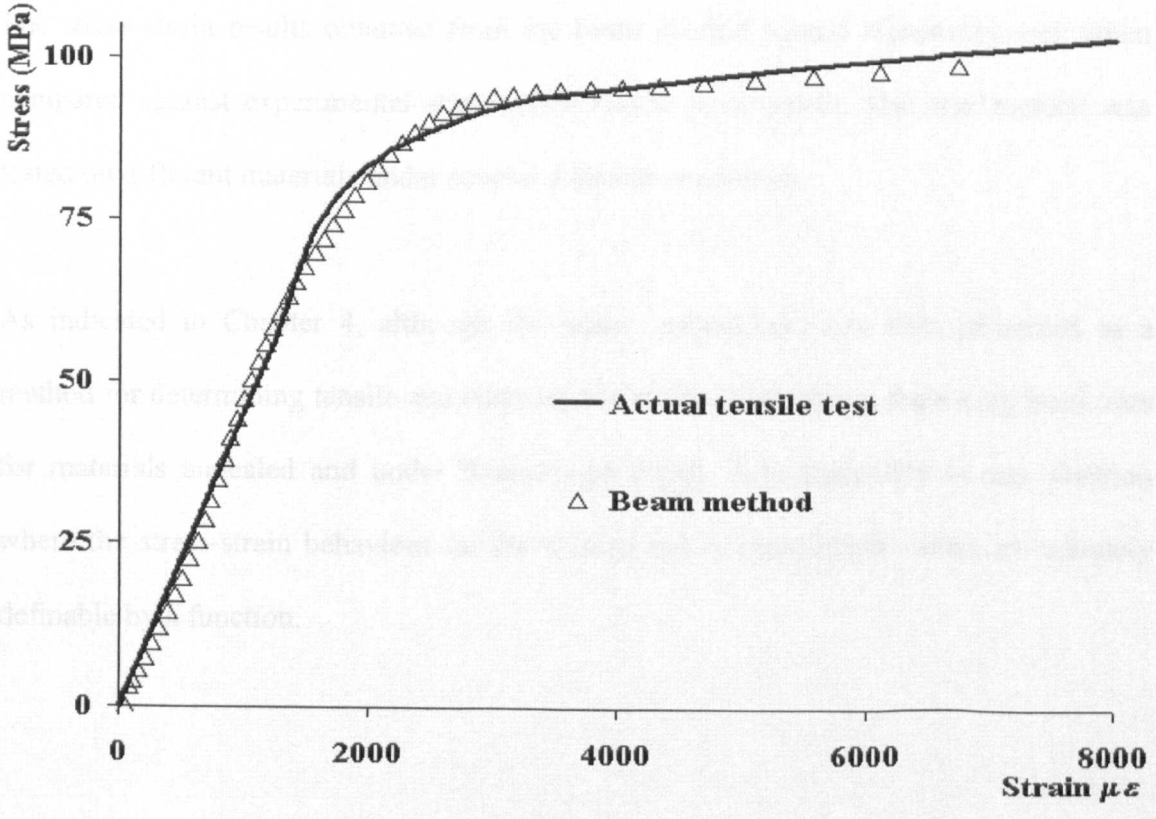

Figure 5.29- Tensile stress-strain results for AA 6082 T6 alloy fully annealed, strain hardened to 30000 microstrain

5.6. Summary.

Mechanical testing including, tensile, compressive and bend tests were performed to determine the stress-strain curves of different materials with different initial strain levels. Tensile, compressive and bend tests that were carried out showed that EN 1A and EN 8 steels and aluminium alloy AA 6082 T6 used in this study exhibited strain hardening and Bauschinger effects, as desired.

When specimens that had been strain hardened were uniaxially tensile tested they showed higher yield stress and if the uniaxial load was reversed the compression yield stress showed lower yield. In all bending tests of pre-pulled specimens the strain gauge results on the compression side (top surface) of the beams showed earlier yielding compared to strain gauge results on the tensile side (bottom surface).

The stress-strain results obtained from the beam method agreed reasonably well when compared against experimental stress-strain results in all cases. The new method was tested on different materials under several different conditions.

As indicated in Chapter 4, although the beam method here has been presented as a method for determining tensile and compression stress-strain curves from only bend tests for materials annealed and under Bauschinger effect, it is applicable to any situation where the stress-strain behaviour on the tension and or compression sides are uniquely definable by a function.

Chapter 6

Crack compliance methods

6.1. Introduction.

The main method used for the determination of residual stresses in this thesis is the crack compliance method. Some aspects of the method such as the practical implementation of the material removal and calculation of weight function were further extended and improved upon in this thesis.

Vaidyanathan and Finnie [1971] were the first to properly experimentally determine residual stresses acting in a component by the crack compliance method. Later *Cheng and Finnie [1986, 1994 and 1997]* developed an approach based on the method and applied it successfully to obtain residual stresses in components of different shapes. The method is based on introducing a crack or a cut into a body that contains residual stresses and increasing the crack length incrementally. Residual stresses are released at the newly created surfaces and cause the stress field to be rearranged in the entire body (Figure 6.1a). From the change of strain at a location (e.g. at M or at N or both) due to the progressive cutting starting at the rear surface (Figure 6.1b) it is possible to calculate the stress that acted along the corresponding axis x in the initial un-cracked state [*Schindler, 1995*].

Compared to other destructive techniques, the crack compliance method contributes unique capabilities for the determination of residual stresses. The technique is a relatively simple method to determine the stress intensity factor caused by a crack in a residual stress field and provides a means to measure crack closure stresses. It can be applied fairly easily with commonly available equipment such as strain gauges and electric discharge or conventional machining. It offers increased spatial resolution of residual stresses and sensitivity to low stresses.

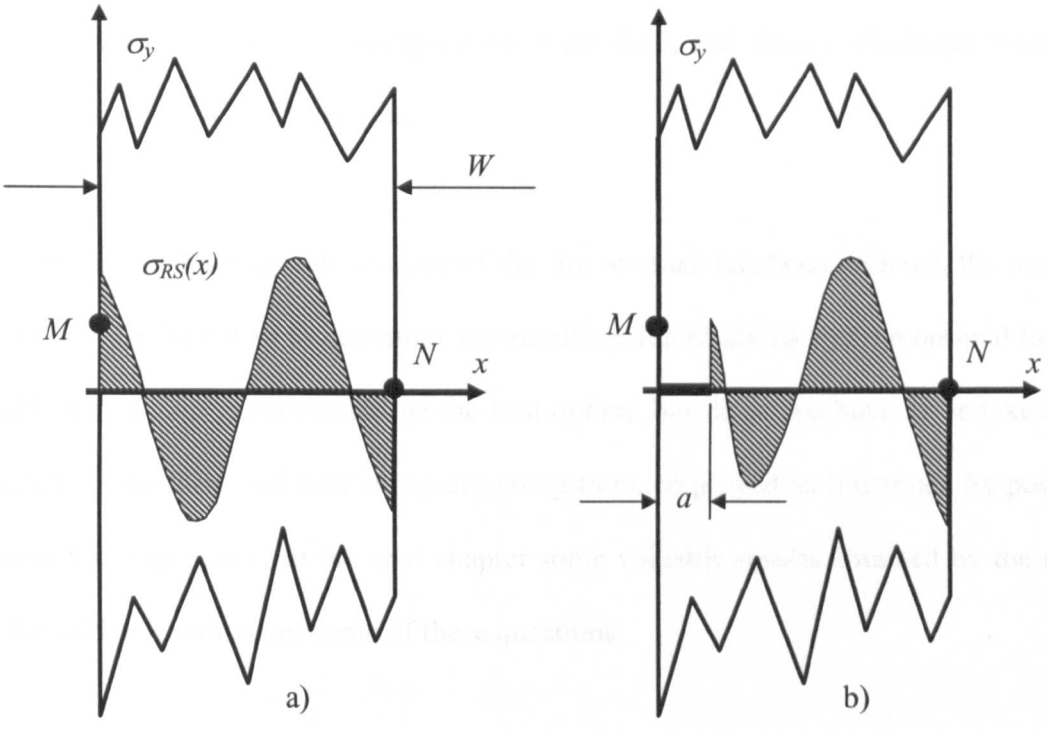

Figure 6.1.- Schematic representation of an arbitrary bidimensional body a) initial residual stress state b) stress rearrangement due to an introduction of a crack or a cut

The crack compliance method can be applied to many distinctive materials; some examples include several different metals, polymers and composites. Different geometrical configurations that have been tested include surface and through thickness measurements, axial stresses in plates (beams and strips), axi-symmetric stress in cylindrical components, pre-cracked specimens, central holes, and others.

Although the method is confined to the laboratory there are several experimental choices to be made. The first and perhaps the most important is how the slot or crack is introduced. Options include saws, milling cutters, and electric discharge machining, but the selection of the method may depend on the nature of the stress field. For example, mechanical saws tend to introduce or change the original residual stress field, cutters tend

to break when cutting into a compressive stress field, and electric discharge machining does not work on plastic materials.

After the method for the introduction of the slot or crack has been selected, the next step is to select the best way to determine the resulting deformations and the optimal location to obtain it. Strain gauges could be the best option, but decisions have to be taken as to where to place them and how many are going to be employed as illustrated by positions *M* and *N* in Figure 6.1. In the next chapter some valuable results obtained by the use of FEA could help to answer some of these questions.

6.2. Theory.

The analytical solution using the crack compliance method can be carried out only when the relaxed strain readings have been obtained from cutting a component with inherent residual stresses. In general, the analysis for the determination of the residual stresses from the strain data collected is performed in two stages; the forward solution stage followed by the inverse solution stage. These solutions are based on linear elastic isotropic material considerations. The forward and inverse solutions used in this thesis are explained in what follows:

6.2.1. The incremental inverse method for residual stress.

Consider a 2-D arbitrary body suffering from the effects of a crack of length a and unknown residual stresses (Figure 6.2). By extending the crack a small increment δa, the change of the surface strain $\delta\varepsilon_M$ produce by the crack extending can be obtained by using strain gauges, at an arbitrary point M on the top or bottom surface, for example (Figure 6.2) [*Schindler and Landolt, 1997*].

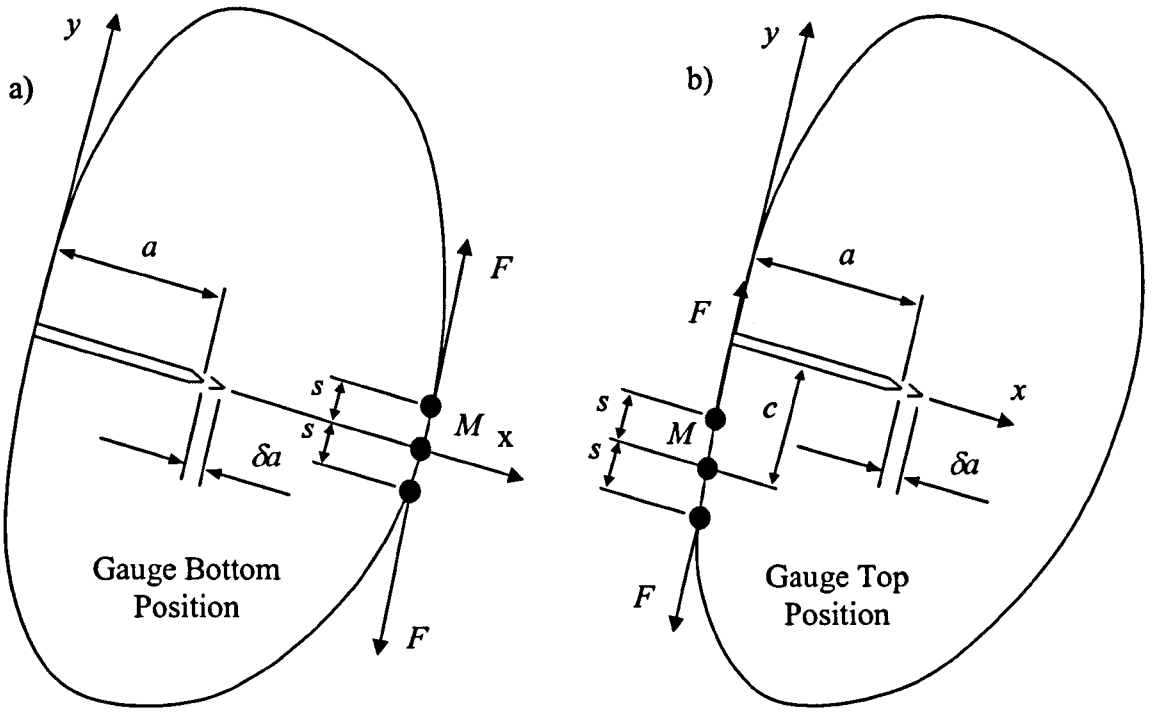

Figure 6.2.- Mechanical system considered to establish the relationship between the stress intensity factor and the strain at an arbitrary point *M* at top and bottom surfaces [*Schindler and Landolt, 1997*]

The strain increment $\delta\varepsilon_M$ can be expressed by the means of Castigliano's theorem [*Todd, 1981*] as:

$$\delta\varepsilon_M = \frac{1}{2}\frac{\partial^2 \delta U}{\partial F \partial s}\bigg|_{\substack{F=0 \\ s=0}} \qquad 6.1$$

where δU is the difference in the elastic energy stored before and after the extension of the crack, F is a virtual force acting tangentially to the surface at M, and s is the distance between the arbitrary point M and the point of the application of the line force F. The reaction forces F can be introduced arbitrarily. In most cases the force is positioned at symmetrical locations with respect to the point M (Figure 6.2). The difference in the elastic energy stored before and after the extension of the crack can be expressed as [*Irwin, 1957*]:

$$\delta U = \frac{B}{E'}\left\{\left[K_{Irs} + K_{IF}\right]^2 + \left[K_{IIrs} + K_{IIF}\right]^2\right\}\delta a \qquad 6.2$$

where E' is the generalized Young's modulus ($E' = E$ for plane stress condition and $E' = E/(1-\nu^2)$ for plane strain), B is the thickness of the part. At the crack tip, K_{Irs} and K_{IIrs} are the stress intensity factors due to the residual stress and K_{IF} and K_{IIF} are the stress intensity factors due to the virtual force. By inserting Equation 6.2 in Equation 6.1 and because K_{IF} is a linear function of F and K_{Irs} is independent of s we have [*Schindler et al, 1997*]:

$$\delta\varepsilon_M = \frac{B}{E'F}\left[K_{Irs}\left.\frac{\partial K_{IF}}{\partial s}\right|_{s=0} + K_{IIrs}\left.\frac{\partial K_{IIF}}{\partial s}\right|_{s=0}\right]\delta a \qquad 6.3$$

This thesis considered systems in which both K_{IIF} and K_{IIrs} vanish (which is the case for symmetrical systems with respect to the crack plane or if the forces F do not produce shearing stresses at the plane y = 0) [*Schindler, Cheng and Finnie, 1997*]. Therefore

$$\delta\varepsilon_M = \frac{B}{E'F}K_{Irs}\left.\frac{\partial K_{IF}}{\partial s}\right|_{s=0}\delta a \qquad 6.3a$$

From Equation 6.3a it is possible to obtain the relationship between the strain change at the arbitrary point M and the stress intensity factor at incremental crack lengths. Equation 6.3a can be re-arranged to give Equation 6.4 [*Schindler and Bertschinger, 1997*].

$$K_{Irs}(a) = \frac{E'}{Z(a)}\frac{d\varepsilon_M}{da} \qquad 6.4$$

where $Z(a)$ is a geometry dependent function which reflects the sensitivity of the strain at M with respect to stresses released at the crack tip, and is given by Equation 6.5 [*Schindler and Bertschinger, 1997*].

$$Z(a) = \frac{B}{F}\left(\left.\frac{\partial K_{IF}}{\partial s}\right|_{s=0}\right) \qquad 6.5$$

Z(a) called the influence function, can be obtained by analytical or numerical (finite element method) methods. By determining the change in the strain caused by the extension of the crack by *da* and substituting the $(d\varepsilon_M / da)$ obtained in Equation 6.4, the stress intensity factor due to a crack in a residual stress field can be obtained, provided that *Z(a)* for the configuration is known.

It should be stated clearly, that the influence function *Z(a)* is a unique function that depends on the geometry of the part, the crack plane and the measurement point *M*, but not on the residual stress distribution. The function *Z(a)* also provides information about the sensitivity of the measurements at point *M* with respect to the relaxed stresses at the crack tip. The higher the value of *Z(a)*, the more sensitive the measurement. *Z(a)* is independent of the stress distribution, so that it need only be determined once for a given configuration.

6.2.2. The inverse solution for the stresses.

Now, from a known $K_{Irs}(a)$ as given in Equation 6.4, it is possible to calculate the normal residual stress distribution $\sigma_{rs}(x)$ acting prior to cutting the cross section $y = 0$, by the inversion of the integral equation 6.6 [*Schindler, 1995*];

$$K_{Irs}(a) = \int h(x,a) \cdot \sigma_{rs}(x) \cdot dx \qquad 6.6$$

where the acting axis has being chosen to coincide with the direction of the growing crack and *h(x,a)* is the weight function [*Bückner, 1970*], which is universal for a given crack geometry. Weight functions are known for several crack configurations [*Wu and Carlson, 1970 and Fett and Munz, 1997*]. Emphasis must be laid on adequate accuracy requirement for the weight functions. This is essential in order to determine residual stresses accurately. The straightforward solution to Equation 6.6 is obtained by applying

a step-by-step incremental procedure. The residual stress distribution $\sigma_{rs}(x)$ is approximated by a series of small steps (Figure 6.3), so that the stress level at each step can be obtained by Equation 6.6. The average stress over the first increment, σ_o, which is the average stress acting near the front surface in the range of $0 < x < a_o$ (where $a_o <<$ depth) was given by *Tada [1973]* as:

$$\sigma_o = \frac{K_{Irs}(a_o)}{1.12\sqrt{\pi a_o}} \qquad 6.7$$

Figure 6.3.- Approximation of the residual stress profile by step function [*Schindler and Bertschinger, 1997*]

To calculate the next step stress, σ_1 (in the range $a_o < x < a_o + \Delta a$) the crack is extended by Δa. Equation 6.6 is expanded to give Equation 6.8 [*Schindler, 1995*]:

$$K_{Irs}(a_o + \Delta a) = \sigma_o \cdot \int_0^{a_o} h(x, a_o + \Delta a)dx + \sigma_1 \cdot \int_{a_o}^{a_o+\Delta a} h(x, a_o + \Delta a)dx \qquad 6.8$$

and since σ_o is known from the last step and $K_{Irs}(a_o + \Delta a)$ is obtained from measurement then σ_1 can by obtained. By using this procedure and allowing the crack to propagate by Δa, the average stress σ_2 in the next step ($a_o + \Delta a < x < a_o + 2\Delta a$) can be calculated. By repenting this process incrementally, the entire stress profile can be determined. The residual stresses at the depth a_i correspond to the i^{th} increment is given by [*Schindler, 1995*]:

$$K_{Irs}(a_i) = \sigma_o \cdot \int_0^{a_o} h(x, a_i)dx + \sum_{j=1}^{i=1} \sigma_j \int_{a_j-1}^{a_j} h(x, a_i)dx + \sigma_i \int_{a_i-1}^{a_i} h(x, a_i)dx \qquad 6.9$$

The accuracy of the approximation can be adjusted by selecting a sufficiently small step length Δa and the step-shape approximation converges to the exact solution as $\Delta a \rightarrow 0$. When calculating the residual stress in a component using this approach, some difficulties may arise [*Schindler and Bertschinger, 1997*], in the sensitive region near the rear surface ($W - a << W$) because the weight function might be inaccurate in this range. This problem is solved in two ways; the first is by using a weight function that includes the correct limiting behaviour as $W - a \rightarrow 0$ [*Schindler and Bertschinger, 1997*], and the second method is by changing the calculation procedure as follows. For $W - a << W$, which means for $a > 3W/4$, the stress intensity factor is calculated by an empirical formula that was developed by *Schindler* [*1995*] and is shown in Equation 6.10;

$$K_{Irs}(a) = \sum_{j=0}^{i} \left\{ \frac{3.97\sigma_j \Delta a\left[0.264W + 0.736a_i - (a_O + j\Delta a)\right]}{(W - a_i)^{\frac{3}{2}}} + \frac{1.4\sigma_j \Delta a}{(W - a_i)^{\frac{1}{2}}} \right\} + 2\sigma_i \sqrt{\frac{2}{\pi} q(W - a_i)} \qquad 6.10$$

where $a_i = a_o + i\,\Delta a$ and the non-dimensional factor q is a constant that is about 0.03 for the further steps.

6.2.3. The global polynomial residual stress field inverse method.

Iain Finnie at the University of California, Berkeley, introduced the crack compliance approach in *1971* and he has been instrumental in its development [*Vaidyanathan and Finnie, 1971*]. Considered as a strip of depth t and unit thickness, Figure 6.4 [*Cheng and Finnie, 1994*].

Figure 6.4.- Measurement of strains near the cut or on the back face
[*Cheng and Finnie, 1994*]

The surface traction $\sigma_y(x)$ is the unknown residual stress that has to be deduced from measurement of the strain ε at some location (for example $x = 0$, $y = s$ or at $x = t, y = 0$),

as shown in Figure 6.4. Furthermore, let the unknown residual stress distribution in the beam to be represented as an n^{th} order polynomial series as [*Cheng and Finnie, 1994*]:

$$\sigma_y(x) = \sum_{i=0}^{n} A_i P_i(x) \qquad 6.11a$$

where A_i are the coefficients that have to be obtained and P_i are a power series, x^0, x^1, x^2, ... x^n etc., Legendre polynomials are also used. However, the crack compliance method includes a step which assumes that a stress distribution, $\sigma_y(x) = P_i(x)$, interacting with the crack is known. This known stress field is used to obtain the crack compliance function C by using Castigliano's approach.

To illustrate the determination of the compliance functions, a strip of unit thickness and unit width in the z direction with an edge crack of length a as illustrated in Figure 6.5, is taken. In order to obtain the horizontal displacement u at (l, s) we introduce a pair of virtual forces F at that location in the horizontal direction (Figure 6.5). The forces may be located at either the top or bottom surface.

Figure 6.5.- Edge-Cracked strip subjected to surface loading and virtual force [*Cheng, Prime and Finnie, 1997*]

The change in the strain energy due to the presence of the crack and the virtual force is given by [*Cheng, Prime and Finnie, 1997*]:

$$U = \frac{1}{E'} \int_0^a (K_I + K_{IF})^2 da \qquad 6.12$$

where K_I is the stress intensity factor due to the known stress field and K_{IF} is the stress intensity factor due to the virtual force F. Applying Castigliano's theorem, the displacement $u(a,s)$ can be determined by taking a derivative of the strain energy with respect to the virtual force, as [*Cheng and Finnie, 1994*]:

$$u(a,s) = \frac{1}{2}\frac{\partial u}{\partial F}\Big|_{F=0} = \frac{1}{E'} \int_0^a K_I \frac{\partial K_{IF}(a,s)}{\partial F} da\Big|_{F=0} \qquad 6.13$$

Differentiating now with respect to the distance s, the strain in the x-direction is given by Equation 6.14 [*Cheng and Finnie, 1994*]:

$$\varepsilon(a_j,s) = \frac{1}{E'} \int_0^a K_I(a) \frac{\partial^2 K_{IF}(a,s)}{\partial F \partial s} da \qquad 6.14$$

This strain ϵ (a,s) due to the stress $P_i(x)$ is known as the compliance function $C_i(a,s)$ so that;

$$C_i(a_j,s) = \frac{1}{E'} \int_0^{a_j} K_I(a) \frac{\partial^2 K_{IF}(a,s)}{\partial F \partial S} da \qquad 6.14a$$

Due to the linearity of K_{IF} with F, the second term under the integral sign in Equation 6.14a is the same as $Z(a)$ in Equation 6.5 with $B = 1$, Therefore we can write

$$C_i(a_j,s) = \frac{1}{E'} \int_0^{a_j} K_I(a) Z(a) da \qquad 6.14b$$

By following the approach in *Schindler et. al.* [*1997*] *and Kang et. al.* [*1989*] for the case of a beam having the strain measurement point M at the base, Figure 6.5, $K_I(a)$ and $Z(a)$ can be expressed as

$$K_I(a) = \int_0^a h(x,a)\sigma_y(x) dx \qquad 6.14c$$

$$Z(a) = 4.283 \int_0^a h(x,a)(1-2x)dx \qquad 6.14d$$

where $\sigma_y(x) = P_i(x)$ and $h(x,a)$ is known as the weight function [*Wu and Carlsson, 1991*]. The reference contains tabulated values of $h(x,a)$ for given values of a and x. We can therefore determine $C_i(a_j,s)$ from Equation 6.14d by integrating numerically. Appendix I describes a direct method developed in this thesis for the determination of $h(x,a)$ without relying on tabulated values. This approach gives more flexibility for the determination of function $h(x,a)$.

Once the $C_i(a,s)$ solutions have been obtained we can obtain the expected strain due to the stress components in 6.11a as [*Cheng and Finnie, 1994*]:

$$\varepsilon(a_j,s) = \sum_{i=0}^{n} A_i C_i(a_j,s) \qquad 6.15$$

The unknown terms A_i now have to be determined so that the strains given by Equation 6.15 matches those from strains measured in the experiment during cutting $\varepsilon(a_j,s)_{actual}$. To minimise the average error over all data points for the n^{th} order approximation, the method of least squares is used to obtain the values A_i. Therefore the number of cutting increments m is often chosen to be greater than the order of the polynomials P_i i.e. $m > n$. Typically $m = n + 1$ is used [*Cheng and Finnie, 1994*]. This work used $n = 8$ and $m = 9$, the least square solution is obtained by minimising the square of the error relative to the unknown constant A_i, i.e. as in Equation 6.16 [*Cheng and Finnie, 1994*]:

$$\frac{\partial}{\partial A_i} \sum_{j=1}^{m} \left[\varepsilon(a,s)_{actual} - \sum_{k=0}^{n} A_k C_k(a_j,s) \right]^2 = 0 \qquad i = 0, \ldots, n \qquad 6.16$$

This gives

$$[H]\{A\} = \{J\} \qquad 6.16a$$

where $[H] = [C]^T[C]$ and $\{J\}=[C]^T\{\varepsilon_j\}_{actual}$ [*Press et. al., 1987*]. Equation 6.16a gives a simple set of simultaneous linear equations. For the problems considered in this work, *[H]* is a *8x8* matrix. The numerical procedure was implemented in a FORTRAN program using the Compac Visual FORTRAN package and Equation 6.16a was solved using the LU Decompositor (LUDCMP) and Backsubstitution (LUBKSB) routines [*Press et. al., 1987*]. The actual residual stress distribution was then determined by using equation 6.11a.

6.4. Summary.

In this chapter, the analytical formulation of the crack compliance method has been explained and an analytical evaluation of the weight function is correspondingly highlighted in Appendix I. The crack compliance method followed in this work used the compliance function and the polynomial representation of the residual stresses as the forward solution and the inverse solution stages. This approach was assessed to be less prone to error propagation problems. Error propagation can occur in the method based on the incremental solution method.

Chapter 7

FEA evaluation of the crack compliance method

7.1. Introduction.

The theory related to the use of the crack compliance was explained in Chapter 6 of this thesis. During the review of literature, it was noticed that there is a lack of information on how some basic functions such as the weight and the geometry dependent functions used in the CCM are evaluated. It was additionally apparent that although several authors used the method there was not enough effort placed on the analysis of the sensitivity of the parameters used.

In this chapter, functions such as the influence and weight functions, which are used in the CCM, were calculated using the FEM. The chapter also demonstrate the simulation of the cutting of a component under the influence of residual stresses in order to obtain resulting strains and study sensitivity to cutting dimensions. The effect of the change in the locations of the virtual forces and the incremental change, *ds*, the location of distance between the forces for the determination of the functions were also investigated using FEM. Other analysis carried out in this chapter shows how the relative positions of the crack plane to the location of the measurement position affect the influence function. The aim of this aspect of the work was to investigate the ease of using FEM to determine essential functions values required for CCM without needing to find analytical solutions for every new problem case.

The results of the FEM analyses carried out for the influence function are compared against analytical solutions found in the literature. To facilitate the analysis carried out in this chapter, all the models used were reduced in dimension as much as possible. Almost all the models analysed were created in 2-D in order to save computer resources and time.

In this chapter ANSYS 5.5 and ABAQUS 6.3 finite element computer programs were used for the analyses carried out.

7.2. Determination of the influence function *Z(a)* using FEM.

The principle of the CCM used for the determination of residual stresses involves the removal of a sufficient amount of material resulting in the deformation of the body in terms of displacements or strains. The modelling carried out in this chapter used this same idea and simulated the introduction of a narrow growing slot into the body in order to determine influence function *Z(a)*, and evaluate its sensitivity to the location of strain measurement and virtual force position.

In the finite element analysis it was necessary to remove small elements in order to simulate the introduced slot for the use of the crack compliance method. The deletion of elements produces a strain relaxation that can be employed to recalculate the residual stress profile. The removal of elements in the model causes a redistribution of the residual stress field, in the same way as happens in real specimens.

A narrow slot, in a material behaving elastically, is nearly equivalent to a crack and the well-known equations of linear elastic fracture mechanics can be used to establish the required mathematical relations. The general relationship between the stress intensity factor of a crack in a residual stress field and the strain change was highlighted in Chapter 6. The three fundamental variables used in the crack compliance method are; the stress intensity factor, the influence function and the weight function. All of these three variables can be obtained analytically and/or numerically, but literature on the determination of the influence and weight functions by numerical methods is rare.

In this section particular attention is given to the technique used to determine the influence function by FEA. Additionally, some FEA carried out on the influence of the distance between the loads acting on a crack and the mode I stress intensity factors are presented.

7.2.1. Determination of the influence functions by FEA.

The influence function, *Z(a)*, is independent of the actual residual stress distribution and only needs to be determined once for a certain geometry. As seen in Chapter 6, the influence function can be expressed as;

$$Z(a) = \frac{B}{F}\left(\frac{\partial K_{IF}}{\partial s}\bigg|_{s=0}\right) \qquad 7.1$$

The influence function is essentially given by the derivative of the stress intensity factor, of a crack configuration of interest due to the line force, F, with respect to the distance tangent to the surface at the strain measurement point (Chapter 6, Figure 6.2). Also as indicated in Chapter 6, *Z(a)* can also be calculated using;

$$Z(a) = \frac{E'}{K_{Iref}(a)}\frac{d\varepsilon_{Mref}}{da}(a) \qquad 7.2$$

where K_{Iref} and ε_{Mref} denote the stress intensity factor and the relieved strain at the selected reference point respectively when the crack length is equal to a.

Equation 7.2 appears easier to implement but in fact the same type of parameters are required in both methods. The position s of the force F and either a differential movement ds or da is required. Equation 7.1 was chosen for the parametric studies carried out. In the following sections several examples for the calculation of the influence function are presented and some factors involved in these calculations are changed in order to check their effect on the final results.

7.2.2. Empirical solution for *Z(a)*.

The first case examined in this section, is the most cited geometry examined by several authors using the crack compliance method, i.e. the beam. The example presented is the determination of the influence function for a beam with an increasing crack length.

Consider a beam of length L and depth W, which contains an initial crack of depth a_o, as illustrated in Figure 7.1. A semi-empirical expression for $Z(a)$ is given in *Schindler, 1996*, as Equation 7.3a and 7.3b below.

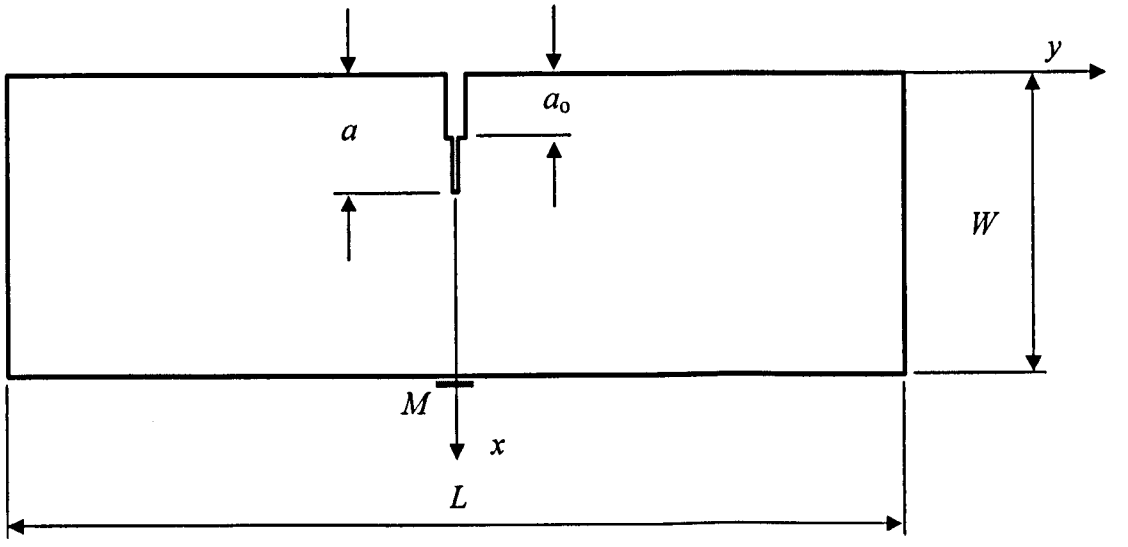

Figure 7.1.- Beam containing an edge crack

$$Z(a) = \frac{2.532}{(W-a)^{\frac{3}{2}}}\sqrt{(1-25)\left(\left(\frac{a}{W}\right)-0.2\right)^2}\left[5.926\left(0.2-\left(\frac{a}{W}\right)\right)^2 - 0.288\left(0.2-\frac{a}{W}\right)+1\right] \quad 7.3a$$

For $a/W \leq 0.2$

$$Z(a) = \frac{2.532}{(W-a)^{\frac{3}{2}}} \qquad 7.3b$$

For $0.2 \leq a/W \leq 1$

The functions relate to strain measurement at the point *M*, Figure 7.1. These equations were deduced from analytical solutions for disks and empirically fitted to the case of beams [*Schindler, 1996*]. The FEA approach provides a means to determine the function without empirical considerations and also potentially take account of the finiteness of dimensions better.

In this section a comparison between the results of Equations 7.3a and 7.3b against the ones determined by the use of FEA with Equations 7.1 and 7.2 was carried out. A typical FE mesh used for the analysis is shown in Figure 7.2. The figure shows the crack length *a* and the distance *s* for the location of the virtual force *F*. The ANSYS 5.5 finite element package was used. To save computational resources and time, the analysis was carried out using 2 dimensional modelling.

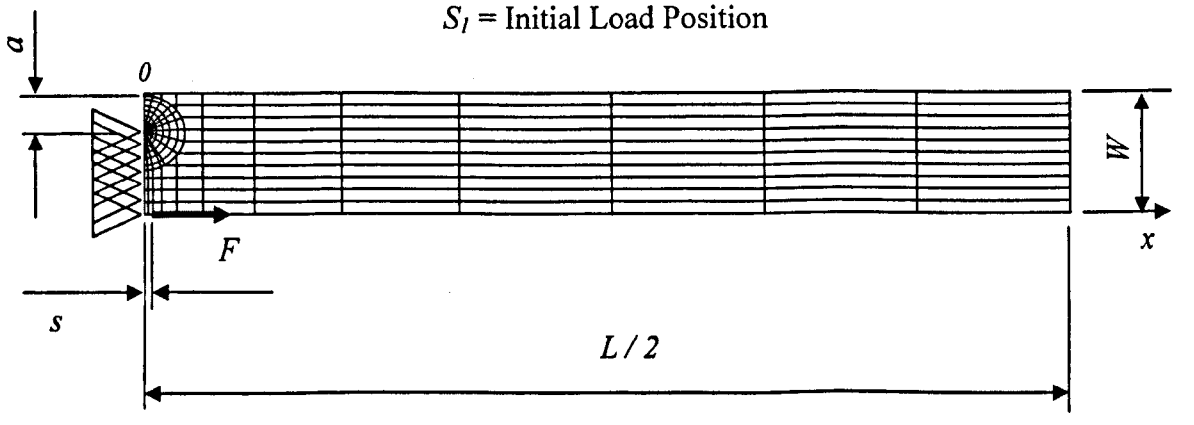

Figure 7.2.- FE beam model containing an edge crack

Only one half of the beam was modelled because of the symmetry of the geometry (Figure 7.2). By constructing the model in this way, the geometry of the beam, the load position and the crack length can be easily modified as required. Eight noded quadratic elements, that provide accurate results and can model irregular shapes appropriately without loss of accuracy, were used (Figure 7.2). The length of the main beam analysed was 200 mm and the depth was 10 mm. The convergence of the model was checked by refining the mesh and verifying that there were no significant differences between results from the meshes. Theoretical calculations were also carried out to validate simulation results wherever possible.

The Young's modulus and Poisson's ratio employed for all the analyses in this section were 210 GPa and 0.3 respectively. FE modelling was used to determine the stress intensity factor (mode I) for several different loading situations, as required for the calculation of the influence function using Equation 7.2. The point force used was 100 N in all cases and the crack length was increased in all cases by 1 mm steps.

The modelling considered the effect of locating the force F at different normalised distances s/W varying from 0.025 to 0.225 in steps of 0.025 increments. The effect of the change in Δs on Equation 7.1 was also studied. These studies were carried out with the aim to verify existing empirical solutions and to ascertain the level of flexibility that FEM can give compared to derivation of analytical solutions for $Z(a)$. The crack length was increased by normalised crack increment $\Delta a/W$ equal to 0.1 in each step and the stress intensity factor was determined for each location s and crack increment length Δa. The analysis was carried out until the crack length reached $0.9W$. The numerical results obtained for the stress intensity factor (mode I) for each load configuration are presented

in Table 7.1. The numerical results obtained for the influence function *Z(a)* for the location *s/W* = 0.025 showing the effect of different values of *ds/W* are shown in Table 7.2.

Table 7.1.- Stress intensity factor K_I (MPa$\sqrt{m}$) for a beam (L = 200 mm and W = 10 mm) with different crack lengths and different loading setting, plane stress analysis

Crack Length *a/W*	*ds/W*								
	0.025	**0.050**	**0.075**	**0.100**	**0.125**	**0.150**	**0.175**	**0.200**	**0.225**
0.1	2.0998	4.2143	6.2486	8.2563	10.221	12.141	13.987	15.775	17.467
0.2	2.7552	5.5259	8.1992	10.834	13.409	15.917	18.326	20.651	22.846
0.3	3.4126	6.8325	10.146	13.401	16.561	19.623	22.541	25.331	27.954
0.4	4.2987	8.6010	12.753	16.807	20.701	24.436	27.946	31.261	34.324
0.5	5.6355	11.259	16.642	21.842	26.753	31.377	35.627	39.545	43.068
0.6	7.8559	15.644	22.986	29.934	36.300	42.097	47.224	51.74	55.642
0.7	12.055	23.828	34.568	44.304	52.690	59.846	65.698	70.459	74.226
0.8	22.041	42.577	59.724	73.630	83.876	91.329	96.475	99.925	102.23
0.9	60.453	106.19	131.80	144.44	149.82	151.54	152.21	151.94	151.69

Table 7.2.- Influence function $Z(a) = (B/F)(dK_I/ds)$, calculation made by taking *s/W* = 0.025 as a start point

Crack Length *a/W*	Analy-tical value	*ds/W*							
		0.025	**0.05**	**0.075**	**0.1**	**0.125**	**0.15**	**0.175**	**0.2**
0.1	0.0938	0.0846	0.0830	0.0821	0.0812	0.0803	0.0792	0.0781	0.0768
0.2	0.1119	0.1108	0.1089	0.1077	0.1065	0.1053	0.1038	0.1023	0.1005
0.3	0.1360	0.1368	0.1347	0.1332	0.1315	0.1297	0.1275	0.1252	0.1227
0.4	0.1720	0.1721	0.1691	0.1668	0.1640	0.1611	0.1576	0.1541	0.1501
0.5	0.2264	0.2249	0.2201	0.2161	0.2112	0.2059	0.1999	0.1938	0.1872
0.6	0.3165	0.3115	0.3026	0.2944	0.2844	0.2739	0.2625	0.2508	0.2389
0.7	0.4870	0.4709	0.4503	0.4300	0.4064	0.3823	0.3576	0.3337	0.3109
0.8	0.8950	0.8214	0.7537	0.6879	0.6184	0.5543	0.4962	0.4451	0.4009
0.9	2.5320	1.8295	1.4269	1.1198	0.8937	0.7287	0.6117	0.5228	0.4562

Figure 7.3 compares the results obtained using FEA against semi-empirical Equation 7.3. The closeness of the results can be seen especially for small values of *ds/W*. The results shows that *ds/W* should be less than or equal to 0.025 for crack lengths up to 0.8*W*. The

difference at $a/W = 0.8$ is about 8%. The difference at lower values such as $a/W = 0.2$ is less than 1%.

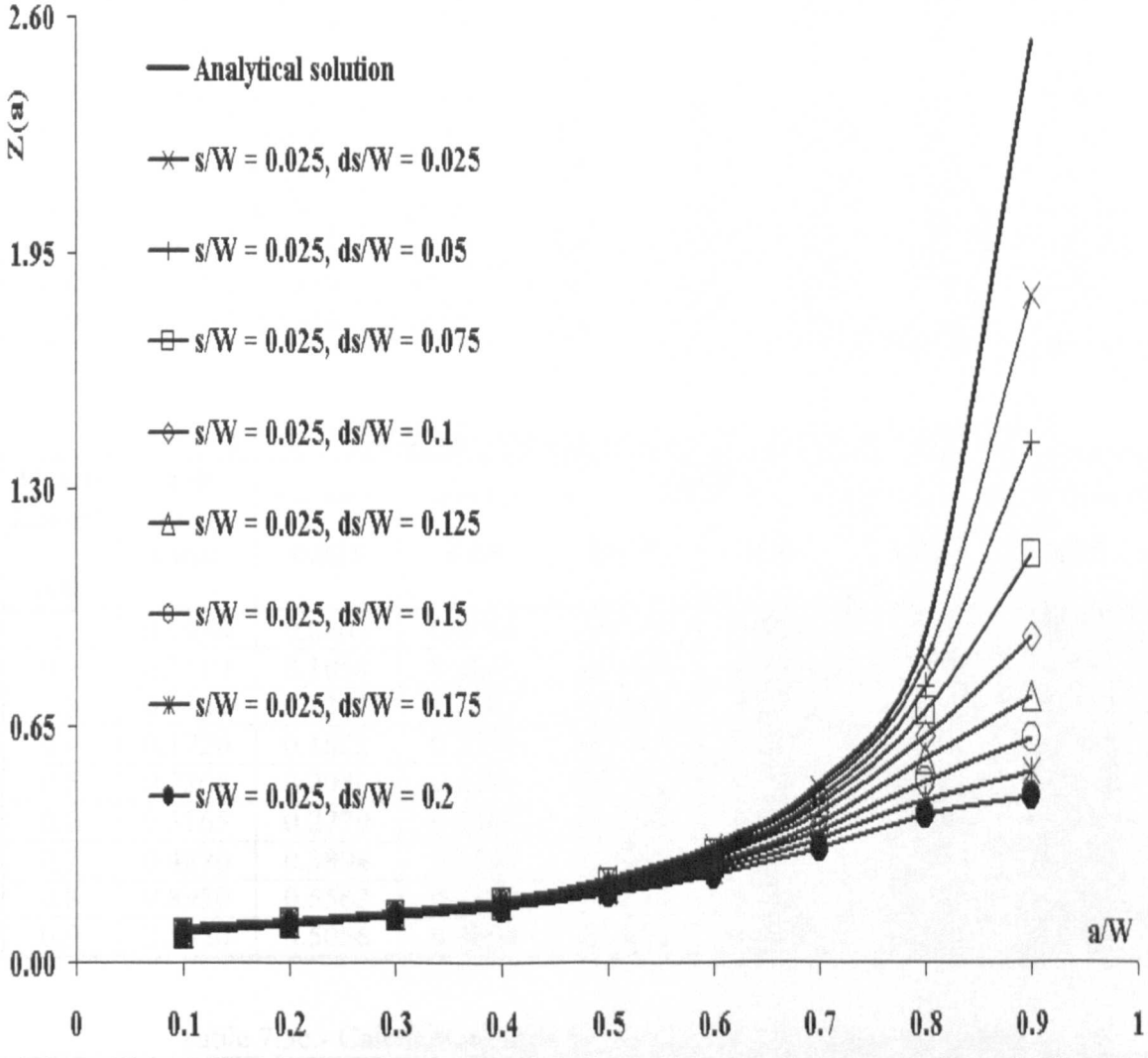

Figure 7.3.- Influence function results from initial loading distance of $s/W = 0.025$ and increasing the separation of the loading distance

Numerical results for the study of the effect of the starting location of the point force can be seen in Tables 7.3 for different values of ds/W. The response of the influence function to the change of the position of the load and also the response of the influence to different ds distances is presented in Figures 7.4. Figure 7.5 presents comparisons between calculations of the influence function where the positions of the point load is varied, but the distance ds is kept constant and the analytical solution.

Table 7.3.- Influence function $Z(a) = (B/F)(dK_I/ds)$

Table 7.3a.- Calculation made by taking $s/W = 0.05$ as a start point

Crack Length a/W	Analytical value	ds/W						
		0.025	**0.05**	**0.075**	**0.10**	**0.125**	**0.15**	**0.175**
0.1	0.0938	0.0814	0.0808	0.0801	0.0793	0.0782	0.0771	0.0641
0.2	0.1119	0.1069	0.1062	0.1051	0.1039	0.1024	0.1008	0.0837
0.3	0.1360	0.1325	0.1314	0.1297	0.1279	0.1257	0.1233	0.1018
0.4	0.1720	0.1661	0.1641	0.1613	0.1584	0.1548	0.1511	0.1233
0.5	0.2264	0.2153	0.2117	0.2066	0.2012	0.1949	0.1886	0.1510
0.6	0.3165	0.2937	0.2858	0.2754	0.2645	0.2526	0.2406	0.1866
0.7	0.4870	0.4296	0.4095	0.3848	0.3602	0.3350	0.3109	0.2266
0.8	0.8950	0.6859	0.6211	0.5507	0.4875	0.4312	0.3823	0.2429
0.9	2.5320	1.0244	0.7650	0.5817	0.4535	0.3682	0.3050	0.1137

Table 7.3b.- Calculation made by taking $s/W = 0.075$ as a start point

Crack Length a/W	Analytical value	ds/W					
		0.025	**0.05**	**0.075**	**0.10**	**0.125**	**0.15**
0.1	0.0938	0.0803	0.0794	0.0786	0.0774	0.0762	0.0737
0.2	0.1119	0.1054	0.1042	0.1029	0.1013	0.0996	0.0961
0.3	0.1360	0.1302	0.1283	0.1264	0.1240	0.1215	0.1164
0.4	0.1720	0.1622	0.1590	0.1558	0.1519	0.1481	0.1401
0.5	0.2264	0.2080	0.2022	0.1965	0.1899	0.1832	0.1698
0.6	0.3165	0.2779	0.2663	0.2548	0.2424	0.2300	0.2057
0.7	0.4870	0.3894	0.3624	0.3370	0.3113	0.2871	0.2394
0.8	0.8950	0.5562	0.4830	0.4214	0.3675	0.3216	0.2288
0.9	2.5320	0.5056	0.3604	0.2632	0.2041	0.1611	0.0580

Table 7.3c.- Calculation made by taking $s/W = 0.10$ as a start point

Crack Length a/W	Analytical value	ds/W				
		0.025	**0.05**	**0.075**	**0.10**	**0.125**
0.1	0.0938	0.0786	0.0777	0.0764	0.0752	0.0737
0.2	0.1119	0.1030	0.1017	0.0999	0.0982	0.0961
0.3	0.1360	0.1264	0.1244	0.1219	0.1193	0.1164
0.4	0.1720	0.1558	0.1526	0.1485	0.1445	0.1401
0.5	0.2264	0.1964	0.1907	0.1838	0.1770	0.1698
0.6	0.3165	0.2546	0.2433	0.2305	0.2181	0.2057
0.7	0.4870	0.3354	0.3108	0.2853	0.2616	0.2394
0.8	0.8950	0.4098	0.3540	0.3046	0.2630	0.2288
0.9	2.5320	0.2152	0.1420	0.1036	0.0750	0.0580

Table 7.3d.- Calculation made by taking $s/W = 0.125$ and $s/W = 0.15$ as a start point

Crack Length a/W	Analy-tical value	*ds/W*				*ds/W*		
		0.025	**0.05**	**0.075**	**0.10**	**0.025**	**0.05**	**0.075**
0.1	0.0938	0.0768	0.0753	0.0741	0.0725	0.0738	0.0727	0.0710
0.2	0.1119	0.1003	0.0983	0.0966	0.0944	0.0964	0.0947	0.0924
0.3	0.1360	0.1225	0.1196	0.1169	0.1139	0.1167	0.1142	0.1111
0.4	0.1720	0.1494	0.1449	0.1408	0.1362	0.1404	0.1365	0.1318
0.5	0.2264	0.1850	0.1775	0.1706	0.1632	0.1700	0.1634	0.1559
0.6	0.3165	0.2319	0.2185	0.2059	0.1934	0.2051	0.1929	0.1806
0.7	0.4870	0.2862	0.2602	0.2369	0.2154	0.2341	0.2123	0.1917
0.8	0.8950	0.2981	0.2520	0.2140	0.1835	0.2058	0.1719	0.1453
0.9	2.5320	0.0688	0.0478	0.0283	0.0187	0.0268	0.0080	0.0020

Table 7.3e.- Calculation made by taking $s/W = 0.175$ and $s/W = 0.20$ as a start point

Crack Length a/W	Analytical value	*ds/W*		*ds/W*
		0.025	**0.05**	**0.025**
0.1	0.0938	0.0715	0.0696	0.0677
0.2	0.1119	0.0930	0.0904	0.0878
0.3	0.1360	0.1116	0.1083	0.1049
0.4	0.1720	0.1326	0.1276	0.1225
0.5	0.2264	0.1567	0.1488	0.1409
0.6	0.3165	0.1806	0.1684	0.1561
0.7	0.4870	0.1904	0.1706	0.1507
0.8	0.8950	0.1380	0.1151	0.0922
0.9	2.5320	-0.0108	-0.0104	-0.0100

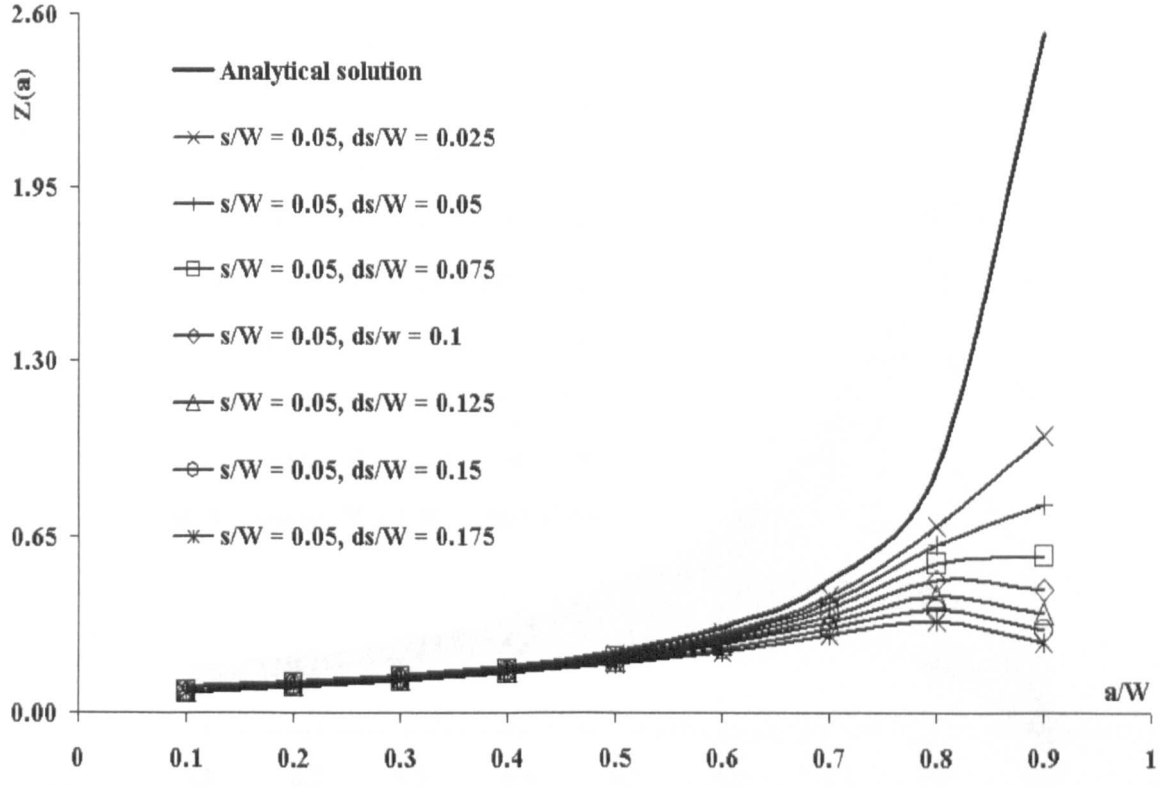

Figure 7.4.- Influence function results from initial loading distance of $s/W = 0.05$ and increasing the separation of the loading distance

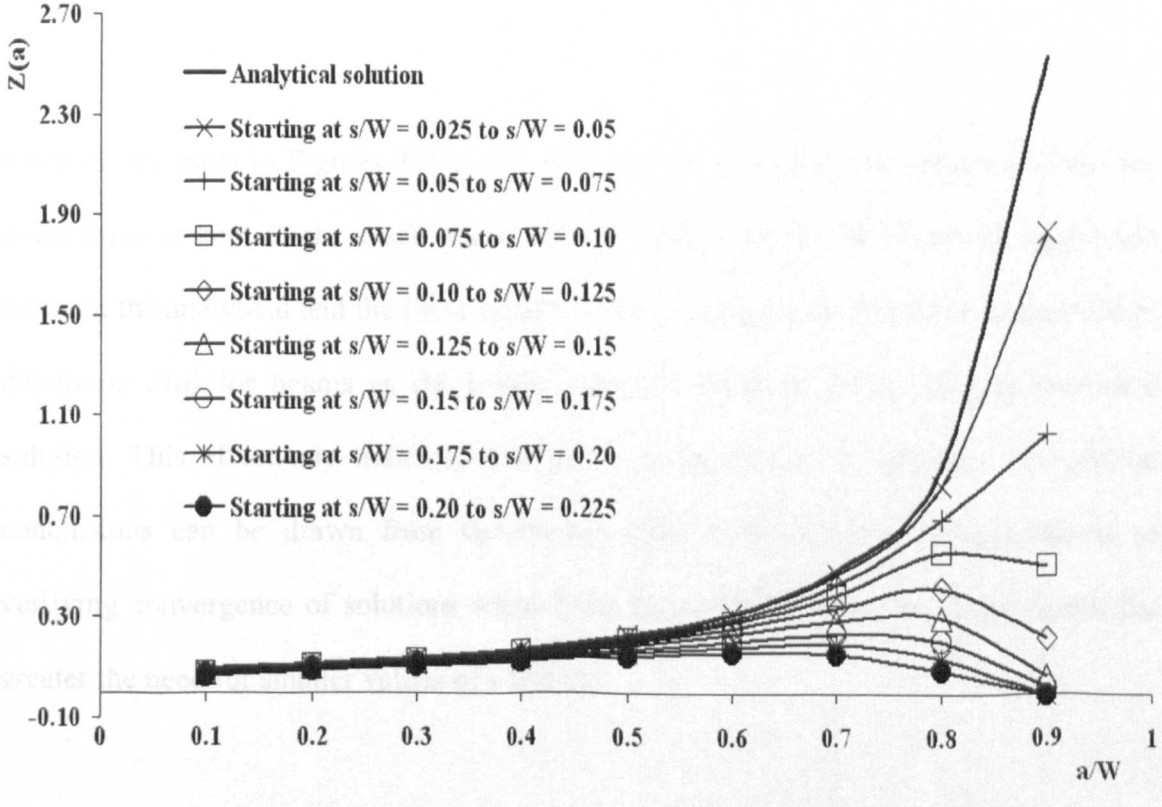

Figure 7.5a.- Influence function results for loading between nearest nodes at different starting points

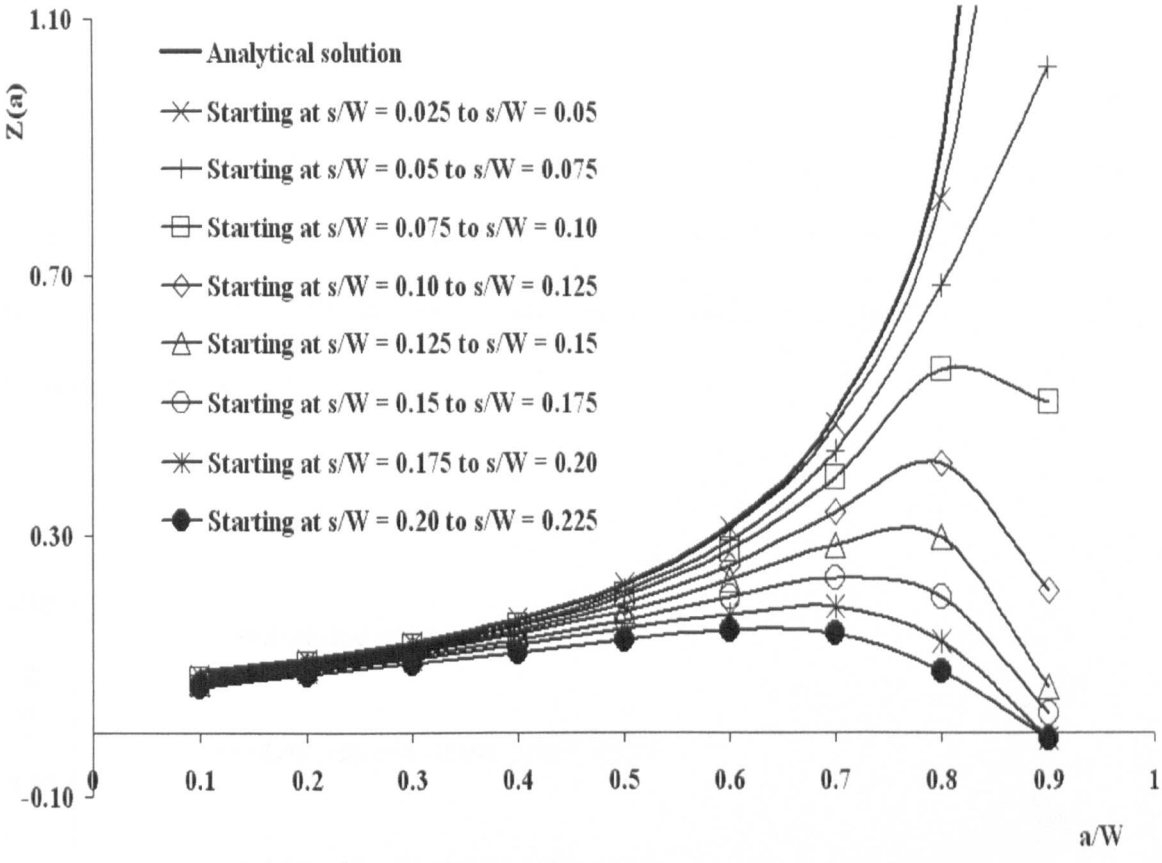

Figure 7.5b.- Close up of the influence function results for loading between nearest nodes at different starting points

From all the plots in Figures 7.3 to 7.5, it is clear as to be expected, that the closer the point force is kept to the crack plane and the smaller Δs is, the closer the agreement between the analytical and the FEM results. There is no apparent benefit in using FEM to determine $Z(a)$ for beams as the results obtained converge to the existing empirical solution. This effectively indicates that the existing solution is adequate. No general conclusions can be drawn from the studies other than the known requirements of verifying convergence of solutions when FEM is used. The longer the crack length the greater the need for smaller values of s and ds.

After the effect of the positions of loading was evaluated, it was considered necessary to analyse the effect of change in geometry by means of the length/depth ratio (L/W) on the influence function. Initially two cases based on $L/W = 2.5$ and $L/W = 1$ were considered. Further parameters considered were $s/W = 0.025$ and $ds/W = 0.025$. Results can be seen in Figures 7.6a and 7.6b. In these cases greater divergence in results is noticed toward extreme values of a/W.

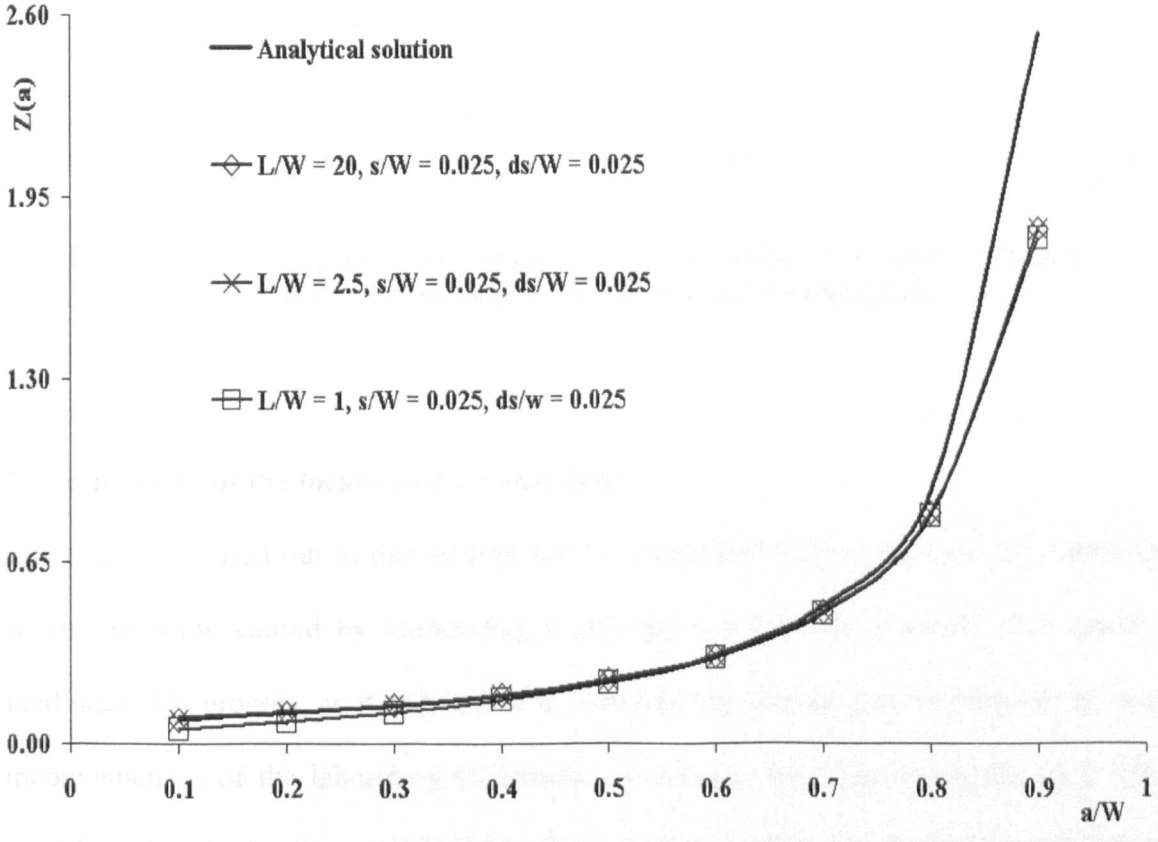

Figure 7.6a.- Comparison between different influence functions for beams and rectangular plates at same loading points

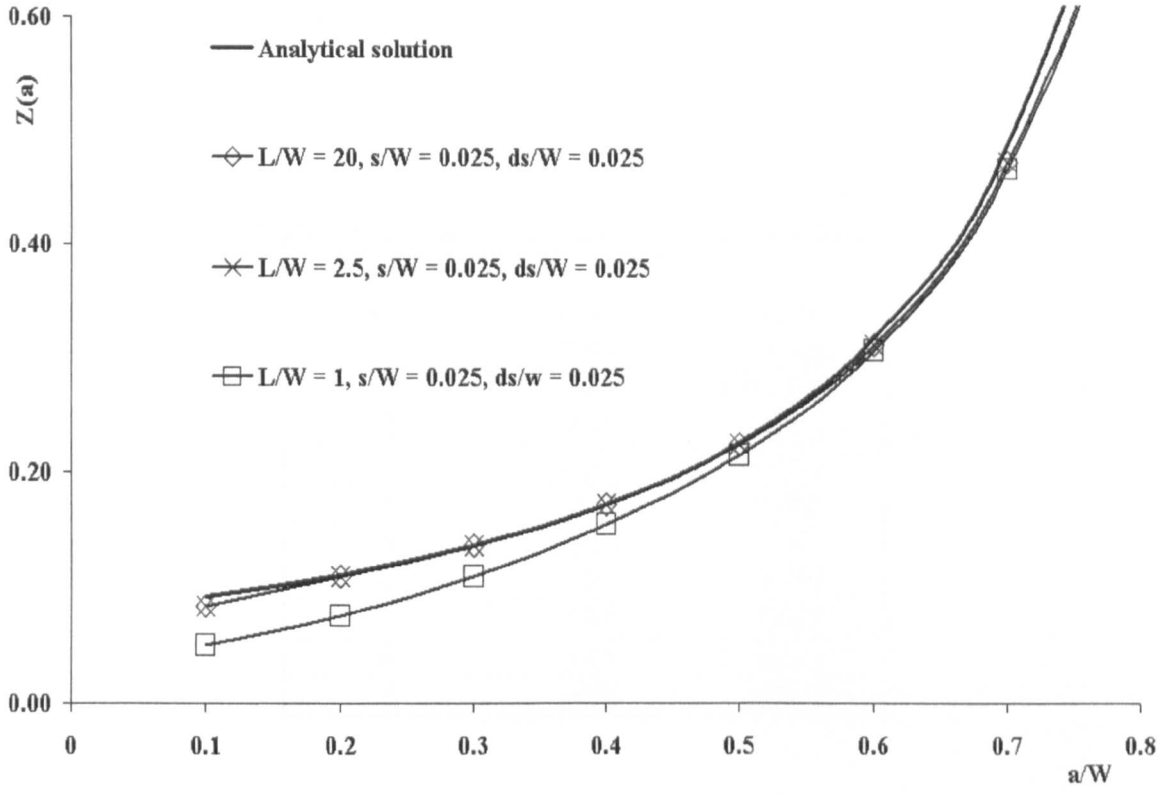

Figure 7.6b.- Close up of the comparison between different influence functions for beams and rectangular plates at same loading points

7.3. Sensitivity of the location of strain gauges.

The analysis carried out in this section was to determine the best location for obtaining strain relaxation caused by introducing a growing slot into the material. FEA greatly facilitates this process, as it is possible to simulate the cutting process without the real inconveniences of the laboratory (Vibration, movement, noise in the signal, etc.). The model used in this section was similar to the one used to determine the influence function for a beam.

The material considered was Waspaloy. The decision to simulate this material by FEA was taken because a few authors [*Nowell, Tochilin and Hills, 2000* and *Ezeilo and Webster, 2000*] have reported their findings on the material. This material has a Young's

modulus equal to 223 GPa and Poisson ratio of 0.285. Multi-isotropic hardening was employed and the material properties used are given in Table 7.4.

Table 7.4.- Waspaloy beam stress-strain behaviour

Point	Stress MPa	Total Strain
1	680	0.00304932
2	830	0.004
3	900	0.005
4	940	0.006
5	967	0.007
6	981	0.008
7	988	0.009
8	995	0.010
9	1050	0.015

Figure 7.7 shows construction points and lines used in order to be able to produce an appropriate mesh for the study. The slot was cut along the centre line of the beam.

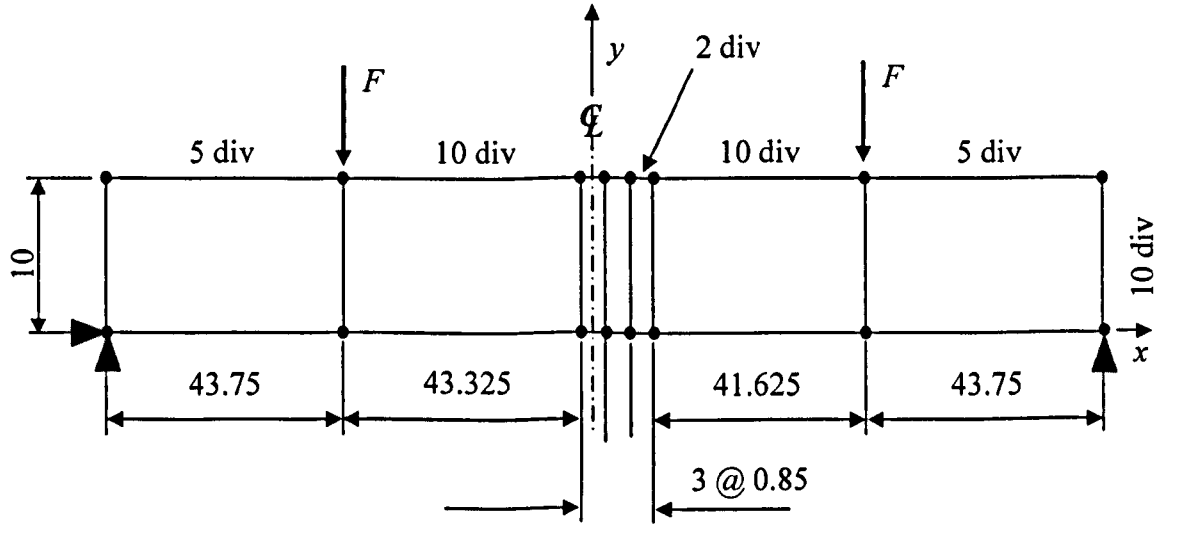

Figure 7.7.- Finite element model of a Waspaloy steel beam

Restrictions of freedom were set at the edges of the beam along the x and y directions at the bottom left node, and along the y direction at the bottom right node. Loading was applied as a four point bending configuration with a point force of 532.5 N [*Ezeilo and Webster, 2000*] acting in the negative direction with respect to the y-axis as illustrated in Figure 7.7. The model was analysed in sequential steps; first plastically loading, then unloading, then deletion of pairs of elements at the centre of the beam with the stress and strain results obtained at each step. The locations where the strains were obtained is illustrated in Figure 7.8.

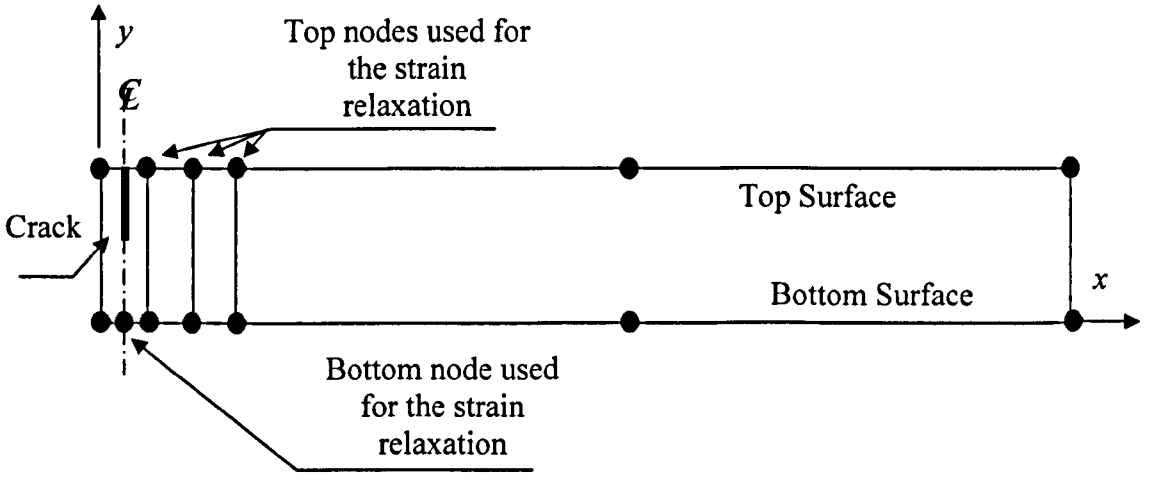

Figure 7.8.- Node location of strain sensitivity reading, top and bottom surfaces

In Figure 7.9 the sensitivity of the strain reading at the top surface is shown. As the strain gauge position was shifted from the cutting plane, the strain reading reduced until it became virtually impossible to detect. The same analysis was carried out for the bottom side of the beam, but different distances were considered and some were located closer to the plane of the crack. In Figure 7.10 a similar phenomenon is illustrated as that occurring for the top surface of the beam.

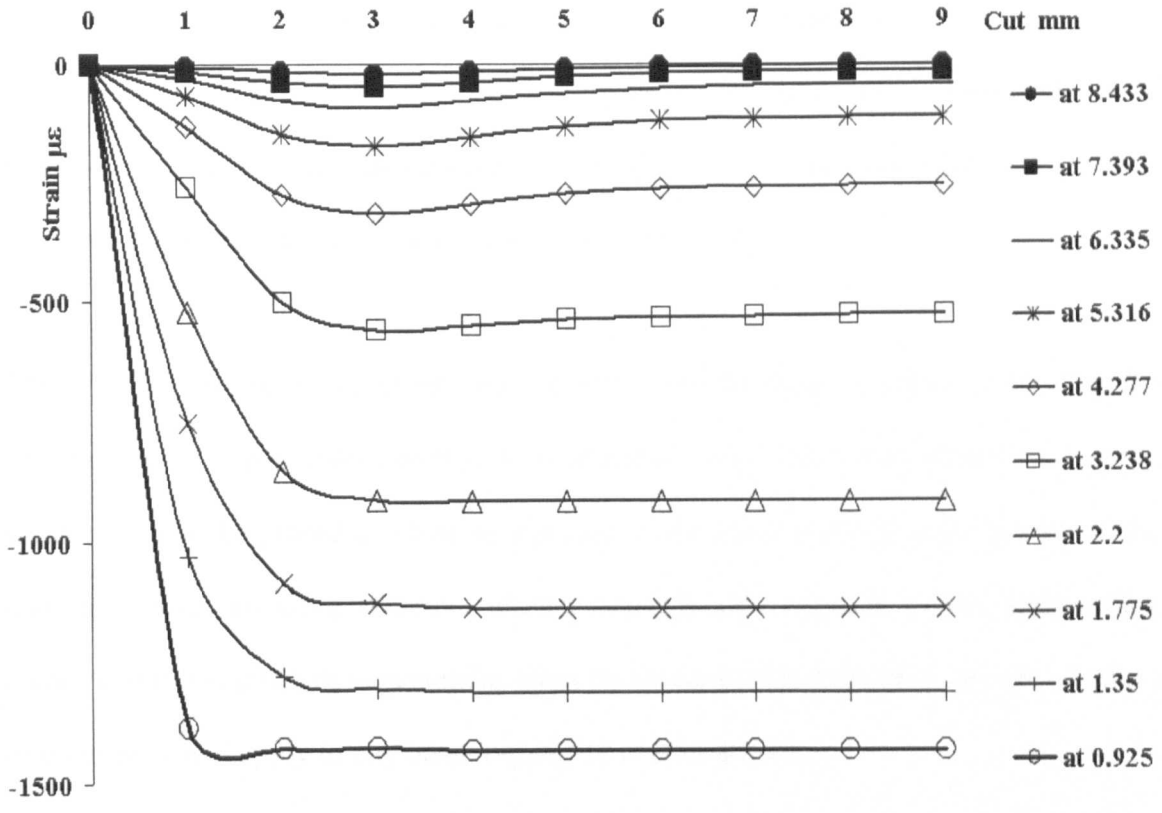

Figure 7.9.- Strain sensitivity at top surface

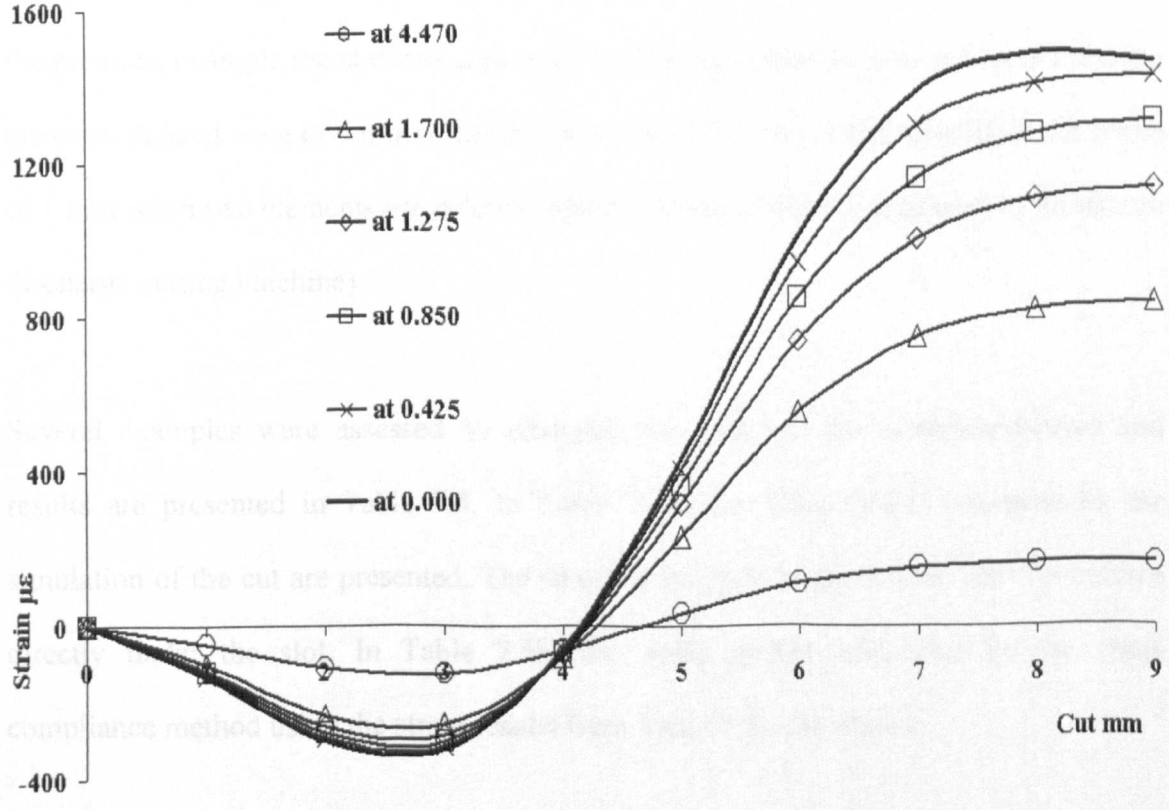

Figure 7.10.- Strain sensitivity at bottom surface

Figures 7.9 and 7.10 gives an indication of the rate of decrease of sensitivity as the position of the strain measurement shifts away from the crack plane. Additionally, as to be expected from the FEA the difference between cutting on the convex (top) or concave (bottom) side is only a change in the sign of the strain values.

The FEA results can be of great value to assess the quantitative effect of locating the strain gauge at a particular position in a laboratory test. The strain gauges on the top surface have to be placed as close as possible to the crack and the strain gauges at the bottom surface are more sensitive when placed directly opposite to the approaching crack. While it is difficult to generalise from the limited study presented, the observations of sensitivity will apply to any beam regardless of dimensions.

7.4. Effect of width of cut.

The next analysis carried out was to evaluate the effect of the thickness on the slot. For the previous example the slot was simulated by deleting elements from the model and the elements deleted were of 1 mm of depth and width of 0.5 mm (which provide a slot width of 1 mm when two elements are deleted, which is close to what is produced by an electro discharge cutting machine).

Several examples were assessed by changing the width of the elements deleted and results are presented in Table 7.5. In Table 7.5a, the strain results produced by the simulation of the cut are presented. The strain readings were taken from the rear surface directly under the slot. In Table 7.5b, the stress profile calculated by the crack compliance method using the strain results from Table 7.5a, are shown.

Table 7.5.- Influence of the slot width on the resulting strain for a Waspaloy beam

7.5a.- Strain (με) relaxation by cut

Cut Length (mm)	Strain (με)					
	Cut Width 1.5 mm	Cut Width 1 mm	Cut Width 0.2 mm	Cut Width 0.1 mm	Cut Width 0.05 mm	Cut Width 0.01 mm
0	0	0	0	0	0	0
1	-148.7	-132.1	-105.4	-104.4	-119	-171.9
2	-318.6	-298	-269.7	-269.5	-284.6	-328.3
3	-331.8	-324.8	-322.9	-323	-323.9	-323.9
4	-36.3	-63	-110.7	-104.9	-79.6	-28.5
5	492.9	431.7	350.6	367.7	409.9	475.2
6	1092.6	1008.5	930.1	959.2	1003.1	1054.9
7	1449.5	1386.6	1368.7	1395.2	1421	1442.3
8	1512.7	1485.7	1521.9	1539.1	1549.9	1555.7
9	1462	1468.3	1464.2	1466.5	1468.1	1469.6

7.5b.- Stress (MPa) calculation by crack compliance, developed by Finnie

Beam Width (mm)	Stress (MPa)					
	Cut Width 1.5 mm	Cut Width 1 mm	Cut Width 0.2 mm	Cut Width 0.1 mm	Cut Width 0.05 mm	Cut Width 0.01 mm
-4	163.10	162.80	169.00	173.80	172.10	118.70
-3	-154.90	-128.20	-81.55	-81.36	-108.40	-181.60
-2	-334.30	-310.40	-280.10	-285.50	-301.10	-316.80
-1	-232.40	-230.80	-241.70	-245.80	-238.40	-207.30
0	46.58	26.35	-12.05	-10.05	8.65	48.68
1	280.90	255.00	222.70	229.70	243.50	262.40
2	299.00	286.50	285.50	291.40	293.50	288.20
3	112.10	120.10	144.20	143.50	137.40	128.90
4	-62.13	-47.36	-38.60	-42.46	-45.17	-65.31

The results plotted in these last tables are also presented in Figures 7.11 and 7.12 for the strain simulation and the residual stress determination respectively. From Figures 7.11 and 7.12 it can be seen that changing the thickness of the induced slot has a small effect in the values and final shape of the residual stress profiles obtained by the CCM using the strain relaxation simulated by FEA.

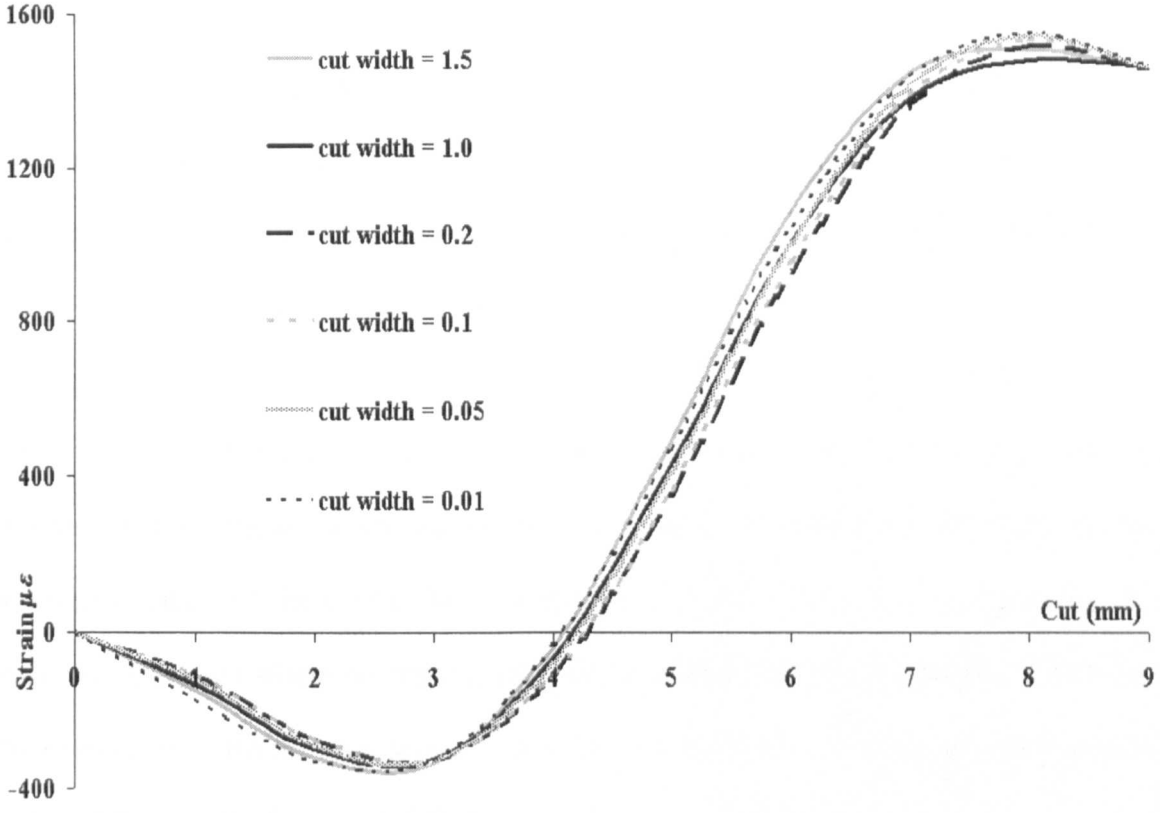

Figure 7.11.- Different widths influence on the strain relaxation cause by the cut simulation

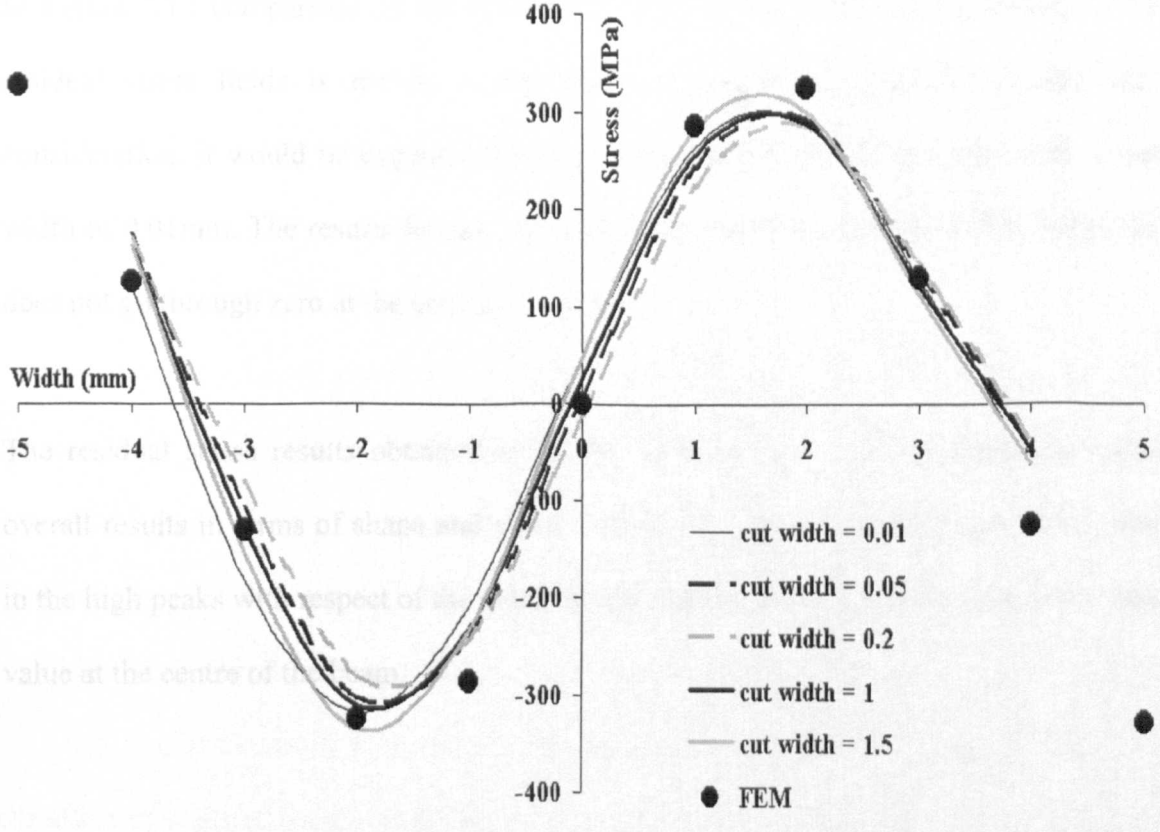

Figure 7.12.- Stress calculations obtained by different widths in the cut simulation

The analysis conducted in this section was based on the fact that CCM uses fracture mechanics theory (where the slot is considered to be a crack, but in reality the produced cut has a width that is much thicker than a crack). So, it was important to assess the effect of the slot width in the determination of residual stresses and how large the width of the cut it can be permitted to obtain accurate results.

From Figure 7.11 it can be seen that the change in width of the slot produces different results for the relaxed strain. Apparently, the shape and height values of the plotted relaxed strain tend to be similar, but if looked at in detail big differences are apparent. For example, the point where the relaxed strain changes from negative to positive is different in all cases and also the high peak values in the relaxed strain (both negative and positive sides) differ greatly from plot to plot.

In Figure 7.12 comparison of the effect of the slot width on the determination of the residual stress fields is shown. If the theory of fracture mechanics is taken into consideration, it would be expected that the best set of results are produced with a slot width of 0.01mm. The results for this slot width seem good at the edges of the beam but does not go through zero at the centre.

The residual stress results obtained by a slot width of 0.05 mm has produced better overall results in terms of shape and values. The residual stress profiles tend to be close in the high peaks with respect of the expected residual stress field and are near to the zero value at the centre of the beam.

The main problem experimentally, is that a slot width of 0.05 mm is not possible to produce. FEA was performed in this section to estimate the effect of a slot width with the results obtained by CCM. From an experimental point of view a slot width of 1 mm is readily achievable. The results presented in Figure 7.12 for a slot width of 1 mm are very close to expected FEA residual stresses and also to those where the slot width was 0.05 mm. One inconvenience is using a 1 mm slot width is that the plot at the centre of the beam does not go through zero.

For the experimental evaluation of the CCM that is presented in the next chapter, it can be concluded that the results determined by a slot width of 1 mm are adequately accurate against expected results obtained by FEA. This section has provided confidence in the ability of the experimental set up to give good results.

7.5. Summary.

The FEA carried out verified the applicability of the published influence function, *Z(a)*, for beams. The need to carry out the verification was due to the empirical approach used for the derivation of the function and the lack of appraisal of the function in the literature.

While FEA can be used to determine *Z(a)* for any geometry configuration, it is difficult to generalise on the selection of the length *s* and *ds* needed to locate the virtual forces required on a mesh.

FEA can provide quantitative guidance on the relative effects of positioning strain gauges for collection of the strain relieved during cutting of slots. Additionally, the assessment of the effect of width of the slot is possible.

Chapter 8

Experimental determination of residual stresses using the crack compliance method

8.1. Introduction.

The aim of this chapter is to present the results of the experimental implementation of the crack compliance method (CCM) described in section 6.2.3. Also in addition to the contribution made in section 6.3.1, a new cutting procedure has been developed for the application of the method. The cutting procedure consists of a simple supporting system and a plate electric discharge machining (EDM) approach. The crack compliance method and the new cutting procedure are evaluated in this chapter by determining residual stresses induced by four-point bending considering the effects of various factors such as:

- types of metal alloys, namely EN 8 and EN 1A steels and AA 6082 T6 aluminium alloy.
- different heat treatment procedures, stress relief annealing and full annealing.
- method of cutting.
- effect of pre-straining.

These factors provided a means to assess the performance of CCM. The cutting process is very important in determining strain relief due to stress relief and the method used is presented in section 8.2 before the results of the evaluation of the CCM is presented in the chapter.

8.2. EDM methodologies for beams with residual stresses.

The most common machine used by researchers to introduce incremental slots in a specimen is the wire electric discharge machining (EDM) method. The principle of the method is to generate an electric discharge (spark) that removes unwanted material. The

method was originally designed to produce holes, slots and other difficult geometries. The machine is on occasions used to produce entire components, manufacture slots in very hard materials or to "rescue" a piece, for example, by removing a broken tap from a component.

A procedure based on the use of EDM with a copper plate instead of a wire is presented in section 8.2.1 below. The working principle is identical to that for a wire electric discharge machining method. In order to allow the cutting operation to be performed properly, a new simple supporting method for specimens was introduced.

8.2.1. Electric discharge machining using a plate.

The new cutting procedure developed focused on producing a straight cut along a desired plane. Firstly, it was important to design a new specimen supporting device that could support different specimen shapes without clamping and ensure that the cut remains in plane. It is also necessary that the weight of the specimen should be prevented from influencing the strain readings and the specimen should displace freely to given accurate strain relaxation readings.

This thesis considered the analysis of uniform rectangular cross-section beams. The weight of the beam can be considered to be uniformly distributed as illustrated in Figure 8.1a. The beam is assumed to be of length $2L$ and the uniformly distributed weight is w (N/m). In order to maintain symmetry, that will assist balance, the supports are assumed to be placed at distance a from the two ends of the beams. The bending moment at the centre of the beam where strain gauges are located is given by:

$$M_{(x=L)} = wL(\frac{L}{2} - a) \qquad 8.1$$

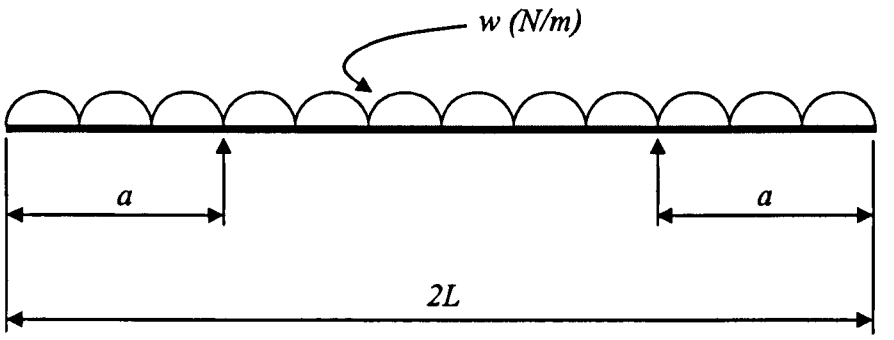

Figure 8.1a.- Consideration for the supporting of uniformly weighted beams

It is therefore obvious that if a is taken to be equal to $L / 2$ in Equation 8.1 that the moment at the centre of the beam will be zero. Therefore no strains will be induced at the centre of the beam due to bending from self-weight. Although zeroing or initialising strain gauge reading could be seen as acceptable if there is a moment at the centre of the beam; additional strain readings will occur as the cutting progresses and the second moment of area, I, at the section changes. The supports were therefore located at distance $a = L / 2$ in the approach used. Figure 8.1b shows the new "supporting rig" which consists of two semi-cylindrical pieces that allow the specimen to rotate freely as the stress is relaxed and prevent the weight of the parts influencing the strain reading.

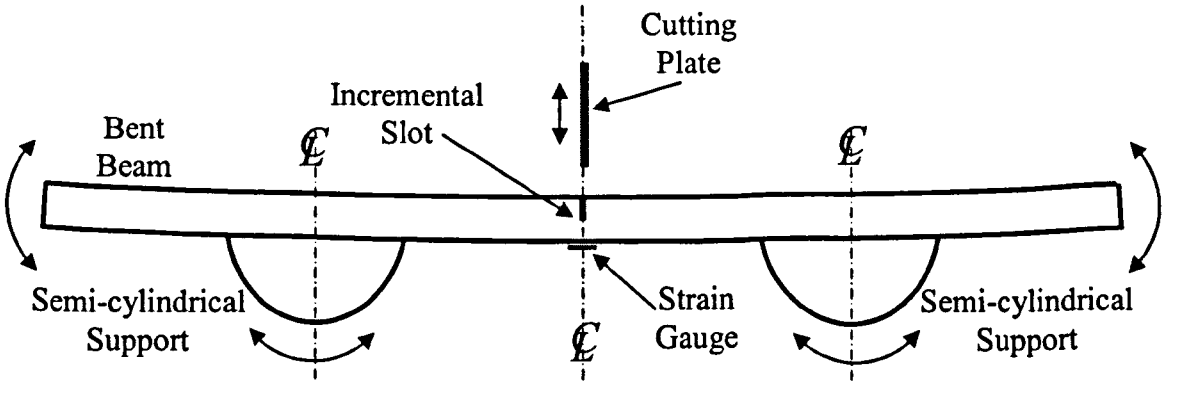

Figure 8.1b.- Cutting procedure of a beam using a plate EDM

The specimen is located so that the centre of gravity of the two parting pieces pass through the centre of the two semi-cylindrical supports as illustrated in Figure 8.1b. The rotation of the supports also has the effect of keeping the slot in the same plane at all times. It is assumed that the rotations due to stress relief will not change the moment distribution significantly.

This is an extremely simple and inexpensive solution, but it took several attempts and studies to obtain. Other authors clamp the specimen as a cantilever at one end and use floats wrapped round the specimen to provide buoyancy to offset weights [*Nowells et. al., 2000*]. The cutting path produced by such methods is not straight, also errors, which can arise from the calculation of the size of appropriate floats, are avoided.

The EDM machine used in this project was an Eurospark F400RP, which uses an AP 35-pulse generator (maximum current output of 35 Amp and maximum power consumption of 3.5 KW). The dielectric fluid employed by the machine is kerosene. The machine can hold different geometries of electrodes, such as plates, wires, bars, spheres and several other more complicate shapes. The cutting plates used in this work were 50 mm by 50 mm with a thickness of 0.35 mm in size. The plates were made from a standard copper sheet.

Figure 8.2 shows a schematic drawing of the electric discharge machining arrangement used in the research. And in Figures 8.3 and 8.4, are illustrated the EDM and one of the specimens ready to be cut.

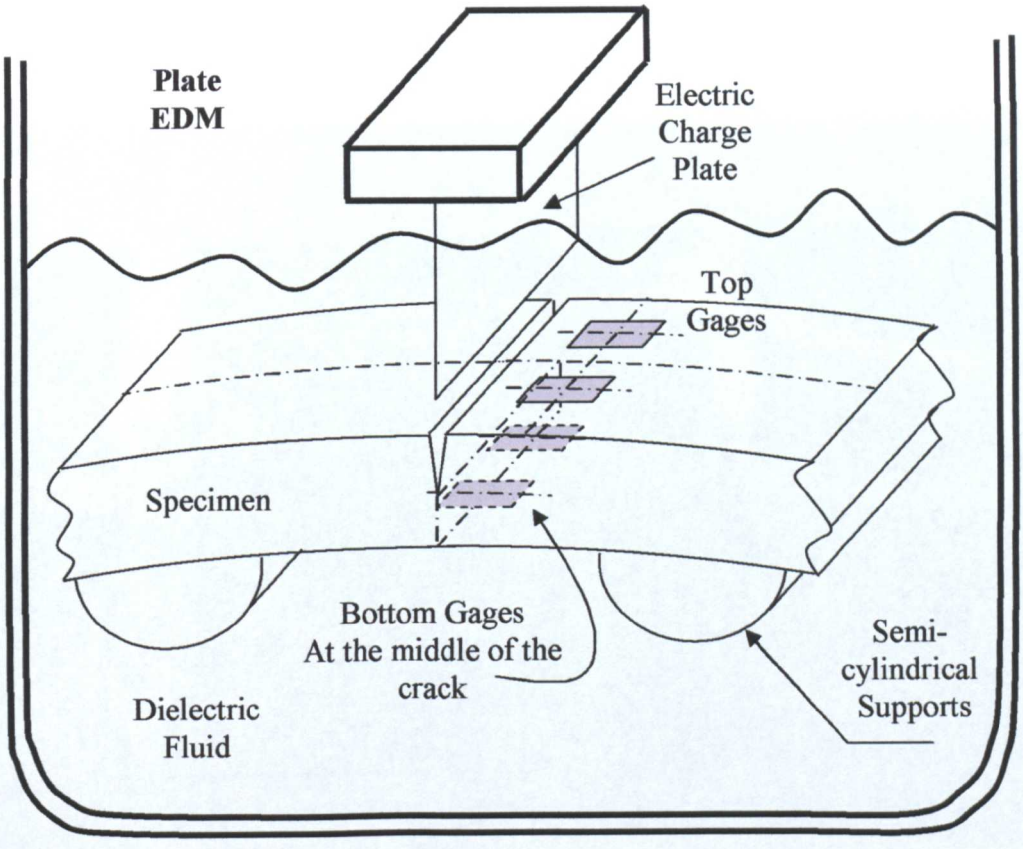

Figure 8.2.- Electric discharge machining using a plate

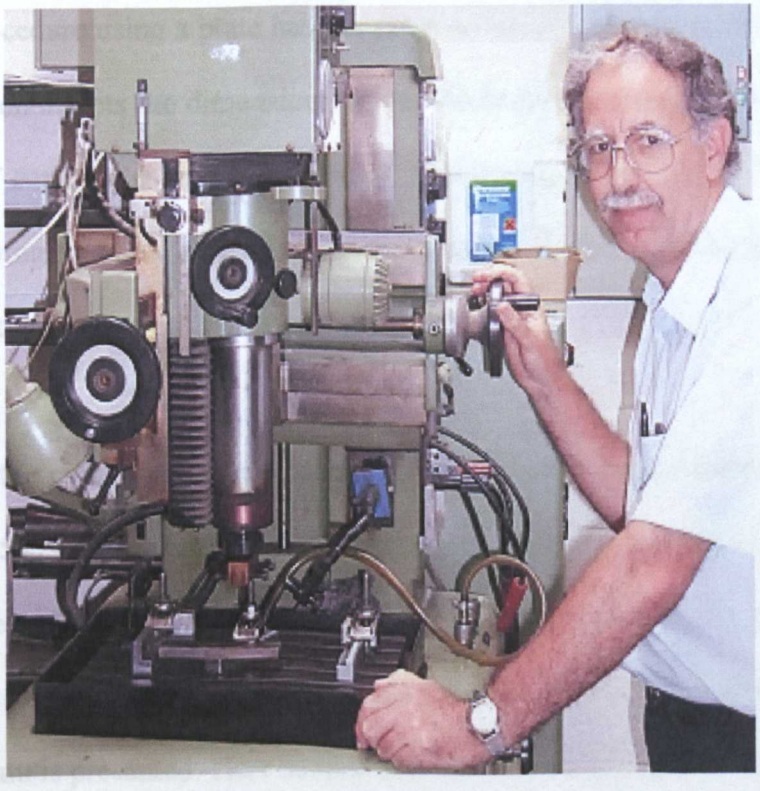

Figure 8.3.- Electric discharge machine

Figure 8.4.- Plastically bent bar ready to be cut

The cutting procedure using a plate has the same erosion of the electrode problem as the wire. The erosion affects the dimensions of the electrode and hence the measurement of actual depth of cut should be done carefully. Performing small cuts of 1 mm long and rotating or moving to a new surface in the plate and re-checking the actual length of the cut can reduce this problem.

In Figures 8.5 the copper plates are shown, illustrating the erosion effect on the cutting edge. Figure 8.5a shows a plate used to erode a specimen with a large width beam. Only one cut can be performed on each edge of the plate and then it has to be rotated to produce a new clean and accurate cut. In Figure 8.5b a plate that had eroded bars with a small width beam is presented. Here several cuts had been produced on each edge.

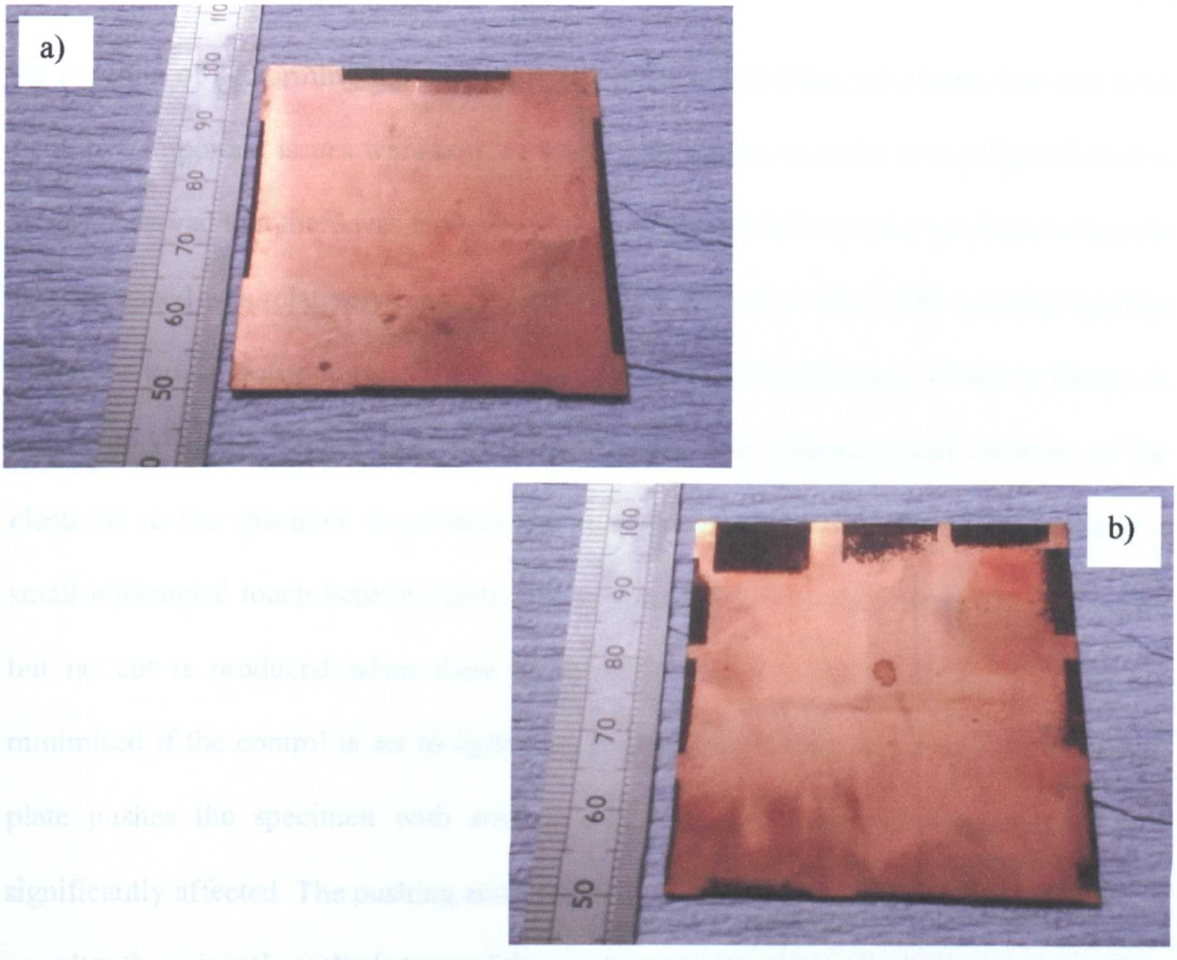

Figure 8.5.- Copper plate electrode a) cutting plate used for EN 8 steel specimens b) cutting plate used for EN 1A steel and aluminium alloy specimens

EDM methods use a dielectric liquid that helps to produce the spark to erode the component. This adds an additional problem to the cutting procedure. The dielectric fluid (kerosene) erodes the coating on gauges and causes short circuits to take place. The solution is to seal the strain gauges with a high tear strength silicon rubber (DOW CORNING 3145 RTV MIL-A-46146) and additionally with a nitrile rubber coating (M-COAT B), which are special products resistant to kerosene. The gauges were coated with two layers of 3145 RTV MIL-A-46146, allowing a drying time of 6 hours between each layer. This layer is protected with at least one layer of M-COAT B and left to dry for at least 24 hours. Both coating products are produced and supplied by the Measurement Group Ltd.

At the time of performing the cuts on the first set of annealed specimens that had been bent, two important issues were noticed that affect the strain results as highlighted below. It was observed that there was a pushing action of the electrode on the specimen when the feeding speed was relatively high. The instruction manual of the EDM specifies that the electrode would not touch the specimen when the cut is performed, which in theory is true. But a weight sensor in the machine controls the closeness and location of the electrode to the specimen to produce the cut automatically. Thus, in reality there is a small interrupted touch between plate and specimen at all times as the cut is performed, but no cut is produced when there is an actual contact. The contact effect can be minimised if the control is set to light feed position. By taking this action the electrode plate pushes the specimen with such a small force that the strain reading is not significantly affected. The pushing action of the electrode can be so severe that at times it can alter the original residual stress of the specimen as the cut is introduced. In fact, when the feeding setting is not adjusted correctly, plastic deformation can be seen in the electrode plate. Heavy feeding can introduce additional residual stresses into the specimen at some stage of the cutting by re-bending the specimen into the plastic region. It was therefore important to set the control to the light feeding position before any cut was done.

When using only the strain gauge opposite the front of the crack, it was found that the calculation of the residual stress field could benefit from performing the calculation on two different bent specimens. One cut is done on the concave side of a beam and the other cut from the convex side of another beam with the same residual stress field (Figure 8.6).

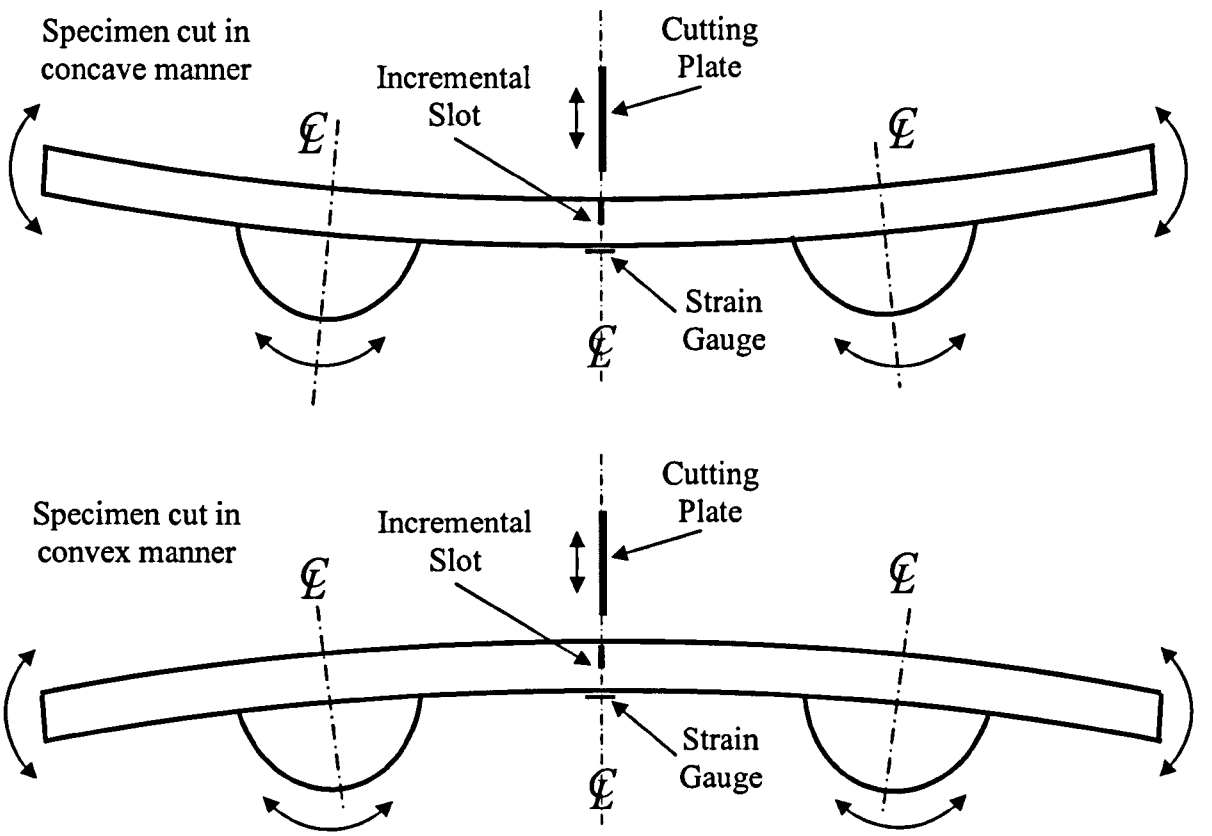

Figure 8.6.- Different cutting procedures (concave and convex)

By obtaining the strain data in this manner the most sensitive results from the cuttings can be used. This results in a better set of calculations for the stresses. This aspect is explained further towards the end of section 8.3.1. All the cutting operations performed in this research were done following this procedure. The residual stress calculations using the crack compliance method and the new cutting procedure are presented in the following sections of this chapter.

8.3. Determination of residual stresses.

All residual stress calculations were carried out using the CCM as described in section 6.2.3. The materials used for this purpose were EN 8 and EN 1A steels, and AA 6082 T6

aluminium alloy. The materials were annealed and strain gauges attached to each specimen as highlighted in Figures 8.1b and 8.2.

Specimens for the study of the Bauschinger effect were pre-pulled to different extents. The extents of pre-pull are indicated in the relevant example cases in this chapter. The specimens were then mounted on a four point bending rig and plastically bent. The bending operation produced residual stress profiles that can be estimated by using the loading and unloading bending stress approach [*Gere and Timoshenko, 1991*]. This will enable the results of residual stresses obtained using the CCM to be evaluated. The loading and unloading stress approach needs the mechanical properties of the materials as determined using the simultaneous derivation of tensile and compressive behaviour developed and presented in Chapter 5.

All the bending operations were performed on an electric screw driven Testometric testing machine with a 50 kN load cell. In Figure 8.7 the electric Testometric machine used for the bending operation can be seen. Different loading conditions were utilized in each case using a specified maximum bending strain value to control the operation. The loading and strain data were collected and recorded using a Measurement Group's System 5000 data logger.

Figure 8.7.- Testometric testing machine

8.3.1. Determination of residual stresses in stress relief annealed EN 8 steel.

Several specimens made from EN 8 steel were stress relief annealed as detailed in Chapter 5. The cross section of the rectangular bars were 38.1 mm by 12.7 mm. The bars were plastically bent to introduce a predictable residual stress field based on well proven superposition of loading and unloading stresses [*Gere and Timoshenko, 1991*]. The bending operation was controlled by the strain reading obtained from the strain gauges attached to the surfaces of the bar. Using the knowledge of the stress strain behaviour of the material, the beams were bent into the plastic range making sure that they did not make contact with the lower surface of the four point bending rig. Figure 8.8 shows a bending moment versus strain result obtained from one of several tests.

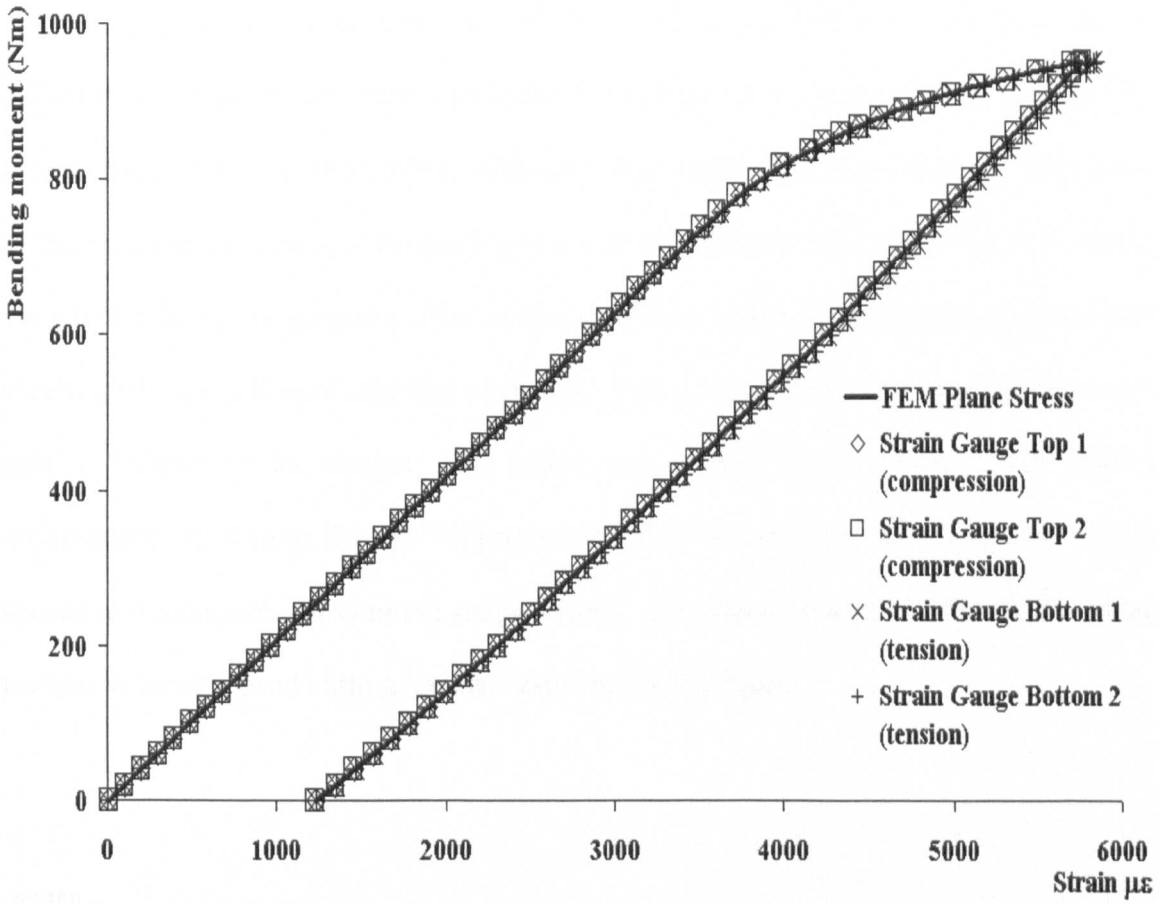

Figure 8.8.- Bend test of stress relief annealed EN 8 steel

This result is representative of the tests carried out on this type of steel that had been stress relief annealed. From the results presented in Figure 8.8 the mechanical properties of the material can be obtained (as presented in Chapter 5) and the residual stress profile can be determined by using the method of superposition of loading and unloading stresses [*Gere and Timoshenko, 1991*].

Results presented in Figure 8.8 shows an almost perfect bending test, because the top and bottom strain gauges gave virtually identical values during loading and unloading. The results also demonstrate a properly carried out annealing process. When the bending procedure was completed, the specimen was cut using the EDM and the cutting supporting system described in section 8.2.1. Several cutting tests were performed,

alternating between cutting from concave and convex sides (top or bottom surfaces). Although the supports are placed to minimise moment at the gauges at the middle; The actual effect of the curvature of the plastically bent beam is not accounted for. This is due to the practical difficulty of measuring and making allowance for the effect of it during the placement of the supports. This means that some effect of self-weight on the strain results still occurs towards the end of the cut. There is still a final rocking to allow each part to balance in its support. This effect was slightly more severe in the convex arrangement. In Figure 8.9 the experimental strain results from both kinds of cutting procedures (concave and convex) are presented. The strain results of a FE model of the process of bending and cutting are also indicated in the figure.

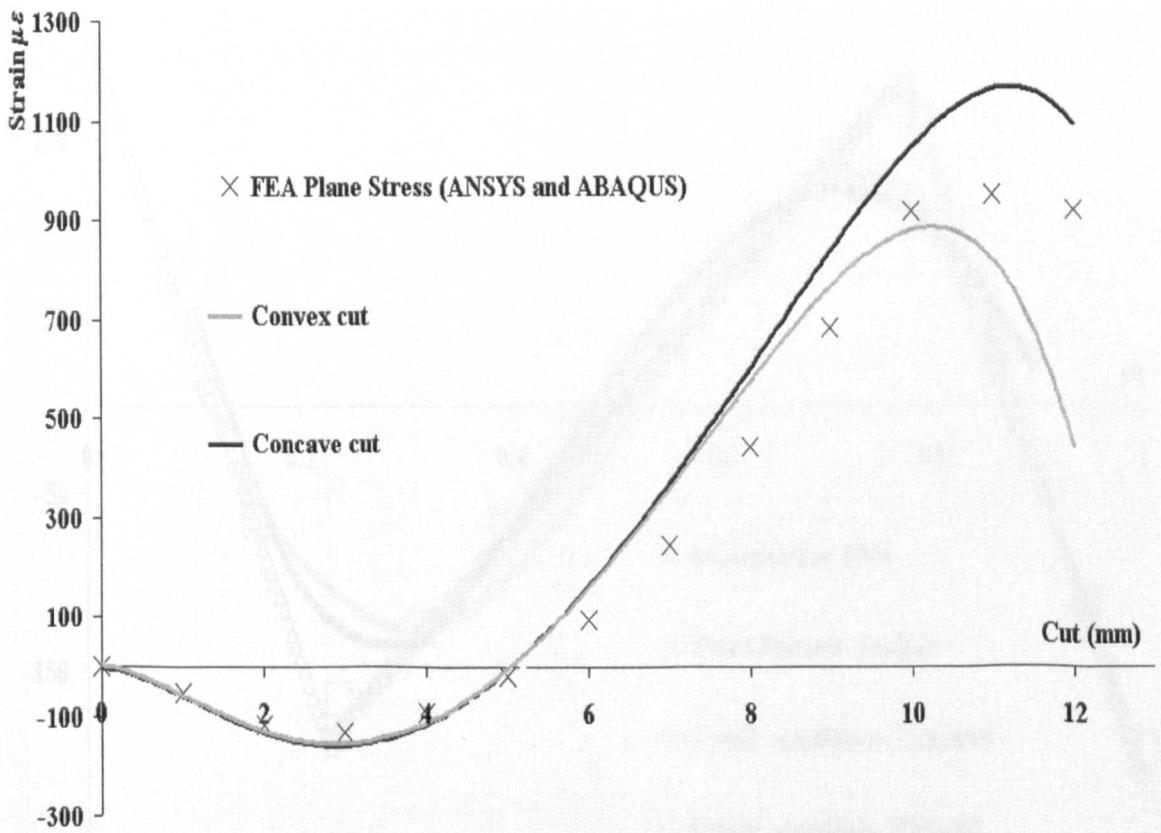

Figure 8.9.- Strain results by cutting for stress relief annealed EN 8 steel

The results of the residual stress field determined using the crack compliance method and strain data for different cases are given in Figure 8.10. The results obtained by FEA are also shown in the figure. It can be seen that the result from data based on cutting from the concave side (top to bottom) agree reasonably well with the expected results (as predicted by FEA) over the range $0 < x/t < 0.8$. The agreement is particularly good in the early parts of the range. It can also be seen that the results from the convex cutting (bottom to top) data agrees well in the range $0.2 < x/t < 1.0$ and are particularly good towards the later part of the range. It therefore appears that a form of averaging in the central part would give a better overall result across the full range. The averaging was carried out at the middle of the range as this position maximised the input from the two gauges.

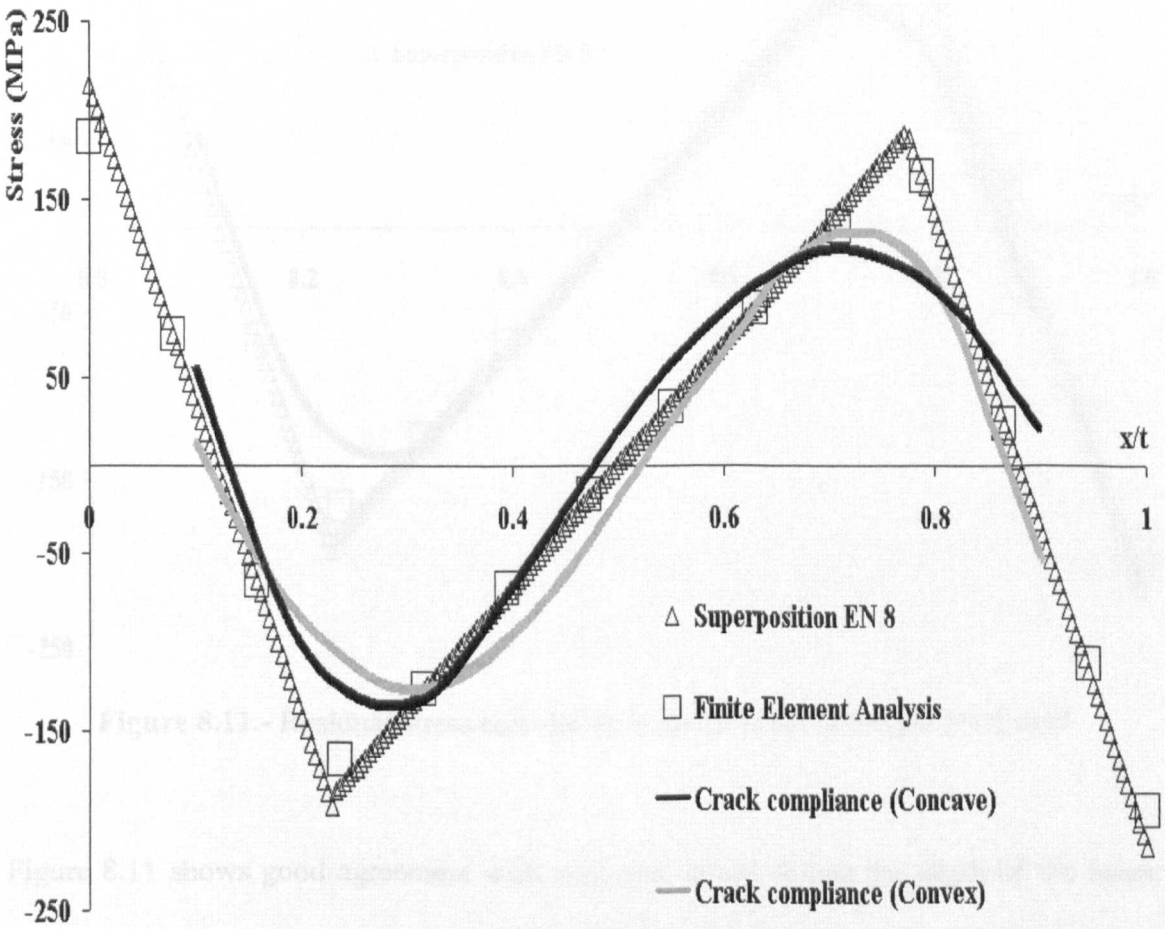

Figure 8.10.- Residual stress calculation for stress relieved EN 8 steel using different cutting direction

This approach assumes that more than one sample with the representative residual stress field is available. The result obtained in this manner is presented in Figure 8.11. In Figure 8.11 a symmetrical residual stress field can be seen, which is centred almost exactly at the mid depth position of the beam. The trend of this result is more symmetrical than those obtained by other researchers such as *Nowells et. al.* [*2000*] and *Schindler and Bertschinger* [*1997*]. This approach was used in all the cases considered in the thesis. The general limitations of the procedure are presented in the discussion in Chapter 10.

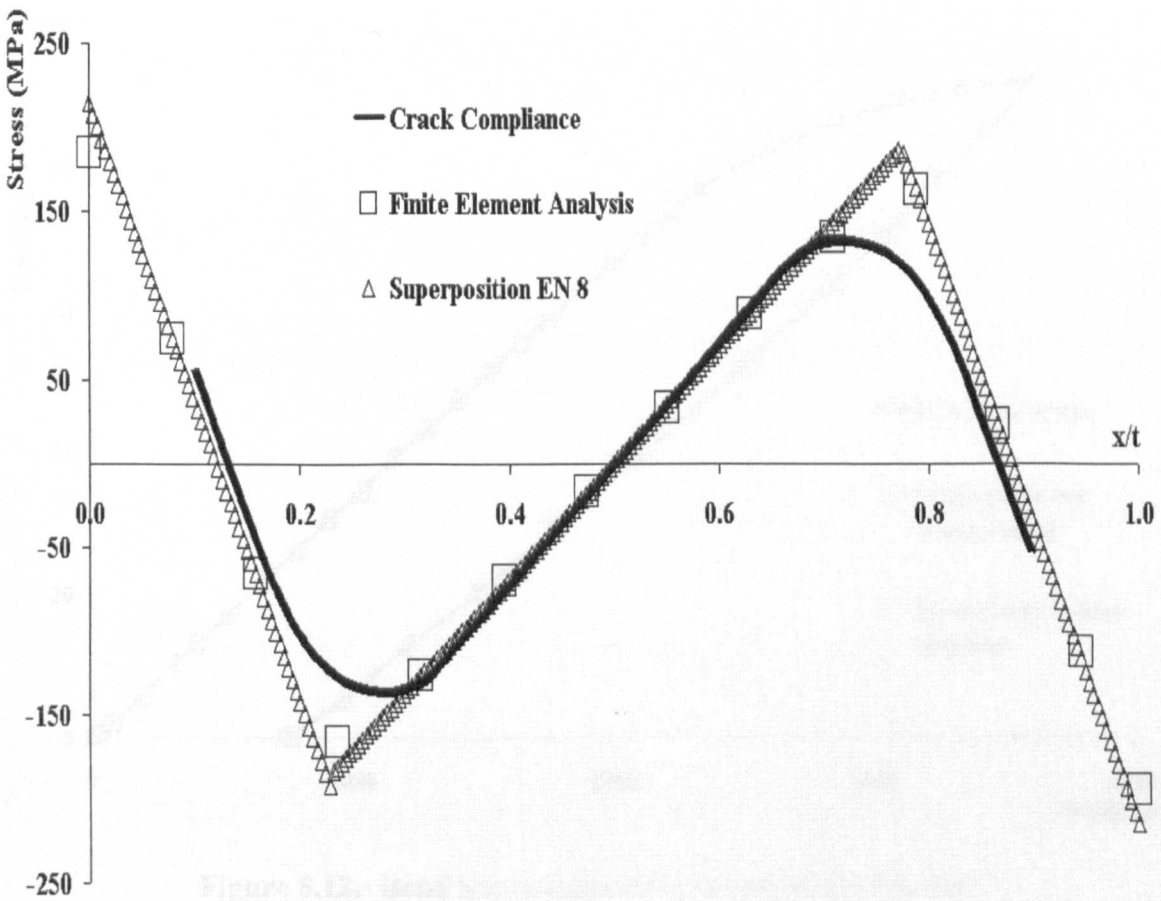

Figure 8.11.- Residual stress calculation in stress relief annealed EN 8 steel

Figure 8.11 shows good agreement with expected results across the depth of the beam. The extrapolation of the curves to the surface also shows that good results will be obtained.

8.3.2. Determination of residual stresses in stress relief annealed EN 1A steel.

In this example another type of steel was tested with different depth compared to that in section 8.3.1. A batch of rectangular EN 1A with 10 mm by 10 mm section bars was stress relief annealed and tested as for the case in section 8.3.1. Figure 8.12 shows a typical bending moment against strain result for the rectangular beams. Once again, it can be observed that the bending tests were performed correctly, giving similar strain values on the tension and compressive sides of the beam.

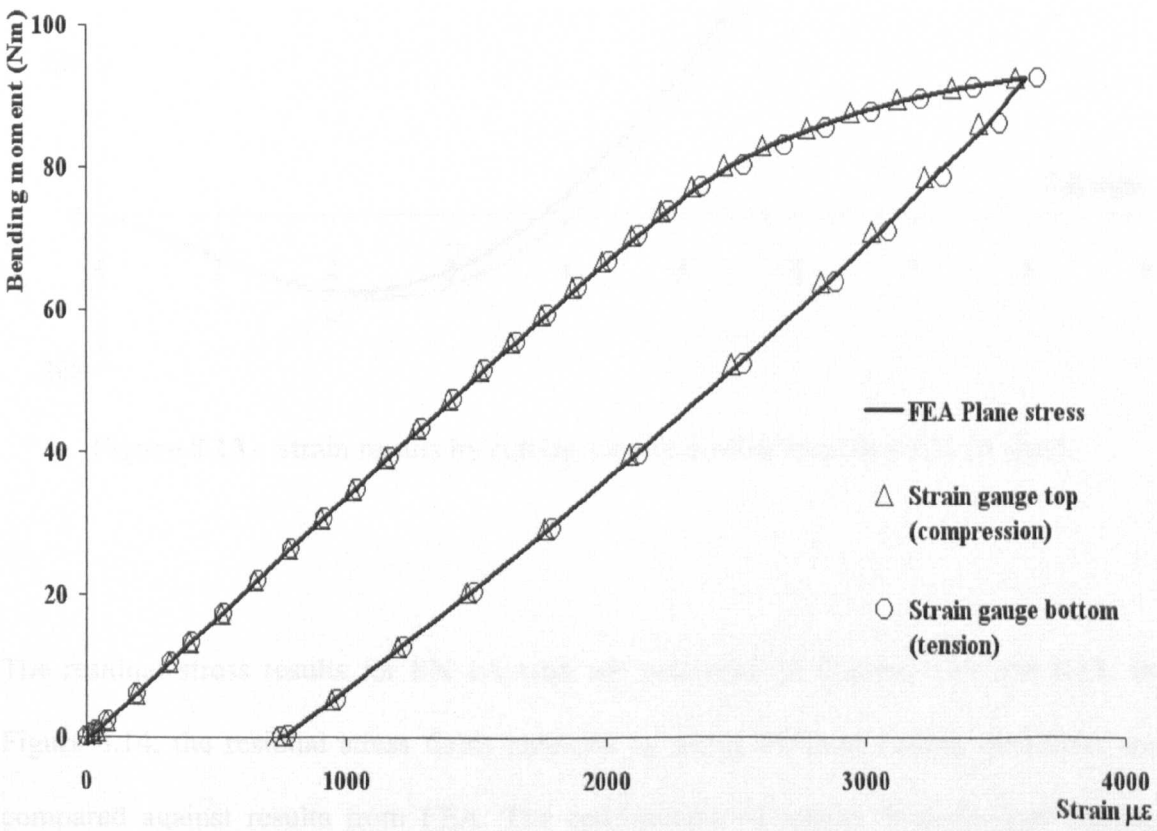

Figure 8.12.- Bend test in stress relief annealed EN 1A steel

In Figure 8.13 the results of cutting the beams from both sides (concave or convex) are presented. The FEA simulation results can also been seen in this figure. The two experimental strain results presented in Figure 8.13 were used in the same way as employed for the EN 8 steel to calculate the residual stress profile.

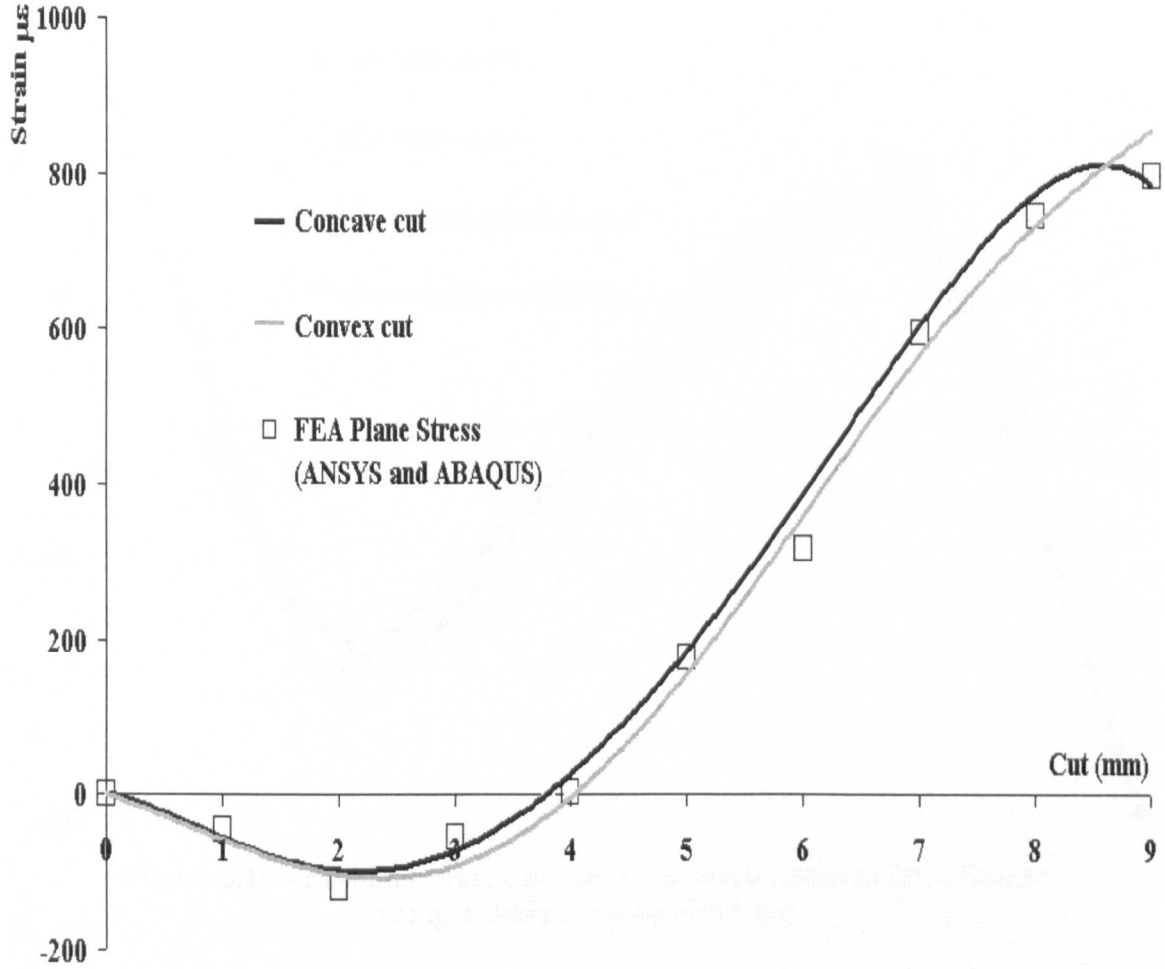

Figure 8.13.- Strain results by cutting for stress relief annealed EN 1A steel

The residual stress results for EN 1A steel are presented in Figures 8.14 and 8.15. In Figure 8.14, the residual stress fields obtained by using different cutting directions are compared against results from FEA. The combination of results from the two cutting directions can be seen to agree very well with expected results in Figure 8.15.

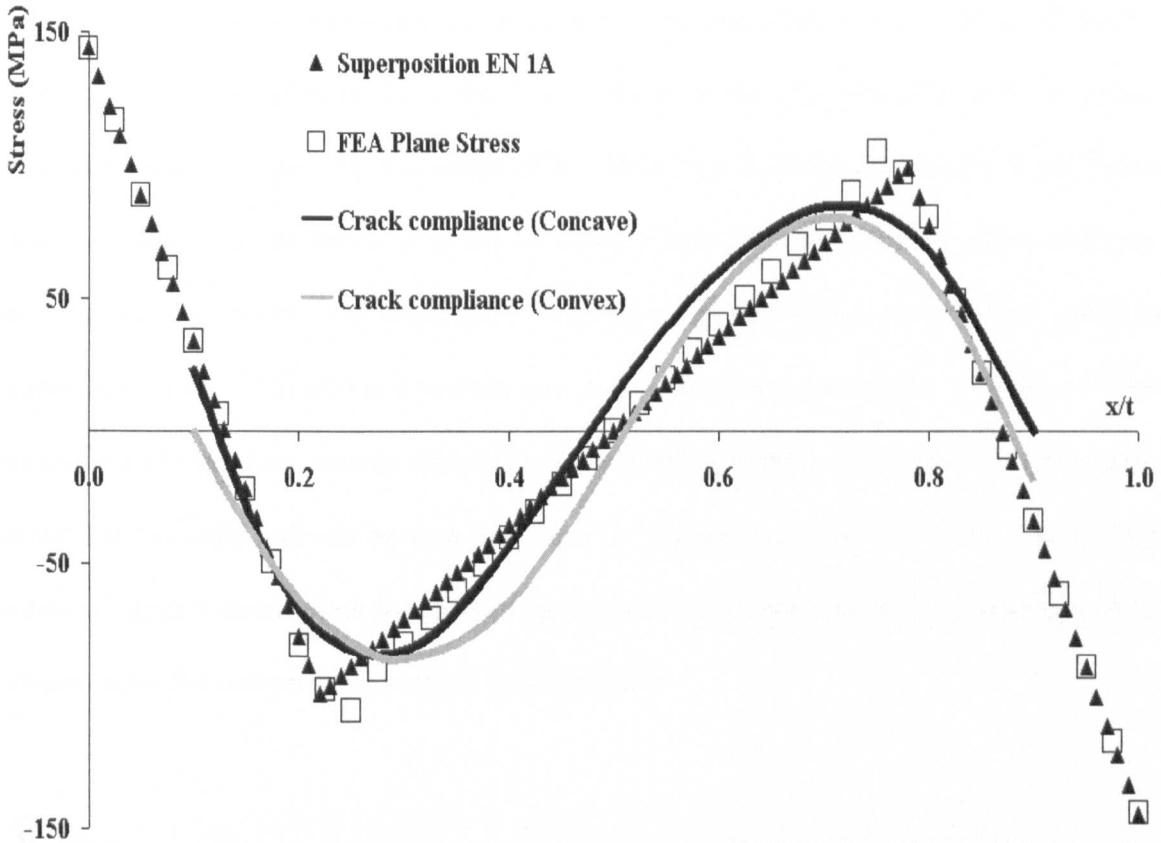

Figure 8.14.- Residual stress calculation for stress relieved EN 1A steel using different cutting direction

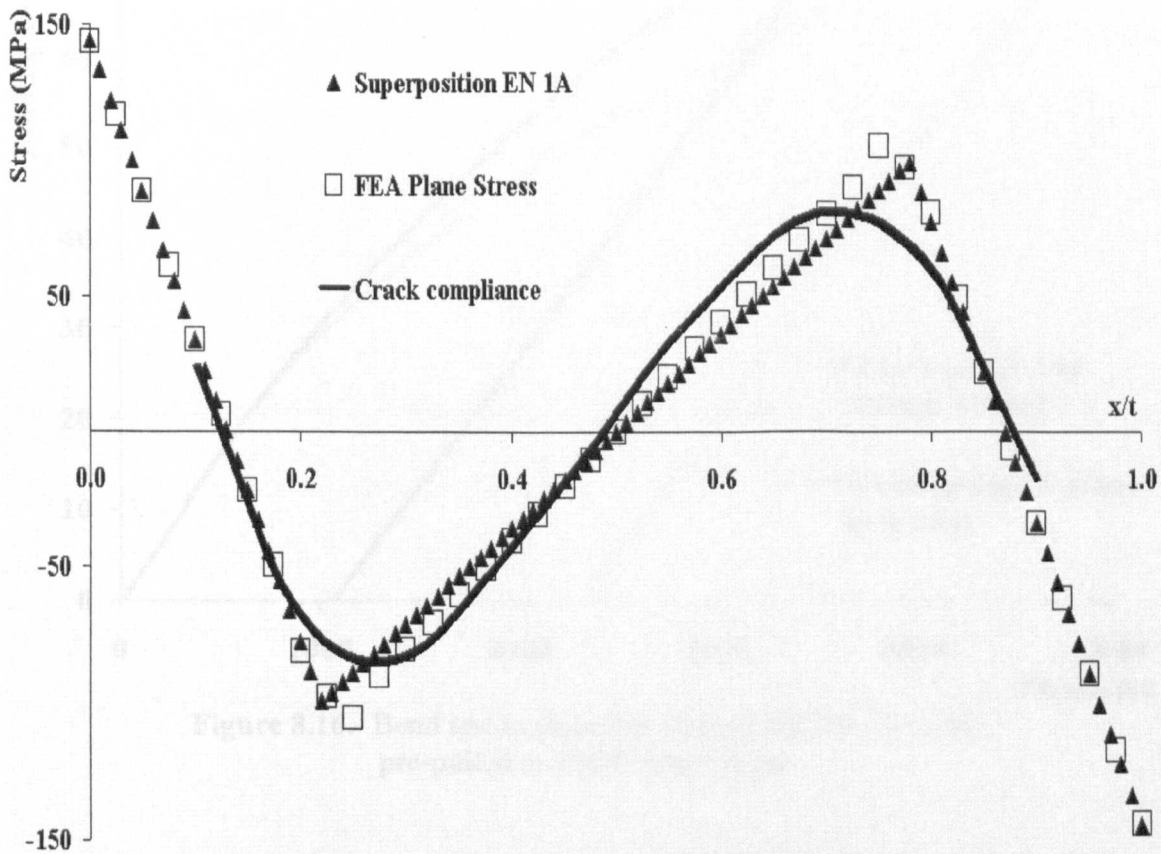

Figure 8.15.- Residual stress calculation in stress relieved annealed EN 1A steel

8.3.3. Determination of residual stresses in EN 1A steel with previous strain history.

A batch of specimens with the same cross-section as the ones detailed in the previous section was used to test for the effect of pre-straining. A mechanical loading operation was performed on the batch in order to induce previous history effect after the stress relief annealing process was completed. A group of the specimens were axially pulled to a moderate level of 10000 microstrain and a second group was axially pulled to 25000 microstrain to produce a more severe level of strain hardening. The plots of load against strain for this axial pull can be seen in Chapter 5. Figures 8.16 and 8.17 show the bending moment against strain plots for each of the pre-pulled groups. An earlier yielding can be observed on the compressive surface of the beams.

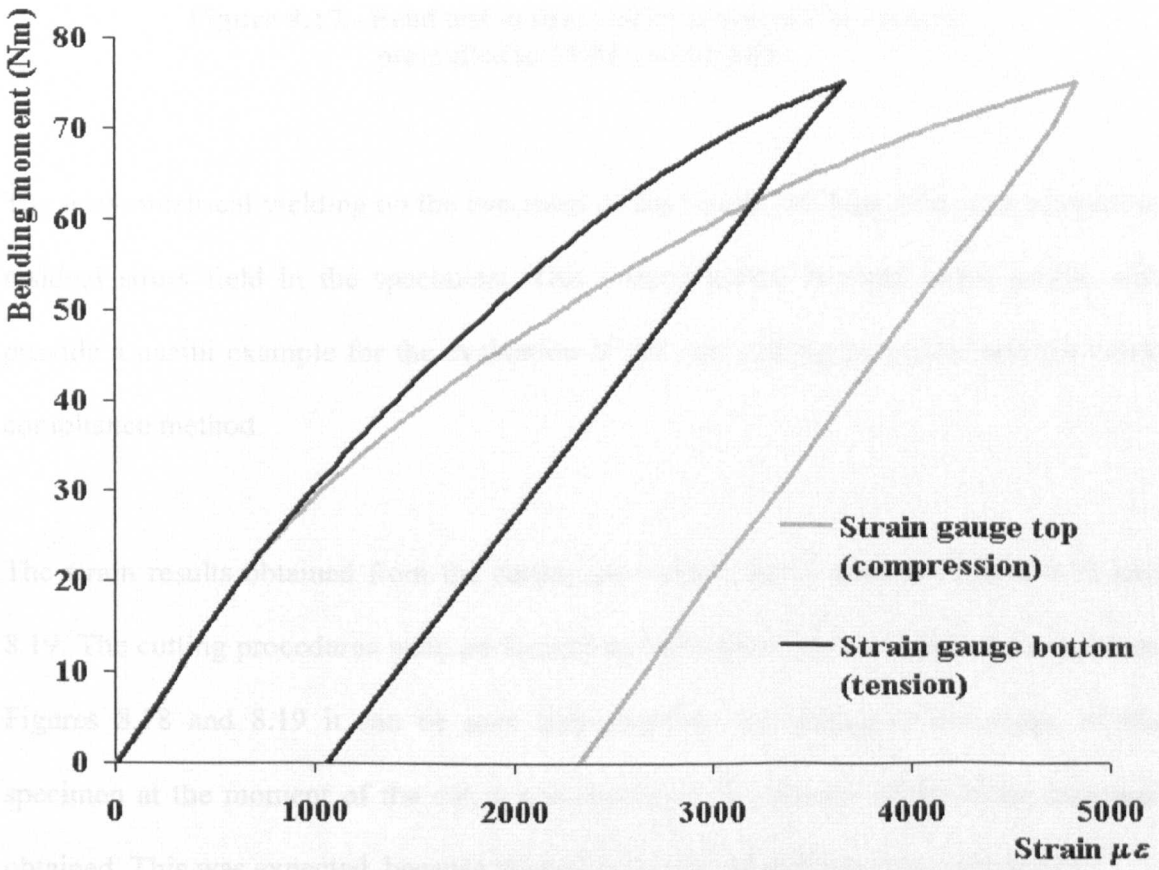

Figure 8.16.- Bend test in stress relief annealed EN 1A steel, pre-pulled to 10000 microstrain

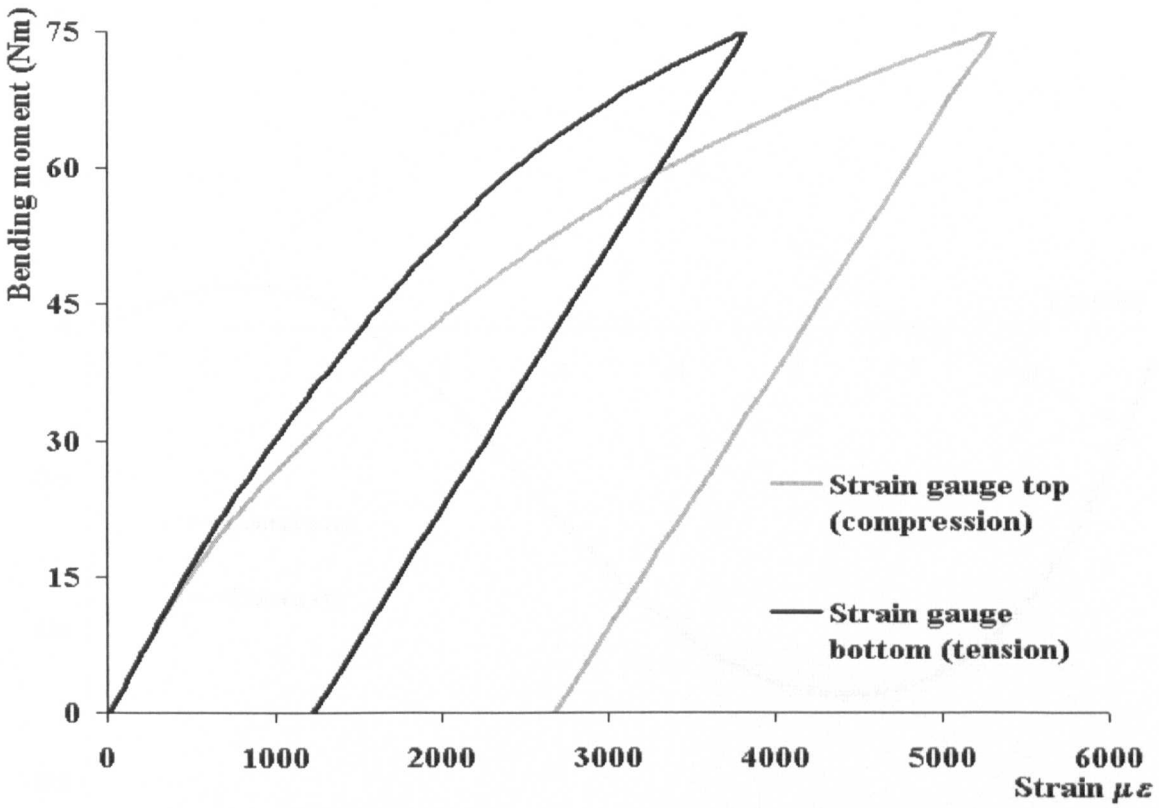

Figure 8.17.- Bend test in stress relief annealed EN 1A steel, pre-pulled to 25000 microstrain

The unsymmetrical yielding on the two sides of the beams will lead to an unsymmetrical residual stress field in the specimens. This unsymmetrical residual stress profile will provide a useful example for the evaluation of the new cutting procedure and the crack compliance method.

The strain results obtained from the cutting procedure can be seen in Figures 8.18 and 8.19. The cutting procedures were performed as highlighted earlier in this chapter. From Figures 8.18 and 8.19 it can be seen that whatever the setting of the shape of the specimen at the moment of the cut, a non-symmetrical response of the strain data was obtained. This was expected, because the residual stress profile was not symmetrical.

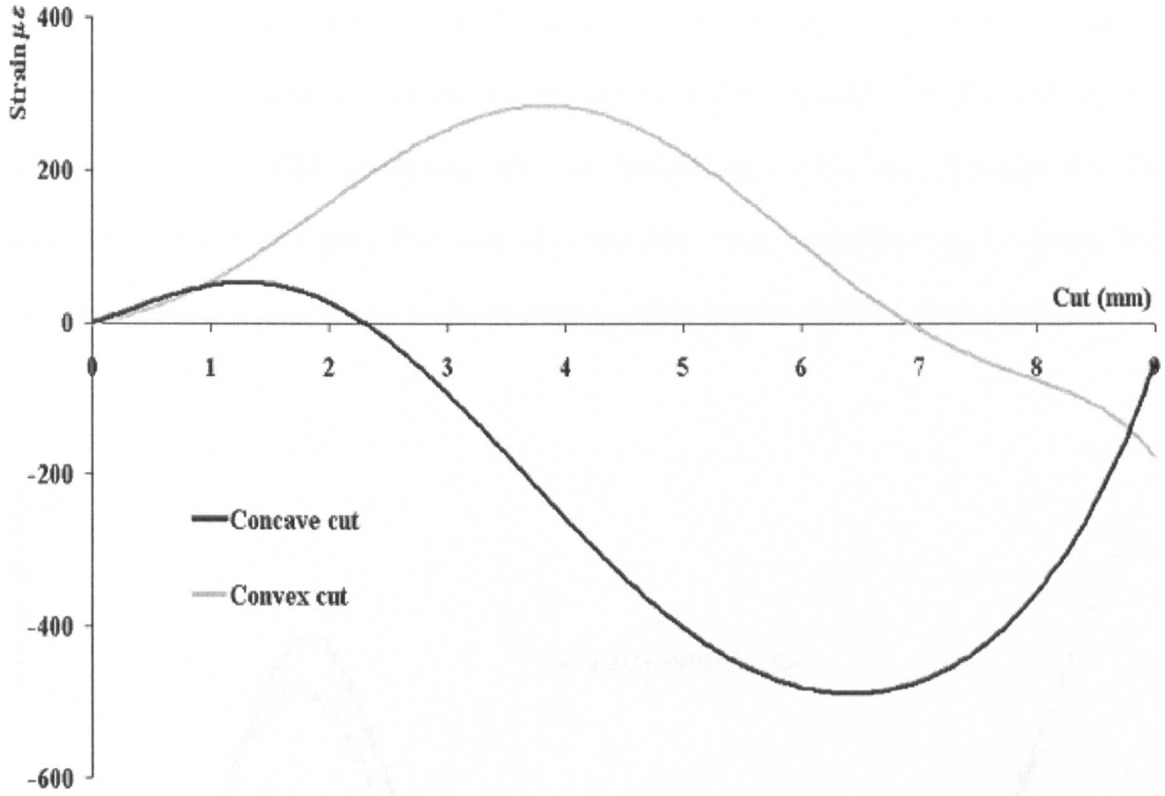

Figure 8.18.- Strain results by cutting for stress relief annealed EN 1A steel, pre-pulled to 10000 microstrain

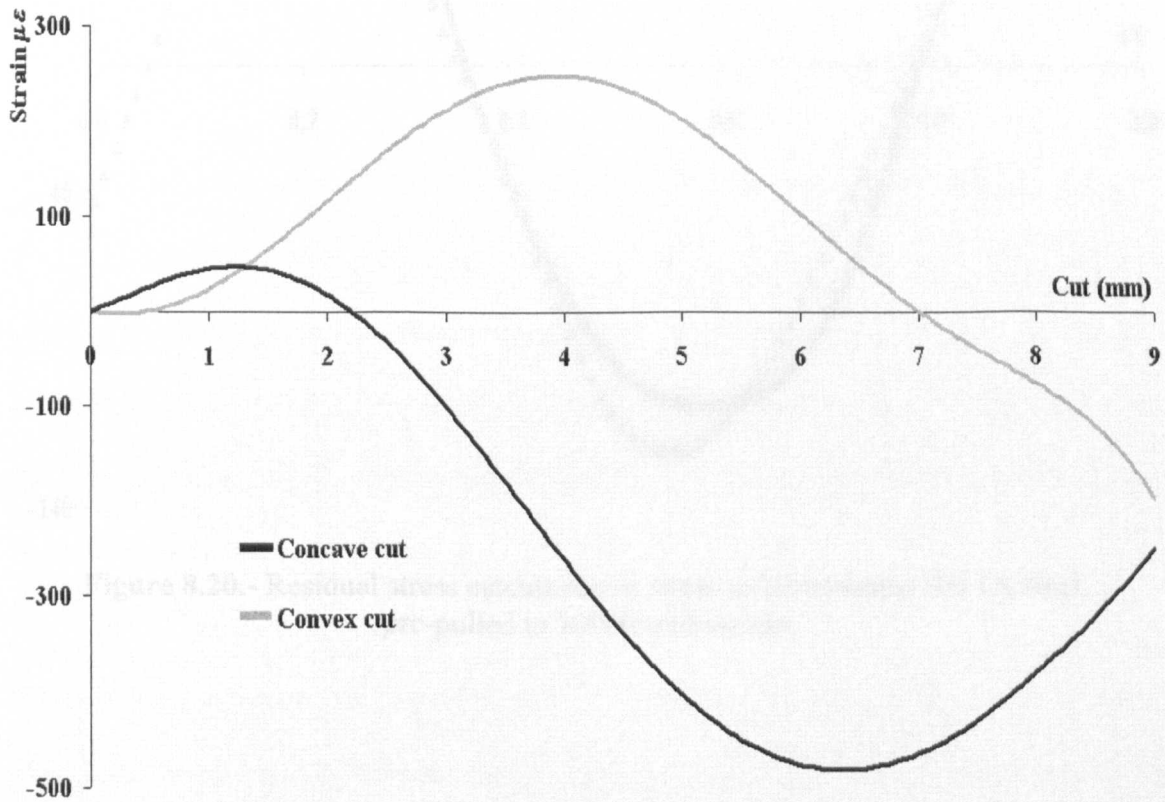

Figure 8.19.- Strain results by cutting for stress relief annealed EN 1A steel, pre-pulled to 25000 microstrain

Figures 8.20 and 8.21 show very good agreement between the results obtained using the crack compliance method and those obtained from superposition of the loading and unloading stresses. FEA modelling was not carried out in this case because data for modelling the Bauschinger effect was not available. Experimental testing to obtain this data would have expanded the scope of the research outside of the original objectives.

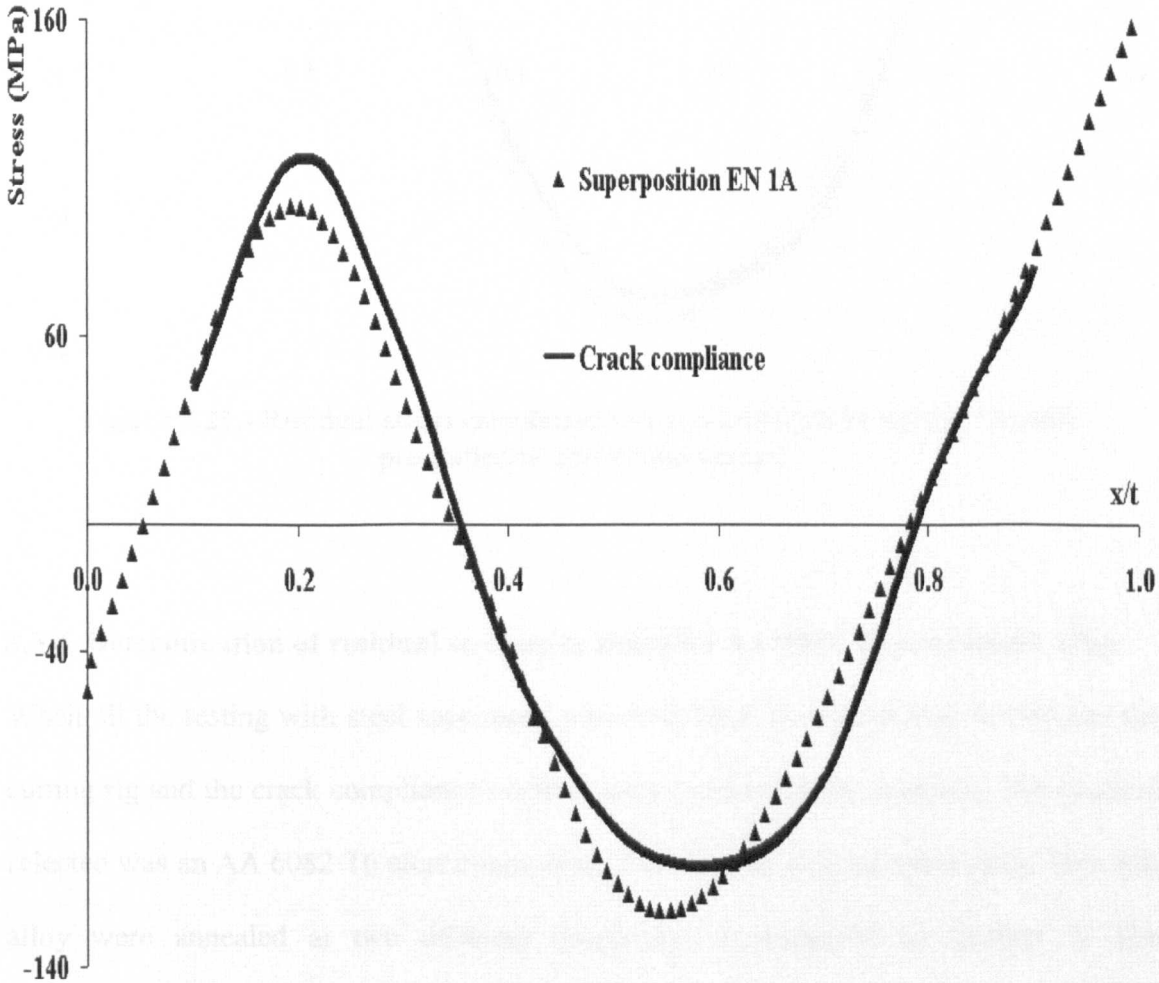

Figure 8.20.- Residual stress calculation in stress relief annealed EN 1A steel, pre-pulled to 10000 microstrain

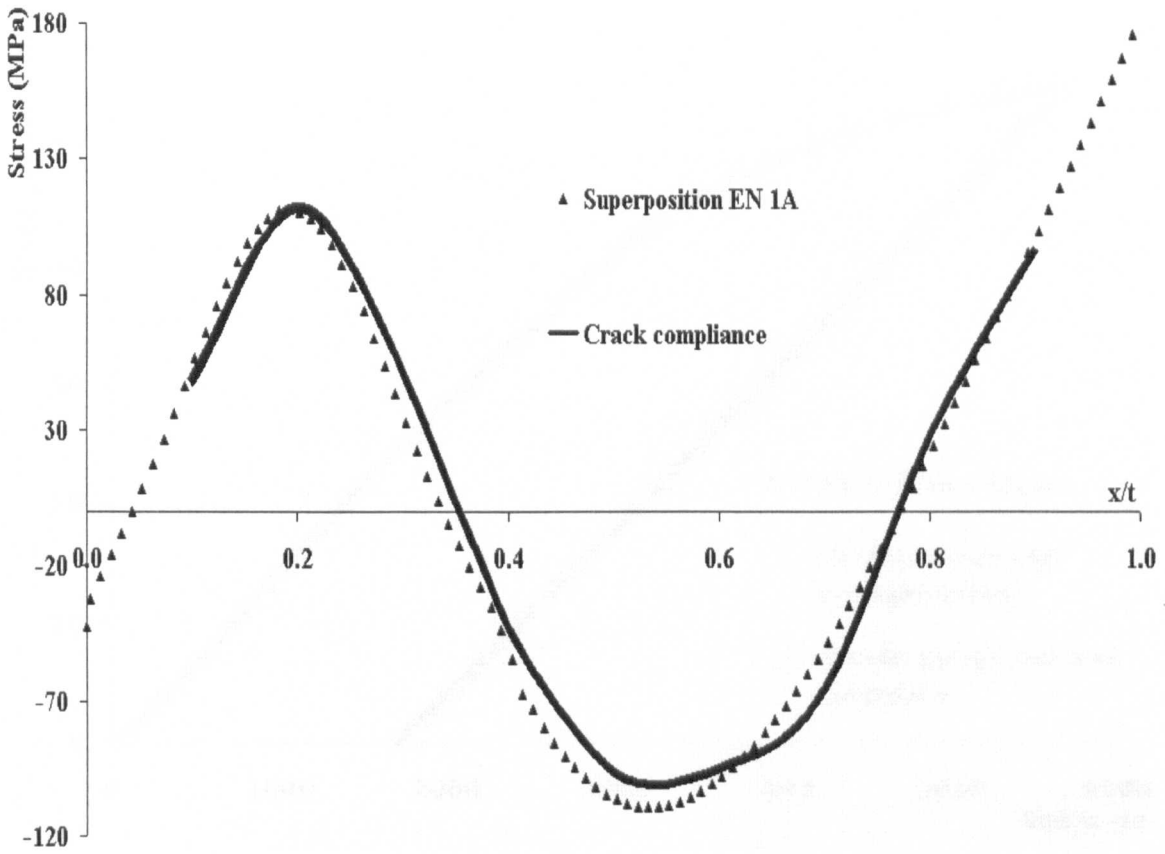

Figure 8.21.- Residual stress calculation in stress relief annealed EN 1A steel, pre-pulled to 25000 microstrain

8.3.4. Determination of residual stresses in annealed AA 6082 T6 aluminium alloy.

When all the testing with steel specimens was completed, it was decided to evaluate the cutting rig and the crack compliance method using another type of material. The material selected was an AA 6082 T6 aluminium alloy. Two batches of specimens made from this alloy were annealed at two different conditions, as indicated in Chapter 5. The rectangular bars had a cross-section of 12.7 mm by 9.8 mm.

The bending procedure was controlled by the use of the strain gauges laid on the surfaces. The plots for all bending results can be seen in Figures 8.22 and 8.23 for each of the annealed conditions.

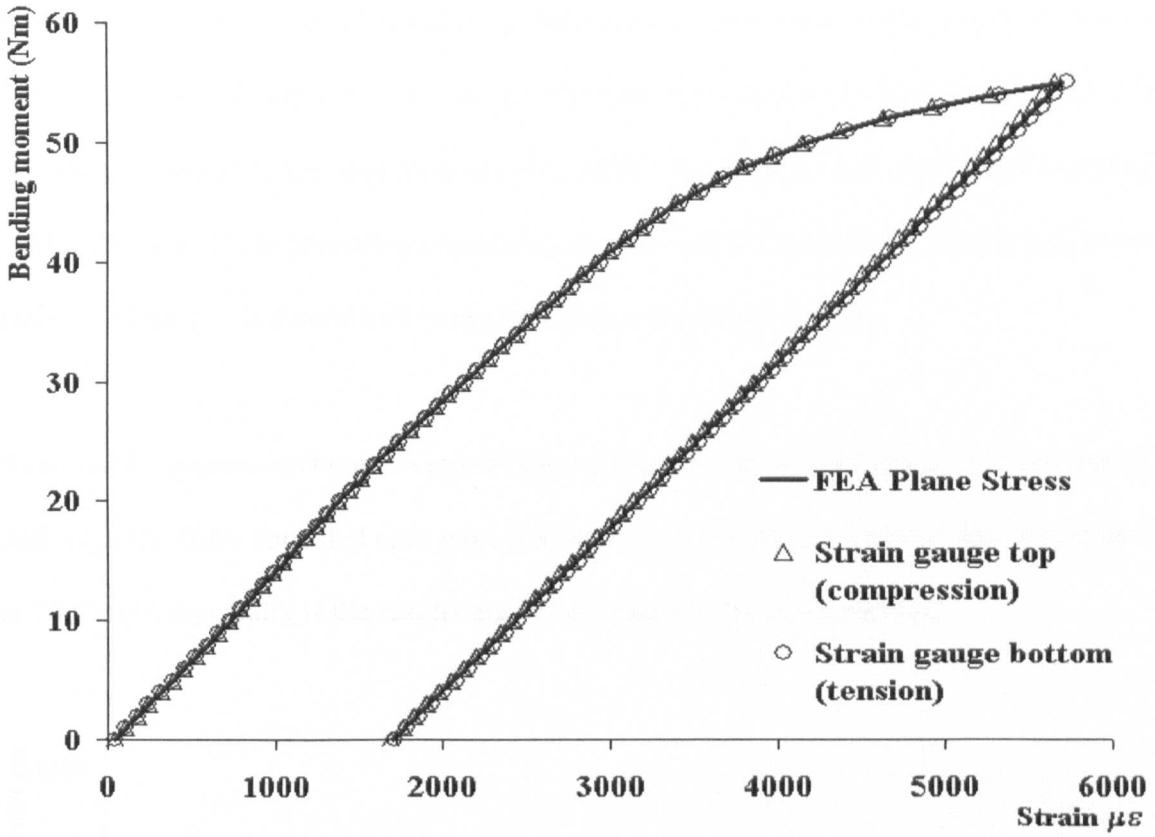

Figure 8.22.- Bend test in stress relief annealed AA 6082 T6 aluminium alloy

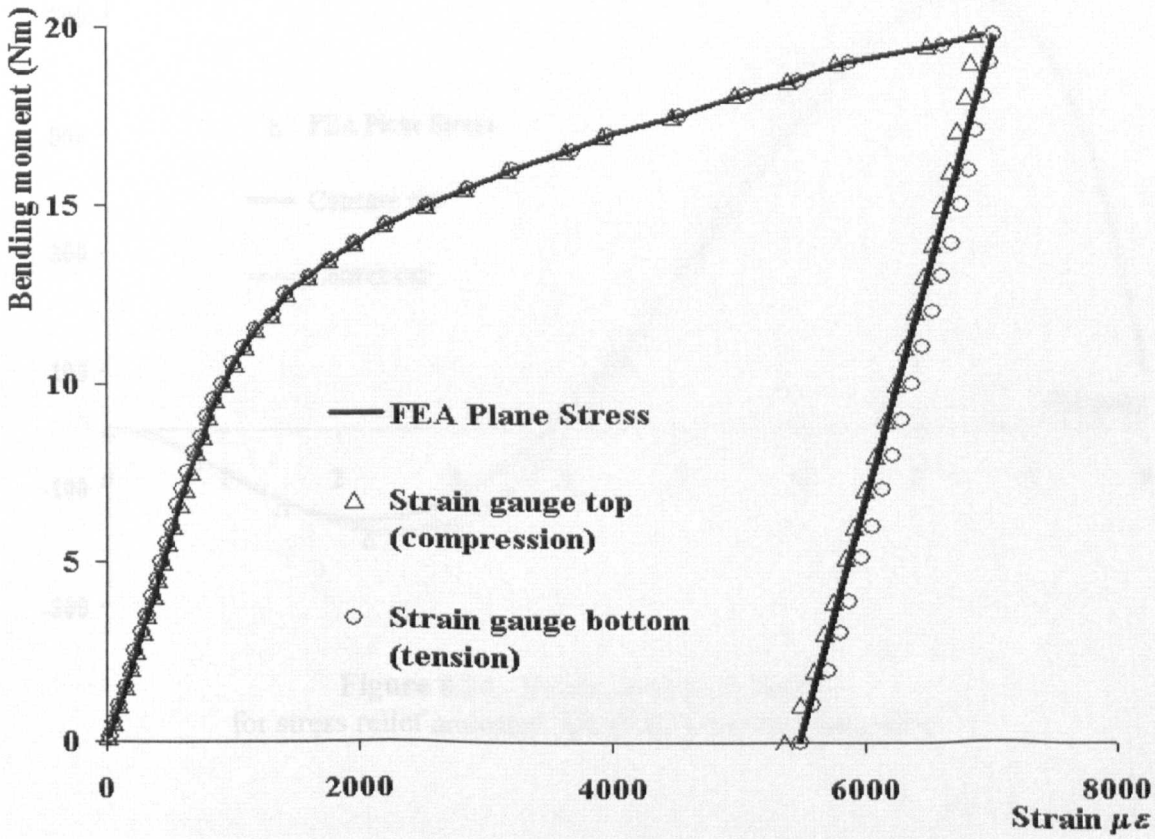

Figure 8.23.- Bend test in fully annealed AA 6082 T6 aluminium alloy

From these figures the mechanical properties can be determined as explained in Chapter 5 and the residual stress results can be obtained by superposition of the loading and unloading stresses [*Gere and Timoshenko, 1991*]. In Figures 8.24 and 8.25 the cutting results for both of the annealing conditions are presented. Figures 8.26 and 8.27 show the residual stress fields determined using the crack compliance method.

Reasonable agreements between results can be seen for the case of stress relief annealing. Although the fully annealed case gave similar trends as expected results, the magnitudes are different especially if the results are extrapolated to the outer surfaces.

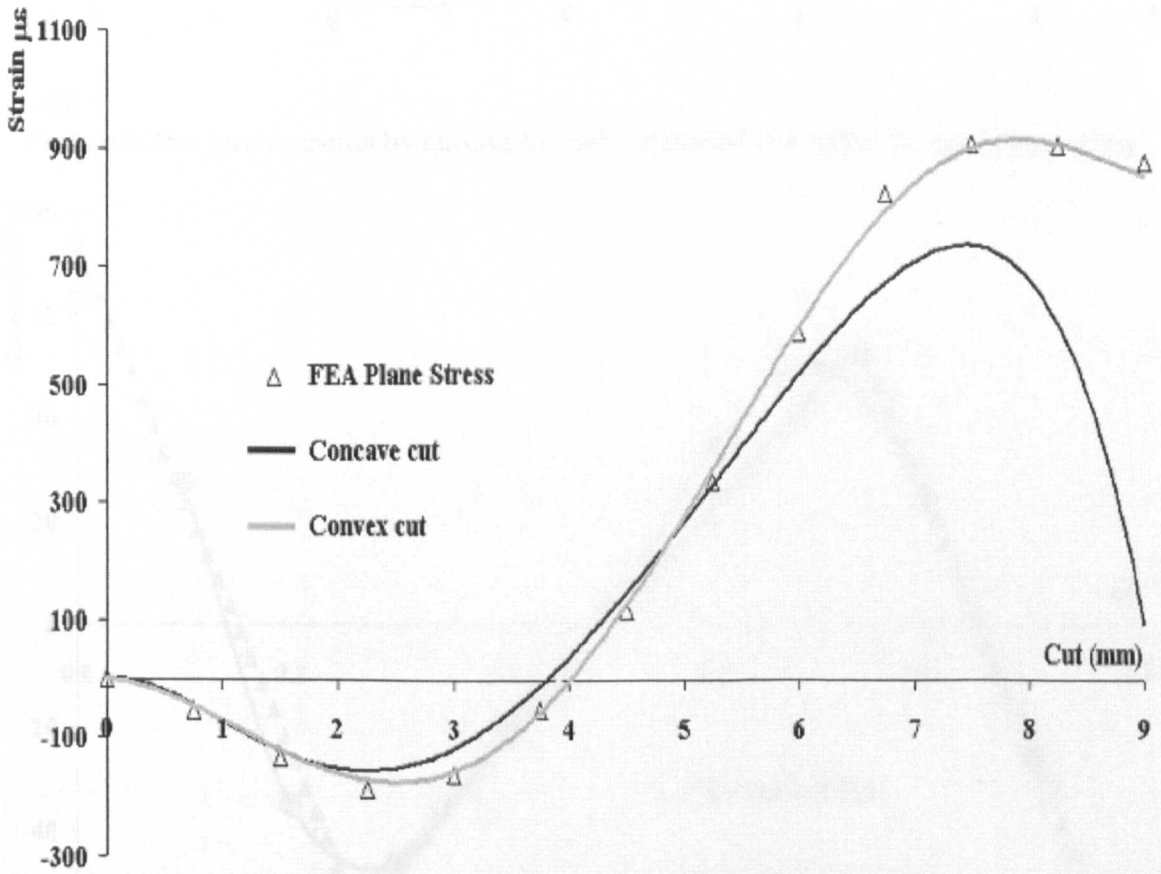

Figure 8.24.- Strain results by cutting
for stress relief annealed AA 6082 T6 aluminium alloy

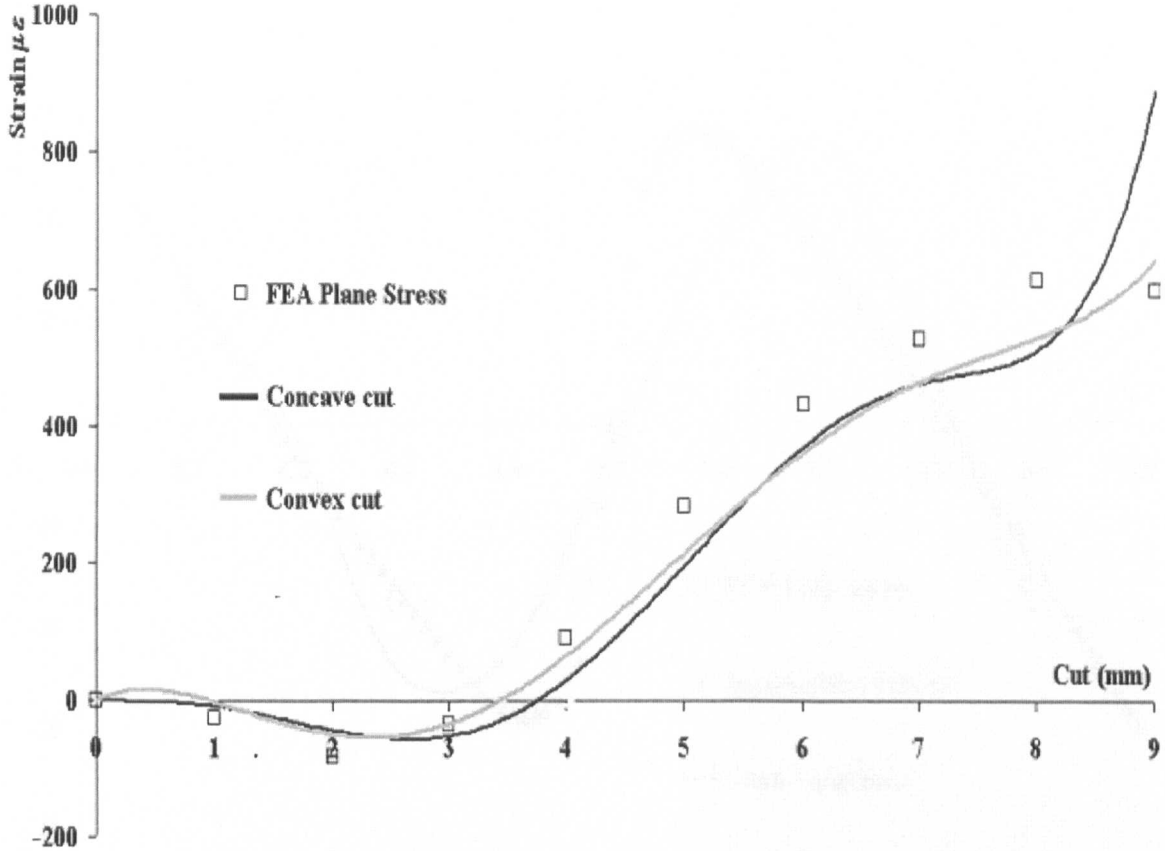

Figure 8.25.- Strain results by cutting for fully annealed AA 6082 T6 aluminium alloy

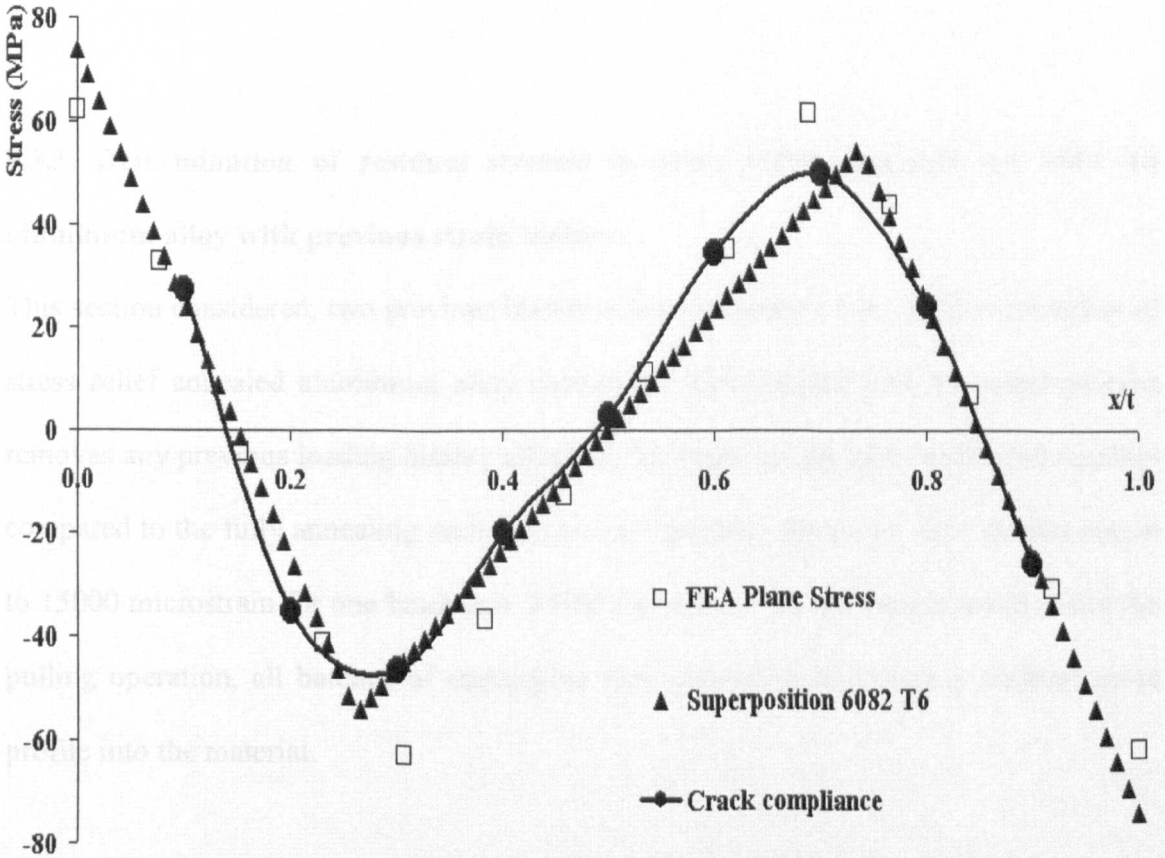

Figure 8.26.- Residual stress calculation for stress relief annealed AA 6082 T6 aluminium alloy

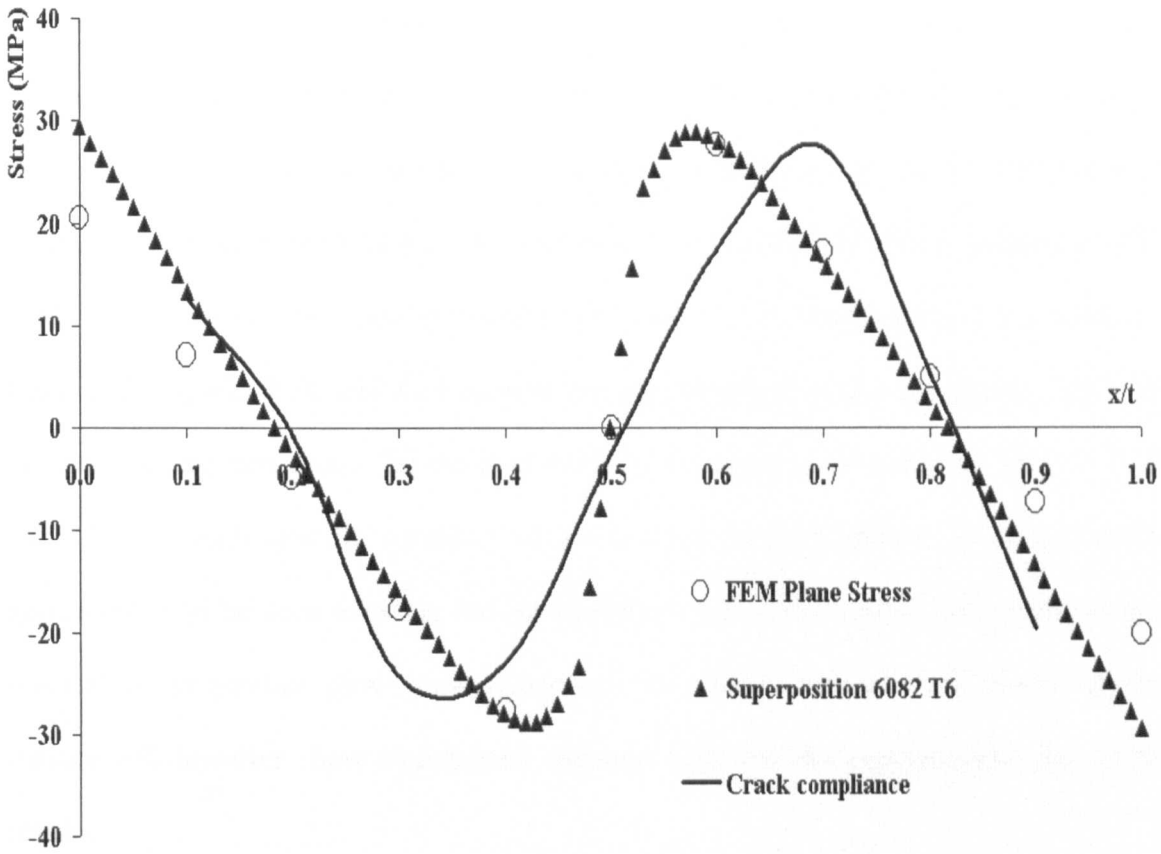

Figure 8.27.- Residual stress calculation for fully annealed AA 6082 T6 aluminium alloy

8.3.5. Determination of residual stresses in stress relief annealed AA 6082 T6 aluminium alloy with previous strain history.

This section considered, two previous history effects imposed on two different batches of stress relief annealed aluminium alloy specimens. The selected heat treatment process removes any previous loading history effects in the material and leads to limited ductility compared to the fully annealing case. The two pre-pulling operations were carried out on to 15000 microstrain for one batch and 30000 microstrain for the second batch. After the pulling operation, all batches of rectangular bars were bent to induce a residual stress profile into the material.

Figures 8.28 and 8.29 present the bending strain plots for the two batches. In all of these figures a clear Bauschinger effect can be seen; the surfaces that experience compressive stress have higher values of strains, when compared with the surfaces under tensile stress. Also, it is clear from both figures that yielding appears earlier on the compressive side. Additionally, from these data mechanical properties were determined as explained in Chapter 5. Figures 8.30 and 8.31 present the experimental results for strains based on different cutting directions. The residual stress calculations are presented in Figures 8.32 and 8.33 for each specific condition of pre-loading in the material. In general good agreements can be seen between the superposition and CCM results. The peaks in the residual stress profiles show good agreement. An extrapolation of the results to the surface will however show significance disparity between the superposition and CCM results.

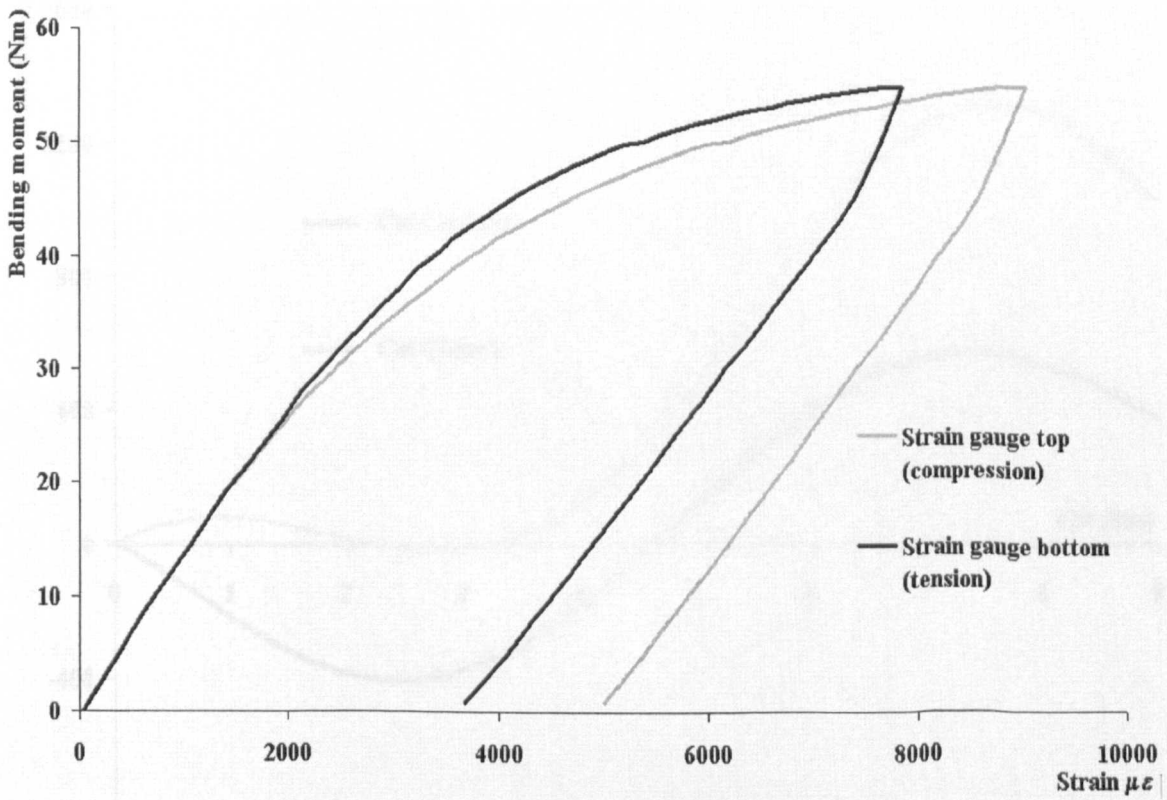

Figure 8.28.- Bend test in stress relief annealed AA 6082 T6 aluminium alloy, pre-pulled to 15000 microstrain

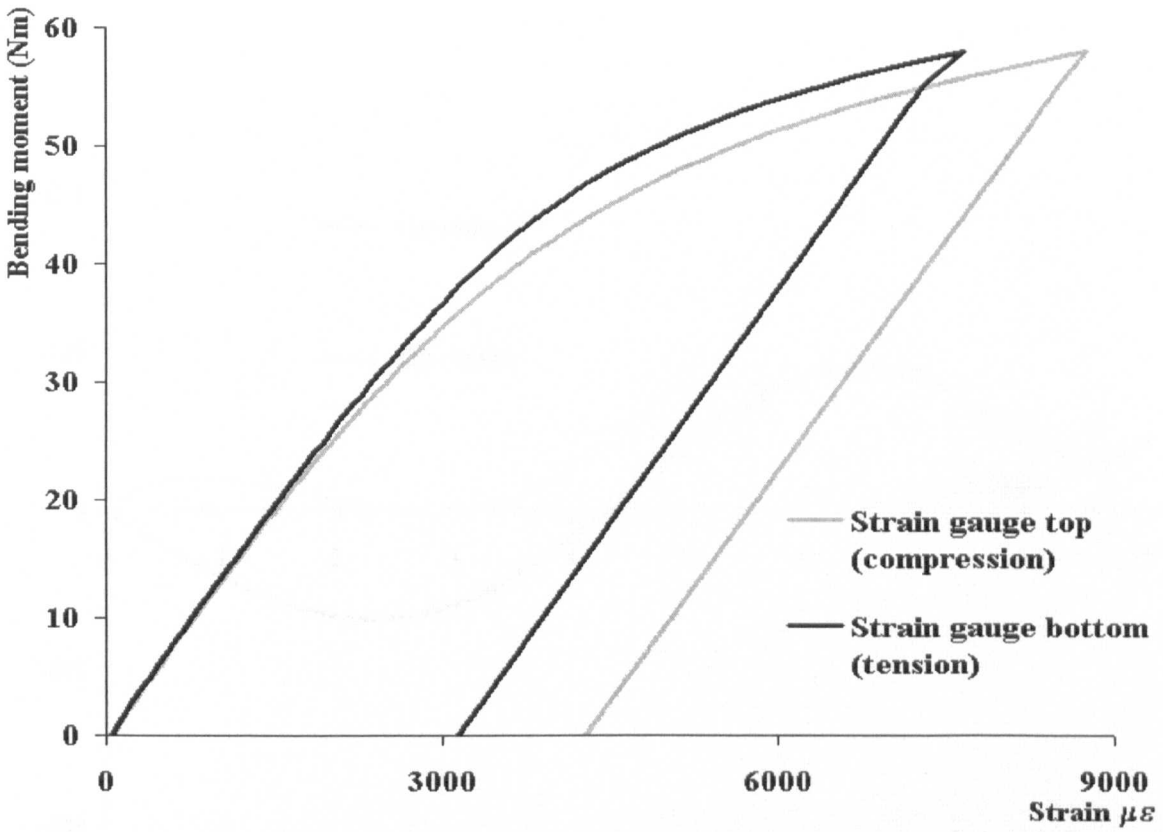

Figure 8.29.- Bend test in stress relief annealed AA 6082 T6 aluminium alloy, pre-pulled to 30000 microstrain

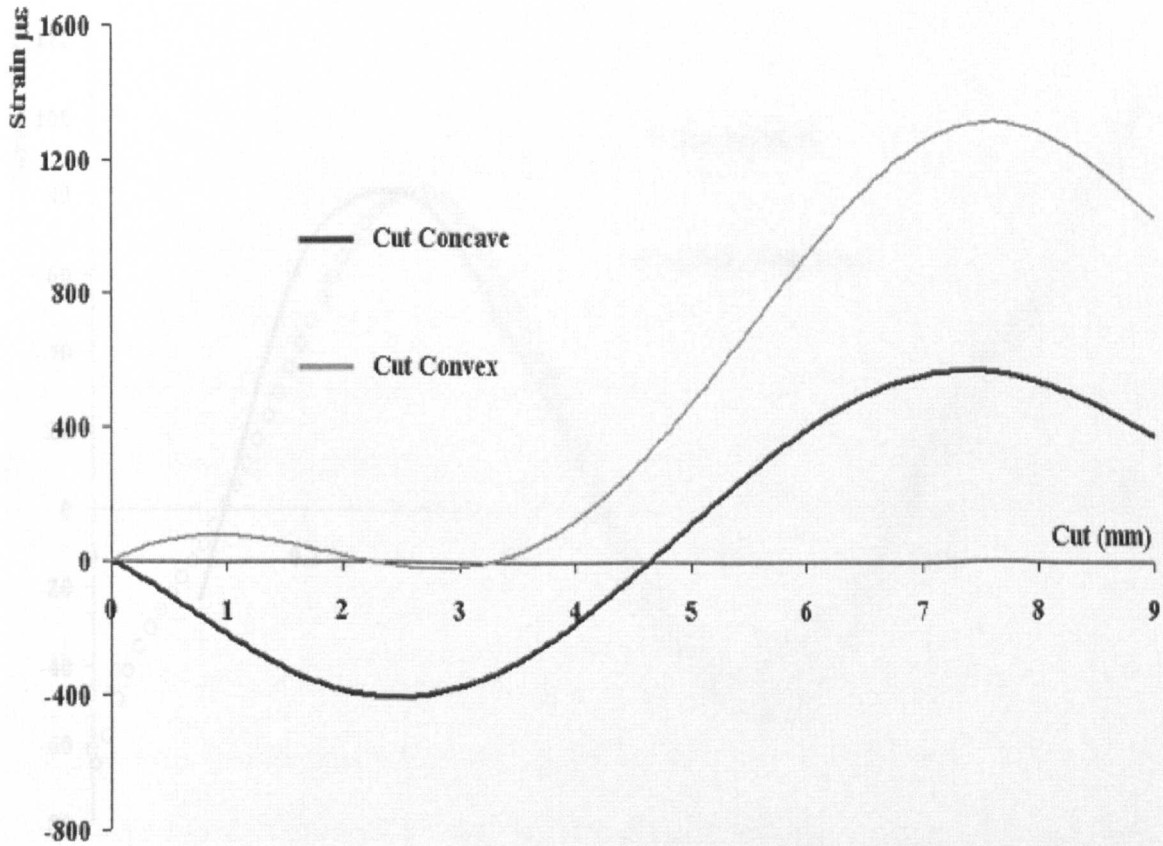

Figure 8.30.- Strain results by cutting for stress relief annealed AA 6082 T6 aluminium alloy, pre-pulled to 15000 microstrain

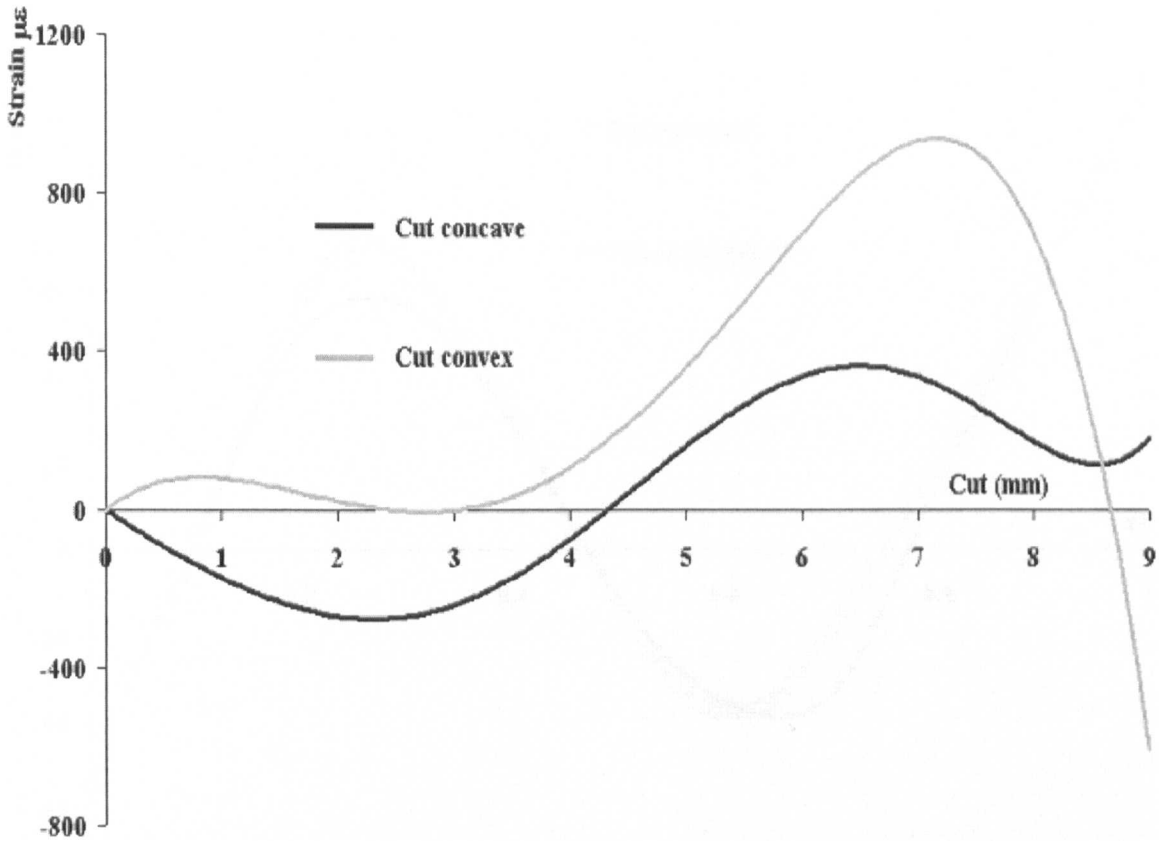

Figure 8.31.- Strain results by cutting for stress relief annealed AA 6082 T6 aluminium alloy, pre-pulled to 30000 microstrain

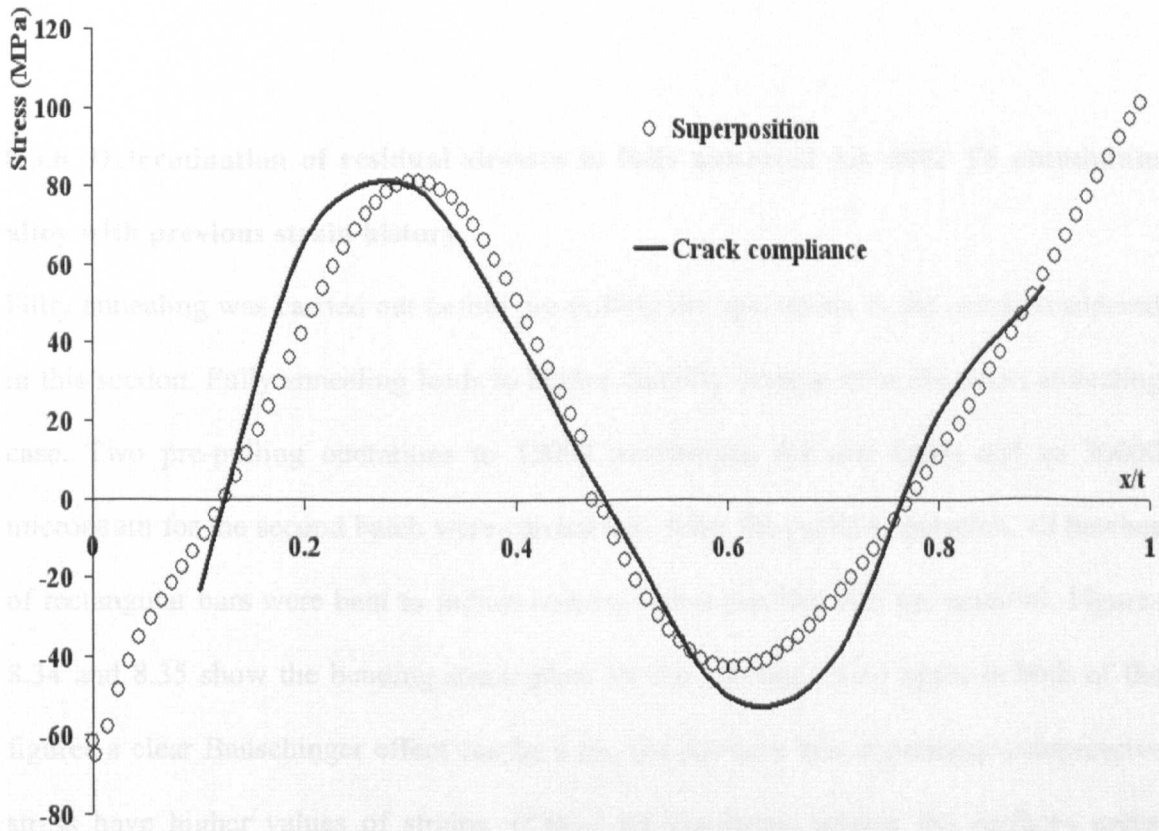

Figure 8.32.- Residual stress calculation in stress relief annealed AA 6082 T6 aluminium alloy, pre-pulled to 15000 microstrain

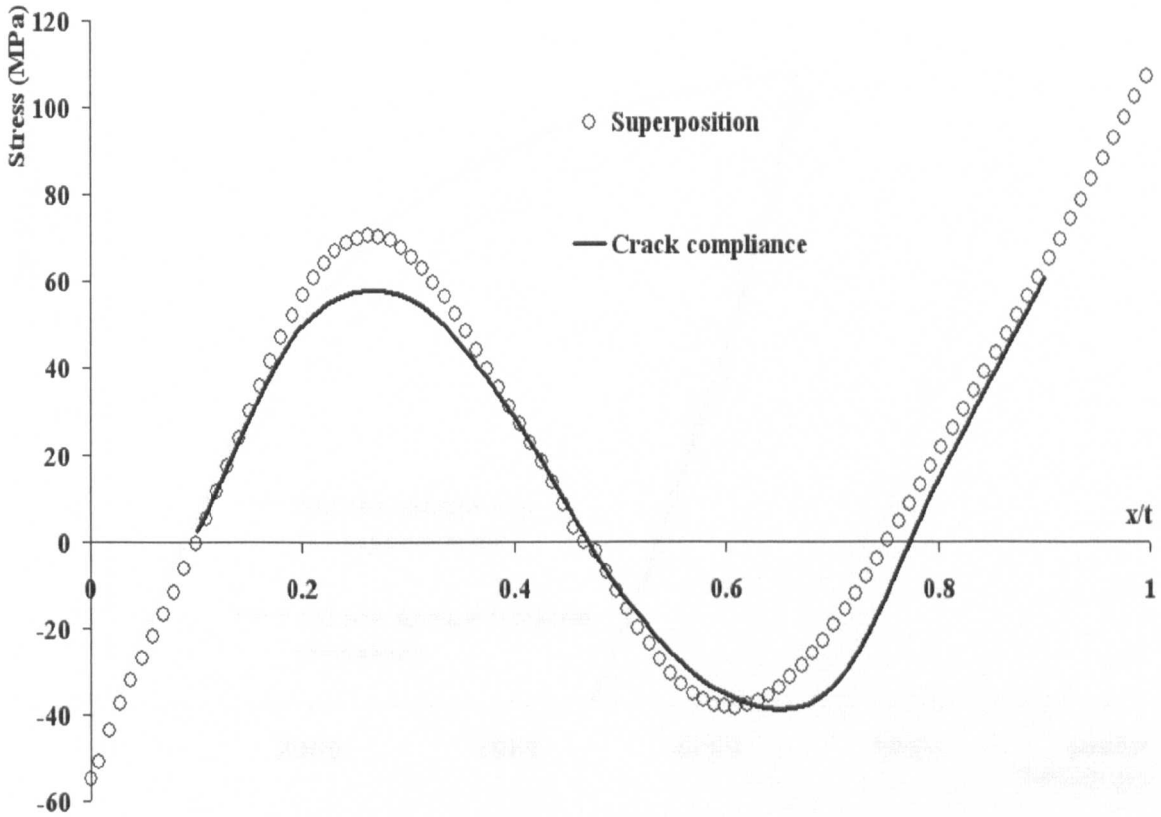

Figure 8.33.- Residual stress calculation in stress relief annealed AA 6082 T6 aluminium alloy, pre-pulled to 30000 microstrain

8.3.6. Determination of residual stresses in fully annealed AA 6082 T6 aluminium alloy with previous strain history.

Fully annealing was carried out before pre-pulling the specimens in the cases considered in this section. Fully annealing leads to higher ductility compared to the stress annealing case. Two pre-pulling operations to 15000 microstrain for one batch and to 30000 microstrain for the second batch were carried out. After the pulling operation, all batches of rectangular bars were bent to induce residual stress profiles into the material. Figures 8.34 and 8.35 show the bending strain plots for the batches. Once again in both of the figures a clear Bauschinger effect can be seen, the surfaces that experience compressive stress have higher values of strains, if they are compared against the surfaces under tensile stress.

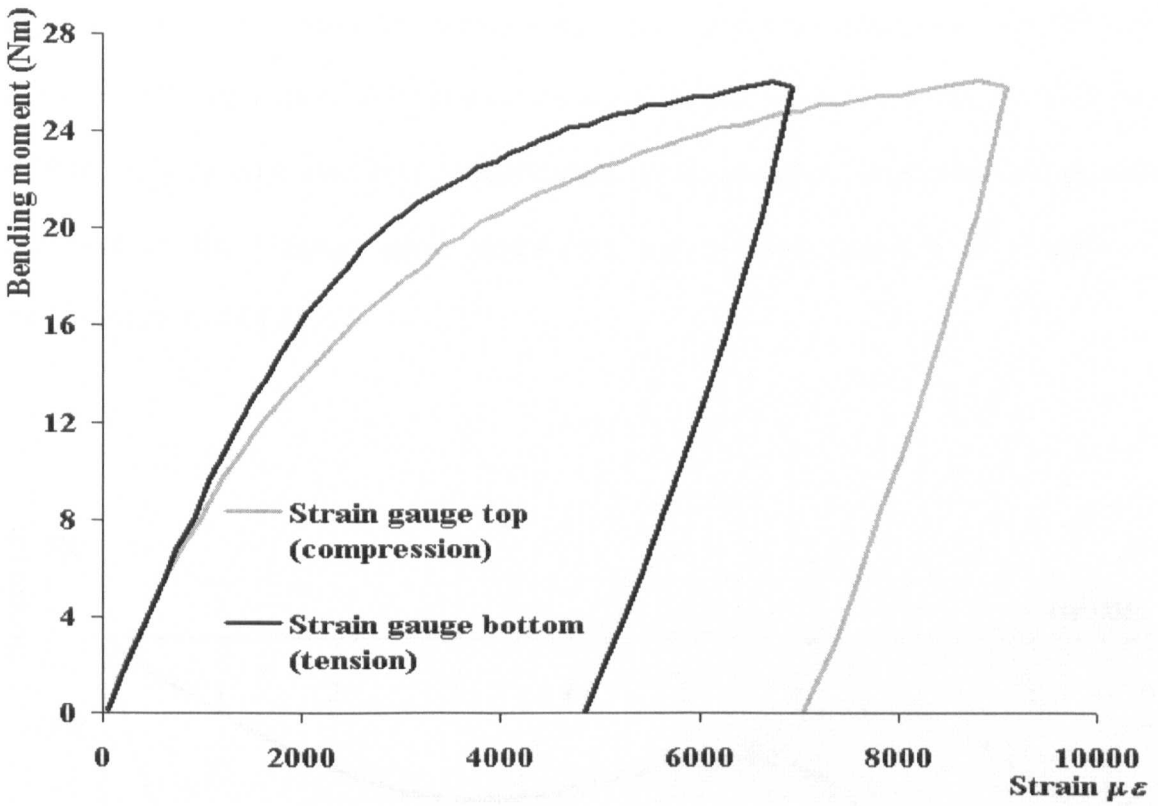

Figure 8.34.- Bend test in fully annealed AA 6082 T6 aluminium alloy, pre-pulled to 15000 microstrain

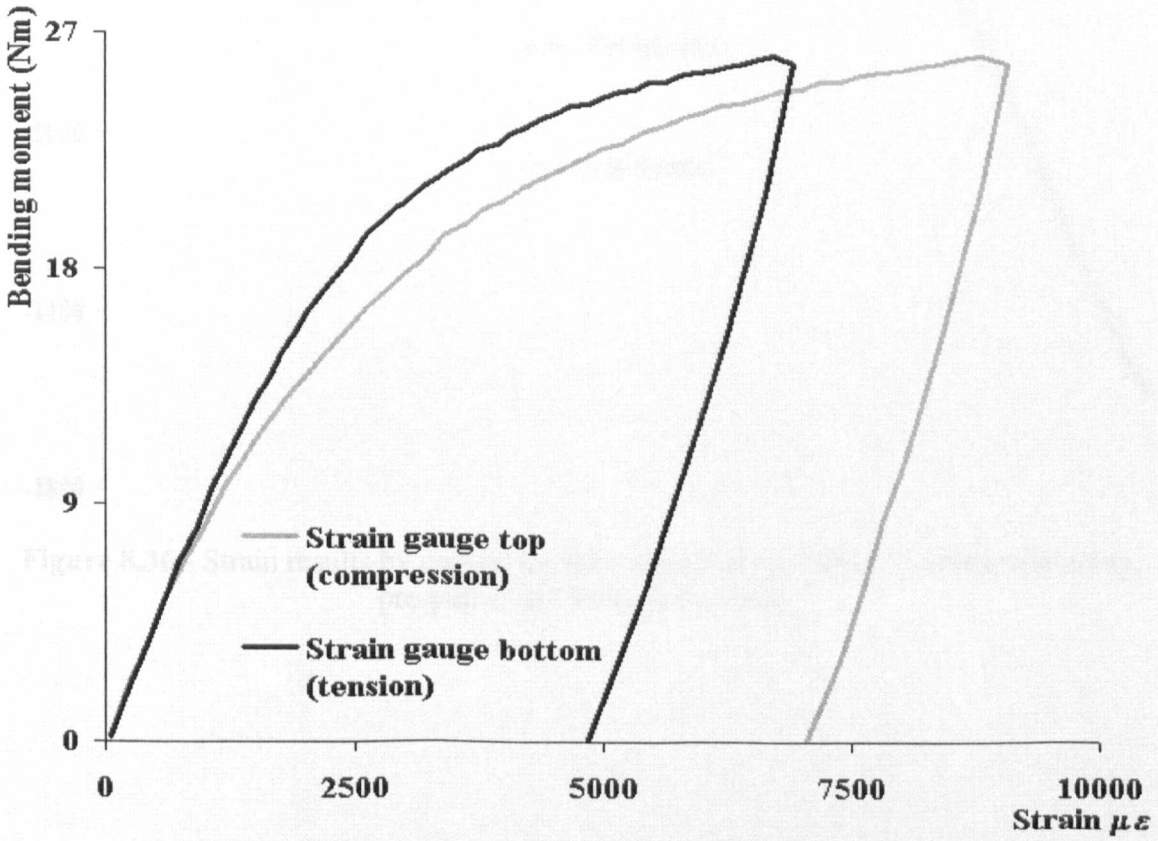

Figure 8.35.- Bend test in fully annealed AA 6082 T6 aluminium alloy, pre-pulled to 30000 microstrain

Figures 8.36 and 8.37 show the experimental strain results for cutting from on different surfaces of the specimen. The residual stress results are presented in Figures 8.38 and 8.39 for each specific condition of pre-loading of the material. As in most of the cases presented in the chapter, good agreements can be seen between the results of superposition and CCM.

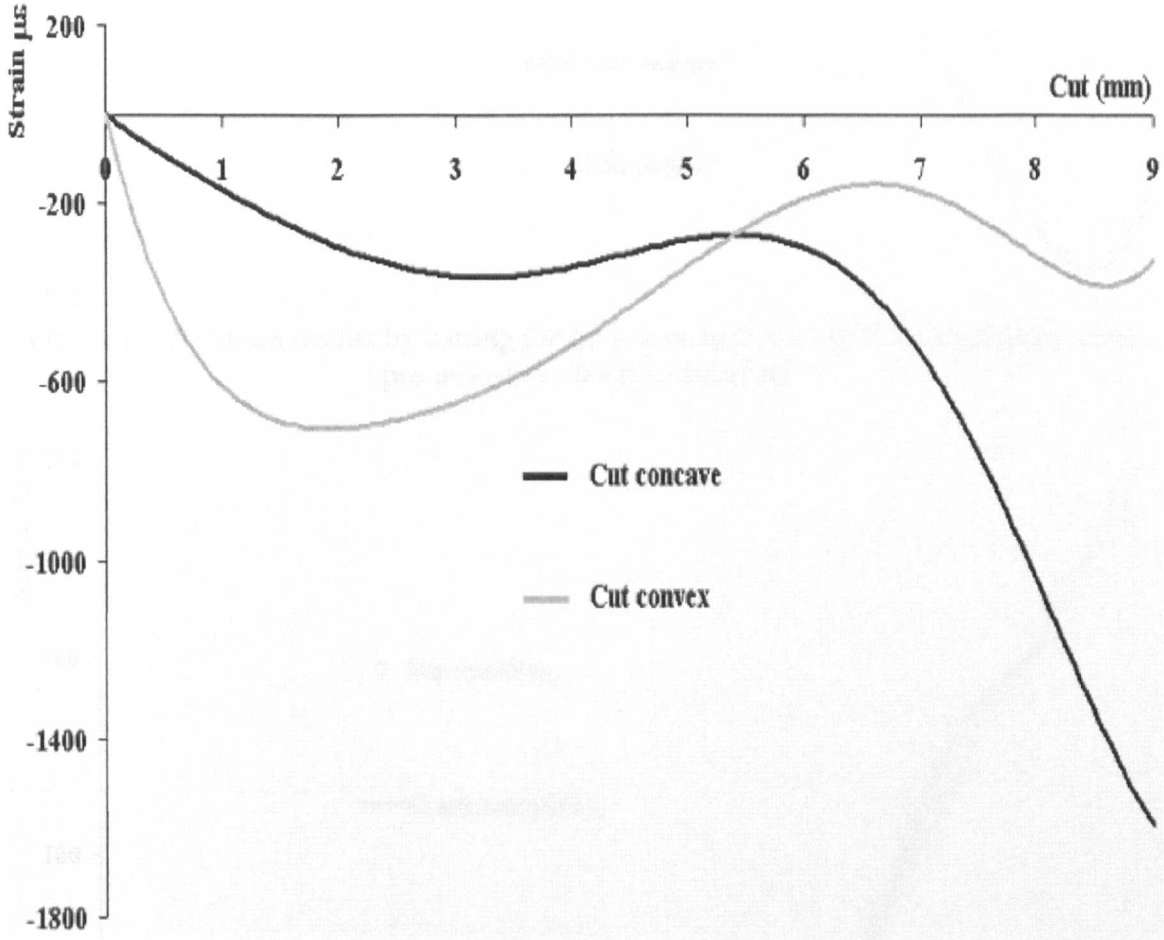

Figure 8.36.- Strain results by cutting for fully annealed AA 6082 T6 aluminium alloy, pre-pulled to 15000 microstrain

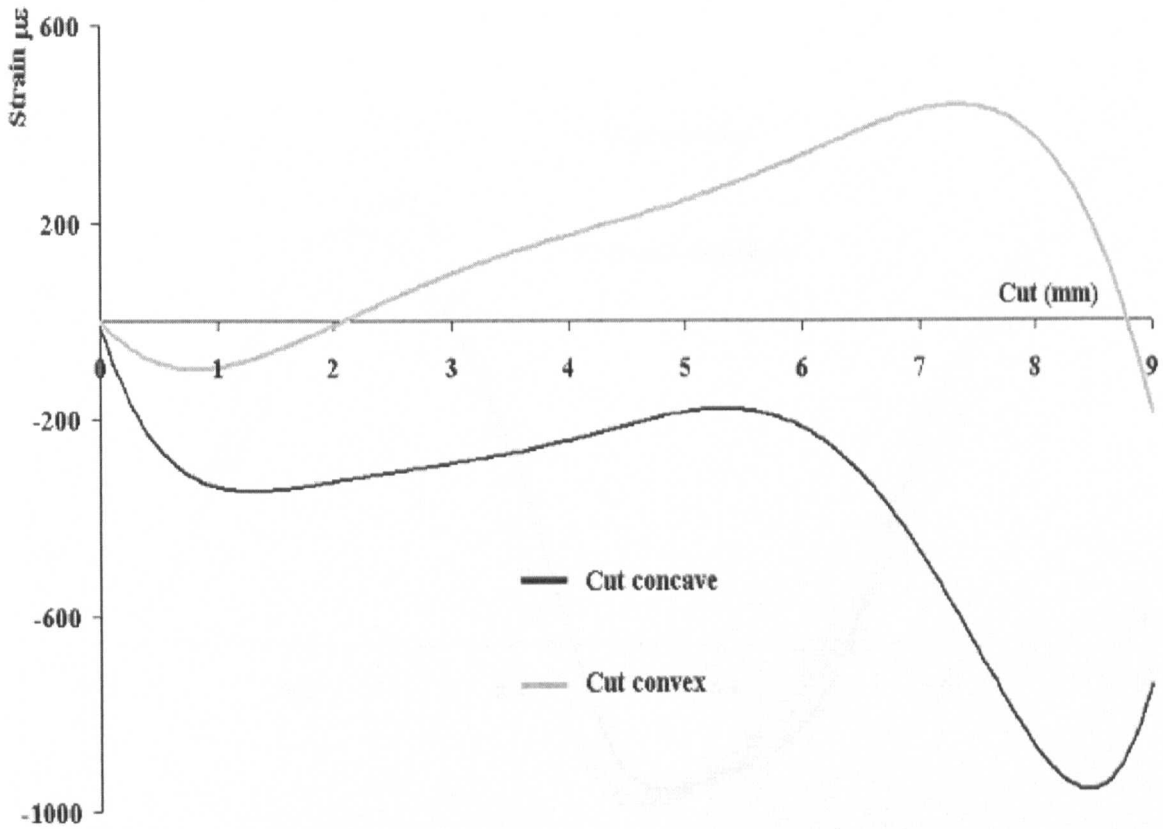

Figure 8.37.- Strain results by cutting for fully annealed AA 6082 T6 aluminium alloy, pre-pulled to 30000 microstrain

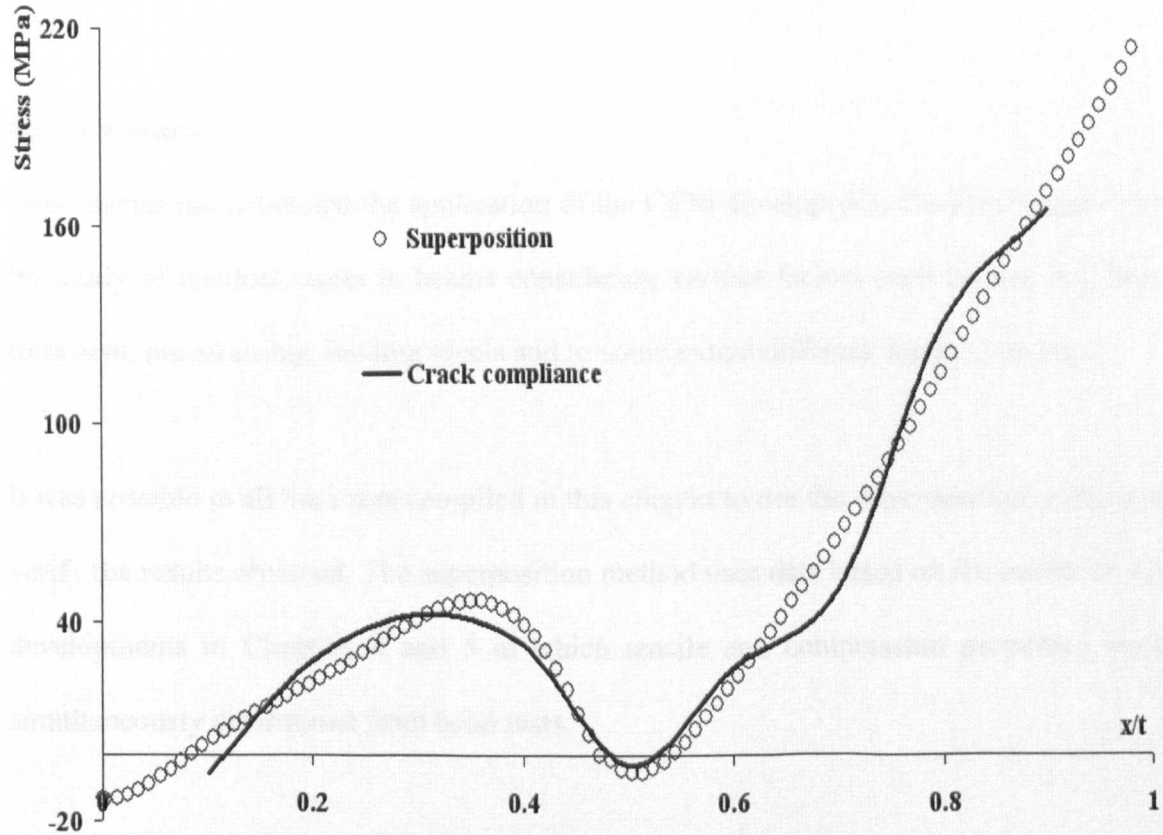

Figure 8.38.- Residual stress calculation in fully annealed AA 6082 T6 aluminium alloy, pre-pulled to 15000 microstrain

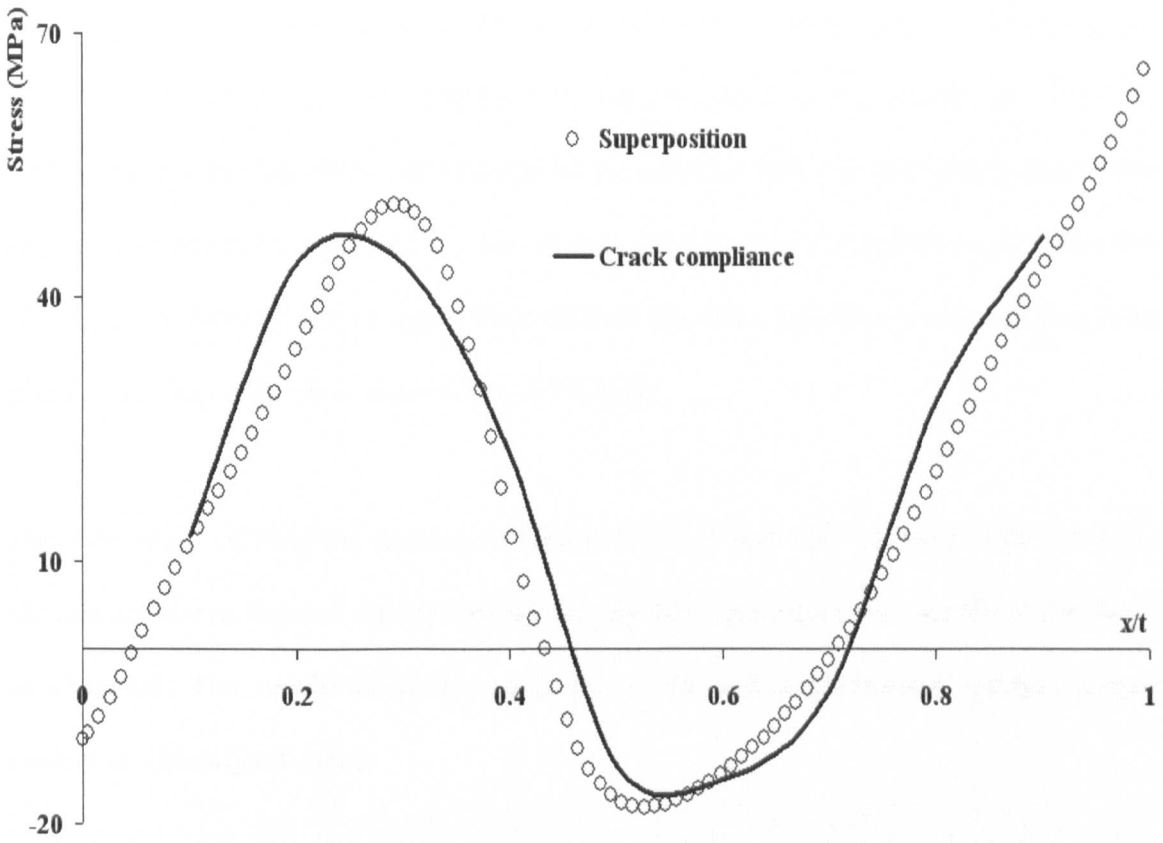

Figure 8.39.- Residual stress calculation in fully annealed AA 6082 T6 aluminium alloy, pre-pulled to 30000 microstrain

8.4. Summary.

This chapter has presented the application of the CCM developed in Chapters 6 and 7 for the study of residual stress in beams considering various factors such as material, heat treatment, pre-straining, loading levels and to some extent different depths of beams.

It was possible in all the cases compiled in this chapter to use the superposition method to verify the results obtained. The superposition method uses data based on the results of the developments in Chapters 4 and 5 in which tensile and compression properties were simultaneously determined from bend tests.

The work in the chapter demonstrates the importance of using appropriate settings for feed rates during EDM. This chapter has also presented a new simple technique for supporting beams that allows deformations due to stress relief to take place freely. The method eliminates the need for the use of floats and removes possibilities of errors that could arise in determining an appropriate size for the float. It is also easier to maintain the plane of cutting in the new approach to be straight.

The evaluation of residual stresses in annealed EN 8 and EN 1A steels and AA 6082 aluminium alloys showed anti-symmetry distribution relating to the middle of the beam as expected. The results obtained using the CCM and superposition method agreed closely in virtually all cases.

The use of the CCM and superposition method showed good agreement between results for residual stresses in materials that had been pre-strained. The residual stress fields in these cases lacked the anti-symmetry of the annealed materials and had different magnitudes of stresses in tension and compression.

The CCM used requires at least two representative samples to be used for the determination of residual stresses. This gives more accurate results in terms of magnitude and distribution of residual stresses. It was also evident that the CCM loses some of it accuracy when it is used to determine small residual stress fields or the induced residual stress is in a highly ductile material. Additionally, the accuracy of the CCM presented in this chapter compared to the superposition method demonstrates that it could be reliably used for other cases. This method is used in Chapter 9 to assess relaxation or maintainability of residual stresses in beams.

Chapter 9

Determination of maintainability of residual stresses using the crack compliance method

9.1. Introduction.

The influence of residual stresses on the behaviour of materials has long been a subject of interest and concern to many investigators [*Noble and Reed, 1974, Herman, 1995 and Badr, 2000*]. In particular, a great amount of work has been carried out on the role that residual stresses play in fatigue.

It is understood that fatigue cracking normally initiates at the surface of components and can be mitigated by the induction of compressive residual stresses at the surface. The extent of mitigation on crack initiation and propagation depends strongly upon the residual stress magnitude and distribution. But, any residual stress relaxation during the component cyclic operation reduces the achievable benefits. So, the evaluation of the effect of residual stresses and their relaxation on fatigue crack initiation and propagation is a helpful aspect of component design and life management.

Chapters 4 and 5 of this work present a new bending method for the accurate determination of mechanical properties of materials. The knowledge of mechanical properties of a material is required in the loading and unloading superposition method [*Timoshenko and Gere, 1991*] for determining residual stresses in a component. Only the stress-strain behaviour of the material and the determination of the loading and unloading stresses from strains at the surfaces are required in this method.

The CCM presented in Chapters 7 and 8 requires only the Young's modulus, Poisson's ratio and the relaxed strains during component cutting. This method was further developed in Chapters 6 and 8 and was verified extensively in Chapter 8. The application of the superposition method is limited to cases where the loading causing the residual

stresses is known. The CCM is applicable whether the loading is known or unknown. This makes the method to be appropriate for the determination of maintainability or relaxation of residual stresses in components.

This chapter presents the application of the crack compliance method given in Chapters 7 and 8 for the determination of maintainability or relaxation of residual stresses in beams that were exposed to cyclic fatigue loading at different levels. There has been no attempt, in the authors' knowledge, to demonstrate fully the redistribution of residual stresses across the full depth of beams subjected to fatigue loading.

The results presented in the next two sections were obtained from two batches of stress relief annealed EN 8 steel specimens subjected to a different four-point bending cyclic loading. Initially both batches of specimens were previously bent, as explained in section 8.3.1 (Figure 8.8), to induce a theoretically known residual stress field. The magnitude of the bending moment applied to induce residual stresses was 950 Nm. The magnitude of the residual stress at top and bottom surfaces of the beam was around 215 MPa (Figure 8.11). Strain gauges attached to the surface were used to monitor changes in the residual stress field as well.

9.2. Determination of maintainability of residual stresses in stress relief annealed EN 8 steel pre-bent, fatigued at 50% of the original bending moment.

The loading applied for the fatigue tests was 50% of the initial bending moment. The maximum nominal bending stress due to this is 463.78 MPa. The minimum alternating bending moment applied was set to 50 Nm in order to keep the machine stable. The total alternating stress range is 414.96 MPa. The selection of the bending moments, were made

taking into consideration, the introduction of a much higher alternating stress in relation to the one determined by fatigue theory for an infinite life ($\Delta\sigma$ = 342.5MPa) [*Bennantine, et. al, 1990*].

A HBM Spider 8 data logger and Catman 4.0 software were used to obtain the strain data results during the fatigue tests. The software was configured to collect data at periodic intervals, every 10000 cycles.

Figure 9.1 presents a plot of the bending moment applied against number of cycles. Figure 9.1 shows that maximum and minimum specified bending loads were maintained during the entire cyclic loading test.

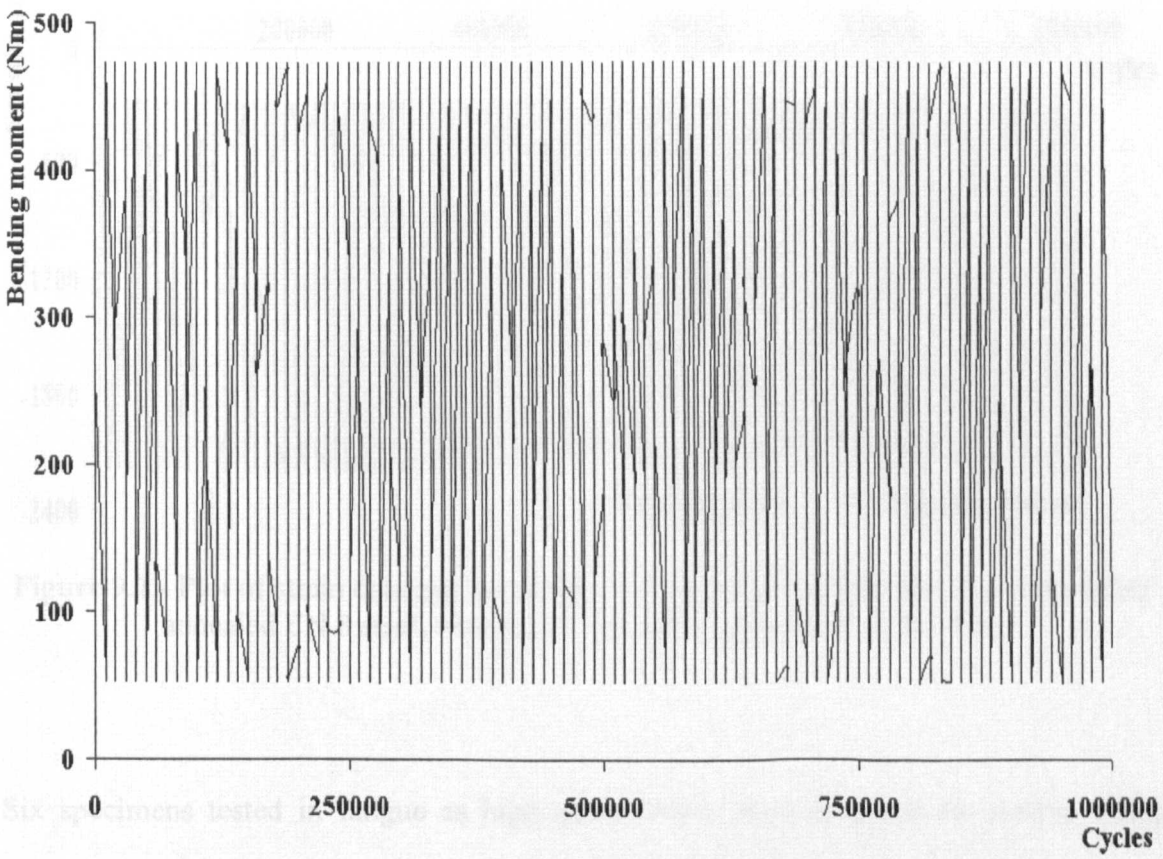

Figure 9.1.- Plot of bending moment against number of cycles in a fatigue test of a stress relief annealed EN 8 steel, with maximum bending moment of 475 Nm

Figure 9.2 illustrated the strain data from the bottom and top surfaces of the beam against number of cycles from the cyclic loading test. The figure shows that the magnitude of strain values at the maximum and minimum loading levels were consistent at about 2200 and 280 microstrain respectively. The fatigue test was stopped after 1000000 cycles, which is a fatigue limit for steels.

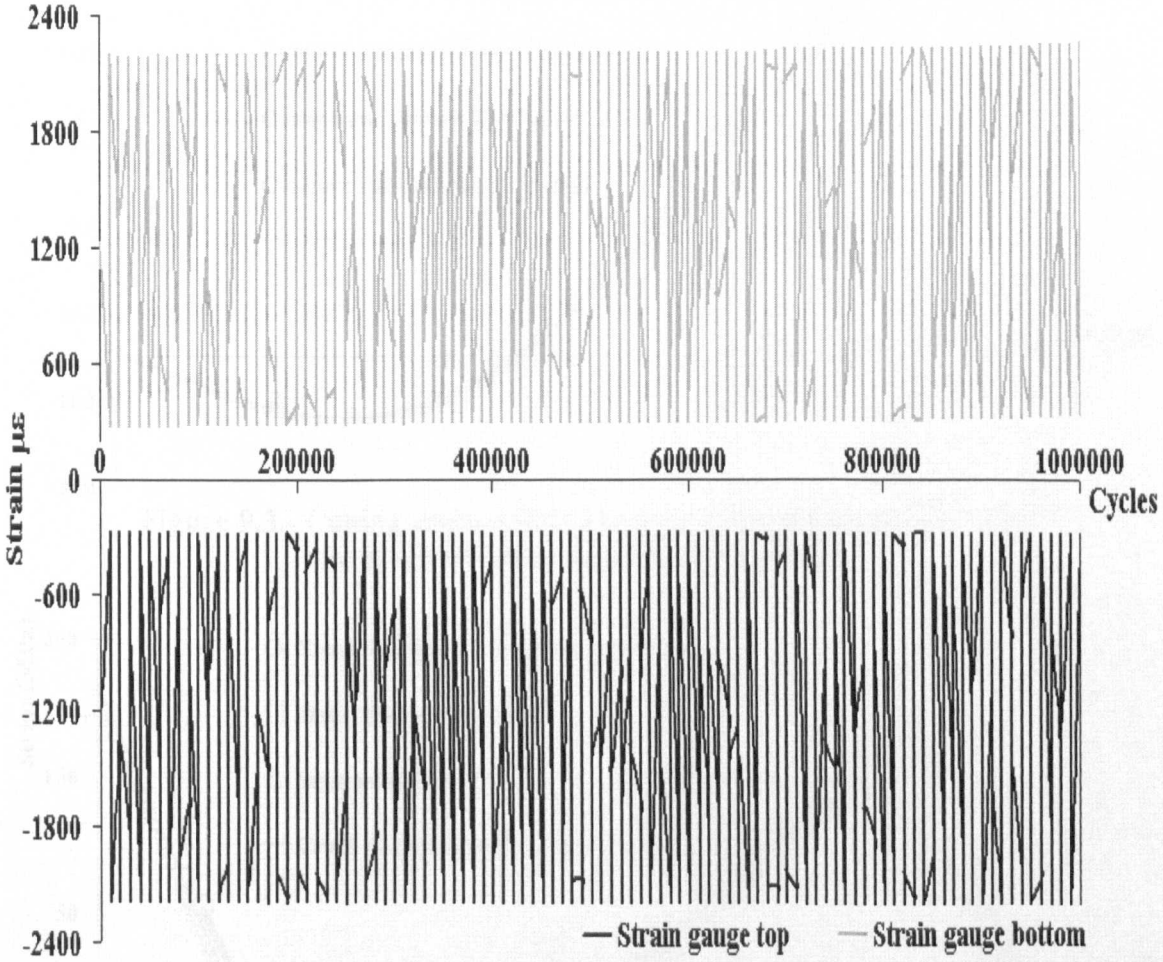

Figure 9.2.- Plot of strain data against number of cycles in a fatigue test of a stress relief annealed EN 8 steel, with maximum bending moment of 475 Nm

Six specimens tested in fatigue as highlighted above were prepared for cutting using EDM as described in Chapter 8. Figure 9.3 shows a typical set of strain results obtained from both of the EDM cutting processes. The results include data from specimens that

were not subjected to fatigue loading. Figure 9.4 shows the residual stress results obtained.

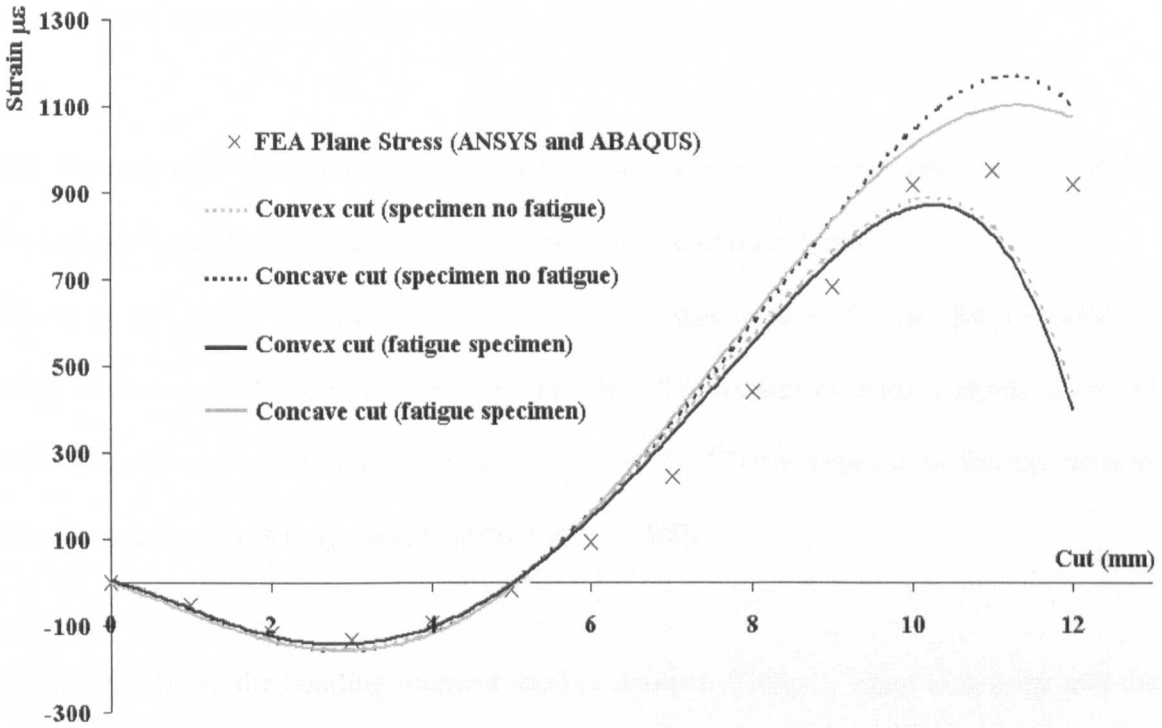

Figure 9.3.- Cutting strain results for stress relief annealed EN 8 steel for residual stress maintainability analysis

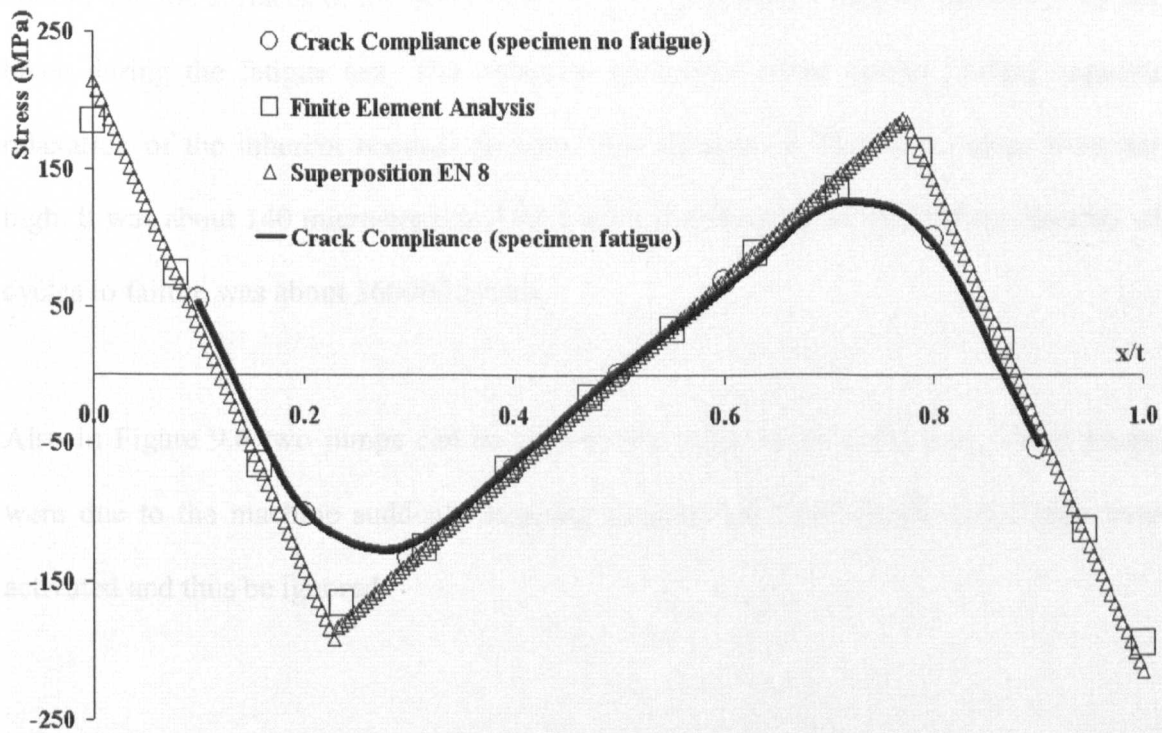

Figure 9.4.- Maintainability of the residual stress field for stress relief annealed EN 8 steel

The results obtained by this manner shows general good agreement. The figure shows that no relaxation of the residual stress field occurred. The results of residual stresses in both cyclically loaded and unloaded specimens were virtually the same and agreed well with the expected stress fields determined using the superposition and FEA methods

9.3. Determination of maintainability of residual stresses in stress relief annealed EN 8 steel pre-bent, fatigued at 60% of the original bending moment.

The next case study was performed on a group of specimens that were fatigue tested at 60% of the originally applied bending moment. The maximum stress applied is 556.53 MPa. The minimum bending moment was kept at the 50 Nm value as in the last section. The alternating stress range was therefore 507.72 MPa.

Figure 9.5 shows the bending moment against number of cycles again indicating that the loading was maintained steady during the tests. Figure 9.6 shows strain data from the bottom and top surfaces of the beam (tension and compression) against number of cycles taken during the fatigue test. The reduction of surface strain during cycling suggests relaxation of the inherent residual stresses. The changes of the strain values were not high. It was about 140 microstrain to 210 microstrain on average. The average number of cycles to failure was about 360000 cycles.

Also in Figure 9.6 two jumps can be seen in the strain-cyclic behaviour. These jumps were due to the machine suddenly stopping because the limit displacement trips were activated and thus be ignored.

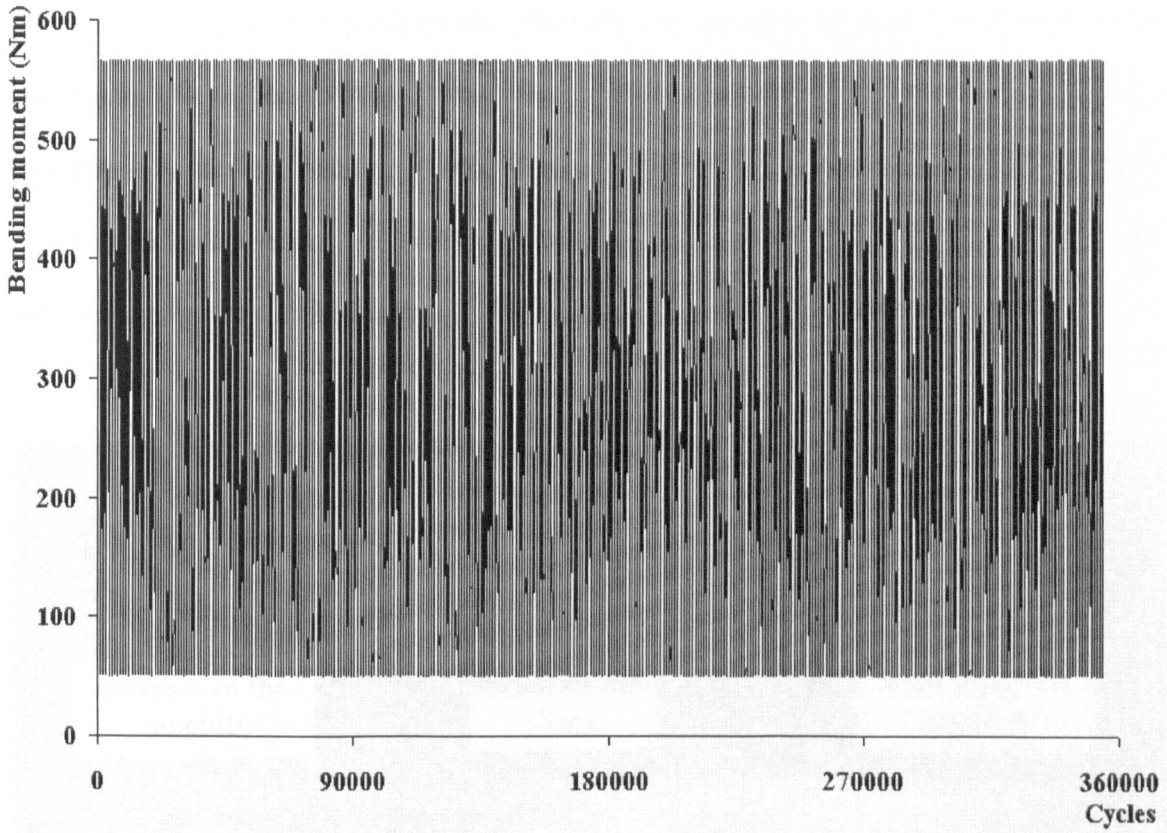

Figure 9.5.- Plot of bending moment against number of cycles in a fatigue test of a stress relief annealed EN 8 steel, with maximum bending moment of 570 Nm

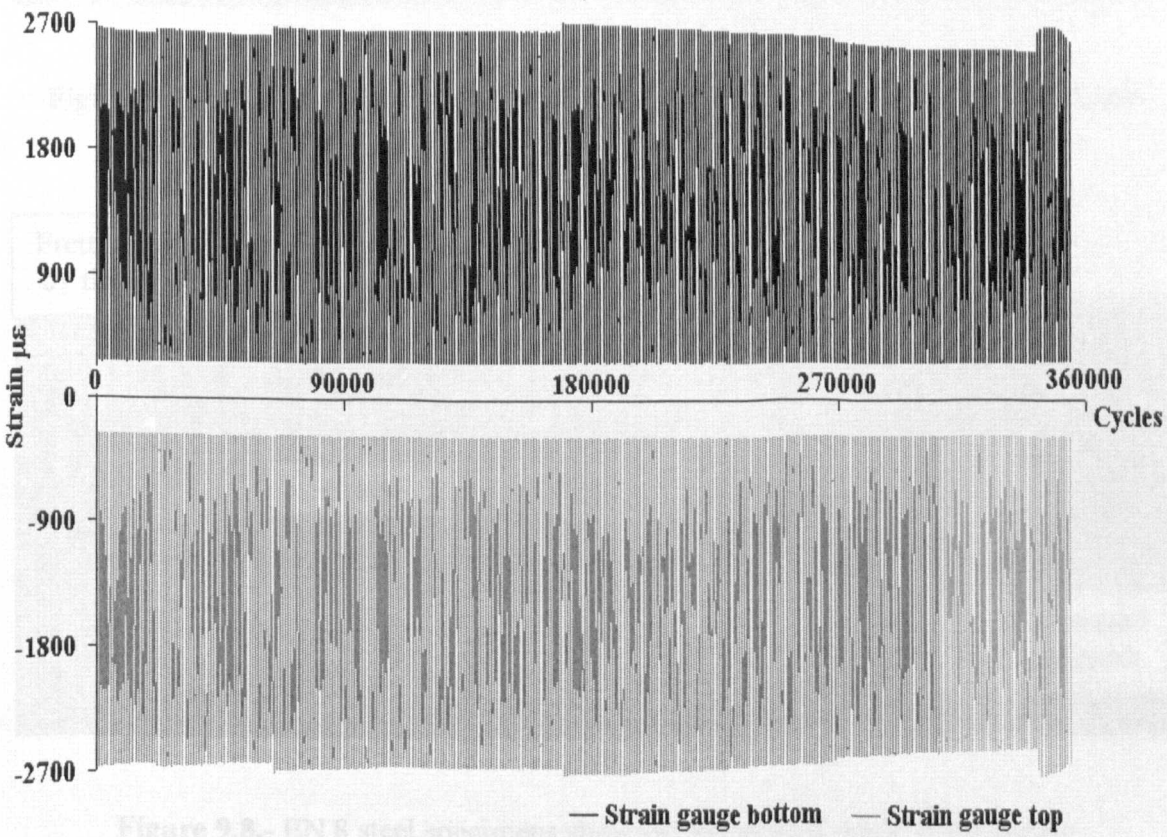

Figure 9.6.- Plot of strain data against number of cycles in a fatigue test of a stress relief annealed EN 8 steel, with maximum bending moment of 570 Nm

Figures 9.7 to 9.10 are photographs showing the location of failure on some of the specimens. It can be seen that failure was randomly located in the middle section of the specimens where the bending moment is maximum and constant due to the four-point bending arrangement. It can also be noticed that failure was not caused by fretting. All failures occurred away from the contact positions of the four-point bending pins.

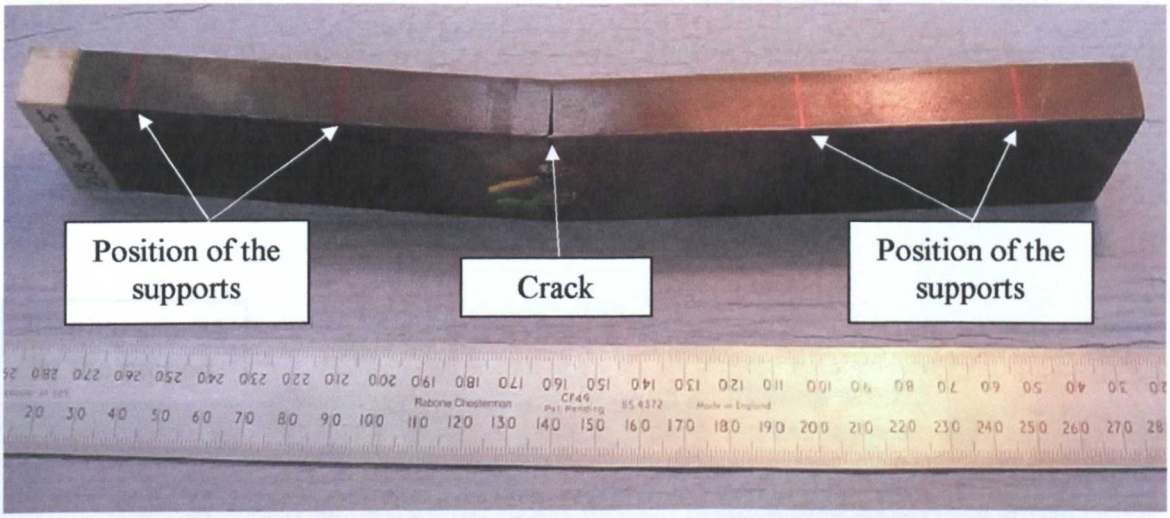

Figure 9.7.- EN 8 steel specimens showing propagated crack at the centre. Specimen cycled to a bending moment of 60% of the initial plastic bending moment

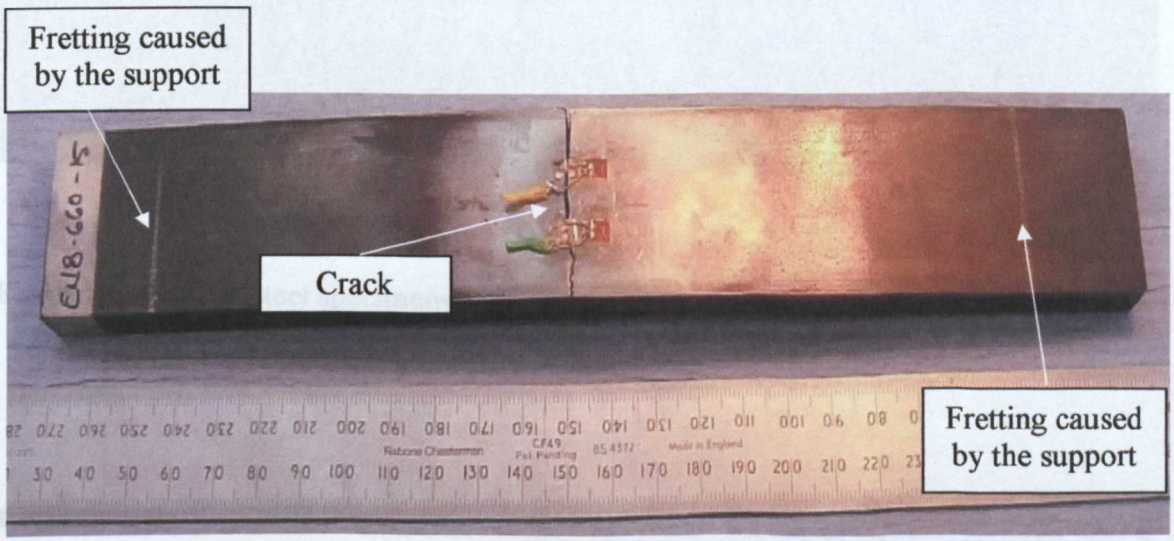

Figure 9.8.- EN 8 steel specimens showing propagated crack at the centre. Crack location is far away from the wear effect caused from loading

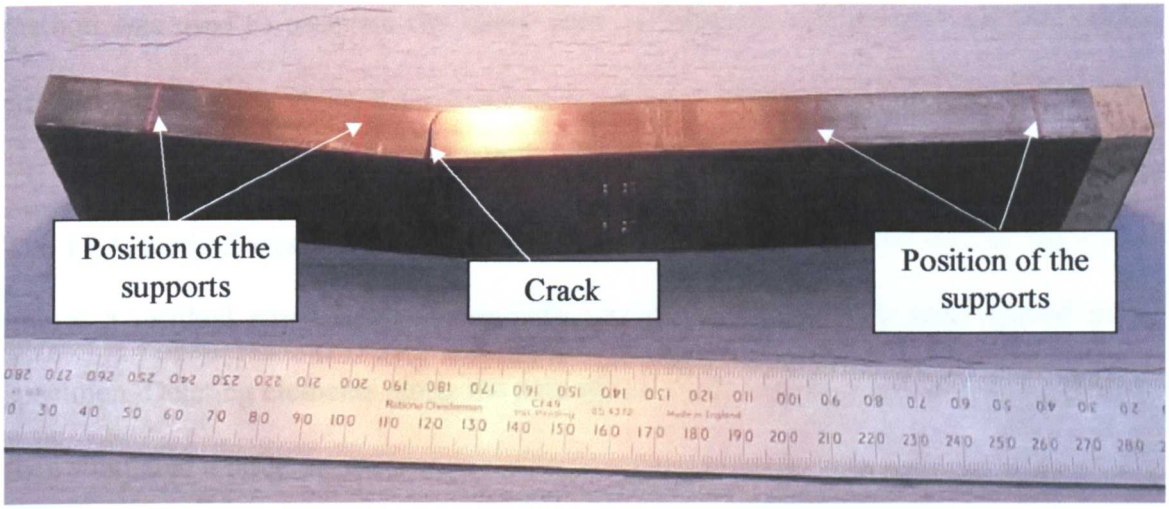

Figure 9.9.- EN 8 steel specimens showing propagated crack at the left side from the centre. Specimen cycled to a bending moment of 60% of the initial plastic bending moment

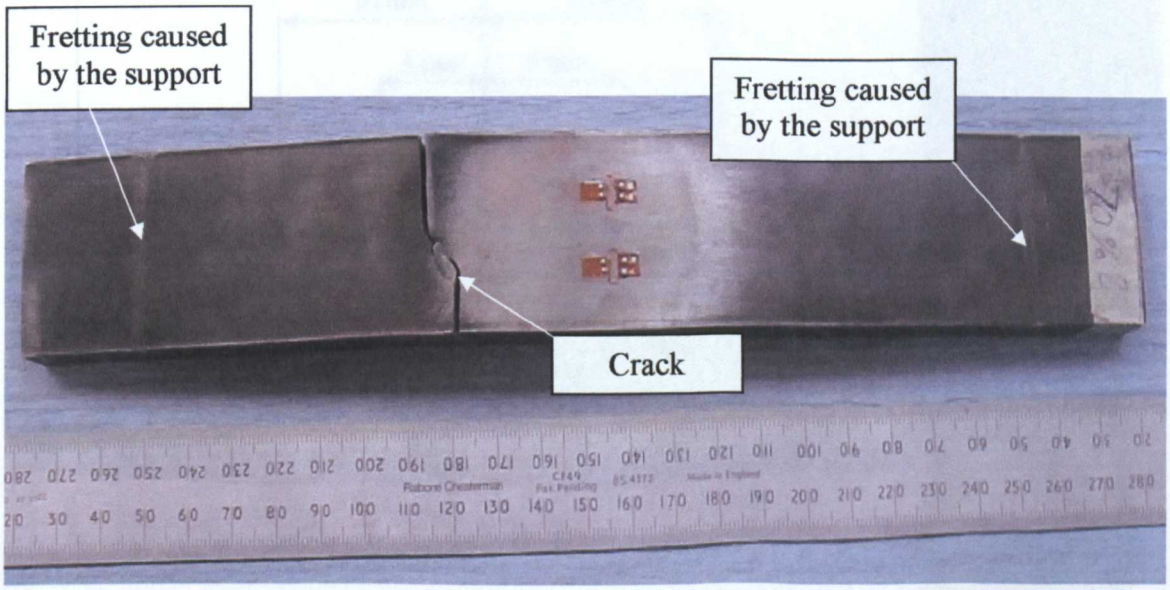

Figure 9.10.- EN 8 steel specimens showing propagated crack at the left side from centre. Crack location is far away from the wear effect caused from loading

It was necessary to establish that the fatigue cracks in the failed specimens only had a local effect on the residual stress fields. X-ray or neutron diffraction methods could be used for this purpose. These were however not available to the researcher. The FEA

method was used to establish the likely zone of influence of the crack on the residual stress field.

The FEA method was used together with the stress-strain behaviour of the material to induce a residual stress field corresponding to the initial 950 Nm load applied to the specimen. Deleting elements along the path of the crack as a cut illustrated in Figure 9.11 then simulated a fatigue crack.

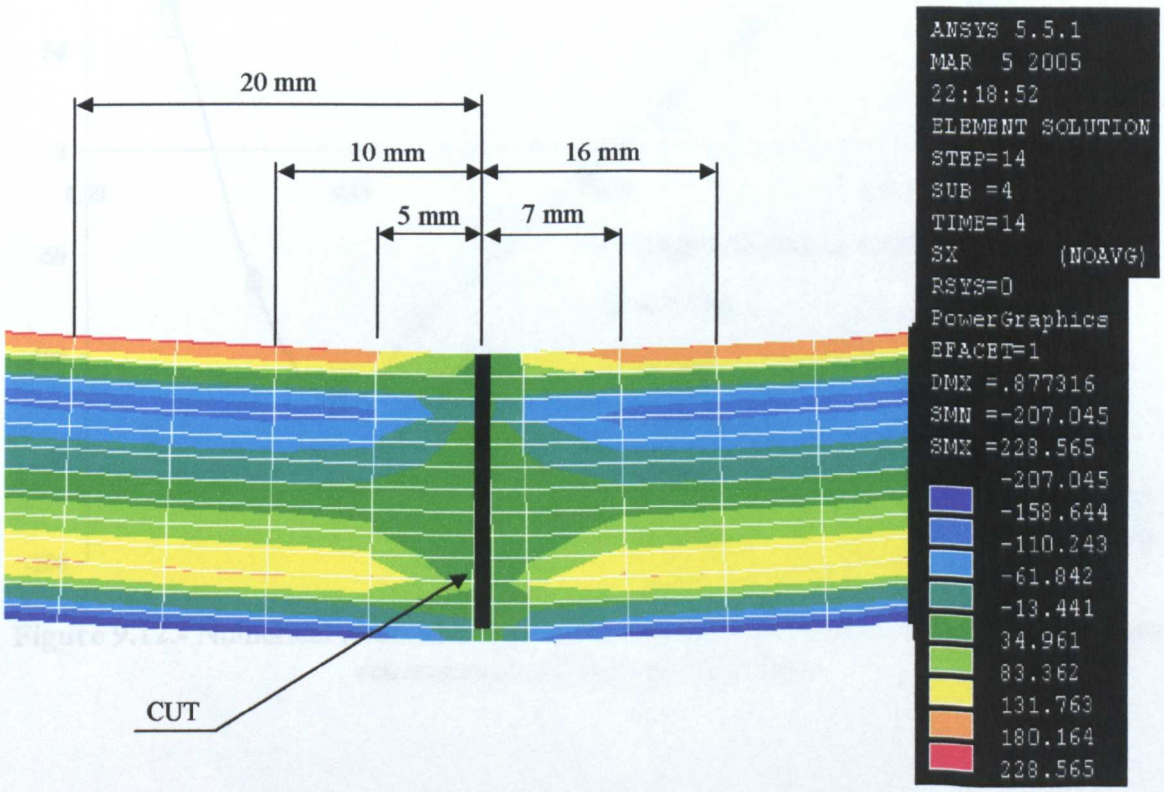

Figure 9.11.- FE cut simulation in stress relief annealed EN 8 steel specimen. Cut located at the centre

Figure 9.12 shows the distribution of residual stresses at different distances from the cut as illustrated in Figure 9.11. It is clear from the figure that for a distance of about 10 mm away from the cut or crack in the specimen, the residual stress profile will not be affected.

It can be seen from the figure that at this distance, the distribution of the residual stress field is as in the case where there is no cut at all. The actual cutting for the CCM analysis was made at a distance of about 20 mm from the failed surface.

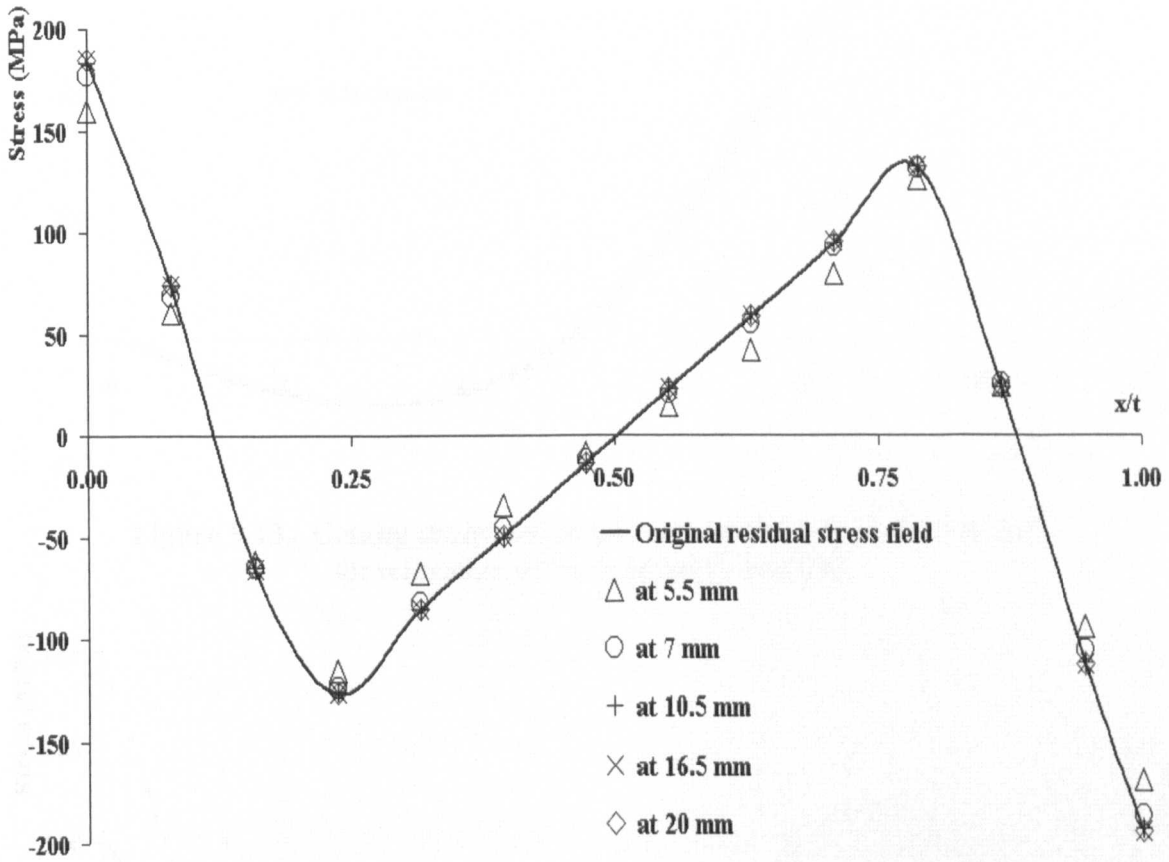

Figure 9.12.- Numerical residual stress values obtained by FE on cut simulation in stress relief annealed EN 8 steel specimen

The plots of strain relief for the cutting results can be seen in Figure 9.13. Figure 9.14 presents the residual stress fields obtained from the strain results. By projecting the curves to the surface, the residual stress at the surface can be seen to have dropped from the about 215 MPa to 113 MPa. It should be noted that this surface, which had a residual tensile stress, was subjected to compressive cyclic stress loading during the maintainability test.

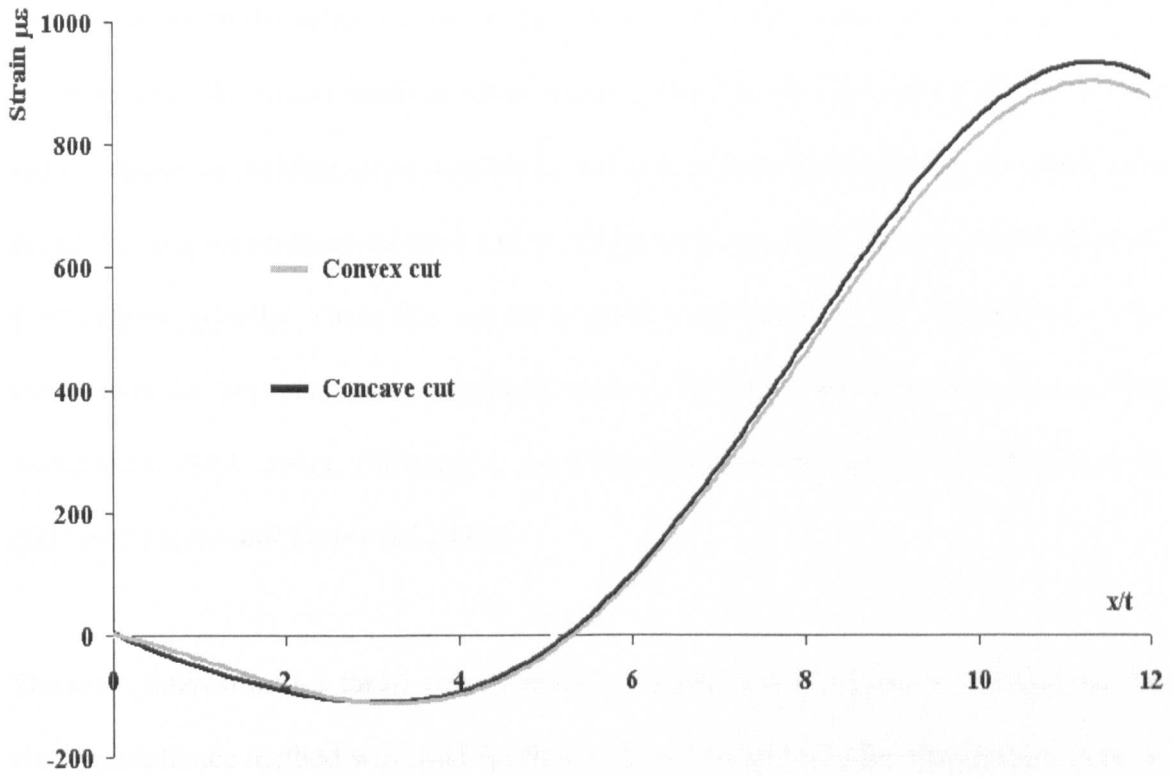

Figure 9.13.- Cutting strain results for stress relief annealed EN 8 steel for relaxation of the residual stress field

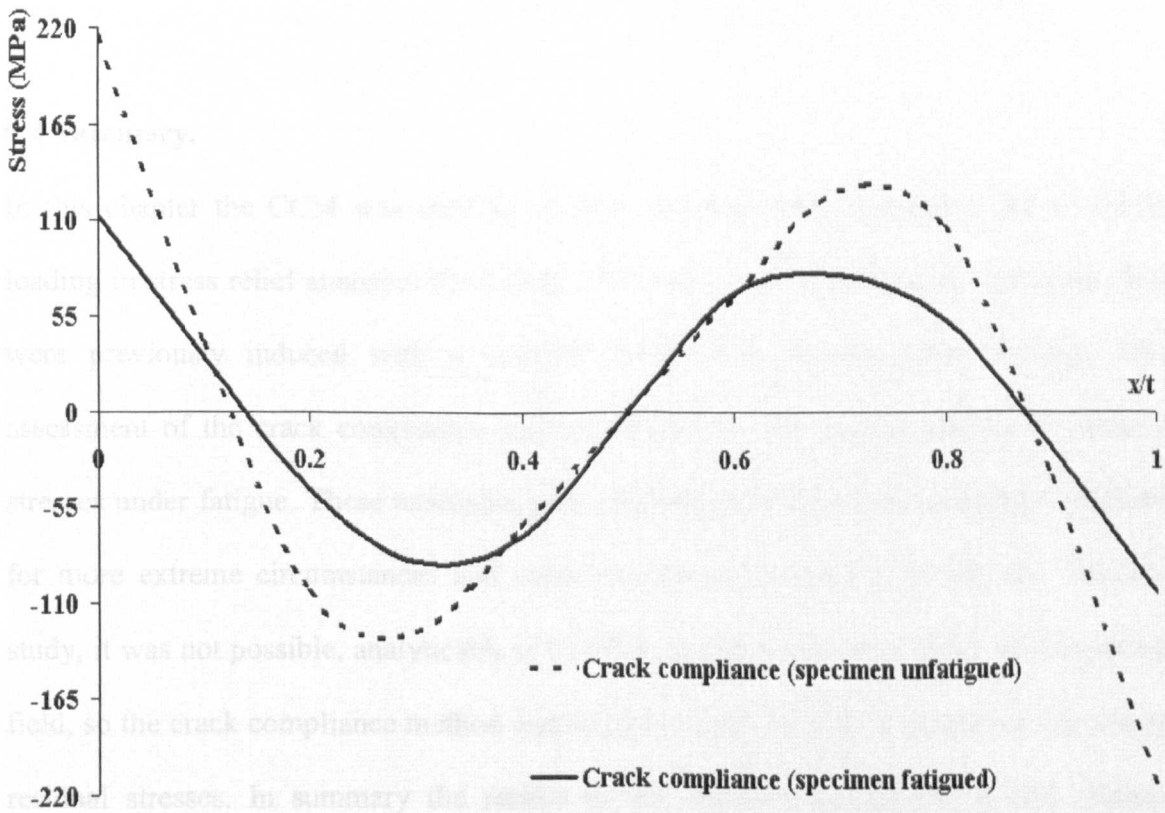

Figure 9.14.- Relaxation of the residual stress field for stress relief annealed EN 8 steel

The reduction on the other surface of the beam, which had compressive residual stress, was similar to the tensile residual stress surface of the beam. The surface of the bar that had compressive residual stress was subjected to a tensile cyclic loading. It appears that the cyclic loading reversed the dislocation effects on both the tensile and the compressive sides almost equally. There has not been good agreement for the explanation of the mechanism for the relaxation of residual stresses by researchers [*Morrow, et. al. 1960, Swindeman, 1981, James, 1982, Lu, et. al. 1988, Chaboche and Jung, 1998, Boyce, et. al. 2002 and Torres and Voorwald, 2002*].

The main interest in this thesis was to provide a quantitative measure for relaxation. The crack compliance method was used for this purpose because no other facilities such as X-ray or neutron methods were available for this research. Initial access was gained to X-ray measurements at Oxford University, but the results obtained were inconclusive.

9.4 Summary.

In this chapter the CCM was used to evaluate residual stress relaxation due to cyclic loading in stress relief annealed EN 8 steel. The study was carried out on specimens that were previously induced with a residual stress field by four-point bending. The assessment of the crack compliance method focused on the maintainability of residual stresses under fatigue. These examples gave confidence in the crack compliance method for more extreme circumstances and under more realistic loading conditions. For this study, it was not possible, analytically or by FEA, to check the state of the residual stress field, so the crack compliance method was the only effective way to determine the acting residual stresses. In summary the results of the analyses carried out in this chapter indicate that:

- The results of a qualitative surface strain approach agreed with the crack compliance solution to indicate that no relaxation of residual stresses occurred under the low load condition, of about 50% of the original plastic load applied to the material tested.
- The results of the comparison in Section 9.3 showed relaxation of residual stresses with cyclic fatigue loading. The trend of the relaxation appeared linear with cycling. The CCM provided a quantitative evaluation of the residual stress field at the end of the cyclic loading. The relaxed stress field was similar in distribution to the original stress field and was symmetrical about the middle of the beam.
- The work in this chapter fulfilled the initial aim of the thesis. The scope of the work expanded to include an efficient way to determine the tensile and mechanical properties of materials and the effect of initial straining on residual stress distribution in beams. These wider aims were achieved as indicated in Chapters 4, 5, 6, 7 and 8.

Chapter 10

Discussions, conclusions and future work

10.1. Conclusions.

The background and the literature review carried out in this thesis showed that there was scope to further develop the methods of obtaining the mechanical properties of materials with previous strain history effect and to determine residual stresses. The research focussed on beams because they provide a simple configuration for the development and verification of the technique proposed in the thesis. This chapter gives conclusions on the various aspects covered.

A new beam method for the simultaneous determination of tensile and compression stress-strain data from bending test data has been presented. The method can reduce the number of tests that need to be carried out. FE simulation was used to assess the method considering elastic-perfectly plastic, isotropic, linear Ziegler, non-linear Ziegler and combined isotropic / kinematic hardening material behaviours.

The results obtained from the new proposed method showed excellent agreement against expected results. The elastic zone was almost perfectly determined by the new method for all the simulated cases. Generally, excellent results were also obtained in the plastic region. However, oscillation was noticed as the material was loaded beyond the yield point. These oscillations are due to the inability of FEA packages to model Bauschinger effect smoothly. Nevertheless, the results converge and agree reasonably with expected results. This encouraged further experimental verification of the method.

The experimental evaluation of the beam method was carried out in Chapter 5. Tensile, compression and bend tests were performed to determine the stress-strain curves of different materials under different annealing and under a number of initial pre-strain

conditions. Strain hardening and Bauschinger effects were exhibited by tensile, compression and bending tests on EN 1A and EN 8 steels and aluminium alloy AA 6082 T6.

The stress-strain results obtained from the beam method agreed reasonably well when compared against experimental stress-strain results in all cases. In all evaluation cases where the state of the material was in an annealed condition, excellent agreement was noticed in the elastic and plastic parts of the stress-strain curve. The evaluation of the method on pre-strained materials was generally very good. All tests carried out on aluminium alloy gave excellent agreement between the results obtained from the beam method and the expected results. The agreements obtained in the case of the steel materials were generally good although some difference was noticed in the plastic region. However, the differences in all plastic regions were not higher than 9%. Analysis of the data used in both the simulation and experimental testing showed that no more than one hundred load increments is required to generate a proper stress-strain curve. The maximum strain considered in this study due to bending alone was less than 5%.

Although the beam method was presented as a method for deriving tensile and compression stress-strain curves from bend tests for materials under Bauschinger effect, it is applicable to any situation where the stress strain behaviour in the tensile part is unique and that in compression part is also unique. This will not be the case for situations where a material has non uniform macro residual stress inherent. In such situations each material point will have a stress strain behaviour that is generally different from other parts of the same material.

The limitations of the derivation of the beam method lie primarily in the assumptions of the bending theory. The theory assumes that the strain at any point in the beam is proportional to the distance of the point from the neutral axis. This assumption is said to hold provided the cross sectional dimensions of the beam is much smaller than the radius of curvature, typically less than one-tenth.

It is not possible to determine the ultimate tensile strength with the beam approach because of the absence of possibility of necking especially for very ductile materials. In this regard, the approach is not less disadvantaged compared to compression tests because barrelling occurs. None of the bending analysis considered here exceeded the 5% strain limit at which Poisson's lateral deformation effects can be considerable. Exceeding 5% strain will have necessitated the consideration of true stress-strain behaviour. This effect was considered in the calculation but did not change the results obtained significantly.

The beam method presented gives the possibility of obtaining tensile and compressive stress-strain curves from bend tests alone. This will reduce the number of tests that need to be carried out, saving time and cost.

The work in this thesis developed several aspects of the crack compliance method further and applied it to the determination of maintainability of residual stresses in beams. Several parameters such as material type, heat treatment, strain hardening, type of loading (static or cyclic) and specimen dimensions were considered to different extents. The conclusions that may be drawn on several aspects of the work carried out may be summarised as follows.

A plate EDM technique was developed for the experimental part of the CCM presented. As part of this development, a new support system was introduced. The support, through its cylindrically shaped base, allows easier rocking of specimens and relaxation of residual stresses. This reduces the possibility of the weight of the specimens from affecting strain readings during the cutting of slots in specimens. The support also allows the cutting plane to be better maintained than other existing methods used. Although electrodes do not theoretically make contact with specimens during cutting, they do in practise touch the specimen and can, if care is not taken, cause plastic deformation that can alter the inherent residual stress field. This showed that very good care needs to be taken in selecting the feed rate of the plate EDM.

It was found helpful to combine the residual stress field results based on strain data obtained from cutting specimens from two different sides in order to determine the full stress fields more accurately.

Some conclusions can be drawn from the FEA carried out in the work. The results of the analysis carried out showed that the currently available influence function in the literature are validated using FEA. Although FEA could be used to determine this function, extreme care needs to be taken to ensure that convergence conditions are satisfied. It is not feasible to generalise on guidelines for selection of the parameters *s* and *ds* needed to locate the determination of *Z(a)* especially for components of a general configuration other than a beam.

The results of FEA carried out showed that the width of slots cut during CCM does not affect significantly the magnitude of the residual stresses determined. The difference in

the magnitude of the residual stresses when slots of width ranging from 0.01 mm to 1 mm were considered was about 30 MPa. FEA was also helpful in highlighting the likely sensitivity of the effect of the location of strain gauges on measuring relaxed strain during cutting. This guided some aspects of the experimental work and the interpretation of results, especially in the studies on maintainability of residual stresses.

The analytical work on the weight function $h(a,x)$ allows the constants required for its evaluation to be carried out more flexibly. This removes the need to rely on the evaluation of the function using tabulated values in reference books.

Generally, the CCM procedure developed in this work produced results that agree closely with results of other methods, such as the loading and unloading stress superposition method. There was good agreement in all cases, covering different levels of strain hardening, different types of heat treatment and depth of beams. Less agreement was however obtained in the cases where the residual stress magnitude is low or the material is very ductile.

The CCM developed was thereafter applied to residual stress maintainability problems. It was not possible to evaluate the results of this analysis by other means. The performance of the CCM developed over a range of problems provided confidence in its ability to analyse other similar problems as posed by residual stress changes due to cyclic fatigue loading. The general outcomes from the CCM analyses may be summaries as follows.

Residual stress field in annealed plastically bent beams showed same magnitudes on the tensile as on the compressive sides. There is a lack of symmetry and variation in the magnitude of stresses in pre-strained or strain hardened beams.

The CCM was applied to study maintainability or relaxation of residual stresses due to cyclic loading in beams. Two load cases were considered. In one case the maximum cyclic load was set to 50% of the magnitude of the original load applied, which caused the residual stress field. In the second case the maximum cyclic load was set to 60% of the original residual stress load that was applied. In both cases the minimum cyclic load was set to 50 Nm. No relaxation was noticed in the 50% load case, while relaxation was noticed in the 60% load case.

The relaxations on the tensile and compressive surfaces were fairly symmetrical. This appears to indicate a similar reversal of dislocation effects on the tensile and compressive residual stress surfaces.

In closing this thesis has presented a new approach for the simultaneous determination of asymmetric tensile and compressive stress-strain behaviour using bend tests only. The CCM has been developed further, verified and applied to study maintainability of residual stresses in cyclic loaded beams.

10.2. Recommendation for future work.

The study presented in this thesis, attempted to provide a complete assessment of two topics, which are strongly related to the subject of residual stresses. The first is the use of bend test to determine the mechanical properties of a material and as a mechanical

process for inducing residual stresses. The second is the use of the crack compliance method to determine residual stresses in beams.

From the research performed in each of the areas highlighted, it was noticed that a number of improvements can be carried out to obtain experimental methods that will be more versatile, easier to apply and more accurate for the determination of results. On this basis suggestion for further work has been divided in to two categories as follows:

1) Determination of mechanical properties.

a) The beam method for the simultaneous determination of tensile and compressive stress strain data from bend tests should be tested further on composite materials. Some composite materials present a different behaviour in tension compared to compression.

b) Mechanical properties were obtained by using only a bending procedure, but the yield point was more difficult to determine from the results than those from uniaxial testing. There is a smother transition into non-linear behaviour in the bend test results. More research can be carried out with respect to this issue.

c) The ultimate tensile strength has not been found using bend tests. The ultimate tensile strength is easily found in axial testing, as the load at which the specimen starts to experience necking is directly measureable. It would be helpful to carry out analyses to determine how to determine the strength of a material using the bending approach.

d) It can be useful to check if a similar procedure for the determination of mechanical properties can be based on torsion testing.

e) The determination of mechanical properties by four point bend tests can be used in the future to help the estimation and/or evaluation of spring-back response. The aim is to simplify the process by eliminating the need for uni-axial testing required and to reduce the time of the analysis.

f) The investigation from the work so far shows that there is no standard for using the bend test to simultaneously determine asymmetric tensile and compressive stress-strain behaviours. This aspect can be taken as further work.

2. Determination of residual stress profiles by the use of the CCM.

a) The research carried out on the CCM was applied only in four-point bending of beams. In the future it will be helpful to evaluate the performance of the new rig for other types of configuration (or to design a new rig, depending on the situation). Examples of other geometries that could be considered are welded pieces, tubes, etc.

b) Metallic composite materials are being used in industry. The CCM and the new cutting system could be used to determine residual stress profiles in these kinds of materials. The new cutting rig can make the erosion process simpler.

This section has attempted to highlight areas where the work carried out in this thesis can be expanded.

Appendix I

Analytical calculation of the weight function $h(a,x)$

Appendix I.

The weight function *h(x,a)* used in this work were derived based on the equations given in *Wu and Carlson* [*1991*]. The reference gives tables of values for *h(x,a)* at different values of *x* for a given crack length *a*. This is however very restrictive, therefore a more flexible procedure was developed. The geometry considered is a single crack in a finite width plate and the length of the plate is at least two times the width, so that the effect of finite length does not need to be considered (Figure A.1).

Figure A.1.- A single edge crack in a finite width plate [*Wu and Carlson, 1991*]
a) dimensional arrangement b) non-dimensional arrangement

In order to obtain the weight function for this system, the reference force *P*, Figure A.1, was chosen as a uniform tensile load. The corresponding weight function is given by the fitting Equation A.1 [*Wu and Carlson, 1991*]:

$$h(a,x)=\frac{1}{\sqrt{2\pi a}}\sum_{i=1}^{5}\beta_i(a)\left(1-\frac{a}{x}\right)^{i-\frac{3}{2}} \qquad \text{A.1}$$

where;

$$\beta_1 = 2.0$$

$$\beta_2 = \frac{\left[4af_r'(a) + 2f_r(a) + \frac{3}{2}F_2(a)\right]}{f_r(a)}$$

$$\beta_3 = \frac{\left[aF_2'(a) + \frac{1}{2}\left[5F_3(a) - F_2(a)\right]\right]}{f_r(a)} \qquad \text{A.2}$$

$$\beta_4 = \frac{\left[aF_3'(a) + \frac{1}{2}\left[7F_4(a) - 3F_3(a)\right]\right]}{f_r(a)}$$

$$\beta_5 = \frac{\left[aF_4'(a) - \frac{5}{2}F_4(a)\right]}{f_r(a)}$$

The functions $F_j(a)$ and $fr(a)$ are given by [*Wu and Carlson, 1991*].

$$F_1(a) = 4f_r(a) \qquad \text{A.3}$$

$$F_2(a) = \frac{1}{12\sqrt{2}}\left[315\pi\phi(a) - 105V_r(a) - 208\sqrt{2}f_r(a)\right] \qquad \text{A.4}$$

$$F_2'(a) = \frac{1}{12\sqrt{2}}\left[315\pi\phi'(a) - 105V_r'(a) - 208\sqrt{2}f_r'(a)\right] \qquad \text{A.5}$$

$$F_3(a) = \frac{1}{30\sqrt{2}}\left[-1260\pi\phi(a) + 525V_r(a) + 616\sqrt{2}f_r(a)\right] \qquad \text{A.6}$$

$$F_3'(a) = \frac{1}{30\sqrt{2}}\left[-1260\pi\phi'(a) + 525V_r'(a) + 616\sqrt{2}f_r'(a)\right] \qquad \text{A.7}$$

$$F_4(a) = \sqrt{2}\ V_r(a) - \left[F_1(a) + F_2(a) + F_3(a)\right] \qquad \text{A.8}$$

$$F_4'(a) = \sqrt{2}\ V_r'(a) - \left[F_1'(a) + F_2'(a) + F_3'(a)\right] \qquad \text{A.9}$$

and

$$f_r(a) = \frac{1}{(1-a)^{3/2}}\sum_{i=0}^{7}\alpha_i a^i \qquad \text{A.10}$$

$$f_r'(a) = \sum_{i=0}^{7}\alpha_i\left[\frac{i(1-a)^{3/2}a^{i-1} + (3/2)(1-a)^{1/2}a^i}{(1-a)^3}\right] \qquad \text{A.11}$$

where $$V_r(a) = \sum_{i=0}^{7} \frac{\gamma_i a^i}{(1-a)^2} \quad \text{A.12}$$

and $$\phi(a) = \frac{1}{a^2} \int_0^a s[f_r(s)]^2 ds \quad \text{A.13}$$

It can be seen from Equations A.1 to A.13 that if $\phi(a)$ is evaluated, the terms $F_i(a)$ and $F_i'(a)$ can be evaluated in terms of a and we can subsequently determine $\beta_i(a)$ that are required for the evaluation of the weight function $h(a,x)$. From Equation A.10, we can write that;

$$[f_r(s)]^2 = \frac{1}{(1-s)^{3/2}} \sum_{i=0}^{7} \alpha_i s^i \frac{1}{(1-s)^{3/2}} \sum_{j=0}^{7} \alpha_j s^j = \frac{1}{(1-s)^3} \left[\sum_{i=0}^{7} \sum_{j=0}^{7} \alpha_i \alpha_j s^{i+j} \right] \quad \text{A.14}$$

and from Equation A.13

$$\phi(a) = \frac{1}{a^2} \int_0^a \sum_{i=0}^{7} \sum_{j=0}^{7} \frac{\alpha_i \alpha_j s^{i+j+1}}{(1-s)^3} ds \quad \text{A.15}$$

In order to perform the integration in Equation A.15, it is helpful to make the transformation $x = 1-s$ from which it follows that $s = 1-x$, $ds = -dx$; $s = a$ when $x = 1-a$, and $x = 1$ when $s = 0$. Therefore we can re-write Equation A.15 as in Equation A.16.

$$\phi(a) = -\frac{1}{a^2} \int_1^{(1-a)} \sum_{i=0}^{7} \sum_{j=0}^{7} \frac{\alpha_i \alpha_j (1-x)^p}{x^3} dx \quad \text{A.16}$$

where $p = i + j + 1$. For $x \leq 1$ and by applying binomials expansions [*Spiegel, 1998*], we have Equation A.16a

$$(1-x)^p = \sum_{k=0}^{p} \binom{p}{k} (-x)^k \quad \text{A.16a}$$

where $\binom{p}{k}$ is the combination factorial

$$\binom{p}{k} = \frac{p!}{(p-k)!k!} \quad \text{A.16b}$$

Therefore A.16 can be written as

$$\phi(a) = -\frac{1}{a^2}\int_1^{(1-a)} \sum_{i=0}^{7}\sum_{j=0}^{7}\sum_{k=0}^{p} \alpha_i\alpha_j(-1)^{k-3}\binom{p}{k}(x)^{k-3}\,dx \qquad \text{A.17}$$

which after integration gives

$$\phi(a) = -\frac{1}{a2}\left[\sum_{i=0}^{7}\sum_{j=0}^{7}\sum_{k=0}^{p} \alpha_i\alpha_j(-1)^{k-3}\binom{p}{k}I(x)\right]_1^{1-a} \qquad \text{A.18}$$

where $$I(x) = \frac{x^{k-2}}{k-2} \qquad \text{for k} \neq 2 \qquad \text{A.19a}$$

or $$I(x) = ln(x) \qquad \text{for k} = 2 \qquad \text{A.19b}$$

and finally after simplifying gives

$$\phi(a) = -\sum_{i=0}^{7}\sum_{j=0}^{7}\sum_{k=0}^{p} \alpha_i\alpha_j(-1)^{k-3}\binom{p}{k}I(a) \qquad \text{A.20}$$

where $$I(a) = \frac{[(1-a)^{k-2}-1)]}{[a^2(k-2)]} \qquad \text{for } k \neq 2 \qquad \text{A.21a}$$

or $$I(a) = \frac{ln(1-a)}{a^2} \qquad \text{for } k = 2 \qquad \text{A.21b}$$

It should be noted that a singularity does not actually occur during the use of Equation A.21b because for real cracks $a < 1$. The differential of ϕ with respect to a is given by

$$\varphi'(a) = -\frac{1}{a^2}\left[\sum_{i=0}^{7}\sum_{j=0}^{7}\sum_{k=0}^{p} \alpha_i\alpha_j(-1)^{k-3}\binom{p}{k}I'(x)\right]_1^{1-a} \qquad \text{A.22}$$

where $$I'(a) = \frac{-((k-2)a^2(1-a)^{k-3}) - 2a[(1-a)^{k-2}-1]}{((k-2)a^4)} \qquad \text{for } k \neq 2 \qquad \text{A.23a}$$

or $$I'(a) = -\left[\frac{1}{a^4}\frac{a^2}{((1-a)-2a\ln(1-a))}\right] \qquad \text{for } k = 2 \qquad \text{A.23b}$$

References

References

ABAQUS, Version 6.3, *Standard user's manual,* Vol. II. 2002.

Al-Hassani, S. T. S., Mechanical aspects of residual stress development in shot peening, *Conference Proceeding ICSP-1*, pp. 583–602, 1981.

ANSYS, Version 5.3, *Standard user's manual,* 2004.

Ashby, M. F., Work hardening of dispersion-hardened crystals, *Philosophic Magazine*, vol. 14, pp. 1157-1178, 1966.

Atkinson, J. D., Brown, L. M. and Stobbs, L. M., *Philosophic Magazine*, vol. 30, pp. 1247-1280, 1974.

Bach, C. and Baumann, R., *Elastizitat und festigkeit.* 1924.

Bader, W. and Lode, W., *Dissertations,* University of Gottingen, 1930.

Badr, E. A., A modified compact tension specimen for the study of residual stress maintainability, *Experimental techniques*, vol. 24, no. 3, pp. 25-27, 2000.

Bainbridge, A. T., *Residual* stresses arising from machining and fabrication, *AGARD Conf. Proc. 53, Symposium on Eng. Practice to Avoid SCC*, Istanbul, Turkey, 8-1 to 8-21, Oct, 1969.

Bairstow, L., *Phil. Trans. Roy. Soc.*, A, pp. 210–235, 1911.

Baltov, A. and Sawczuk, A., A rule of anisotropic hardening, *Acta Mechanica.* 1, pp. 81-92, 1965.

Bannantine, J. A., Comer, J. J. and Handrock, J. L., *Fundamentals of metal fatigue analysis*, Prentince-Hall, Inc. pp. 1-39, 1990.

Bauschinger, J., Changes of the elastic limit and the modulus of elasticity on various metals, *Zivilingenieur*, 27, pp. 289-353, 1881.

Bauschinger, J., On the changes of the elastic limit and strength of iron and steel, by drawing out, by heating and cooling, and by repetition of loading, *Mittheilungen aus dem mechanischen technischen laboratoriumder k*, Hochschule in Munchen, pp. 463-465, 1886.

Beaney, E. M. and Procter, E., A critical evaluation of the centre hole technique for the measurement of residual stresses, *Strain*, pp. 7–14, January, 1974.

Beaney, E., M., Accurate measurement of residual stress on any steel using the centre hole method, *Strain*, vol. 2, no. 3, pp. 99-106, 1976.

Beghini, M. and Bertini, L., Residual stress modelling by experimental measurements and finite element analysis, *Journal of strain analysis*, vol. 25, no. 2, pp. 103–108, 1990.

Bonner, N. W., *Measurement of residual stresses in thick-section steel welds.* Ph. D. thesis, Department of Mechanical Engineering, University of Bristol, pp. 7, 1996.

Boyce, B. L., Chen, X., Peters, J. O., Hutchinson, J. W. and Ritchie, R. O., Mechanical relaxation of localized residual stresses associated with foreign object damage, *Report No. UCB/R/02/A1191 LBNL – 50157*, May, pp. 1–32, 2002.

BSI 10002, *Tensile testing of metallic materials; part 1 and 4.* British Standards Institution, BS EN 10002-1 and BS EN 10002-4, 1990.

Bückner, H., Novel Principle for Computation of Stress Intensity Factors, *Zeitschrift für angew. Mathematik and Mechanik,* (ZAMM), 50, 1970.

Bühler, V. H. and Buchlotz, H., Effect of residual stresses upon bending fatigue strength, *Stahl and Eisen*, vol. 53, no. 53, pp. 1330–1332, 1933.

Canal, J. R., *Investigation of the Bauschinger effect in copper.* MIT Master Thesis, 1960.

Cardenas-Garcia, J. F. The hole drilling method in photo-elasticity applications of an optimisation approach, *Strain*, pp. 9–17, February, 2000.

Chaboche, J. L. and Jung, O., Application of kinematic hardening viscoplasticity model with thresholds to the residual stress relaxation, *International journal of plasticity*, vol. 13 no. 10, pp. 785–807, 1998.

Chen, P. C. T., Bauschinger and hardening effects on residual stresses in autofrettaged thick-walled cylinders, *Journal of Pressure Vessels Technology*, vol. 108, February, pp. 108–112, 1986.

Cheng, W. and Finnie, I., A method for measurement of axisymmetric residual stresses in circumferentially welded thin-walled cylinders, *Journal of engineering materials and technology*, vol. 107, pp. 181–185, 1985.

Cheng, W. and Finnie, I., Measurement of residual hoop stress in cylinders using the compliance method, *Journal of engineering materials and technology*, vol.108, pp. 87–92, 1986.

Cheng, W. and Finnie, I., A new method of measurement of residual axial stresses applied to a multi-pass butt welded cylinder, *Journal of engineering materials and technology*, vol. 109, pp. 337–342, 1987.

Cheng, W. and Finnie, I., The crack compliance method for residual stresses measurements, *Welding in the world*, vol. 28, pp. 103–110, 1990.

Cheng, W., Finnie, I. and Vardar, Ö., Measurement of residual stresses near the surface using the crack compliance method, *Journal of engineering materials and technology*, vol. 113, pp. 199–204, 1991.

Cheng. W. and Finnie. I., An Overview of the Crack Compliance Method for Residual Stress Measurement, *Proc. 4th Int. Conf. Residual Stress*, Baltimore, Maryland, Society for Experimental Mechanics, pp. 449–458, 1994.

Cheng. W., Prime, M., B. and Finnie, I., Measurements of Residual Stresses Through the Thickness of a Strip Using the Crack Compliance Method, *Residual Stress III – Science and Technology Proceedings 3rd International Conference of Residual Stress*, vol. 2, pp. 1127–1132, 1997.

Cohen, J. B., X-ray techniques for the measurement of residual stresses in the real world, *Residual stress for designers and metallurgist*, pp. 211–221, 1992.

Dieter, G.E., *Mechanical metallurgy*, Mc Graw Hill, 1981.

Dowling, N. E., *Mechanical Behaviour of Materials,* Prentice-Hall International Editions, pp. 527–530, 1993.

Dye, D., Roberts, S. M., Withers, P. J. and Reed, R. C., The determination of the residual strains and stresses in a tungsten inert gas welded sheet of IN718 super-alloy using neutron diffraction, *Journal of strain analysis*, vol. 35, no. 4, pp. 247-259, 2000.

Edelman, F. and Drucker, D. C., Some extensions to elementary plasticity theory. *J. Franklin Inst.* 251, pp. 581-605, 1951.

Ezeilo, A. N. and Webster, G. A., Neutron diffraction analysis of the residual stress distribution in a bent bar, *Journal of strain analysis*, vol. 35, no. 4, pp. 235-246, 2000.

Fett, T. and Munz, D., *Stress intensity factors and weight functions,* Computational Mechanics Publications, Southampton, UK, 1997.

Fett, T. and Thun, G., Residual stresses in PVC-cylinders determined with the weight function method, *Journal engineering fracture mechanics*, vol. 55, no. 5, pp. 859–863, 1996.

Gauthier, J., Krause, T. W. and Atherton, D. L., Measurement of residual stress in steel using the magnetic Barkhausen noise technique, *Insight*, vol. 31, no. 1, pp. 23-31, 1998.

Gere, J. M. and Timoshenko, S. P., *Mechanics of materials,* PWS, 1997.

Gould, D. D., Hirsch, P. B. and Humphreys, F. J., The Bauschinger effect, work-hardening and recovery in dispersion-hardened copper crystals, *Philosophic magazine*, pp. 1353-1375, 1974.

Gremaud, M., Cheng, W., Prime, M. and Finnie, I., Measurement of residual stress in laser treated layers using the crack compliance method, *Proc. Int. Conf. Laser Advanced Mat. Proc.*, Matasunawa A. and Katayama S. (eds), pp. 713–718, 1992.

Gremaud, M., Cheng, W., Finnie, I. and Prime, M., *The compliance method for measurement of near surface residual stress – analytical background,* Journal of engineering materials and technology, vol. 116, pp. 550-555, 1994.

Grimberg, R., Savin, A., Chifan, S. and Leitoiu, A., Incremental permeability method - One option for non-destructive evaluation of boilers tubes, *NDE Science & Technology; Proceedings of the 14th World Conference on Non-Destructive Testing*, New Delhi, 8-13, vol. 3, pp. 1643–1646, December, 1996.

Güngör, S., Residual stress measurements in fibre reinforced titanium alloy composites, *Journal of strain analysis*, in press, 2001.

Hearn, E. J., *Mechanics of materials, vol 1: An Introduction to the Mechanics of Elastic and Plastic Deformation of Solid and Structural Components*. Butterworth Heinemann, Oxford, 1997.

Herbert, H., Uber den Zusammenhang der Biegungselastizitat des gusseisens mit seiner zug- and druckelastizatat. (On the connection between bending deformation and tension compression deformation for cast iron), *Mitt. Und Forschungsarb. Ver deut Ing.* 89, pp. 39-81, 1910.

Herman, R., Crack growth and residual stress in Al-Li metal matrix composites under far-field cyclic compression, *Journal of materials science*, pp. 3782–3790, 1995.

Heyn, E., Theory of the cancelled elastic stresses, *Metall und Erz, Zeischrift*, 15, pp. 411-422, November, 1918.

Hodge, P. G., Discussion on Prager W, A new method of analysing stresses and strains in work hardening plastic solids. *Journal of applied mechanics,* 24, pp. 482-483, 1957.

Huang, D. J., Mayo, W. E. and Chen, Y., Residual stress measurement in time-controlled quenched austenitic steel, *Journal of experimental mechanics*, pp. 359–363, 1988.

Irwin, G., R., Analysis of Stresses and Strains Near the End of a Crack Traversing a Plate, *Journal of applied mechanics,* vol. 24, pp. 361 – 363, 1957.

James, M. R., The relaxation of residual stresses during fatigue, *Experimental Techniques*, The Soc. for Exp. Mech. Inc, pp. 297–314, 1982.

Kandil, F. A., Lord, J. D., Fry, T. A. and Grant, P. V., A review of residual stress measurement methods – A guide to technique selection, *Project CPM 4.5, Measurement of residual stress in components, NPL Report MAT(A) 04*, Feb. 2001.

Kang, K. J., Song, J. H. and Earmme, Y. Y., A method for the measurement of residual stresses using a fracture mechanics approach, *Journal of strain analysis*, vol. 24, 23–30, 1989.

Kashiwaya, K., Sakamoto, H. and Inoue, Y., *Non-destructive measurement of residual stress using magnetic sensors*, pp. 30–35, 1989.

Keil, S., Experimental determination of residual stresses with the ring core method and on-line measuring system, *Experimental techniques*, The Soc. For Exp. Mech. Inc., pp. 17–24, 1992.

Korsunsky, A. M. and Whithers, P. J., Plastic bending of residually stresses beam, *International journal of solids structures*, vol. 34, no. 16, pp. 1985-2002, 1997.

Lambrineas, P., Finlayson, T. R., Griffiths, J. R., Howard, C. J. and Smith, T. F., Neutron diffraction residual stress measurements on a thin steel plate, *NDT International*, vol. 20, no. 5, pp. 285–290, October, 1987.

Laws, V., Derivation of the tensile stress strain curve from bending data, *Journal of materials and science*, 16, pp. 1299-1304, 1981.

Leeman, E. R. and Hayes, D. J., A technique for determining the complete state of stress in rock using a single borehole, *Proc. 1st Congress Int. Soc. of Rock Mech.*, Lisbon, Portugal, pp. 17–24, Sept/Oct, 1966.

Lindgren, M. and Lepistö, T., Effect of mean stress on residual stress relaxation in steel specimens, *Material science and technology*, vol. 18, pp. 845–849, August, 2002.

Lloyd, D. J., The Bauschinger effect in polycrystalline aluminium containing coarse particles, *Acta Metallurgica*, vol. 25, pp. 459–466, 1977.

Lu, J., Flavenot, J., F. and Turbat, A., Prediction of residual stress relaxation during fatigue, Mechanical Relaxation of Residual Stresses, *ASTM STP 993*, L. Morfin, Ed., *American Society for Testing and Materials*, Philadelphia, pp. 75–90, 1988.

Macherauch, E. and Kloos, K. H., Origin, measurement and evaluation of residual stresses, *Residual stresses in science and technology*, ISBN3-88355-099-X, vol. 1, pp. 3-26, 1986.

Mac Readys, *Steel Catalogue*, pp. 6, 1991.

Marin, J., *Mechanical behaviour of engineering materials*, Prentice Hall, 1962.

Masing, G., *Zeitschrift fur Metallkunde*, 17, pp. 268, 1925.

Masubuchi, K., *Analysis of welded structures*, pp. 92-94, 1980.

Mayville, R A. and Finnie, I., Uniaxial stress-strain curves from a bending test, *Experimental mechanics*, pp. 192-201, 1982.

Measurements Group, *Student manual for strain gage technology*, Bulletin 309D, pp. 17-23, 1992.

Middleton, J. C., Residual stresses and X-rays, *NDT International*, vol. 20, no. 5, pp. 291–294, October, 1987.

Moore, H. and Beckinsale, S. J., The removal of internal stress in 70:30 brass by low temperature annealing, *Journal of the institute of metals*, vol. 23, pp. 225-245, 1920.

Morrow, J. D., Ross, A. S. and Sinclair, G. M., Relaxation of residual stresses due to fatigue loading, *SAE Transactions*, vol. 68, pp. 40–48, 1960.

Mroz, Z., On the description of anisotropic work-hardening, *Journal of the mechanics and physics of solids*, vol. 15, pp. 163-173, 1967.

Nabertherm, *Hardening guide and other heat treatments of steel*, 1997.

Nadai, A., *Plasticity*, McGraw-Hill, 1931.

Noble, H. J. and Reed, E. C., The influence of residual stress in nickel and chromium plates on fatigue, *Journal of experimental mechanics*, pp. 463–467, 1974.

Nowell, D., Tochilin, S. and Hills, D. A., Measurement of residual stress in beams and plates using the crack compliance technique, *Journal of strain analysis*, vol. 35, no. 4, pp. 277–285, 2000.

Orowan, E., *Internal stresses and fatigue of metals*, N. Y. Elsevier, pp. 1-29, 1959.

Pacyna, J. and Kokosza, A., Residual stress measurement in steel mill rolls using magnetic Barkhausen noise analysis, *NDT.net*, August, vol. 4, no.2, pp. 1-7, 1999.

Parlane, A. J. A., The determination of residual stresses: A review of contemporary measurement techniques, *Residual stresses in welded construction and their effects*, pp. 63–78, 1979.

Prager, W., A new method of analysing stresses and strains in work hardening plastic solids. *Journal of applied mechanics*, 24, pp. 493-496, 1956.

Press, W. H., Flannery, B. P., Teukolsky, S. A. and Vetterling, W. T., *Numerical recipes*, Cambridge University Press, 1987.

Prevéy, P. S., X-ray diffraction residual stress techniques, *Metals Handbook*, 10, American Society for Metals, pp. 380–392, 1986.

Prime, M., B., Residual stress measurement by successive extension of a slot: The crack compliance method, *Applied mechanics reviews*, vol. 52, no. 2, pp. 75–96, 1999.

Prime, M. B., Rangaswamy, P. and Bourke. M. A. M., Measuring spatial variation of residual stresses in a MMC using crack compliance, *7th International Conference on Composites Engineering*, pp. 711–712, 2000.

Prime, M. B., Cross-sectional mapping of residual stress by measuring the surface contour after a cut, *Journal of engineering materials and technology*, vol. 123, pp. 162–168, 2001.

Rees, D. W. A., Anisotropic hardening theory and the Bauschinger effect, *Journal of strain analysis*, vol. 16, no. 2, pp. 85-95, 1981.

Ritchie, D. and Leggatt, R. H., The measurement of the distribution of residual stress through the thickness of a welded joint, *Strain*, vol. 23, no. 2, pp. 61–70, 1987.

Rosenthal, D., Sines, G. and Zizicas, G., Effect of residuals compression on fatigue, Ibid., vol. 28, no. 3, *Research Suppl.*, pp. 98–103, 1949.

Ruud, C. O., Nondestructive and semidestructive methods for residual stress measurement, *Residual stress effects in fatigue*, pp. 3–5, 1982.

Sachs, G. and Espey, G., The measurement of residual stresses in metal, *The iron age*, pp. 63–71, 1941.

Sachs, W. and Shoji, H. *Z., Physik,* 45, pp. 776, 1927.

Sarnatski, V. M., Krasnoschekova, N. A., Popov, A. M. and Filev, A. K., Magneto-elastic properties of doped ferrites, *XI Session of the Russian Acoustical Society*, Moscow, November, pp. 19-23, 2001.

Schindler, H., J. and Bertschinger, P., Some Steps Towards Automation of the Crack Compliance Method to Measure Residual Stress Distribution, *5th Int. Conf. on residual stresses*, June 16 - 18, Linköping, Sweden, pp. 682–687, 1997.

Schindler, H. J., Cheng, W. and Finnie, I., Measurement of residual stress distribution in a disk or a solid cylinder using the crack compliance method, *Proc. 4th Int. Conf. Residual Stress*, Baltimore, Maryland, Society for experimental mechanics, pp. 1266–1274, 1994.

Schindler, H. J., Determination of residual stress distributions from measured stress intensity factors, *International journal of fracture*, vol. 74, no. 2, pp. 23–30, 1995.

Schindler, H. J. and Landolt, R., Experimental determination of residual stress and the resulting stress intensity factors in rectangular plates, *4th. European conference on residual stresses,* Cluny, France, pp. 509-517, 1997.

Schindler, H. J., Cheng, W. and Finnie, I., Experimental determination of stress intensity factors due to residual stresses, *Journal of experimental mechanics*, vol. 37, no. 3, pp. 272–277, 1997.

Schindler, J. H., Residual stress measurement in cracked components: Capabilities and limitations of the cut compliance method, *Materials science forum*, vols. 347–349, pp. 150–155, 2000.

Schwaighofer, J., Determination of residual stresses on the surface of structural parts, *Journal of experimental mechanics*, vol. 4, no. 2, pp. 54–56, 1964.

Sidebottom, O. M. and Chang, C-T., *Influence of the Bauschinger effect on inelastic bending of beams.* University of Illinois, pp. 631–639, 1963.

Smith, D. J., Bouchard, P. J. and George, D., Measurement and prediction of residual stresses in thick-section steel welds, *Journal of strain analysis*, vol. 35, no. 4, pp. 287–305, 2000.

Smithells Metals Reference Book, 7th Edition, E. A. Brandes & G. B. Brook, pp. 22-1 to 22-27, 1992.

Spiegel, M. R., *Mathematical handbook*, McGraw Hill, pp. 3, 1998.

Stänhlkopf, K. and Egan, R. G., Recent advances in residual stress measurement, *Residual stresses in welded construction and their effects*, pp. 321–333, 1979.

Stouffer, D. C., *Dame LT. Inelastic deformation of metals,* John Wiley, 1996.

Swindeman, R. W., Mechanical relaxation response of 2 ¼ Cr – 1 Mo steel, *Residual stress and stress relaxation,* Sagamore Army Materials Research Conference, N. Y. pp. 157–179, 1981.

Tada, H., *The Stress Analysis of Cracks Handbook,* Del Research Corporation, Hellertown, Pennsylvania, 1973.

Takeda, T. and Nasu, Y., *Determination of the Bauschinger effect and planar anisotropy from bending test*, Bull. Yamagata Univ. Eng., vol. 20, no. 2, pp. 169-177, January, 1989.

Thakur, A., Nemat-Nasser, S. and Vecchio, K., S., Dynamic Bauschinger effect, *Acta Metallurgica*, vol. 44, no. 7, pp. 2797–2807, 1996.

Timoshenko, S. P., *Strength of Materials, Part II Advanced,* International Student Editions, pp. 377–381, 1956.

Timoshenko, S. P., *Strength of Materials, Part II Advanced.* Van Norstrand, 1981.

Timoshenko, S. P. and Gere, J. M., *Mechanics of materials,* Third SI Edition, pp. 250–340, 1991.

Todd, J. D., *Structural theory and analysis*, Second Edition, Macmillan Publishers Ltd, pp. 181-189, 1981.

Torres, M. A. S. and Voorwald, H. J. C., An evaluation of shot peening, residual stress and stress relaxation on the fatigue life of AISI 4340 steel, *International journal of fatigue,* vol. 24, pp. 877-886, 2002.

Treuting, R. G., The nature, origin and effects of residual stresses, *Residual stress measurements,* pp. 1– 41, 1952.

Urriolagoitia-Sosa, G., Durodola, J. F. and Fellows, N. A., Determination of residual stress in beams under Bauschinger effect using surface strain measurements, *Strain*, ISSN 0039-2103, Vol. 39, No. 4, November, pp. 177-185, 2003.

Vaidyanathan, S. and Finnie, I., Determination of residual stresses from stress intensity factor measurements, *Journal Basic Engineering*, vol. 93, pp. 242–246, 1971.

Vanderveld, R. A., Carpenter, J. H. and Dahmen, K. A., Hysteresis in magnetic materials: Analyzing the size and shape of subloops near the critical point,

http://www.physics.uiuc.edu/Education/UnderGrad/REU/FinalPapers/2000/Vanderveld.pdf, 2000.

Vöhringer, O., Relaxation of residual stresses by annealing or mechanical treatment, Advances in surface treatments, *International guidebook on residual stresses*, Pergamon Press, pp. 367–396, 1987.

Wadsley, N., *Residual stress analysis*, M. Sc. Thesis, Oxford Brookes University, pp. 12, 1994.

Wallace, W. P. and Frankel, J. P., Relief of residual stress by a single fatigue cycle, pp. 565, November 1949.

Wern, H., A new approach to triaxial residual stress evaluation by the hole drilling method, *Strain*, pp. 121–125, November, 1997.

Wilson, O. V., Magnetic properties, internal strains and the Bauschinger effect in metals, *Nature*, London, vol. pp. 170, 30-31, 1952.

Wolley, R. L., Bauschinger effect in some face-centred and body-centred cubic metals, *Philosophical Magazine*, vol. 44, no. 353, pp. 597-618, 1953.

Wolley, R. I., *Rep. Conf. On Str. Of Solids, Bristol,* London Phys. Soc., 1958.

Wu, XR. and Carlsson, A. J., *Weight function and stress intensity factor solutions.* Pergamon Press, Oxford, England, 1991.

Zhang, XD., Ginter, T. J., Cornell, B., Evans, D. J. and Fraser, H. L., Effect of stretching on the strength (Bauschinger's effect) of Ti-6Al-2Cr-2Mo-2Sn-2Zr alloy, *Journal of advanced material,* vol. 32, no. 1, pp. 34-38, 2000.

Ziegler, H., A modification of Prager's hardening rule. *Quart. Appl. Maths.* 17, pp. 55-65, 1959.

Publications from this work

Journal paper:

1.- Urriolagoitia-Sosa, G., Durodola, J. F. and Fellows, N. A., Determination of residual stress in beams under Bauschinger effect using surface strain measurements, *Strain*, ISSN 0039-2103, Vol. 39, No. 4, November, pp. 177-185, 2003.

Conference paper:

1.- Urriolagoitia-Sosa, G., Durodola, J. F. and Fellows, N. A., Determination of tensile and compressive stress-strain curves from bend tests, Advances in Experimental Mechanics, ISBN=0-87849-955-5, *Applied Mechanics and Materials*, Vol. 1-2, ISSN=1660-9336, pp. 133-138, 2004.

Conference abstracts/presentations:

1.- Urriolagoitia-Sosa, G., Durodola, J. F. and Fellows, N. A., Residual stress comparison by diverse method between bending beams and cylinders subjected to internal pressure, *Proceedings of the 5th International Congress of Electro-mechanic Engineering and Systems*, pp. 155-159, November 27th – 30th, D. F., México, 2000.

2.- Urriolagoitia-Sosa, G., Durodola, J. F. and Fellows, N. A., Determination of the compression stress-strain behaviour of a bend beam under Bausshinger effect, *Proceedings of the 7th International Conference on Advanced Materials, ICAM 2001*, pp. 31, August 26th – 30th, Cancún, Q. R., México, 2001.

3.- Urriolagoitia-Sosa, G., Durodola, J. F. and Fellows, N. A., On the use of the crack compliance method for measurement of residual stress, *Proceedings of the 11th International Materials Research Congress 2002*, pp. 21-10, August 25th – 29th, Cancún, México, 2002.

4.- Urriolagoitia-Sosa, G., Durodola, J. F. and Fellows, N. A., Determination of residual stress relaxation by the use of the crack compliance method, *Proceedings of the 14th International Materials Research Congress, IMRC 2005*, Accepted, August 21th – 25th, Cancún, México, 2005.